



The University of Strathclyde

Department of Mechanical and Aerospace Engineering

**Regenerating the strength of thermally
recycled glass fibres using chemical
treatments**

Eduardo Sáez-Rodríguez

A thesis presented for the degree of Doctor of Philosophy

Glasgow, Scotland

United Kingdom

September 2017

DECLARATION OF AUTHENTICITY AND AUTHOR'S RIGHTS

This thesis is the result of the author's original research. It has been composed by the author and has not been previously submitted for examination which has led to the award of a degree.

The copyright of this thesis belongs to the author under the terms of the United Kingdom Copyright Acts as qualified by University of Strathclyde Regulation 3.50.

Due acknowledgement must always be made of the use of any material contained in or derived from this thesis.

Signed:

A handwritten signature in blue ink, appearing to read 'Eduardo Sáez-Rodríguez', written in a cursive style.

Eduardo Sáez-Rodríguez

Date: 16th of September of 2017

ACKNOWLEDGEMENTS

Firstly, I would like to express my sincere gratitude to my supervisor, Professor James Thomason, for giving me the opportunity of pursuing a Ph.D on this composite research project, excellent guidance, and for his continuous support, motivation and inestimable research discussions. I very much appreciate the trust and confidence he placed in me, expressed as freedom to tackle the problems independently. He helped me to develop my research and restless thinking, improved my communication skills and he cared about my welfare.

Besides my supervisor, I would like to thank my colleagues and friends, Dr Liu Yang, Dr Chi-Chuan Kao, Dr Durai Prabhakaran, Dr Fiona Cullinane, Susan Roch, Kerrie Downes, Jose Luis Rudeiros Fernandez, Peter Jenkins, Ulf Nagel, Kyle Pender and Ross Minty, for their advice and support on my work, their friendship and the good times spent together.

My sincere thanks also go to Dr Fiona Sillars from the Advanced Materials Research Laboratory and Jim Doherty and James Kelly of the Department of Mechanical Engineering for their great technical support to my laboratory work; Dr Simson McCreath for his help with the use of NMR and his knowledge in the field of polymer chemistry; Dr Leung Tang for his help with the IR equipment; Dr John Liggat, of the Department of Pure and Applied Chemistry for the access to his laboratories.

I thank the Engineering and Physical Science Research Council (EPSRC) for the financial support.

I would also like to have a special mention to my parents and brother, who have given me everything: support, guidance, consolation and love.

But my special mention is for my wonderful and devoted girlfriend, Irene, without whose tireless support, care and love, none of that would have been possible.

Contents

Abstract	VIII
List of symbols	X
List of abbreviations	XII
List of figures	XIV
List of tables	XXII
Introduction	1
Chapter 1 Literature review	3
1.1 Glass	3
1.2 Glass Fibre	5
1.2.1 Manufacture of Glass Fibres.	8
1.2.2 Basic structural differences between glass and glass fibres	10
1.2.3 E-glass	11
1.3 Mechanical properties of glass fibres	13
1.3.1 Strength	13
1.3.2 Flaws and cracks	13
1.3.3 Diameter and length dependence	19
1.3.4 Weibull distribution	20
1.4 Silane coupling agents	23
1.4.1 Types of silane coupling agents	24
1.4.2 Conditioning of silane coupling agents	25
1.4.3 Types of silane coupling agent layer adsorption and deposition	31
1.4.4 Effect of silane coupling agent on glass fibre surface and strength	34

1.5	Amino Silanes.....	36
1.6	The effect of pH on hydrolysis and self-condensation reactions of APS	40
1.7	The effect of temperature on hydrolysis and self-condensation reactions of APS 40	
1.8	Effect of thermal conditioning on glass fibre properties	41
1.9	Acid and basic treatments.....	47
1.9.1	Hydrofluoric acid treatment	47
1.9.2	Hydrochloric acid treatment.....	51
1.9.3	Sodium hydroxide treatments.....	52
Chapter 2	Experimental.....	59
2.1	Materials	59
2.1.1	Glass fibres.....	59
2.1.2	Chemicals.....	59
2.2	Silanes solution treatments	60
2.3	Thermal degradation (TD).....	63
2.4	Acid and base treatments	64
2.4.1	HCl treatment	64
2.4.2	NaOH treatments.....	64
2.5	Single fibre tension test	65
2.6	Nuclear Magnetic Resonance (NMR)	69
2.7	Fourier Transform Infrared (FTIR)	70
2.8	Scanning Electron Microscope (SEM)	72
Chapter 3	Results and Discussion	73
3.1	Regeneration of glass fibre strength	73

3.1.1	Strength of as received and commercially coated glass fibres.....	73
3.1.2	Strength of as received self-coated glass fibres	73
3.1.3	Strength statistical analysis of as received, commercially silane coated and as received self-coated with RT and ET APS GFs.....	76
3.1.4	Thermally degraded GFs.....	80
3.1.5	Effect of chemical treatments on the strength of thermally conditioned commercially coated GFs.....	83
3.1.6	Effect of ET APS on the strength of thermally degraded commercially coated GFs.....	88
3.1.7	Effect of pre-washing of APS from commercially coated GFs	89
3.1.8	Combined effect of Prewashing, HCl, NaOH and ET APS	90
3.2	NMR investigation of ethanol removal from APS solution	93
3.3	FTIR characterisation of ET APS.....	98
3.3.1	FTIR characterisation of ET APS in solution	98
3.3.2	FTIR characterisation of ET APS films	110
3.4	ET APS polymerisation Hypothesis	113
3.5	DRIFT study of treatments effects on GFs.....	116
3.6	SEM surface characterisation	120
Chapter 4	Conclusions	126
Chapter 5	Summary and future work	130
Chapter 6	References	136
Chapter 7	Appendix	146
7.1	Fourier Transform Infrared spectroscopy (FTIR).....	146
7.1.1	FTIR spectra	150

7.2	Nuclear Magnetic Resonance	154
7.2.1	NMR spectra	159
7.3	Bundle tension tests	163
7.3.1	Materials.....	163
7.3.2	Chemicals.....	163
7.3.3	Silane solution preparation.....	163
7.3.4	Experimental	166
7.3.5	Results and discussion.....	169
7.4	Weibull analysis plots.....	174

Abstract

The processing and reuse of end-of-life composite products in an environmentally friendly manner is one of the most important challenges facing the industry and community. The development of an economically viable process for regenerating the properties of thermally recycled glass fibres (GFs) would have major technological, societal, economic and environmental impacts. The ultimate goal of this project is to enable cost-effective regeneration of the mechanical properties of GFs which have been produced from thermal recycling of end-of-life glass reinforced structural composites from automotive and wind energy applications.

This work investigates the loss, and regeneration, of GF strength after thermal degradation at typical GRP recycling temperatures. The mechanical properties of APS sized and water sized (uncoated) Boron-free-E-glass fibres were first characterised using a conventional single fibre tension test. A substantial higher average strength was obtained from the APS sized fibres. Further investigation with GFs, coated with different silanes was carried out to determine any beneficial effect on GF mechanical properties. It was found that γ -Methacryloxypropyltrimethoxy Silane (MPS) and γ -Glycidoxypropyltrimethoxy Silane (GPS) prepared for 24 hours at RT and solution medium pH 5-5.5 in deionised water and γ -Aminopropyltriethoxy Silane prepared at 83^oC for 5 hours at solution medium natural pH (ET APS) in deionised water showed the higher increases in GF mechanical properties. Moreover, it was found that preparing the hydrolysed APS solution at elevated temperatures, had a beneficial effect on GF strength in comparison to a solution prepared at RT over 24 h (RT APS).

Further investigation was carried out to identify any changes to the final products in solution and any structural differences between APS prepared at RT and at ET, that would lead to a conclusion about the difference in mechanical properties achieved. Using techniques such as Nuclear Magnetic Resonance (¹H NMR) and Fourier Transform Infrared Spectroscopy (FTIR), several differences were identified. The results showed that ET APS contained less ethanol in solution after preparation, showing a relationship between the preparation temperature and the ethanol lost from the solution. On the other hand, the FTIR spectra indicated a higher polymerisation

level of the ET APS, which suggested that a higher polymer may positively affect the mechanical performance of GFs. Hydrolysis at elevated temperature was found to be a novel and relatively easy way to prepare APS that improves the beneficial effect on GF strength.

Thermal degradation of the APS sized Boron-free-E-glass fibres was also investigated across a wide range of temperatures. The results suggested that at temperatures around 350⁰C, the APS coating on the GFs surface starts to degrade and disappear, consequently reducing the protection provided by the APS layer. The effect of high temperature on GFs also creates cracks and flaws that may also contribute to the strength loss seen in these results which are consistent with the creation of defects for high temperature.

Two other chemical treatments were investigated for their ability to regenerate the mechanical properties of the thermally conditioned GFs. An acidic treatment with hydrochloric acid (HCl) 37% v/v did produce a small increase of the average fibre strength, whilst a base treatment using concentrated sodium hydroxide (NaOH) solution at high temperature (95⁰C) substantially improved the mechanical properties of thermal conditioned GFs, achieving up to 200% increase in fibre strength in comparison with the thermally degraded GFs.

The optimum NaOH treatment conditions were further characterised in terms of treatment time, NaOH concentration and GF surface state and the effect on GF surface (i.e. OH groups on the surface) and reactions that occur with the glass. It is concluded that a number of very promising treatments with the potential to regenerate the mechanical properties of GFs recycled from composites have been identified.

List of symbols

A	Cross section area
A_p	Prefactor
D	Diameter
D_0	Pre-exponential factor
D_D	Water diffusion coefficient
E	Elastic modulus
E_a	Activation energy
F	Load
F_{max}	Maximum load
i	Rank value
K_{IC}	Fracture toughness
L	Length
L_0	Length of a conceptual link
l_0	Fibre gauge length
m	Shape parameter in Weibull analysis
m_0	Initial weight of the crushed glass
m_1	Shape parameter of population 1 in Weibull analysis
m_2	Shape parameter of population 2 in Weibull analysis
m_t	Residue weight at t time
Δm	Difference between m_0 and m_t
N	Fibre specimens
P	Hydrostatic pressure
P_F	Probability of failure
q	Mixing parameter in Weibull analysis
Q_D	Activation energy of water diffusion
R	Hydrolysable group
T_a	Absolute temperature

T_g	Glass transition temperature
ΔV	Activation volume
W_{loss}	Weight loss
X	Reactive or resin compatible functional group
α	half the crack length
δ	Tolerance
σ	Stress
σ_0	Scale parameter in Weibull analysis
σ_{01}	Scale parameter of population 1 in Weibull analysis
σ_{02}	Scale parameter of population 2 in Weibull analysis
σ_1	Surface submicrocracks
σ_2	Flawless massive glasses after etching
σ_3	Flawless glass fibre
σ_E	Extrinsic environmental fatigue strength
σ^*_E	Intrinsic environmental fatigue strength
σ_F	Fatigue-free Extrinsic strength
σ^*_F	Fatigue-free Intrinsic strength
σ_{FAIL}	Stress at fail
σ_i	Extrinsic inert strength
σ^*_i	Intrinsic inert strength
σ_{sm}	Surface microcracks
σ_T	Threshold stress

List of abbreviations

AFM	Atomic force microscope
APS	γ -Aminopropyltriethoxy Silane
ATR	Attenuated total reflectance infrared spectroscopy
Av.	Average
CLTE	Coefficient of linear thermal expansion
DRIFT	Diffuse reflectance infrared Fourier spectroscopy
ET	Elevated temperature
FTIR	Fourier transform infrared spectroscopy
GF	Glass fibre
GFs	Glass fibres
GPS	γ -Glycidoxypropyltrimethoxy silane
GRP	Glass reinforced plastics
^1H NMR	Proton nuclear magnetic resonance spectroscopy
LSs	Least squares regression method
ML	Maximum likelihood analysis method
MPS	γ -Methacryloxypropyltriethoxy silane
NMR	Nuclear magnetic resonance spectroscopy
O.C.	Owens Corning
PW	Prewash
RT	Room temperature
SEM	Scanning electron microscope
Si	Silicon
SPS	γ -Mercaptopropyltrimethoxy silane
T	Temperature
TD	Thermal degradation
ToF-SIMS	Time-of-life secondary ion mass spectroscopy
VS	Vinyltriethoxy silane

XPS X-ray photoelectron spectroscopy

List of figures

Figure 1.1 Schematic representation of (a) ordered crystalline and (b) random-network glassy form of silica [3].	3
Figure 1.2 The silica tetrahedron, the basic structural unit of silicates and silica glasses.	4
Figure 1.3 GF forming process.	8
Figure 1.4 Schematic representation of the axial cross-section of a GF with a surface layer and different types of surface flaws: surface microcracks (σ_{sm}), surface submicrocraks (σ_1), flawless massive glasses after etching (σ_2) and flawless glass fibres (σ_3) [13].	14
Figure 1.5 Fish-bone chart of the experimental parameters which may influence the measured strength of melt-dawn fibres [9].	17
Figure 1.6 2-point bending fibre fracture strain technique.	18
Figure 1.7 Simple schematic of silanes at an interface.	24
Figure 1.8 Typical GF industry silane coupling agents.	25
Figure 1.9 Hydrolysis and condensation processes of alkoxy silanes [50].	26
Figure 1.10 Reaction between self-condensed alkoxy silane and substrate surface [50].	27
Figure 1.11 Schematic representation of the adsorption of silane coupling agent molecules onto glass fibre surface. A) The silane solution is a concentration below the onset concentration of association, and B) The silane coupling agent concentration above the onset concentration of association. White open circles indicate isolated silanes. Black closed circles indicate hydrogen bonded or oligomeric silane coupling agents.	30
Figure 1.12 Chemical structure of hydrolysed APS on GF [66].	32

Figure 1.13 Interpenetrating network between hydrolysed APS and polyurethane film polymer or sizing [66].	33
Figure 1.14 Interphase in a GF composite where a reacted interpenetrating network between network silane, film former and resin matrix (R) forms [66].	33
Figure 1.15 Types of flaws and the effect of a surface treatments on fibre surface [70].	35
Figure 1.16 Si-O-Si bonding between silica surface and APS.	37
Figure 1.17 APS hydrolysis and self-condensation reactions in water.	39
Figure 1.18 Linear contraction of a single E-glass fibre as a function of temperature and time [16].	41
Figure 1.19 Influence of heat treatment temperature on RT average strength of unsized (water sized) and APS sized GFs [81].	43
Figure 1.20 Variation of tensile strength with period of heat treatment at four temperatures [91].	45
Figure 1.21 Relation between RT strength and heat treatment temperature [92].	46
Figure 1.22. Recovery in RT tensile strength of heat-treated glass fibres as a function of the treatment time of 1 % v/v of HF aqueous solution [108].	50
Figure 1.23 Tensile strength of heat-treated glass fibres as a function of fibre diameter reduction and an example for the 600 ⁰ C-treated fibres with semi-circular and straight-fronted cracks [108].	50
Figure 1.24 Variation of etching rate for 4" Oyrex glass (Corning 7740) with the composition of the solution in pure HF, 10:0.5, 10:1 and 10:1.5 of HF:HCl [109].	51
Figure 1.25 Weight loss (Δm is the difference between m_0 and m_t) of SB versus time in function of the nature of alkaline solution (NaOH and KOH) at 70 ⁰ C [113].	53
Figure 1.26 Weight loss (Δm is the difference between m_0 and m_t) of SB versus time in function of the concentration of alkaline solution (NaOH) at 70 ⁰ C [113].	54

Figure 1.27 Mass loss ratio-treating time behaviour (alkali treatment). The error bars represent the standard deviation [118].	56
Figure 1.28 Strength maintenance ratio-treating time behaviour at 98 ⁰ C (alkali treatment). The error bars represent the standard deviation [118].	56
Figure 1.29 SEM images of the GF (E-glass) surfaces after treatment in NaOH solution [118].	57
Figure 2.1 Bundles Steel Rig.	62
Figure 2.2 Bundles Steel Rig. A) GF Bundle. B) Nut, bolt and washer.	63
Figure 2.3 Single fibre test template.	65
Figure 2.4 Single fibre separation from GF bundle.	66
Figure 2.5 Measurement of GF diameter using an optical microscope.	67
Figure 2.6 Typical load-extension curve for a single fibre test.	68
Figure 2.7 Lid used to prepare APS films for DRIFT analysis.	71
Figure 3.1 Weibull plot of as received GFs, self-coated with RT and ET APS and commercially coated GFs.	76
Figure 3.2 Cumulative failure probability for as received GFs, self-coated with RT and ET APS and commercially coated GFs.	77
Figure 3.3 Cumulative failure probability for self-coated RT and ET APS GFs.	79
Figure 3.4 Cumulative failure probability for self-coated ET APS and commercially silane coated GFs.	79
Figure 3.5 Cumulative failure probability for self-coated RT APS and commercially silane coated GFs.	80
Figure 3.6 Plot of the average single fibre strength for commercially coated GFs at different TD temperatures.	81
Figure 3.7 Plot of the average single fibre strength for commercially coated GFs at different TD temperatures between 350 and 500 ⁰ C.	82

Figure 3.8 NaOH solution concentration effect on average single fibre strength of TD commercially coated GFs.....	87
Figure 3.9 Prewashing effect on average single fibre strength of TD commercially coated GFs.....	90
Figure 3.10 Average single fibre strength for the different treatment combinations.1: TD; 2: PW and TD; 3: PW, TD and ET APS; 4: PW, TD, NaOH; 5: PW, TD, NaOH and ET APS.....	91
Figure 3.11 ¹ H NMR spectrum of APS in Chloroform at 20 ⁰ C (RT).....	93
Figure 3.12 Predicted ¹ H chemical shifts (ppm) for γ -APS.....	94
Figure 3.13 ¹ H chemical shifts of 25% v/v RT APS in D ₂ O.	95
Figure 3.14 ¹ H chemical shifts of 25% v/v ET APS in D ₂ O.....	96
Figure 3.15 Ethanol presence during 25% v/v APS in D ₂ O preparation at different temperatures.....	97
Figure 3.16 ATR spectra of 10% v/v APS in deionised water solution prepared at RT and ET, and an equivalent % of ethanol released by APS in deionised water solution (7.5% v/v).....	99
Figure 3.17 Magnification of ATR spectra of 10% v/v APS in deionised water solution prepared at RT and ET, and an equivalent % of ethanol released by APS in deionised water solution (7.5% v/v) between 3100 and 2700 cm ⁻¹	99
Figure 3.18 Magnification of ATR spectra of 10% v/v APS in deionised water solution prepared at RT and ET, and an equivalent % of ethanol released by APS in deionised water solution (7.5% v/v) between 1350 and 850 cm ⁻¹	100
Figure 3.19 ATR spectra of 10% v/v APS 10 in D ₂ O solution prepared at RT and ET, and an equivalent % of ethanol released by APS in D ₂ O (7.5% v/v).	101
Figure 3.20 Magnification of ATR spectra of 10% v/v APS in D ₂ O solution prepared at RT and ET, and an equivalent % of ethanol released by APS in D ₂ O (7.5% v/v) between 3100 and 2700 cm ⁻¹	101

Figure 3.21 Magnification of ATR spectra of 10% v/v APS in D ₂ O solution prepared at RT and ET, and an equivalent % of ethanol released by APS in D ₂ O (7.5% v/v) between 1350 and 850 cm ⁻¹	102
Figure 3.22 Magnification of ATR spectra of 10% v/v APS in D ₂ O solution prepared at RT and ET, and an equivalent % of ethanol released by APS in deionised water solution (7.5% v/v) between 1600 and 1250 cm ⁻¹	103
Figure 3.23 Dialpath transmission spectra of 10% v/v APS in deionised water solution prepared at RT and ET.	104
Figure 3.24 Dialpath transmission spectra of 10% v/v APS in D ₂ O solution prepared at RT and ET.	105
Figure 3.25 Magnification of dialpath transmission spectra of 10% v/v APS 10 in D ₂ O solution prepared at RT and ET between 1600 and 1250 cm ⁻¹	105
Figure 3.26 ATR spectra for 10% v/v ET APS in deionised water and D ₂ O between 1150 and 900 cm ⁻¹	109
Figure 3.27 Dialpath transmission spectra for 10% v/v ET APS in deionised water and D ₂ O between 1150 and 900 cm ⁻¹	109
Figure 3.28 ATR derivative of the spectra for 10% v/v ET APS in deionised water and D ₂ O between 1150 and 900 cm ⁻¹	110
Figure 3.29 DRIFT spectra for 10% v/v APS prepared at RT and ET in deionised water, dried for 48h at 83 ^o C.	111
Figure 3.30 DRIFT spectra for 10% v/v APS prepared at RT and ET in D ₂ O, dried for 48h at 83 ^o C.	112
Figure 3.31 The different species formed during the hydrolysis reaction determined with solid state NMR relaxation time measurements. Molecule structures are T ⁰ _R : pristine silane; T ⁰ _H : silanol group from hydrolysis; T ¹ : dimer or chain end; T ² : linear link; T ³ : three dimensional [140].	113
Figure 3.32 DRIFT spectra for TD commercially coated GFs treated with NaOH and then rinsed in deionised water.	117

Figure 3.33 DRIFT spectra for TD commercially coated GFs treated with NaOH and then rinsed in HCl.	118
Figure 3.34 DRIFT spectra for TD commercially coated GFs treated with NaOH, wash with deionised water and then treated with APS.	119
Figure 3.35 DRIFT spectra for TD commercially coated GFs treated with NaOH, wash with deionised water and then treated with MPS.	119
Figure 3.36 Commercially coated GFs TD at 450 ⁰ C. a) Flat surface GF; b) bump in GF surface.	120
Figure 3.37 Commercially coated GF TD at 450 ⁰ C with HCl 10% v/v for 1 hour treatment surface.	121
Figure 3.38 Commercially coated GFs TD at 450 ⁰ C coated with a) MPS b) RT APS.	121
Figure 3.39 Commercially coated GFs TD at 450 ⁰ C treated with a)10% v/v HCl and MPS b)10% v/v HCl and RT APS.	122
Figure 3.40. As received GFs treated 5 hours with NaOH 3M.	123
Figure 3.41. As received GFs treated 5 hours with NaOH 3M and washed with 37% v/v HCl.	123
Figure 3.42. As received GFs treated 10 minutes with NaOH 3M.	124
Figure 3.43 As received GFs treated 1)10 minutes NaOH 3M washed with HCl, 2) 20 minutes NaOH 3M washed with HCl and 3) 30 minutes NaOH 3M washed with HCl.	125
Figure 7.1 The oscillation electric field of photon generates oscillating, oppositely directed forces on the positive and negative charges of the molecular dipole. The dipole oscillates with the same frequency as the incident photon [142].	147
Figure 7.2 Stretching and bending vibrations [143].	148
Figure 7.3 Symmetric and asymmetric vibrations [143].	149
Figure 7.4 Different types of bending vibrations [143].	149

Figure 7.5 DRIFT spectra for 10% v/v APS prepared at RT and ET in D ₂ O, dried for 3h at 83 ⁰ C.....	150
Figure 7.6 DRIFT spectra for 10% v/v APS prepared at RT and ET in deionised water, dried for 3h at 83 ⁰ C.....	150
Figure 7.7 DRIFT spectra for 10% v/v ET APS prepared in deionised water and deuterated water, dried for 3h at 83 ⁰ C.	151
Figure 7.8 DRIFT spectra for 10% v/v RT APS prepared in deionised water and deuterated water, dried for 3h at 83 ⁰ C.	151
Figure 7.9 ATR spectra for pure ethanol.	152
Figure 7.10 ATR spectra for pure APS.....	152
Figure 7.11 ATR spectra for dibutylamine, ethanolamine and triethylamine.....	153
Figure 7.12 ATR spectra for pure deionised water and D ₂ O.	153
Figure 7.13 The ¹ H-NMR spectrum of ethanol. The bold letters denote the protons giving rise to the resonance peak, and the step-like curve is the integrated signal (Atkins, 1998) [145].....	156
Figure 7.14 The range of typical chemical shifts for (a) ¹ H resonances and (b) ¹³ C resonances.	158
Figure 7.15 NMR spectra of APS prepared for 24 hours at 20 ⁰ C in D ₂ O.....	159
Figure 7.16 NMR spectra of APS prepared for 5 hours at 45 ⁰ C in D ₂ O.....	160
Figure 7.17 NMR spectra of APS prepared for 5 hours at 75 ⁰ C in D ₂ O.....	161
Figure 7.18 NMR spectra of APS prepared for 5 hours at 83 ⁰ C in D ₂ O.....	162
Figure 7.19 Fibre bundle template.	167
Figure 7.20 Bundle sample in Testometric M250-2.5CT	168
Figure 7.21 Typical force-elongation curve for a fibre bundle test. A) As received GF. B) commercially coated GF.	169

Figure 7.22 Weibull analysis. Comparison of as received GFs, RT and ET APS self-coated GFs..... 174

Figure 7.23 Weibull analysis. Comparison of RT APS self-coated GFs and commercially coated GFS 175

Figure 7.24 Weibull analysis. Comparison of as received ET APS self-coated and commercially coated GFs..... 176

List of tables

Table 1.1 Compositions ranges of commercial GFs (weight %) [6].	6
Table 1.2 Properties of commercial glass fibres [6].	7
Table 1.3 Types of measured strengths [28].	17
Table 2.1 Silanes 1% (v/v) preparation.	61
Table 2.2 Range of thermal degradation temperatures.	63
Table 3.1 Average single fibre strength of as received and commercially silane coated GFs.	73
Table 3.2 Average single fibre strength for as received GFs self-coated with silanes prepared in different conditions.	74
Table 3.3 Average single fibre strength for commercially silane coated GFs at different TD temperatures.	81
Table 3.4 Average single fibre strength for 450 ⁰ C commercially coated thermally degraded GFs with different combinations using HCl 10% v/v.	84
Table 3.5 NaOH concentration effect on average single fibre strength of thermally degraded commercially coated GFs.	86
Table 3.6 3M NaOH solution treatment time effect on average single fibre strength of TD commercially coated GFs.	87
Table 3.7 Average single fibre strength of TD commercially coated GFs self-coated with ET APS.	88
Table 3.8 Summary of average single fibre strength of the commercially coated GFs TD at different temperatures using new treatment combinations.	91
Table 3.9 ¹ H chemical shifts of carbons which form the APS and 1, 4-Dioxane at RT.	94
Table 3.10 DRIFT different bands of the spectra.	111

Table 3.11 Comparison between RT and ET APS.....	114
Table 7.1 Silanes 1% (v/v) preparation for bundle tensile tests.....	164
Table 7.2 Blends of silanes 1% (v/v) preparation for bundle tensile tests.....	164
Table 7.3 Temperature effect investigation on APS 1% (v/v) for bundle tensile tests.	165
Table 7.4 Concentration effect of MPS and APS 1 and 2% (v/v) applied to water sized GFs for bundle tensile tests.....	165
Table 7.5 Average peak force of as received and commercially coated GF bundles.	169
Table 7.6 Average peak force for as received GFs coated with different silanes....	170
Table 7.7 Average peak force for as received GF bundles coated with different silane blends.....	171
Table 7.8 Average peak force for as received GFs coated with APS 1% (v/v) prepared at solution medium natural pH, 83°C and changing the preparation time and leaving the lid open or closed.....	172
Table 7.9 Average peak force for MPS and APS 2% (v/v) prepared in different ways.	173
Table 7.10 Summary of parameters for Weibull distribution for as received, RT APS and ET APS self-coated GFs.....	174
Table 7.11 Summary of parameters for Weibull distribution of as received RT APS self-coated and commercially coated GFs.....	175
Table 7.12 Summary of parameters for Weibull distribution as received ET APS self- coated and commercially coated GFs.....	176

Introduction

The processing and reuse of end-of-life composite products in an environmentally friendly manner is one of the most important challenges facing the industry and community. The development of an economically viable process for regenerating the properties of thermally recycled glass fibres (GFs) would have major technological, societal, economic and environmental impacts. The ultimate goal of this project is to enable cost-effective regeneration of the mechanical properties of GFs which have been produced from thermal recycling of end-of-life glass reinforced structural composites from automotive and wind energy applications. The global annual production of glass reinforced composite materials is rapidly approaching 10 million tons, of which approximately 60% is thermoset based. A breakthrough in the regeneration of recycled glass fibre performance has the potential to totally transform the economics of recycling such glass fibre reinforced plastics composites (GRP) which would otherwise most likely be disposed of to landfill. This will enable such recycled fibres to compete with, and replace, pristine materials in many large volume composite applications. The reuse of these materials could result in a huge reduction in the environmental impact of the glass-fibre composites supply industry.

There are a few possible routes available to recycle GRP, such as solvolysis, pyrolysis, grinding or other applications such as concrete production. Of these possible routes, thermal recycling (pyrolysis) is probably the most advanced technologically.

Nowadays, nearly all these options deliver recycled fibre materials which suffer from a lack of cost competitiveness with pristine first-pass materials. A key factor in this equation is that there is a huge drop in the performance of thermally recycled GFs (80-90%) in comparison to its original state. Consequently, recycled GFs have a very poor performance to cost ratio, and in most cases are considered unsuitable for reprocessing and reuse as a valuable reinforcement of composites. For these reasons, landfill is currently the most common way of composite disposal. However, expanding the use of the landfill option is increasingly being perceived as environmentally and economically unacceptable. These are the reasons for the challenge of recycling GFs that will be able to compete with, and replace, pristine materials in many large volume

composite applications. The reuse of these materials could result in a huge reduction in the environmental impact of the glass-fibre composites supply industry. Furthermore, finding a solution for cost-effective composite recycling, would imply increased economic benefits due to the money saved on sanctions and greater income from new products.

In this work, the mechanical characterisation of uncoated (or “as received”) and γ -aminopropyltriethoxy Silane (APS) coated (or “commercially coated”) GFs was firstly carried out to understand the differences produced by a thin layer of silane on GF properties. The mechanical performance was carried out using conventional single fibre tension tests. Further mechanical characterisation of as received GFs coated with 3 different silanes was also carried out. A new preparation procedure for APS was developed which enhanced the positive effect of silanes on GF mechanical properties. Due to the results obtained with the new APS preparation procedure, the characterisation of APS was investigated using Nuclear Magnetic Resonance (^1H NMR) and Fourier Transform Infrared Spectroscopy (FTIR). The differences obtained for APS prepared in this new way, and prepared using classic methods, were compared and discussed. In order to investigate the effect of high temperature on GF mechanical properties, several thermal degradation temperatures were applied to APS coated GFs to see the effect on them without any other post-treatments. Two chemical methods, using HCl or NaOH, were investigated to regenerate the mechanical properties of degraded GFs due to the high temperatures when they are thermally degraded. Both experienced increases. The NaOH treatment, which provided substantial GF strength increases, opens the possibility of finding a new way to regenerate the strength of GFs recycled from end of life composite materials. These mechanical characterisation results used single fibre tension tests and were further supported by Scanning Electron Microscope (SEM) of the GF surfaces and FTIR to analyse the GF surface.

Chapter 1 Literature review

1.1 Glass

Glass is one of the most common substances in everyday life, playing an imperative role from bygone times to present days in different fields such as scientific, industry and everyday life. Glass is defined as an inorganic substance which is continuous when in the liquid state of that substance but which, due to a reversible change in viscosity when the liquid cools and solidifies, it becomes a rigid glass for all practical purposes as long as no crystallisation has occurred [1]. Therefore, glass can be considered as an amorphous solid (non-crystalline) material formed by rapid cooling from its very low viscosity state. Such melt quenching results is an insufficient time that molecules would need for arrangement into a regular structure (i.e. crystallisation). In lieu of a reorganization of the molecules during the cooling process, they solidify in the positions they had in the liquid phase. This explains why their structure has no long-range order or three-dimensional periodicity [2].

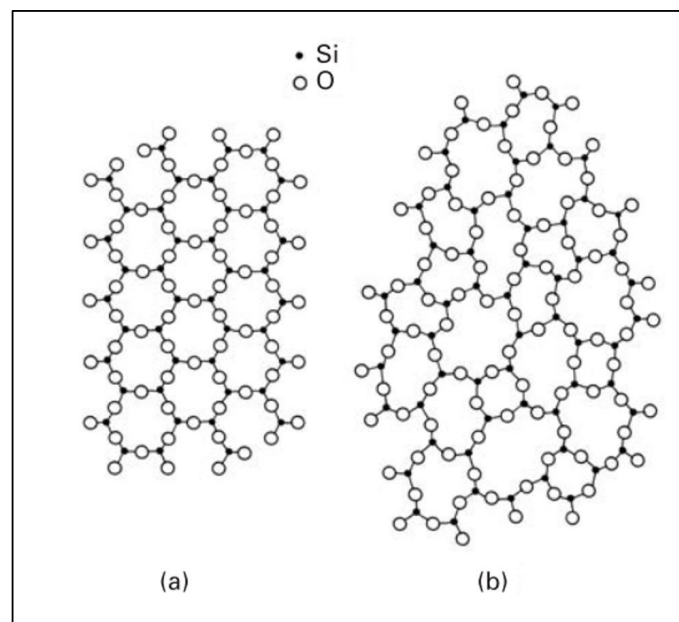


Figure 1.1 Schematic representation of (a) ordered crystalline and (b) random-network glassy form of silica [3].

Nevertheless, a high degree of short range order (i.e. at the scale of a few angstroms) is the reason for the rigidity of glasses. Solids that exhibit this type of positional disorder are called glasses (Figure 1.1) [3]. Silica (SiO_2) forms the basis of almost all commercial glasses. The molecule SiO_2 does not exist in the way the chemical formula assumes; but rather as a polymer $(\text{SiO}_2)_n$. In its various crystalline forms it consists of rings of SiO_4 groups, achieving a link between the groups by the sharing of O^{2-} between Si^{4+} ions. The basic unit (SiO_4) has a tetrahedral structure with the four oxygens at the corners and the silicon at the centre of the tetrahedron. Silica in the form of quartz is a clear example of this three-dimensional network of repeated rings containing 3 or 6 SiO_4 groups (Figure 1.2).

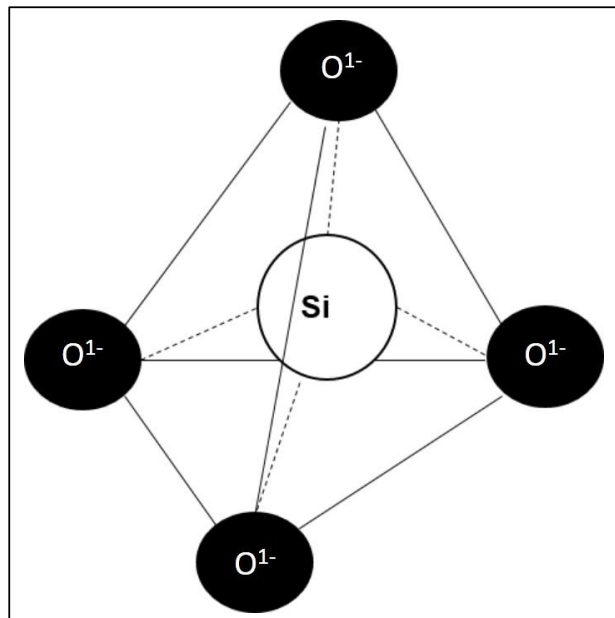


Figure 1.2 The silica tetrahedron, the basic structural unit of silicates and silica glasses.

Fused silica glasses, i.e. almost pure silica glasses, will form after silica is heated at 2000°C until fluid and then rapidly quenched. Crystallisation occurs if a temperature of about 1200°C is applied instead of cooling. Glass or glass fibres (GF) made of silica have advantages such as good chemical and temperature resistance, low coefficient of thermal expansion, high modulus and strength. However, a disadvantage of fused silica glasses or GF is the high temperature needed for glass formation, making processing

costs too high for this to be a viable commercial material. Hence, commercial silica based glasses are produced with addition of oxides. The mixture of silica and these metal oxides reduces the processing temperature to 1300 °C – 1600 °C. These oxides can modify the silica network by interrupting its continuity and in turn making its structure more irregular. Hence, the addition of these oxides improves the formability of the glass but causes a stiffness and strength decrease in comparison with silica glass. The oxides that are commonly added to the silica based glass production are divided into three groups [1]:

- I. Network formers such as B_2O_3 and Al_2O_3 ; which are capable of forming their own network.
- II. Network modifiers such as CaO , BaO , Na_2O and K_2O ; which can modify the silica network.
- III. Intermediate oxides such as MgO , BeO , TiO_2 ; which can do both.

The manipulation of these ingredients can lead to a variety of compositions that have been commercially established to provide a wide range of glass products with different properties and having a wide market due to their different applications.

1.2 Glass Fibre

One of the major applications of glass is for the production of GFs used as the reinforcement in polymer matrix composites. In such composites the reinforcement, either fibrous or particulate, is embedded in the polymer matrix. Fibrous reinforcement materials are most often used because of the high performance which can be achieved. Indeed, since commercial production of reinforced polymers began, GF have remained the highest volume fibre reinforcement for plastics [4] despite the increase in the use of carbon and natural fibres during recent years. One of the main reasons for this continued high demand is the high performance, i.e. specific tensile strength and specific modulus, per unit cost of the GF reinforcement.

Commercial GFs can be divided in two categories: premium special-purpose fibres and low-cost general-purpose fibres, the latter accounting for over 90% of all GFs. These fibres are designated by the letter E as E-glass. The remaining GFs, designated

with the letters A, C and S, are premium special-purpose GFs [5]. Each letter represents a small range of compositions as shown above in Table 1.1.

Table 1.1 Compositions ranges of commercial GFs (weight %) [6].

	E	A	C	S
SiO₂	52-56	72-72.5	60-65	64.3-65
Al₂O₃	12-16	0.6-1.5	2-6	24.8-25
B₂O₃	0-13		2-7	
CaO	13-25	9-10	13-16	0.01
MgO	0-6	2.5-3.5	3-4	10-10.3
K₂O			0-2	
Na₂O	0-1	13-14.2	7.5-12	0-0.27
TiO₂	0-0.4			
Fe₂O₃	0.05-0.4			0-0.2
F₂	0-0.5			
SO₃		0.7		

Letter designations relate to special properties. E is from electrical, for low electrical conductivity GFs; A is from alkali, for soda lime GFs; C is from chemical, for high chemical durability; and S is from strength, for high strength GFs. The properties of these GFs are list in Table 1.2.

As it can be seen E-glass fibre has fairly high strength, high Young's modulus and relatively low liquidus temperature, which substantially reduces the production costs. Failure strength and Young's modulus are usually the parameters of greatest interest when it comes to reinforcement materials, due to these determining the resultant level of reinforcement supplied to the composite materials.

Table 1.2 Properties of commercial glass fibres [6].

Properties	E	A	C	S
Specific gravity: Fibre	2.54-2.55	2.50	2.49	2.48-2.49
Specific gravity: thermally compacted fibre	2.58-2.62		2.54	2.51-2.52
Index of refraction at 589.3nm: fibre	1.547	1.512	1.541	1.523
Dielectric Constant: thermally compacted fibre (at 21⁰C, 10⁶hz).	5.66-6.60	6.90	6.24-6.30	4.53-4.60
Specific heat (cal g⁻¹ °C⁻¹)	0.192		0.19-.021	0.176
Linear expansion coefficient (x10⁻⁶ K⁻¹)	4.9-6.0	9.0	7.0-7.2	2.9-5.0
Liquidus temperature (°C)	1120-1140			1500
Fiberizing temperature (°C)	1270-1300	1280		1565
Softening point (°C)	845	695-720	750	968
Young's modulus: fibre(GPa)	72.1-76	72.5	70	84-88
Virgin fibre tensile strength at room temperature (RT) (GPa)	3.5	2.41	2.7-3.1	4.6

1.2.1 Manufacture of Glass Fibres.

The properties of GFs depend upon both the composition and forming history, which involves the temperature of molten glass and thermo-mechanical history during fibre attenuation [7]. The variation in these conditions may affect the bonding and underlying atomistic structure of GFs.

Almost all continuous GFs are manufactured by the attenuation of molten glass flowing from nozzles located in the base of a special fibre drawing plate called a bushing. The bushing has a large number of nozzles with small separations between them [8]. These nozzles range from 0.75 to 2.0 mm internal diameter [1]. The bushing is one of the most important parts of the manufacturing process equipment since this is where the glass is transformed into fibres; because of the high temperature resistance required it is necessary to use very expensive platinum-rhodium alloy as the bushing material [8].

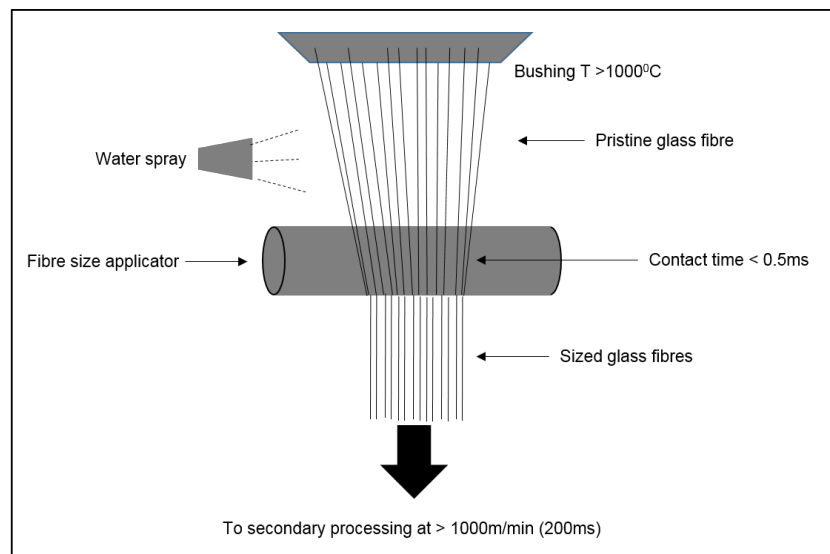


Figure 1.3 GF forming process.

Figure 1.3 shows a typical GF forming process. Once the molten glass is deposited above the bushing, it flows under gravity through the nozzles and is immediately attenuated and then cooled down by fine water sprays below the bushing. Immediately after fibre drawing a fibre size applicator provides a moving surface, often a cylinder,

coated with fibre size with which the cooled filaments makes contact; the sizing pickup occurs over a contact distance of approximately 10 mm [1].

Once the fibre strands have been formed and sized, they are guided to the last stage in which they will be convert onto final products, i.e. rovings, chopped strands, yarns, mats or fabrics [1].

The fibre diameter can be controlled by adjusting the viscosity of the glass (dependent on composition and temperature), the diameter of the nozzles and the winding speed [7]. The GFs formed between the bushing and the fibre size applicator, right after the bushing, are often considered as the pristine or virgin fibres [9]. These fibres are considered not to have severe defects caused by subsequent manufacturing process and handling but might still have defects related to the thermal fluctuations suffered during the cooling process. They are also called flaw free fibres [9]. The size is applied after a rapid contact with the fibre size applicator, usually a rolling applicator. Sizing is a thin surface coating of mainly organic materials applied to GF. It must impart good processing characteristics during manufacturing of the fibres, during transportation and handling of the glass product, and during conversion to composite parts. Sizing is probably the key component influencing the success or failure of most reinforcement products and their composites. GF could not be manufactured in a high volume cost-effective manner without the correct sizing formulations, applied in the appropriate manner. In the same way, most composite production processes could not be operated in a cost-effective manner without appropriately sized GFs. This is the reason why the optimization of the fibre sizing and the closely associated fibre-matrix interphase in the composite critically influences the short and long term composite performance. Optimization of the formulation of GFs is a complex art which involves a compromise of manufacturing, marketing technical and economic factors [10]. The deposition onto the GF surface of specific chemicals controls the adhesion between the GF and the polymer. Those factors will determine the physical and chemical properties of the composite made from them [1]. The GF sizes generally consist of the following main components:

- I. Film former, which, when dried holds the filaments together in a strand and protects the filaments from damage through fibre-fibre contact and fibre-

process contacts. They are chosen to be as closely compatible to the intended polymer matrix as possible and still fulfil all the other requirements of a sizing.

- II. Organofunctional silane or coupling agents with general structure $[X-Si(OR)_3]$. They have several roles apart from the fibre-matrix link, such as improvements in interphase strength and hydrothermal resistance of the composite interphase.
- III. Other additives, such as anti-static agents, emulsifiers, chopping aids, wetting additives and antioxidants [10].

The general structure of the organofunctional groups of the silane coupling agent are $X-Si(OR)_3$. X refers to the reactive or resin compatible functional group which may interact with the matrix resin and R refers to a methyl (CH_3) or ethyl group (C_2H_5). In the aqueous size, the Si-OR groups hydrolyse and then self-condense or the free silanol (Si-OH) may react with GF surface. This process is often catalysed with acetic acid to adjust the pH to approximately 5.5 [11]. The free silanol groups may react with the free OH groups from the GF surface leading to a complex deposition of the silane. Jones [11] and Wang [12] carried out investigations about the interaction of organosilane coupling agents with the GF surface. It is generally assumed that the interaction between organosilane coupling agents and GFs results in a 3-dimensional graded network on the glass surface. The three distinct layers or components deposited differ in their hydrolytic stabilities:

- I. Strong chemisorbed layer hydrolytically resistant at the immediate glass surface.
- II. 3-dimensional chemisorbed layer of polysiloxane.
- III. Physisorbed layer of cyclic and linear oligomers.

1.2.2 Basic structural differences between glass and glass fibres

There are two basic but important differences between GF and bulk glass of the same composition. The first is the rapid cooling from the molten state, which is often of the order of 10^4 - 10^3 s⁰/C. The rapid quenching from very high temperatures results in the structure-related properties being different for the fibre than for the bulk glass. The density is about 2% lower, with the refractive index of 0.1-0.40% lower, and the

Young's modulus lower as well in comparison with the bulk glass [1]. The rapid quenching also increases the temperature gradient from the fibre surface to the core, which may lead to a thin surface layer whose structure differs from that in the core. Bartenev [13] carried out an investigation of the structure and strength of GFs of different chemical compositions. He suggested that there exists a thin surface layer, which can increase the fibre strength due to freezing in of a more homogeneous high temperature glass structure in the surface layer, a molecular orientation of the structural network of the glass along the axis of the fibre and occurrence of tempering compressive stresses in the surface layer. Nevertheless, there is no experimental evidence of the presence of residual stresses in GFs with diameter of 20 μm or smaller and theoretical estimates also indicate that these stresses are negligible in fibres [6].

The second important difference between GF and bulk glass is the ratio of surface area to weight. GF ratio of surface area to weight is much higher than bulk glass. For an average fibre diameter of 10 μm , 10 g of fibre has a surface area of about 2 m^2 [1]. Another difference between GF and bulk glass might be the chain orientation of GFs. The mechanical loading experienced by GF is along its axis. This mechanical loading applied during cooling of the fibre, i.e. fibre attenuation, may cause freezing of the chains in their oriented positions along the longitudinal direction [14]. Nevertheless, other authors like R.T. Brannan [15] and W.H. Otto [16] disagree with the orientation in structure in GFs. This still remains under discussion and it cannot be confirmed that there exists an orientation difference between GF and bulk glass.

Regarding composite materials, fibre surface plays a very critical role. Composites require larger surface area of the fibre-matrix interface for higher ductility and toughness, and better transfer of loads from the matrix to fibre, for example, for the same volume fraction of fibres in a composite, the area of the fibre-matrix interface is inversely proportional to the diameter of the fibre [17]. This special zone termed as interphase may have, due to its different composition and structure, properties completely different from fibre and matrix.

1.2.3 E-glass

E-glass is used in the production of continuous fibre to be used in manufacturing of structural, insulating, and radio-engineering materials, due to its high thermal and

moisture resistance. This glass was developed over 60 years ago by Owens Corning for electrical engineering applications. Over time the area of application of this composition significantly expanded, and now nearly 90% of all GF has the composition of E-glass [1]. E-glass is mainly calcium, aluminium and borosilicate containing less than 1% alkali oxide. The actual content of alkalis and the presence of traces of other elements are a function of the raw materials. Most glasses contain small quantities of fluorine, which facilitates the dissolution of raw materials, decreases the melt liquidus temperature, and improves fibre formation. The presence of ferric oxide in raw materials also has a significant effect on the stability of fibre formation, since iron ions increase the rate of infrared absorption of the melt, and the rate of heat transfer in glass exiting from the bushing increases. Glasses used in the production of E-glass fibre can contain a relatively high, up to 10%, amount of boric oxide, which is a costly and scarce component. Furthermore, the substantial volatilization of boric oxide in melting has a negative effect on the environmental safety of the production facility. At present, various products are made from E-glass [18]:

- I. Fibreglass fabrics and meshes for various purposes.
- II. Non-woven materials.
- III. Fibreglass plastics based on these materials.

However, E-glass has a number of technological disadvantages. The most important is the presence of boron oxide and fluorine, which intensely evaporate in melting due to their relatively high volatility in comparison with the rest of the components of E-glass. This often leads to the variability of the chemical homogeneity of the glass and, simultaneously, pollutes the environment. The problem of volatilization of raw materials can be partly solved by electrical melting of glass under a cold batch layer. Another substantial shortcoming of E-glass is the high aggressiveness in terms of corrosion of the glass melt with respect to the majority of refractories used in containing the molten glass. The use of expensive refractories and boric oxide, significantly increases the GF production cost. Finally, the fibre made of E-glass is insufficiently resistant to acids, which in some cases restricts its application. Therefore, numerous researchers and GF manufacturers have been developing low-boron and boron-free glasses, which in their service properties are not inferior to E-glass. Some

of the most successful developments in this field are the ECR and Advantex GFs developed by Owens Corning. The viscosity curves of such glasses are 60 – 70°C higher than those of standard E-glass. At the same time, Advantex glass surpasses the standard alkali-free aluminium-borosilicate glass in its resistance to chemical agents, and the strength of fibre made of this glass in corrosive media declines much more slowly than in E-glass fibres [18].

1.3 Mechanical properties of glass fibres

1.3.1 Strength

The stress at a point on a body (σ) represents the internal resistance of a body to an external force. The load per unit area of the force (F) applied per cross-section area (A), are related to stress by the equation of forces (1.1). As will be indicated later, the strength of glass and GF is a surface controlled phenomenon. Under an applied tensile load, stress is concentrated on the flaws present on the glass surface and consequently weakening the surface. Nevertheless, the ultimate strength of a composite does not only depend on the strength of the GFs. It depends on the sum of each component's material property times its volume fraction [19]. Based on the fact that GF is a brittle material we can assume that the strength (i.e. tensile strength) is the tensile stress at break. (1.2).

$$\text{Stress} = \frac{F}{A} \quad (1.1)$$

$$\text{Strength} = \frac{F_{\text{Max}}}{A} \quad (1.2)$$

1.3.2 Flaws and cracks

We can define a flaw as an extrinsic defect in the glass. These 3-dimensional flaws are commonly scratches, inclusions or devitrified regions or trapped gas bubbles. Sometimes intrinsic inhomogeneities present in glass are called intrinsic flaws, such

as point defects, structural inhomogeneities caused by frozen-in density and composition fluctuations and nanoscale roughness on glass surface [9].

On the other hand, a crack is a 2-dimensional flaw, that is, an area across which the bonds are broken. Crack tip is the name attributed to the boundary of this area. The curvature (normal to the plane of the crack) at the tip is assumed to be infinitely sharp in the continuum models but is of atomistic dimensions in real materials [9] although it is still unresolved [20]. A silica glass has a crack tip with a radius of curvature on the order of 0.3 nm, that is, approximately the size of a single siloxane bridge (Si-O-Si). It is important to know that cracks can only grow under tensile stress. 3-dimensional flaws cannot grow [9]. As can be seen in Figure 1.4, three different types of surface flaws have been determined as a function of their strength levels [13].

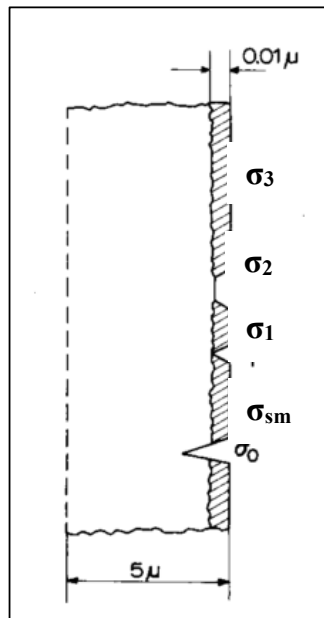


Figure 1.4 Schematic representation of the axial cross-section of a GF with a surface layer and different types of surface flaws: surface microcracks (σ_{sm}), surface submicrocracks (σ_1), flawless massive glasses after etching (σ_2) and flawless glass fibres (σ_3) [13].

Three different types of flaws have been proposed [21]:

- I. Flaw Type A (σ_{sm}): severe surface flaws with an average separation of 20 mm which arise from handling and processing.

- II. Flaw Type B (σ_1): mild surface flaws with an average separation of 0.1 mm. It is likely from the flaw severity that these flaws are etch pits, but it is not known if these are present as drawn, grow by corrosion in the absence of stress, or grow by a stress corrosion mechanism during the tensile test.
- III. Flaw Type C (σ_2, σ_3): can only be observed when gauge lengths of less than 1 mm. are tested. The proportion of failures controlled by type C flaws increases as the gauge length is decreased to 0.25 mm. Extrapolation of this type suggests a flaw separation of 0.01 to 0.001 mm. It is believed that type C flaws are internal, structural defects arising from the heterogeneity of the glass, and thus represent concentrations of terminal cations that interrupt the silica network. These are not flaws in the normal sense of voids, but generate a stress concentration because the weaker bonds at these regions lead to a local reduction of elastic modulus and hence to a stress concentration.

An investigation carried out by Griffith in 1921 [22] originated the Griffith flaw theory.

$$\sigma_{fail} = \frac{K_{IC}}{\sqrt{\pi \alpha}} \quad (1.3)$$

Where σ_{fail} is the stress at fail, K_{IC} is the fracture toughness and α is half the crack length.

He postulated that glass contained a large number of microscopic flaws and cracks. He also postulated that while internal defects had a negative effect on fracture strength, surface defects were even more detrimental. In the case of thin fibres the presence of microscopic flaws on the fibre surface would have a catastrophic effect on strength. Nowadays, surface defects of the Griffith type are believed to be very few on fine fibres, whilst stress corrosion induced by water and ion exchange in the glass surface is probably the main reason [23,24].

Other researchers started to realise that glass fracture was in fact a kinetic process, in which a chemical reaction of the water adsorption on the glass surface is involved, which may be from the atmosphere moisture, and the stressed siloxane bonds at the crack tip.

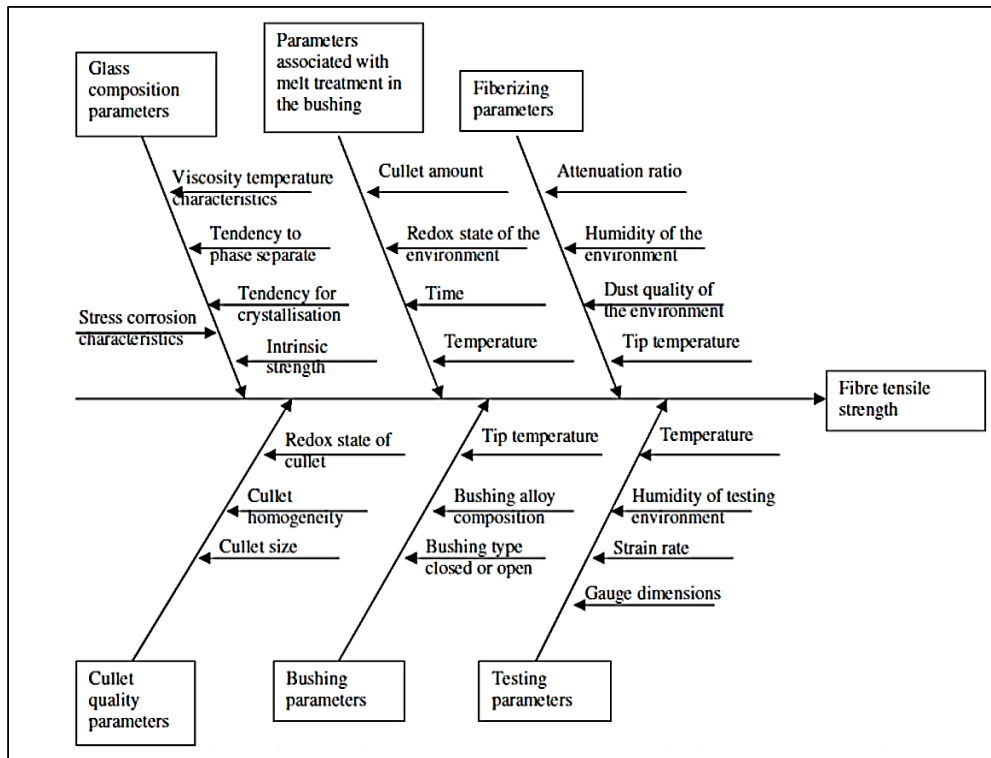


Figure 1.5 Fish-bone chart of the experimental parameters which may influence the measured strength of melt-drawn fibres [9].

Kurkijan et al. [28] introduced new a factor to measure the fibre strength. They differentiated the strength on whether it is intrinsic or extrinsic and depending on whether the fatigue is absent, inert or environmental. These new factors provided six different types of strengths, as we can see in Table 1.3.

Table 1.3 Types of measured strengths [28].

	Types of measured strengths		
	Fatigue free	Inert	Environmental Fatigue
Intrinsic	σ_F^*	σ_i^*	σ_E^*
Extrinsic	σ_F	σ_i	σ_E

The new six different types of strength are as follow [28]:

- Fatigue-free extrinsic strength (σ_F): extrinsic strength in the absence of any fatigue (environmental or inert).

- Fatigue-free intrinsic strength (σ^*_F): intrinsic strength in the absence of any fatigue (environmental or inert) and free from all extrinsic influences.
- Extrinsic inert strength (σ_i): is the strength measured under conditions when there is no environmental fatigue.
- Intrinsic inert strength (σ^*_i): is the strength measured under conditions when there is no environmental fatigue and free from all extrinsic influences.
- Extrinsic environmental fatigue (σ_E): is the strength measured under environmentally enhanced fatigue.
- Intrinsic environmental fatigue (σ^*_E): is the strength measured under environmentally enhanced fatigue and free from all extrinsic influences.

The strength measured in the absence of extrinsic defects is called intrinsic strength. It is challenging to measure intrinsic strength due to the fact that only flaw free surfaces are exempt of extrinsic defects. However, there are several conditions suggested that reduce the probabilities of extrinsic flaws presence [28]:

- I. Use of thin, melt and drawn fibres whose bulk and surface have been protected from extrinsic flaws.
- II. Measure the fracture strain with a 2-point bending technique. This technique allows testing of very short gauge lengths.

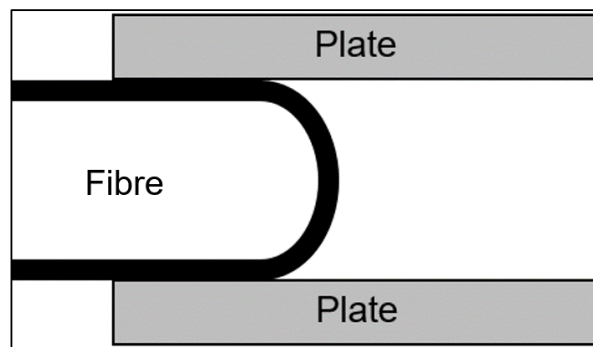


Figure 1.6 2-point bending fibre fracture strain technique.

- III. Testing the fibres as soon as possible after forming to reduce the additional handling. There is a direct relationship between storage time and probability of extrinsic flaws forming on a bare fibre surface.

Regarding fibre testing, three criteria have also been suggested for measuring a set of strength data to be considered intrinsic [28]:

- I. No dependence of measured strength on fibre diameter or length.
- II. The coefficient of variation in strength values is about two times the coefficient of variation in the fibre diameter values.
- III. High measured fracture strengths (or fracture strains).

Only by testing pristine GFs can the intrinsic strength be obtained, due to the fact that they are flaw free, i.e. no extrinsic flaws. An added problem is the difficulty of producing pristine GFs as Gupta [9] explained in his investigation of the strength of GFs. It is noteworthy to say that the intrinsic strength includes the effects caused by all intrinsic defects that are expected to be present (being the result of the thermal fluctuations) and fatigue, i.e. intrinsic fatigue. If the strength measurement is performed in absence of fatigue, it is defined as fatigue-free strength. These terms are also applied to non-pristine fibres. However, these fibres have extrinsic defects which make their measured strength controlled by flaws. For E-glass fibres the intrinsic strength under fatigue is of about 3.5 GPa and the intrinsic strength under inert conditions is about 5.8 GPa.

In this research only extrinsic strength was measured; GFs stored in rovings were tested at only one gauge length (20 mm), at 50 % relative humidity and 23°C.

1.3.3 Diameter and length dependence

In brittle solids like GFs, the strength is determined by randomly distributed surface defects, i.e. flaws of different dimensions. As a matter of volume, the average GF strength measured will decrease proportionally with the increase of the fibre volume. In other words an increase of either the diameter or length of the fibre will produce a strength decrease. Bartenev et al [29] carried out an investigation on the effect of length of GFs on their strength. They showed that the relationship between the GF length and the average strength is due to the frequency of the defects in the fibres and the type of the distribution along the fibre, that is, the larger the sample, the more statistically probable it is for the sample to have severe flaws. They also defined three different

types of strength level related with three different GF lengths. They determined that the highest strength was achieved for the smallest fibre length, having values similar than the pristine GFs. The effect of diameter on GF strength was investigated by Otto [30]. He reported that an increase in tensile strength due to the diameter decrease was evident. Nevertheless, he also pointed that the diameter was not as critical a factor in fibre strength as previously believed by other researchers. Indeed, fibres of different diameters, formed under well controlled conditions, experienced basically the same tensile strengths at break.

Consequently, taking all the points in the foregoing discussion into account, the measured strength of glass fibre usually exhibits a considerable distribution of individual measured values rather than a unique value. These variations are due to the combination of randomness of flaw dimension and the contribution of finiteness of measured sample dimension.

1.3.4 Weibull distribution

Different probabilistic approaches have been used to analyse the unpredictable variation when measuring strength. Among them, Weibull distribution is the most successful treatment, which was pioneered in 1939 by Weibull [31], and later in 1951 he applied the statistical treatment to the fibre strength [32]. The approach is referred to as the weakest-link theory which assumes that a given volume of material will fail at the most detrimental flaw. Thomason [33] carried out an investigation on the application of the Weibull analysis to experimentally determined single fibre strength distributions. He proposed that the analysis relies on the assumption that the failure of fibres as a function of applied load is controlled by the random distribution of a single type of defect (unimodal Weibull) along the length of the fibres. This enables equations to be developed linking the probability of fibre failure (P_F) at a stress level (σ) during a tensile test with a certain test gauge length (or volume in the case of variable fibre diameter). Two parameters (characteristic strength, σ_0 and Weibull modulus, m) are used to describe the density and variability of flaws in the material. When the fibre gauge length and fibre diameter and therefore the tested volume is kept constant then equation (1.4) may be applied.

$$P_F = 1 - \exp \left[-\frac{V}{V_0} \left(\frac{\sigma - \sigma_T}{\sigma_0} \right)^m \right] \quad (1.4)$$

The parameter σ_T is included in the more general three parameter model where σ_T is defined as a threshold stress below which the failure probability is zero. It has been common practice to set the value of σ_T to zero for brittle materials which significantly simplifies the analysis of equation (1.4). Weibull parameters are commonly obtained from the analysis of a dataset obtained at a single gauge length. In this case Equation (1.4) can be rearranged to give:

$$\ln[-\ln(1 - P_F)] = m \ln(\sigma) - m \ln(\sigma_0) \quad (1.5)$$

The experimental fibre strength data plotted in equation (1.5) should give a straight line from whose equation the parameters σ_0 and m , which characterise the density and variability of flaws, can be estimated using the Least Squares (LSs) regression method. σ_0 is a scale parameter, which describes the intensity of the distribution and m is a shape parameter, also called Weibull modulus, which governs the shape of the respective density and distribution functions. A number of authors have indicated application of the Maximum Likelihood (ML) analysis method to such single gauge length datasets produces better estimates of the underlying Weibull parameters than the LS method. However, the quality of the linear relationship in some published unimodal Weibull analysis is frequently questionable. Indeed, further levels of structure can often be observed in Weibull plots of experimental fibre strength data. Some authors choose to ignore such deviations whereas others postulate these deviations as evidence of a more complex physical state of the test material [33].

One such deviation that has received significant attention is an increase in the slope of the line in a Weibull plot at low strength values. Beetz noted such a relationship in a Weibull analysis of single carbon fibre strength results [34]. More recently Zinck et al. have noted similar relationship in a Weibull analysis of single GF strength results [35]. Due to the evidence of multiple populations of defects on the fibre surface, it was postulated that a bimodal Weibull cumulative density function should be applied to the data in [34] and [35]. For the bimodal Weibull cumulative density function P_F is given by:

$$P_F = 1 - q \exp \left[- \left(\frac{\sigma}{\sigma_{01}} \right)^{m_1} \right] - (1 - q) \exp \left[- \left(\frac{\sigma}{\sigma_{02}} \right)^{m_2} \right] \quad (1.6)$$

where q is a mixing parameter, the fraction of failures due to the population (1) of more severe flaws defined by shape parameter m_1 and scale parameter σ_{01} . The remaining fraction of failures is attributed to flaws in another type of population (2) defined by shape parameter m_2 and scale parameter σ_{02} [33]. Apparently it is assumed that no interaction occurs between population (1) and population (2) flaws. The investigation of the strength of brittle fibres requires numerous experiments since fracture is statistical. The experimental approach generally consists of determining the strength of N fibre specimens of the same length taken from a large population of fibres such as a fibre rovings. The N strength values are then ranked in ascending order and the probability of each strength is then estimated from the rank value i and N . The general form of the estimator is given by Equation (1.7), where $\alpha = 0.5$ and $\beta = 0$ is commonly used. The choice of α , β and N have been shown to affect the results of the Weibull graphical analysis [33,36,37].

$$P_F(i) = \frac{(i - \alpha)}{(N - \beta)} \quad (1.7)$$

Those familiar with single fibre testing also know well that for every successful N test results there are a large number of fibres which break during sample preparation and mounting. The probability of any selected fibre breaking before testing depends on a complex combination of factors. Clearly the fibre strength distribution plays a role in defining the number of these “weak” fibres. Fibre breakage will also depend on the force required to remove the fibre from the bundle, in this case the properties and distribution of the fibre sizing plays a critical role. Finally, the experience and abilities of the operator play an important role in determining the minimum level of fibre strength required to isolate and prepare a test fibre without breaking it prior to testing. Consequently, for every population of fibres, there exists a lower limit on the individual fibre strength which is experimentally inaccessible. A review of results in the literature combined with our own experience shows that this limit for GF may be anywhere from 1 GPa down to 0.3 GPa. Any fibres weaker than this limit which are selected from the population will not survive to end up in the strength results to be

analysed. In a somewhat similar fashion the intrinsic material properties provide an upper limit to the experimentally obtainable strength values. For instance, with E-glass fibres not obtaining a room temperature (RT) strength above the accepted pristine fibre strength of approximately 3.5 GPa [33].

1.4 Silane coupling agents

GF sizing generally consists of a water-based formulation containing a film former, a silane coupling agent and a number of auxiliary components [38]. The coupling agent can be defined as a material that improves the chemical resistance of the bond across the fibre-matrix interface. A molecule made from a silicon compound which contains both organic and inorganic reactivities can function as a coupling agent [39], also called organofunctional silane coupling agent, alkoxy silane or simply silane. These molecules have also been reported in other roles such as improvement in interphase strength and hydrothermal resistance of the composite interphase [10]. The main functions of silanes are [40]:

- I. Finish or surface modifier.
- II. Primer or size.
- III. Adhesive.

These functions will result in developments in mechanical properties such as tensile and flexural strength, fracture toughness, and tensile modulus [41]. The general structure of the silane is $[X-Si(OR)_3]$. R is a hydrolysable group, often methyl (CH_3) or ethyl group (C_2H_5). X refers to the reactive or resin compatible functional group which may interact with the matrix resin [10,42]. In Figure 1.7 a simple schematic of silanes at an interface is shown. [43]. Nowadays, a wide range of silanes are available with different specifications/characteristics and they are commercially available on a large scale.

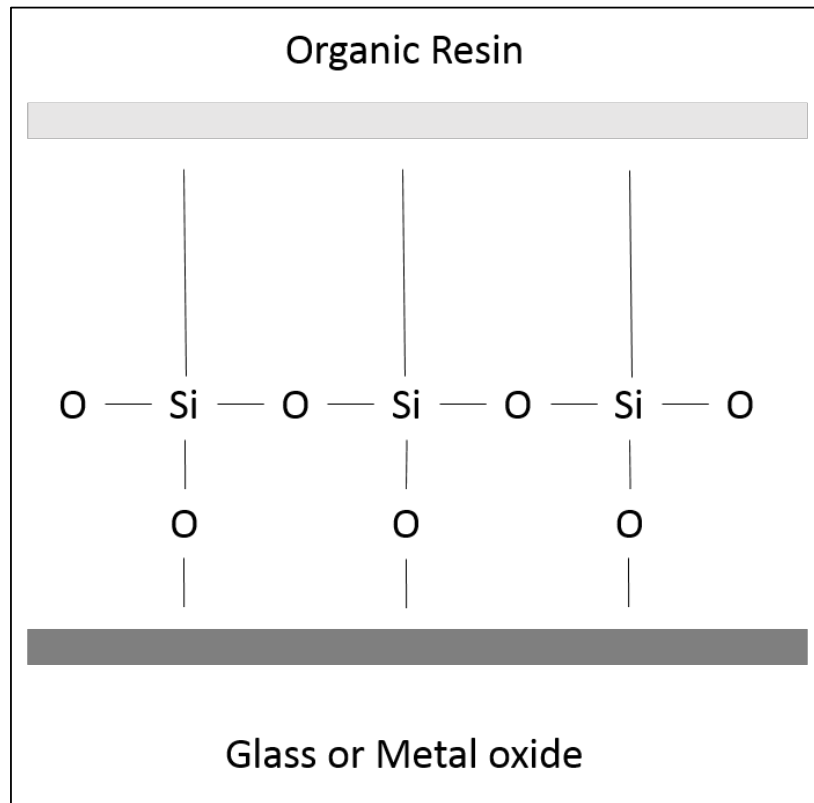


Figure 1.7 Simple schematic of silanes at an interface.

1.4.1 Types of silane coupling agents

As mentioned above, the groups that characterise silane coupling agents are R and X [42]. What is often used to differentiate the silane coupling agents is the group X, which is intended to react with the resin/matrix. Regarding the X group, a wide range of different silane coupling agents are available. Despite the availability of this wide range of different silane coupling agents, the GF industry has focused its sizing products on only four, three of which are shown in Figure 1.8. The X group contains amino, methacryl, epoxide, or alternatively vinyl functionality [44], with the aminosilanes being the largest proportion employed [10,45]. This is due to the reactivity and residual stresses between the aminosilanes and thermoplastics [44] and additionally their good reactivity with thermoset plastics [1]. Other silanes tend to possess good reactivity with resins of similar structure [39], e.g., epoxy silanes with epoxy resins, methacryl silanes with polyesters and vinyl silane with vinylester resin.

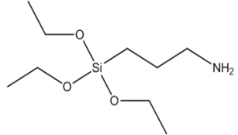
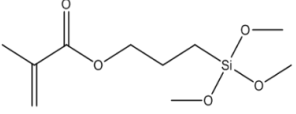
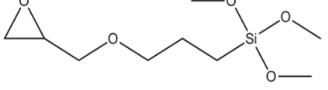
Silane		Structure
APS	γ -Aminopropyltriethoxy Silane	
MPS	γ -Methacryloxypropyltrimethoxy Silane	
GPS	γ -Glycidoxypropyltrimethoxy Silane	

Figure 1.8 Typical GF industry silane coupling agents.

1.4.2 Conditioning of silane coupling agents

Silane coupling agents are mixed in an aqueous solution in which they hydrolyse stepwise to give the corresponding silanols, which can then condense to siloxanes as can be seen in Figure 1.9. A transformation from trialkoxysilane to trihydroxysilane which occurs when alkoxy silanes are in water. Both reactions are strongly dependent on pH [39]. The hydrolysis is often acid catalysed using acetic acid to adjust the pH \sim 3.5 [11], conditions in which the hydrolysis occurs in minutes while the condensation reaction needs hours, that is, hydrolysis is comparatively fast. In general terms, acidic conditions (i.e. pH below 7) accelerate the hydrolysis, but limit the self-condensation reactions. Only amino silanes undergo hydrolysis under neutral conditions (i.e. pH \sim 7) [47,48]. This may be supported by the fact that most commercial alkoxy silanes, with the exception of aminoalkoxy silanes, have initially limited solubility in water until they hydrolyse [48]. An investigation carried out by Naviroj et al. [49], studied the pH effect on the structure and adsorption characterisation of silane coupling agents on silica and E-glass fibres, using three silanes: γ -APS, γ -MPS and VS. They concluded that the mode of adsorption of γ -APS is pH dependent. A maximum adsorption of γ -APS molecules is achieved when the silica is treated at natural pH (10.6), having significant structure changes between pH 6 to 12. On the other hand, adsorption of

both γ -MPS and VS can be considered independent of the pH of the treating solution, as long as the pH is below 10.

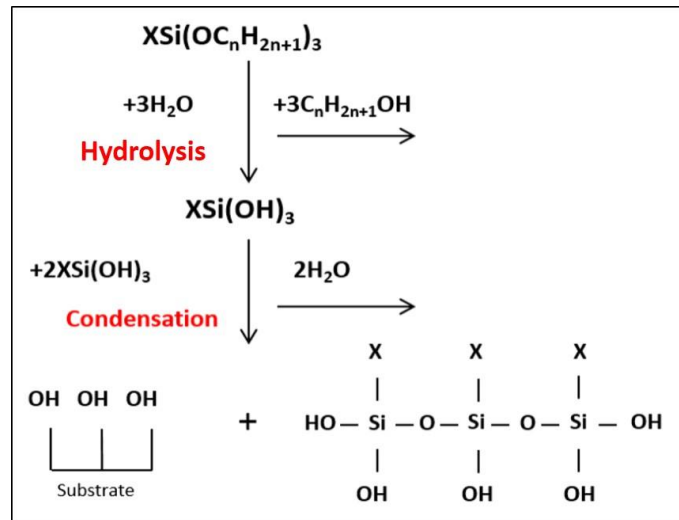


Figure 1.9 Hydrolysis and condensation processes of alkoxy silanes [50].

Two investigations suggested that hydrolysis is faster than condensation. The first, carried out by Peña-Alonso et al. [51], shows that hydrolysis is faster than condensation when the molar ratio H_2O to γ -APS is higher than 2. On the other hand, samples with a molar ratio $\text{H}_2\text{O} / \gamma\text{-APS} = 1$ show that hydrolysis is faster than condensation during the first 50 min of reaction and after such time condensation is the main reaction. The second was carried out by Ogasawara et al. [52], in which they concluded that hydrolysis is three times faster than condensation. Based on these investigations, it is supposed that the hydrolysis is faster than condensation and occurs first.

Once the silanes have been hydrolysed and self-condensed, the last step is the reaction between the free hydroxyl groups (OH) of the silane with the ones on the substrate surface [53]. This attachment to the glass can be made by covalent bonds, as shown in Figure 1.10. Silanes also contain at least one different functional group (X) which can react with the resin during the curing process. For this reason it is believed that silanes act as a bridge to bond the glass with the resin through a chain of primary bonds [50].

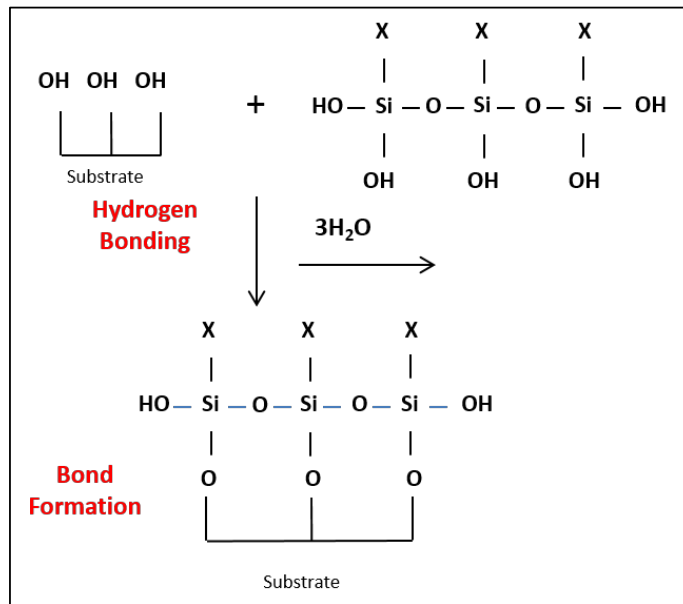


Figure 1.10 Reaction between self-condensed alkoxy silane and substrate surface [50].

It is well known that the application of silanes to the GF surface produce a substantial improvement on the performance of GF reinforced plastics. Several theories have been proposed to interpret the mechanism of reinforcement produced by silanes. These theories include the following:

- i. Chemical bonding theory
- ii. Deformable layer theory
- iii. Preferential adsorption theory
- iv. Restrained layer theory
- v. Coefficient of friction theory
- vi. Surface wettability theory
- vii. Reversible hydrolysable bond theory

Chemical bonding theory states that silanes contain functional groups that can react with OH groups on glass. This attachment to the glass can be made by covalent bonds, with a minor role for hydrogen bonding, that form uniform and continuous films on the glass surface. Apart from these bonds, coupling agents contain at least one different functional group which can react with the matrix resin during the cure. This is the

reason why the silanes act as a bridge to bond the glass with the resin through a chain of primary bonds. Furthermore, there is a chemical structural similarity between glass surface and the silicon moiety of the coupling agent, the silane [54,55].

Deformable layer theory postulates that a flexible, deformable phase seems desirable to accommodate stresses set up at the interface, due to the differential thermal shrinkage between resin and GFs when cooling the composite. Such a deformable layer, or interphase, would be helpful by accommodating stresses set up at the interface [39].

The next two theories are considered to be basically the opposite. Preferential adsorption theory is a modification of the deformable layer theory. It is based on the fact that different types of finishes have different degrees of activity for absorption of certain components from the uncured resin. This leads to an interphase region with properties different from the bulk polymer matrix. This causes an incomplete curing, resulting in the formation of a potentially flexible, ductile interphase region with its consequent alteration on the mechanical properties due to its capability to relieve and transfer stresses between the GFs in load bearing situations. On the other hand, the restrained layer theory suggests that the stress transfer between a high modulus GF and a low modulus matrix can most uniformly occur if the interface between them has a modulus which is intermediate between that of the GF and the matrix, i.e. the matrix surrounds the fibres and produces a layer, which has a modulus value between the matrix and the glass [55–58].

Coefficient of friction theory claims that the frictional resistance to relative movement between the matrix and the reinforcement is the factor which controls the mechanical properties of the composite underplaying the effect produced by the bonding at the glass-matrix interface, i.e. the chemical bonding effect [59].

Surface wettability theory is based on surface wetting but also based on energy effects. It suggests that the silanes improve the wetting of the reinforcement leading to a closer contact between the matrix and the reinforcement. Although good wetting may be a prerequisite for bond formation it does not mean that it will provide maximum performance [59–61].

The final theory is the reversible hydrolysable bond theory. This bonding occurs through a rigid surface and it is a combination of three of the previous theories: chemical bonding theory, the restrained layer theory and the deformable layer theory. The concept of the combination of the theories includes a dynamic equilibrium adhesion mechanism wherein a reversible breaking and remaking of stressed bonds at the interface between a hydrophilic mineral GF and matrix in the presence of water allows relaxation of stresses with loss of adhesion. As molecular dimensions are responsible for stress relaxation, this concept would be the most appropriate to apply to fine GFs [58].

As mentioned above, apart from the chemical bonding theory, the rest of the theories are somewhat outdated due to the fact that they do not explain the data that have been obtained by several researchers. The most accepted theory is the chemical bonding theory since it may explain most of the data that have been obtained. However, the most accurate solution is probably a combination of this theory with some of the others depending on the experimental conditions in which that data was obtained.

Another two important factors which affect the preparation of silanes (i.e. hydrolysis and condensation) are temperature and concentration. Some authors have studied the effect of temperature in the preparation of silane coupling agents. Salon et al. [47] carried out an investigation about the kinetics of hydrolysis and self-condensation reaction of silanes by NMR spectroscopy. They used 3-Methacryloxypropyltrimethoxy silane (MPS) under acidic conditions to study the effect of high temperatures. They started the hydrolysis reaction at RT (25⁰C) for 2 hours followed by an increase in temperature to 70⁰C, keeping this temperature for a long period of time to see if there was any effect. They concluded that the temperature did not affect the hydrolysis, but it generates a large increase in self-condensation reactions, which is in accordance with Arrhenius equation (1.8).

$$k(T_a) = A_p \cdot e^{-\frac{E_a}{RT}} \quad (1.8)$$

Where k is the rate constant dependent on the absolute temperature T_a , A_p is the prefactor, E_a is the activation energy and R the universal gas constant.

Another investigation carried out by Pasternack et al. [62], in which the surfaces of silicon wafers were treated in-situ with APS prepared at 70°C. The effect of this high temperature was an increase in surface organization of the silane at the silicon surface, without compromising the self-termination of the deposition.

A concentration of the order of a fraction of a percent is normally used when a silane, in an aqueous solution, is to be applied. It seems to be that at this concentration range isolated silane monomers are able to form higher molecules due to association between them through hydrogen bonding from the silanol groups. The amount of adsorbed silane (thickness) is linearly proportional to concentration until a critical concentration is reached. This characteristic concentration has been called *onset concentration of association*. Once this concentration is reached the hydrolysed silane molecules start forming hydrogen bonded species and an incomplete dispersion of the silane in the solution occurs [63]. Thus, the orientation of the associated silanes is disturbed and the thickness build-up slows. A solution with a lower concentration than the onset concentration of association yields less physisorbed silane by decreasing the defect of the adsorbed layers [64].

An example of the adsorption in regards of the onset concentration of association effect can be seen in Figure 1.11. In example B) a disturbance in packing due to high concentration is seen with hydrogen bonded or oligomeric silane coupling agents.

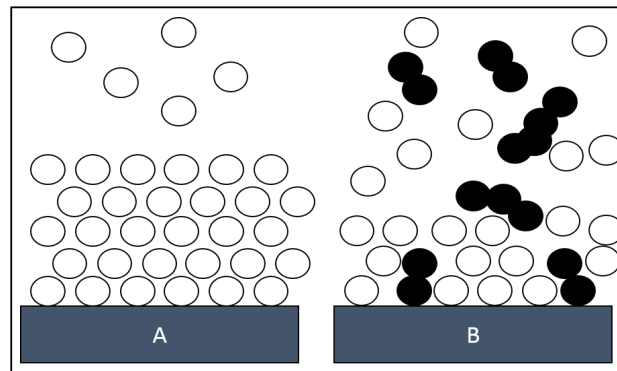


Figure 1.11 Schematic representation of the adsorption of silane coupling agent molecules onto glass fibre surface. A) The silane solution is a concentration below the onset concentration of association, and B) The silane coupling agent concentration above the onset concentration of association. White open circles indicate isolated silanes. Black closed circles indicate hydrogen bonded or oligomeric silane coupling agents.

However, this hypothesis explains the concentration effect from a simplistic point of view. No consideration was taken regarding partially hydrolysed or condensed silane molecules.

1.4.3 Types of silane coupling agent layer adsorption and deposition

The adsorption process of silanes onto the substrate surface depends on the number of functional groups which can react with the surface. Even though it is very difficult to differentiate adsorption from deposition, deposition may occur when the silane is mixed with a solvent which is a poor solvent for silane monomers and/or oligomers. This solubility factor may change as a function of the silane molecular weight. The main difference between them is that adsorption is related to the mechanism which provides an attachment (i.e. anchor) of the molecule to the surface, which involves the participation of the adsorbent toward the substrate. Alternatively, deposition is the process in which adsorbent molecules are forced out of the solution and onto the substrate surface. Based on these assumptions it can be said that deposition often takes place when the solubility of the silane coupling agent is poor or due to changes in concentration regarding solvent evaporation [64].

It is widely assumed that when an interaction occurs between silanes and GFs it results in a three-dimensional graded network on the GF surface. Jones et al. [65] carried out an investigation on a deposit of APS using ToF-SIMS and XPS. They confirmed a three layer structure on the GF. This three-dimensional network consisted of a chemisorbed hydrolytically resistant grafted layer, a chemisorbed three-dimensional layer of polysiloxane and a physisorbed layer of cyclic and linear APS oligomers. This was further investigated by Liu et al. [66] using XPS and AFM; through extraction treatment they confirmed the presence of components of different hydrolytic stability in the APS deposit, which are associated with physisorbed, loosely chemisorbed and strongly chemisorbed components. Ishida et al. [67] investigated the structure of silane coupling agents adsorbed on silicon powder using Diffuse Reflectance Infrared Fourier Transform (DRIFT) spectroscopy to study the basic differences between the chemisorbed and physisorbed layers. The differences described were summarised:

- I. The chemisorbed silane is chemically bonded to the surface through Si-O-Si linkages whilst physisorbed layers are intermolecularly bonded, instead of chemically bonded, through Si-O-Si bonds.
- II. The condensation of physisorbed layers have a higher degree of condensation, i.e. less amount of free Si-OH, than the chemisorbed layers.
- III. In the chemisorbed layers the amine groups form a hydrogen-bonded structure to the surface. These amine groups, when a physisorbed layer is involved, are free or form an aminebicarbonate salt when dried in air.

Figure 1.12 to Figure 1.14 give a schematic of the formation of the glass/silane/matrix interphase, which is represented as a bonded semi-interpenetrating network. An illustration of the deposition of hydrolysed APS onto GF surface, showing a three dimensional polysilane network containing oligomeric silanes, is shown in Figure 1.12.

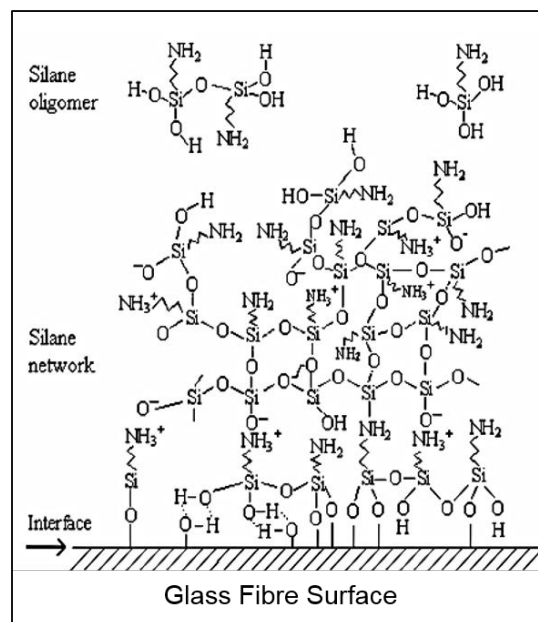


Figure 1.12 Chemical structure of hydrolysed APS on GF [66].

In Figure 1.13 the silane co-deposition, but in this case with a polymeric film former or size, is shown. An interpenetrating network non-exists between the linear polymer film former and the three dimensional network silane. Lastly Figure 1.14, illustrates the structure of the interphase in a composite, consisting of an interpenetrating network

between three components: matrix, film former and silane network. It extends over a length scale of several molecular layers.

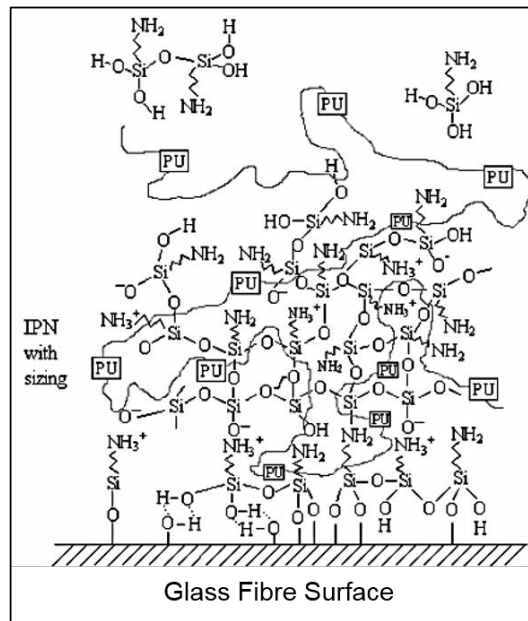


Figure 1.13 Interpenetrating network between hydrolysed APS and polyurethane film polymer or sizing [66].

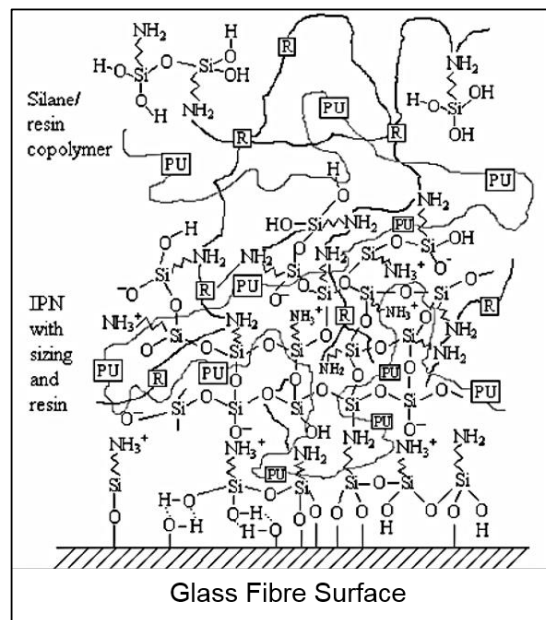


Figure 1.14 Interphase in a GF composite where a reacted interpenetrating network between network silane, film former and resin matrix (R) forms [66].

1.4.4 Effect of silane coupling agent on glass fibre surface and strength

For high performance levels in GF reinforced composites there are at least three key functions that are influenced by applications of sizings:

- i. The need for high level of stress transfer capability across the fibre-matrix interface.
- ii. The need to maintain the highest potential level of fibre strength.
- iii. The need to protect the above two functions against environmental degradation.

These three functions are closely linked with the manner in which sizings interact with fibre surfaces and the manner in which this interaction combines with the protective role of the multifunctional sizings to define the individual GF strength in any particular glass and composite fibre product. The stress transfer capability of the interphase is presumed to be influenced by the ability of the silane to form bonds with the fibre surface, to enhance the wetting of the coated fibre by the resin, and to form links to the matrix. With respect to glass-silane interaction, this is often pictured as a condensation reaction with surface silanols and it could therefore be presumed that a fibres surface concentration of silica might be related to bonding performance.

From the instant of drawing, GFs begin a downward spiral of declining fibre tensile strength as they first cool and then meet with both chemically and mechanically hostile environments [68]. The reaction of the glass surface with water breaks strained Si-O-Si bonds and generates active Si-OH sites. Mechanical abrasion generates flaws, then as the glass is dried and stored before use, water etching can increase the severity of flaws [10]. As explained in 1.3, practical fibre strength is lower than the theoretical strength, due to fibre defects and surface flaws, which may be produced after fibre formation due to physical damage. The increase in flaw severity tends to create stress concentration leading to a premature fracture of the fibre when it is loaded [9,69]. Therefore, fibre strength retention may be strongly influenced by the speed and complexity with which a silane can attach to the surface and form a siloxane network. Silanes are also thought to have a flaw healing ability [10,35,45,70,71], mitigating the usually negative effects of existing flaws on the fibre surface on fibre strength. To maintain the highest level of fibre strength, sizings are designed to contribute to the

protection of the fibre surface against processing damage. On the other hand, silanes also provide protection against environmental degradation. They protect against the ingress and action of moisture in the interphase region [40], due to an increase in hydrophobicity of surfaces [10]. In summary, silanes can act as a promoter on fibre-matrix interaction, but can also contribute significantly to the retained fibre strength [71].

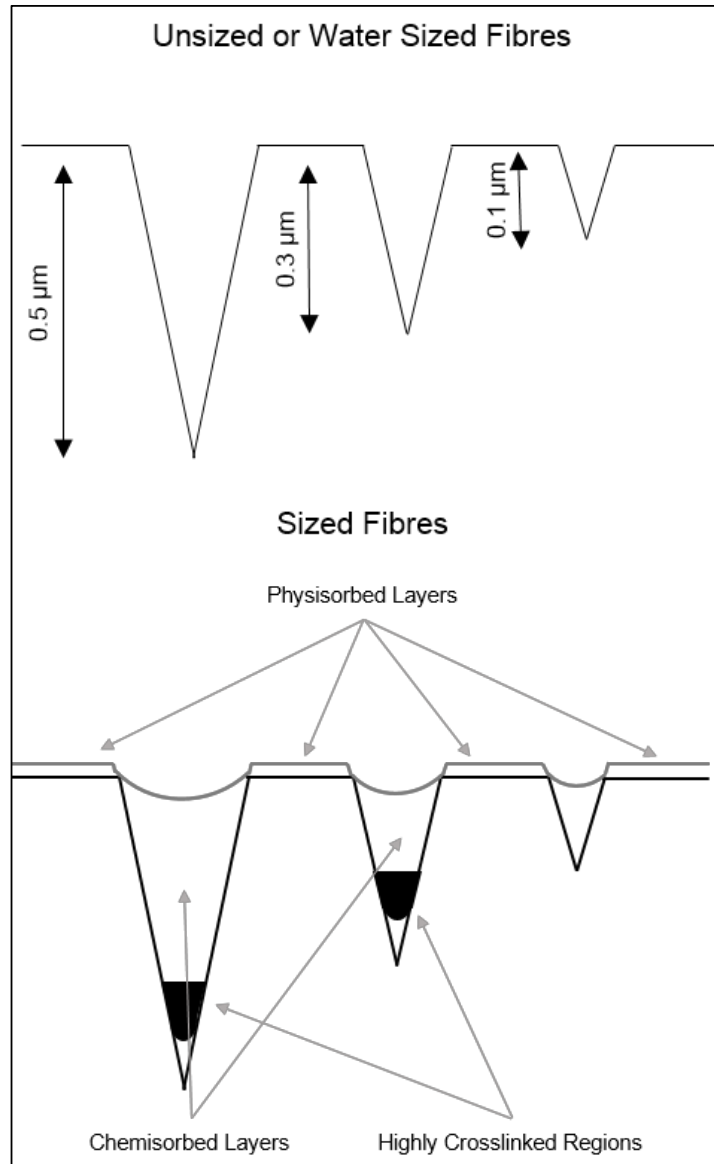


Figure 1.15 Types of flaws and the effect of a surface treatments on fibre surface [70].

The hypothetical effect of silane coupling agents was investigated by Zinck et al. [70]. They carried out an investigation of mechanical characterisation of GFs as an indirect analysis of the effect of surface treatment. In this study they used a bimodal Weibull two parameter cumulative distribution function to analyse the tensile strength of E-glass fibres. They also analysed the effect of silane coupling agents and the effect of its adsorption on the surface, assuming that the flaw distribution is similar for fibres of the same diameter. The three dimensional graded network of the silane coupling agent was proposed to interact with the glass fibres surface making the existing flaws disappear. Silane coupling agents could heal the flaws up to a minimum critical value at which the ratio between the flaw dimension and the molecules (oligomers and polymers) from the silane coupling agent made the flaw healing process no longer possible. This critical dimension up to which defects are not healed was statistically calculated to be 0.1 μm [70]. A graphical example of the deposition of the silane coupling agents healing the flaws up to the critical dimension can be seen in Figure 1.15.

1.5 Amino Silanes

Among the silane coupling agents, aminofunctional silanes are of special interest owing to their bifunctional nature. In the idealized scheme, the ethoxy moiety hydrolyses, which results in the release of ethanol molecules and formation of OH groups on the Si atom in the silane. These OH groups can condense with the surface hydroxyl groups to form a surface Si–O–Si bond whereas the amino functionality extends from the surface [72,73]. Aminofunctional silanes such as APS are commonly used as coupling agents to enhance the durability of GF reinforced composites [74]. APS can act as a surface modifier for GFs and network modifier for hybrid materials (e.g. composite materials) [49,51,75,76]. Water is usually needed for the hydrolysis of the alkoxy groups of the molecules and the amine functional group will self-catalyse the hydrolysis reaction [76]. After hydrolysis, condensation reactions take place where hydrolysed APS molecules react with other APS molecules through a self-condensation process, or react with different molecules containing hydroxyl groups through a condensation reaction. When APS is used as a network former in hybrid materials, the amount of water and the pH of the solution can affect the level of the

silane hydrolysis. However, when a sufficiently large amount of water is used, a complete hydrolysis of APS is achieved [51].

The modified glass surface of silica is often depicted by a uniform structured surface as shown in Figure 1.16. The aminopropyl silane behaves as a “primer” molecule providing an anchor to the surface and a linkage point for the attachment of other molecules to the surface. The unique properties imparted by the amine group along with its capability for reaction with other functionalities have been the source of its popularity as a silanating agent [72].

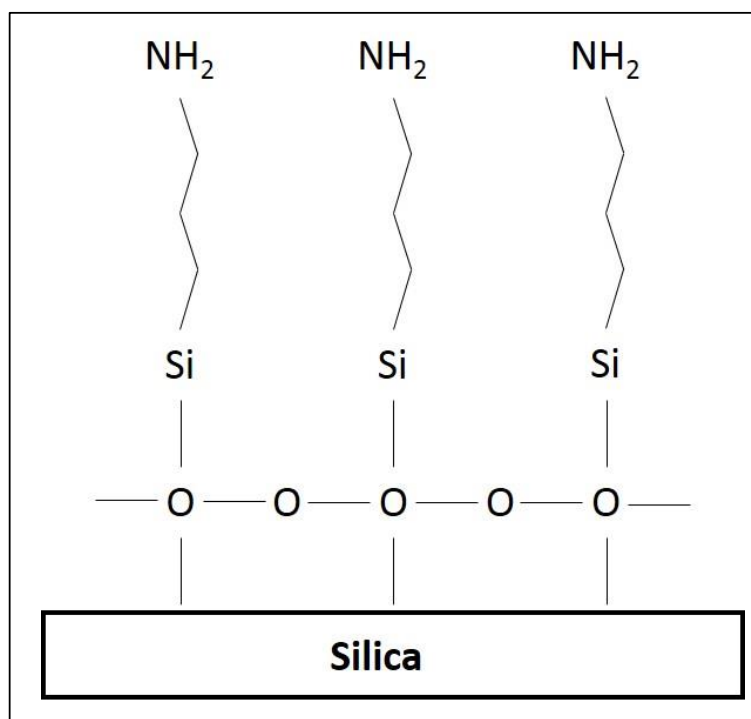


Figure 1.16 Si-O-Si bonding between silica surface and APS.

Although APS is one of the most studied coupling agents, it is also the one which stirs the greatest controversy about its molecular structure during both hydrolysis and condensation. Part of the problem is the variety of process conditions used in sample preparation. In the past, many structures have been proposed for the hydrolysed, partially condensed form of APS on various substrates. In brief, the controversy is over the structure of the amine functionality of the APS coupling agent [77]. The exact mechanism is unclear. It is thought that the ethoxy groups of APS, once they

hydrolyse, condense with the silica surface silanols, releasing ethanol and leaving the amino end group free. The free amino group is then capable of binding to the polymeric resins of the composite [74].

A wide range of differing reaction conditions have been used to deposit APS films. There are, however, some basic mechanisms which are well established and agreed upon. Hydrolysis of silane enables the attachment of the APS to the substrate resulting in siloxane bonds at the substrate surface. Basic functional groups such as amines may self-catalyse the hydrolysis reaction leading to more reactive monolayer formation as compared to non-aminated silanes. The initial hydrolysis step can occur either in solution or at the substrate surface depending on the amount of water present in the system. An excess of water will result in excessive polymerisation occurring in the solvent phase, while a deficiency of water will result in the formation of a monolayer with several remaining ethoxy groups that did not hydrolyse and condense [75].

APS is often pre-hydrolysed in aqueous solution until the mixture reaches an equilibrium of oligomers and polymers prior to deposition [78]. Factors such as pH and temperature affect the pre-hydrolysis process. This process may be divided into two steps:

- i. Hydrolysis: water molecules react with the three ethoxy groups of the APS molecules giving rise to aminopropyltrihydroxy silane molecules and three ethanol molecules per molecule of APS.
- ii. Self-condensation: the aminopropyltrihydroxy silane molecules, and probably a few partially hydrolysed APS molecules, self-condense giving rise to an amino silane polymer.

The sequence of reactions can be seen in Figure 1.17:

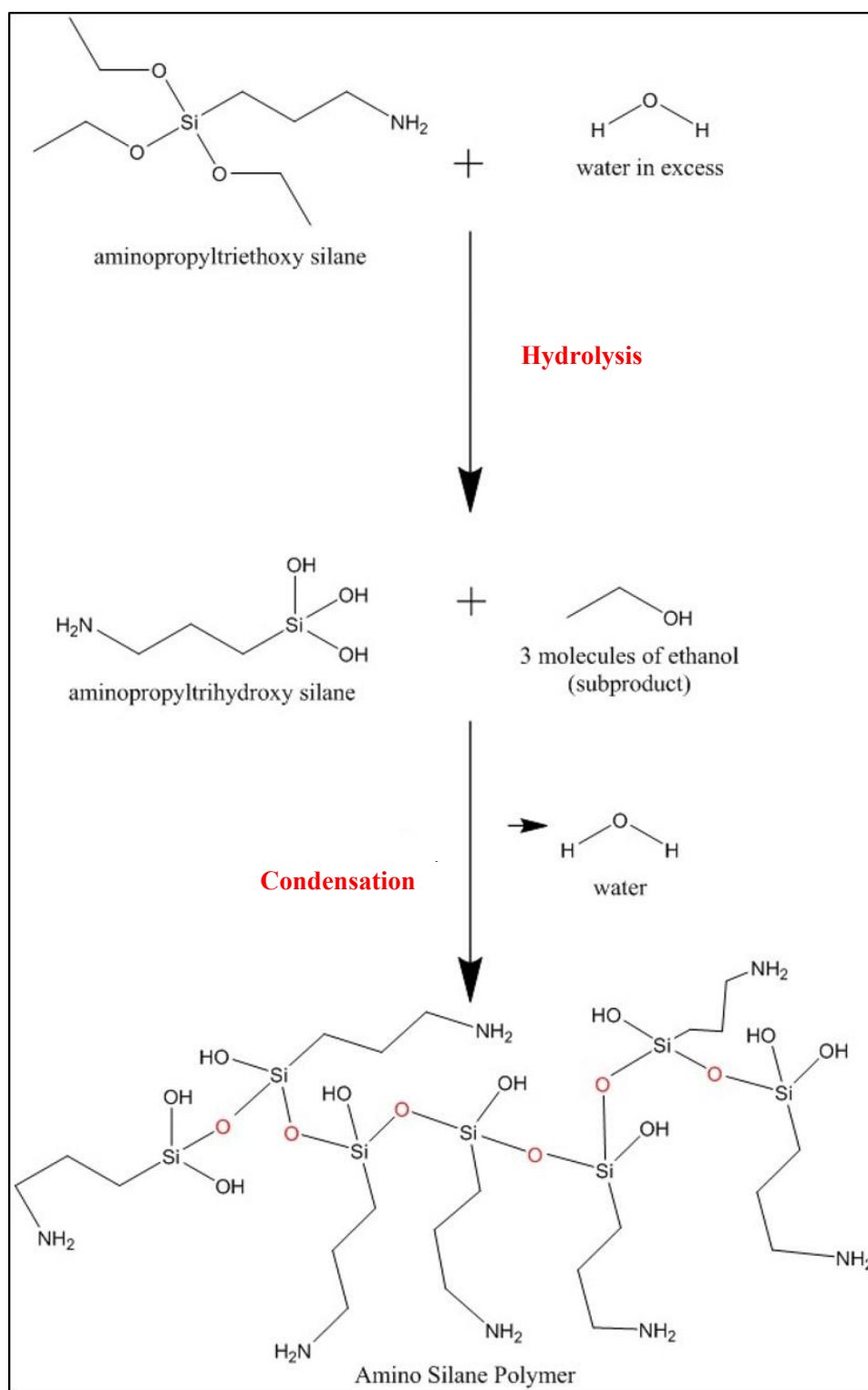


Figure 1.17 APS hydrolysis and self-condensation reactions in water.

1.6 The effect of pH on hydrolysis and self-condensation reactions of APS

Both the intermediate and final structure of APS is highly affected by the pH of the treating solution. As often mentioned above (1.4.2), the pH value of silane solutions is often adjusted to acidic values, which is highly beneficial for most of the silanes, since the majority of the silanes are hydrophobic and an acidic solution (i.e. pH ranging from 3.0 to 4.0) makes them more soluble in water [64]. However, this is not the case for APS. An investigation was carried out by Naviroj et al. [49] in which they studied the structure and adsorption characteristics of silane coupling agents on silica and E-glass fibre depending on pH. They concluded that the structure of APS is highly dependent on the pH of the treating solution. When a silica or E-glass fibre surface is treated with an APS solution at its natural pH (i.e. 10.6), the maximum amount of adsorption was achieved, making it clear that the adsorption and structure of APS is pH dependent. Salon et al. [47] carried out an investigation of the kinetics of hydrolysis and self-condensation reactions of silanes by NMR spectroscopy in which they suggested that pH conditions strongly affected the hydrolysis and self-condensation rates. The hydrolysis rate is accelerated by acidic conditions whilst self-condensation reactions are limited. These conditions also seem to stabilize hydrolysed moieties.

1.7 The effect of temperature on hydrolysis and self-condensation reactions of APS

Changing the temperature of the APS solution may affect the reactions involved in the preparation of APS. Salon et al. [47] suggested that hydrolysis rate is not affected by elevated temperatures, but that self-condensation reactions are strongly accelerated. They also showed that the proportion of silanols in solution drastically decreased with increased temperature [47]. Other researchers also investigated the effect of temperature in other silanes. An investigation carried out by Pasternack et al. [62] has shown that an in situ incubation at elevated temperatures ($\sim 70^{\circ}\text{C}$) increases surface organization without compromising the self-termination of the deposition.

1.8 Effect of thermal conditioning on glass fibre properties

The mechanical and physical properties of glass are determined by the composition and the thermal history of the glass. How the fibre forming process changes the values of the physical properties indicates that the glass in the fibre has a particular structural configuration. There is almost conclusive experimental evidence that intense chilling during the fiber-forming process results in a non-equilibrium form of glass at room temperature, in which most physical properties are affected. Although they are affected, it does not mean that it is unstable at room temperature. It represents equilibrium at some higher temperature since the measured values of density, modulus, and index of refraction are those corresponding to glass at an elevated temperature. When glass fibres (GFs) are subjected to elevated temperatures, temperatures close to the glass transition temperature (T_g point), the physical properties tend to return those values representative of the massive, annealed form of the glass. The term “thermal compaction” has been chosen to describe this phenomenon. Compaction has been experimentally shown as both time and temperature sensitive. This effect can be observed in fibres by measuring the change in length as the fibre is reheated, as can be seen in Figure 1.18 [16].

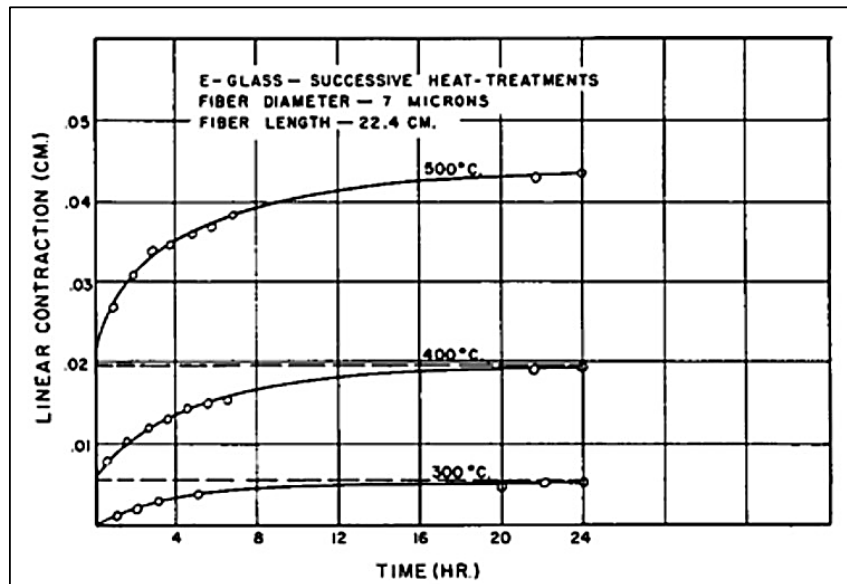


Figure 1.18 Linear contraction of a single E-glass fibre as a function of temperature and time [16].

Fibre length decreased with both time and temperature up to the normal glass softening temperature, which is the temperature at which glasses, non-provided of support, will begin to sag (e.g. 726⁰C for soda-lime glass). The density and compaction during annealing experienced by GFs during processing was investigated by Otto [16].

An investigation carried out by Yang et al. [79] showed that the coefficient of linear thermal expansion (CLTE), of E-glass fibre has no temperature dependence at temperatures below 300⁰C, but at higher temperatures variation in the CLTE were observed with an abrupt length change at temperatures around GF T_g (i.e. temperatures of about 760⁰C). The isothermal measurements that they carried out showed an important length shrinkage at temperatures above 300⁰C. A logarithmic dependence on time was found to represent the length contraction, implying that when hyper-quenched GF is heated to high temperatures, it tends to experience structural relaxation.

Further investigation about temperature effects on GFs was carried out by Feih et al. [80]. They heat treated E-glass fibres under conditions that represented commercial composite thermal recycling processing. They showed that the RT fibre strength decreased rapidly with increasing temperatures above 150-250⁰C. However, in contrast with the results of Yang et al. [79], the Young's modulus was not affected. At temperatures above 450⁰C, the strength for single fibres and fibre bundles decreased 40 and 80% respectively. Once again, they suggested that strength is dependent on both temperature and time of exposure to that temperature.

Thomason et al. studied the properties of GFs after conditioning at composite recycling temperatures [81]. They concluded that the thermal history likely to be encountered by GFs recycled out of end-of-life composite by processing in the 250-600⁰C temperature range can potentially cause dramatic lowering of the RT fibre strength and strain at failure. Using two different types of fibres, E-glass uncoated and APS coated fibres, the exposure to 15 minutes conditioning at 600⁰C reduced the average RT single fibre strength up to 70%. While unsized GFs exhibited an apparent linear decrease in average RT tensile strength with increasing conditioning temperature, APS sized GFs showed relative stability of the single fibre strength up to

250°C, undergoing a severe drop in RT strength for higher conditioning temperatures. The results can be seen in Figure 1.19 [81].

Jenkins et al. [82] also studied the effect of high temperatures, introducing the novel concept of single fibre thermal conditioning GFs. The investigation they carried out comparing single and bundle thermal conditioning suggested a dual effect, which is the combination of thermal and mechanical handling damage on the strength of thermally conditioned GFs. Single fibre thermal conditioning GFs showed the possibility of achieving significantly greater retained tensile strength.

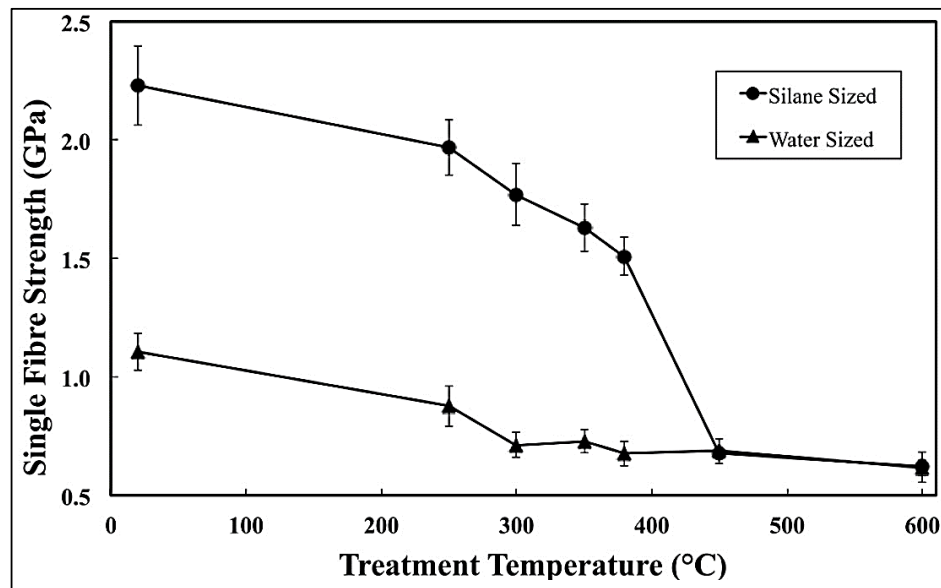


Figure 1.19 Influence of heat treatment temperature on RT average strength of unsized (water sized) and APS sized GFs [81].

On the other hand, the observation carried out using APS sized and unsized GFs, showed a more significant strength reduction in sized GFs rather than unsized, which may be due to sizing degradation during thermal processing. Due to this, a disparity in retained strengths for sized fibre was only observed when thermal conditioning was performed above 300°C, whereas the bare fibre system exhibited the effect even upon heating at relatively low temperatures. Based on thermal conditioning data shown in Figure 1.19, the protective effect of the APS coating against mechanical handling damage is suggested to be up to 500°C, at which temperature the APS is completely removed.

Aslanova [83] studied the relationship between the chemical composition of glass and its strength and Aslanova et al. [84] investigated the effect of chemical composition on the relaxation properties of thin GFs. Experimental data were published using GF's with different diameters and chemical compositions. These were tested over a wide range of temperatures using a low frequency torsion pendulum under vacuum, reporting changes in both shear modulus and internal friction. They observed that the shear modulus of aluminoborosilicate glass decreases with thermal conditioning up to 300⁰C, but begins to increase at higher temperatures, a similar observation to that of Otto [16]. They suggested that it was an effect of the compaction of the glass structure (i.e. density increase during the process), which in turn is suggested to be due to the relaxation of deformation within the fibre structures that are formed during drawing. Due to the importance of this physical effect, the relaxation of glasses has been also studied through mathematical modelling to predict the variations of glass subjected to arbitrary temperature-time histories [85,86].

The thermal conditioning of fused silica was also studied, with similar behaviour. In the temperature range of 0 to 200⁰C, specific surface defects were formed by the bonding of dust contaminants to the silica. Then, for high temperatures of 600 to 800⁰C extensive interaction occurred around these dust particles, which act as a surface stress raiser, reducing the strength of the heat treated silica [87]. Duan et al. [88] studied glass microstructure evaluations using high temperature mechanical spectroscopy measurements, in which they determined that the stiffness of alumina-silicate glass also decreases with temperature increase.

On the other hand, Izmailova et al. [68] did not observe any relationship between the strength of the fibre and the process temperature (i.e. 1200⁰C) in their investigation of the production cycles for GFs without surface defects, where they compared their results with those obtained by Otto [30]. Bartenev et al. [89] investigated the effect of tensile stresses on the strength of heat treated GFs. They observed that thermal conditioning under load does not affect GF strength and in certain cases it increases.

The combined effect of temperature and time has been widely studied by several authors. Sakka [90] investigated the effects of reheating on the strength of glass fibres. He produced laboratory GFs with a given composition (SiO₂ 67.7, B₂O₃ 12.0, BaO

2.0, K₂O 9.2, Al₂O₃ 0.5), heating the fibres for 1 hour at the desired temperature and then cooling to RT before testing. Then they were tested. It was found that for thermal conditioning temperatures up to 200⁰C the strength of the GFs was unchanged, whilst conditioning above 200⁰C resulted in a rapid decrease in fibre strength which was linear with temperature.

In the investigation of the factors likely to affect the strength and properties of E-glass fibres, Thomas [91] studied the effect of heat treatment on the RT strength of GF. He used an apparatus specially designed and constructed to heat treat the GF at the required temperature and a tubular electric furnace also constructed for this purpose. He applied temperatures in the range of 100 up to 600⁰C in intervals from 1 to 4 hours. He showed, as can be seen in Figure 1.20, that the necessary time to reduce the breaking stress to a constant value depends on the temperature of the heat treatment, requiring lower time exposures for high temperatures than for relatively low temperatures (i.e. 150⁰C). He suggested that molecular and structural rearrangements in the glass during the heat treatment probably causes stresses that lead to surface and bulk flaws and cracks.

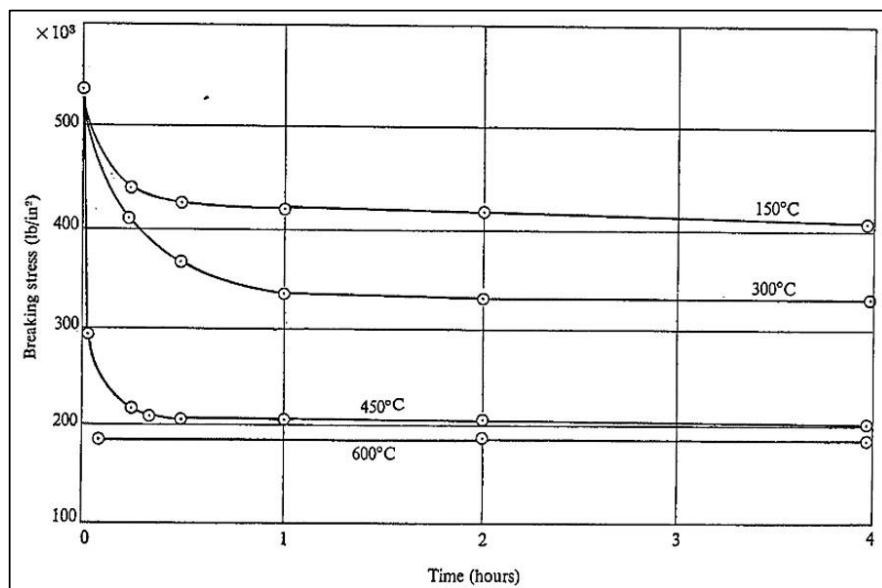


Figure 1.20 Variation of tensile strength with period of heat treatment at four temperatures [91].

Cameron [92] also studied the effect of temperature on GF strength using E-glass fibres. He showed that for temperatures below 100°C, there is no significant decrease in strength, whilst for temperatures above 100°C the RT strength starts to decrease with increasing temperature, as can be seen in Figure 1.21. He concluded by suggesting that the probable cause of weakening is a structural change in the glass due to the temperature.

Further investigations concluded that temperature negatively affects GF strength. Some of them proposed that this weakening of GFs is caused by a twofold effect of heat treatment. The first effect is due to flaw initiation and growth that occurs at a rate which increases with increasing temperature in the range 20 to 600°C. The second effect is due to internal changes with temperature increase [93], with similar suggestions as Thomas [91] and Cameron [92]. Other authors also corroborate these suggestions with their investigations showing similar results for thermal conditioning GFs at high temperatures [81].

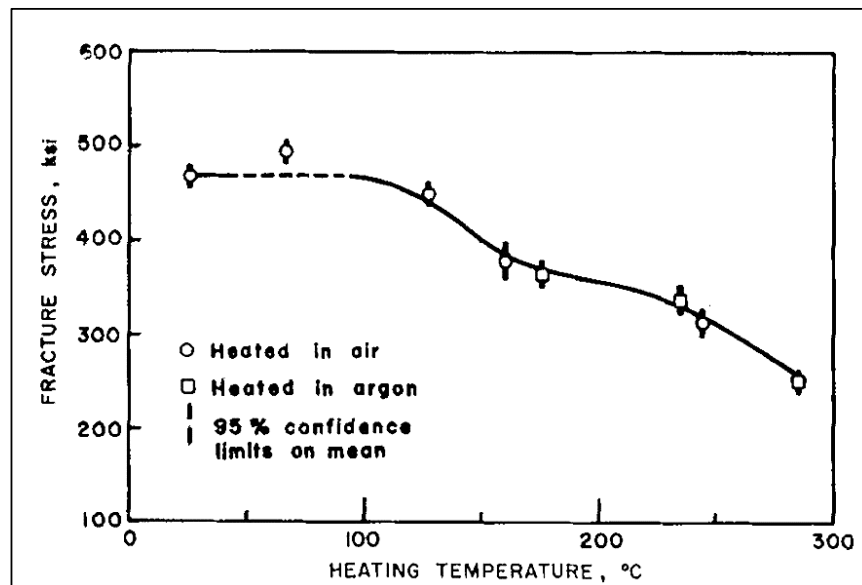


Figure 1.21 Relation between RT strength and heat treatment temperature [92].

The investigation carried out by Aslanova [94] showed that the strength of thin GFs changes sharply as a result of the heat treatment, with a reduction in strength of as

much as 70%, adding that the composition of the glass wields a considerable influence on GF strength of fibres subjected to heat treatment.

Dorzhiev et al. [95] investigated the strength and structure, using magnesium aluminosilicate fibre; they also showed a strength reduction due to heat treatment (200-600°C). They suggested that this is associated with the relaxation of the siliceous phase and the liberation of adsorbed and structurally bonded moisture. The effect of water vapour (moisture) on structural relaxation of silica glasses was also studied by Tomozowa et al. [96]; they carried out experiments using two different types of silica glass, thermally conditioning them at high temperatures under different water vapour conditions. They suggested that surface structural relaxation takes place much more rapidly than the bulk structural relaxation when it is promoted by moisture in the atmosphere, i.e. molecular water, given by the water diffusion coefficient equation (1.9) [97]:

$$D_D = D_0 \exp\left(\frac{-Q_D}{RT}\right) \exp\left(\frac{-P\Delta V}{RT}\right) \quad (1.9)$$

Where D_0 is the pre-exponential factor, Q_D is the activation energy of water diffusion in the absence of stress, P is the hydrostatic pressure and ΔV is the activation volume.

It was also suggested that structural relaxation can take place at room temperature, if it is assisted by water vapour and applied tensile stress [97,98].

1.9 Acid and basic treatments

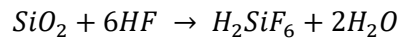
1.9.1 Hydrofluoric acid treatment

The effect of acids on glass has been widely studied. In this chapter only hydrofluoric acid (HF) and hydrochloric acid (HCl) will be investigated in regard of their potential beneficial effect on the strength of glass fibres (GFs).

Silica glasses, and by extension GFs, are materials resistant to most liquids and gases. The exception is HF or other HF containing aqueous solutions, which can dissolve glass even at room temperature. It is used as a cleaning agent, due to its ability

to remove oxides and other impurities and it is also used as an etchant. The latter effect is commonly used in the glass field [99]. Several investigations have been carried out in relationship with HF reactivity with GF. In general terms, HF has been used to etch the GF surface with the aim of removing the possible existing cracks and flaws.

HF reacts with vitreous silica (SiO_2) from glass as shown in the reaction below:



Ray et al. [100] carried out an investigation of the strength of glass by etching and ion-exchange, in which they investigated the factors that could affect the loss in strength of etched glass on heating. They used the etching effect of HF to remove the microcracks in the surface, to which the low strength of bulk glass is attributed. Such microcracks reduce the overall stress needed to cause fracture to a small fraction of the maximum local stress.

In his investigation into glass composition and the strength of GF, Bartenev [101] also used HF to etch GF surface. He showed different behaviour between commercial and flawless GFs. GF strength was increased after chemical etching, whilst flawless GFs strength decreased after chemical etching. This result was due to flawless GFs having a structure presumed to be completely intact, whereas commercial GFs experience significant stresses during drawing, resulting in the development of flaws in the surface layer. Etching the surface can remove these flaws, leading to a strength increase; whereas in the former the damage sustained to the previously pristine surface lowers fibre strength. By controlling the etching process Levengood [102] used HF to etch glass and crystalline surfaces and produce structure variations on them.

Izmaelova et al. [68] investigated the production cycles for GF without surface defects. They, once again, studied the effect of badly damaged GF surface. To compare the damaged GFs and the non-damaged ones they used HF to etch the surface and remove the crack and flaws from the surface layer. This etching effect can be relatively homogeneous for certain conditions such as HF concentration and etching time. Based on this assumption, HF was also used to create flaws, through an HF environment [103]. Uncoated GFs were aged by exposure to the vapour of 1% v/v HF solution,

controlling the corrosion by varying the aging time and/or relative humidity of the aging environment. This HF environment allowed them to create different flaw geometries to study their effect on fibre strength.

Another example of using HF as an etching compound is the investigation carried out by Takahagi et al. [104], in which they investigated the formation of hydrogen passivated silicon-crystal surfaces using ultraviolet cleaning and HF. They used HF to clean the surface through dipping the sample silicon wafers into high purity HF (50%) and low concentration HF aqueous solutions obtained by dilution with ultra-pure water. With this treatment the oxide layer created after the UV cleaning was removed from the surface. With these treatments they cleaned the organic compounds from the silicon wafer surface. In a similar study, also using the same HF concentration solutions, Takahagi et al. [105] carried out an investigation of fluorine-containing species on the HF etched silicon single-crystal surface. They studied the chemical behaviour of fluorine on the HF etched silicon surface. This study was an extension of the previous in which they suggested that the Si-F bonds are rapidly hydrolysed to Si-OH by water rinsing and also gradually hydrolysed by exposure to moisture in air. This would benefit the reaction of GFs after HF treatment with silane.

Tso and Pask [106] studied the reaction of different glasses with HF solutions. The results of the reaction between them were presented, interpreting the reaction mechanism between silica glass and several silicate glasses with different HF acid solutions. They suggested that the reaction between silica and silicate glasses with HF is considered to be transport or diffusion controlled from the glass into the liquid.

Yang et al. [107] in their investigation, showed that the deposition of particles rich in fluorine (probably reaction products like hexafluorosilicic acid) did not appear for short treatment times, i.e. 30 seconds, but deposition began to appear after longer times, i.e. 2.5 minutes for a HF 4% v/v solution in deionised water. They suggested that for short periods of time the GF surface is relatively clean.

A recent study investigated the concept of regenerating thermally degraded GFs for a potential closed-loop recycling of GF thermosetting composites. [108]. In this work, the stress of GFs was thermally reduced for a study of the regeneration of GF strength. GFs thermally conditioned at temperatures between 450 and 600°C, were chemically

treated with HF 1% v/v in deionised water solution for different periods of time. As can be seen in Figure 1.22 [108], the different time treatments resulted in a substantial increase in GF strength.

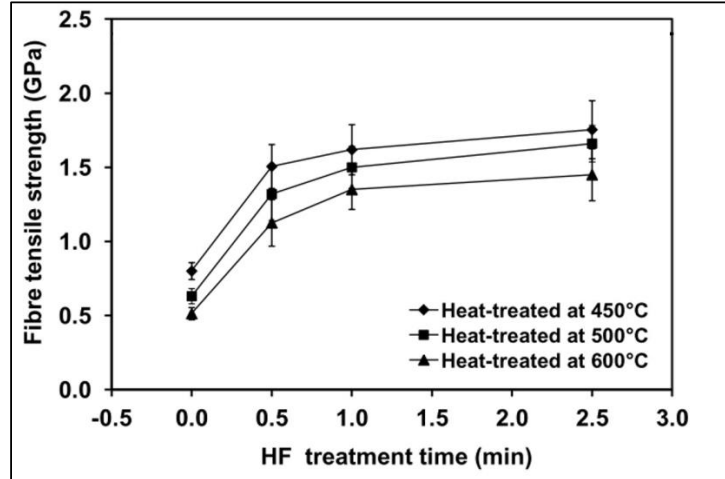


Figure 1.22. Recovery in RT tensile strength of heat-treated glass fibres as a function of the treatment time of 1 % v/v of HF aqueous solution [108].

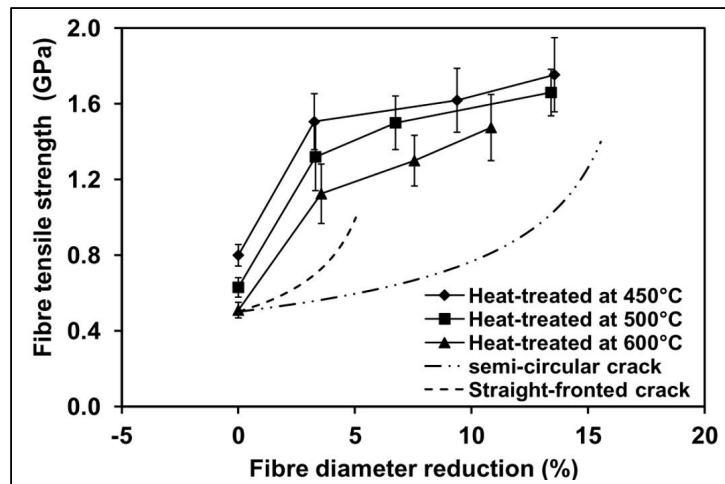


Figure 1.23 Tensile strength of heat-treated glass fibres as a function of fibre diameter reduction and an example for the 600°C-treated fibres with semi-circular and straight-fronted cracks [108].

On the other hand, reaction of HF with GFs, reduced the average fibre diameter due to the loss of material into the solution. The reduction in diameter was correlated with the increase in strength, as shown in Figure 1.23 [108].

For higher diameter reductions, higher strength increase was observed. They showed that the higher fibre tensile strength slope was found to be for fibre diameter reductions up to 3%.

Iliescu et al. [109] used a solution of HF mixed with HCl as a way for improving the quality, i.e. the smoothness and uniformity, of the generated glass surface. In their publication they also carried out an investigation of the reaction of HF / HCl solution with glass through an etching graph as can be seen in Figure 1.24 [109], with a non-linear etching trend regarding the HF concentration in solution. They suggested that there is an optimal composition of the etchant (i.e. HF / HCl solution) that varies based on the glass to be treated.

HF has been also applied to other different uses, e.g. fabrication of intrinsic fibre Fabry-Perot sensors in silica fibres using hydrofluoric acid etching [110], but usually using the same reacting/etching effect that it has over silica compounds.

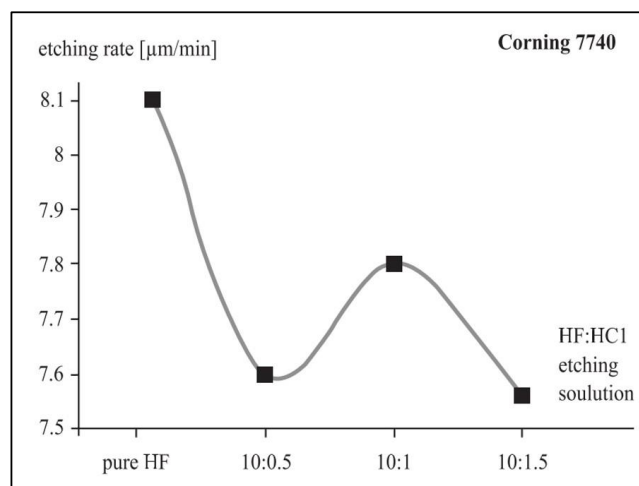


Figure 1.24 Variation of etching rate for 4” Oyrex glass (Corning 7740) with the composition of the solution in pure HF, 10:0.5, 10:1 and 10:1.5 of HF:HCl [109].

1.9.2 Hydrochloric acid treatment

Regarding HCl treatment, Baselga et al. [111] studied the microstructure and wettability of surface pretreated GFs. Their investigation was focused on the influence of different activation pretreatments of GFs on the structure of APS coupling agent layer. They thermally conditioned GFs at 450°C for 1 hour to remove the organic

compounds. After the heat treatment, the surface was reactivated with 10% solution of HCl for 1 and 3h. After acid reactivation the samples were washed several times with distilled water to remove remaining HCl. The fibres were dried at 110⁰C for 1 hour and kept in a desiccator until silanisation. They applied a 1% v/v APS aqueous solution for 10 minutes followed by a drying process of another 1 hour at 110⁰C. They analysed the effect of these treatments using Fourier Transform Infrared Spectroscopy (FTIR) and scanning electron microscope (SEM), suggesting that their results indicated that under acidic conditions, i.e. HCl solution, a great number of silanol groups are generated on the fibre surface.

1.9.3 Sodium hydroxide treatments

Sodium hydroxide (NaOH), commonly called caustic soda, is a highly caustic inorganic compound soluble in water. When pure it is found in solid state as pellets, flakes or granular form. NaOH is known to react with silica based glasses when it is in solution at RT and is particularly reactive at high temperatures. Several authors have investigated this reactivity when applying it to glasses. Rowland et al. [112] carried out an investigation of the corrosion of glasses by alkaline solutions in which they studied the attack of borosilicate glass, lime glass and a lead glass using alkali compounds as NaOH and Na₂CO₃. The temperature of the alkali solution was 90 ± 0.5⁰C, for the 18h treatment time. They concluded that alkaline reagents under 0.5 N attacked the 3 types of glasses mentioned in an expected manner. The strongest bases were found to be hydroxides of Na and K in solution.

An interesting investigation of the dissolution of waste glasses in high alkaline solutions [113] used alkaline solutions of recycled waste glass with the purpose of synthesizing a new mineral binder for particular applications. The waste glasses investigated were SB and SM (bottle glasses obtained from SOLIBRA) and VC (window glass from SIVIMI), two typical soda lime glasses provided by two different companies. The waste glass was simply dissolved in alkaline solution. The chemical reactions involved in glass corrosion include two general concepts which are an ion exchange process or the removal of soluble glass constituents (leaching) and the glass network dissolution in alkali solution (etching). Two alkali solutions were used in this investigation, NaOH and potassium hydroxide (KOH). The results showed that higher

weight loss (W_{loss}) was obtained for the solution of NaOH (Figure 1.25 [113] and Figure 1.26 [113]). The weight loss was calculated by the equation (1.10):

$$W_{\text{loss}} = \frac{m_0 - m_t}{m_0} \quad (1.10)$$

Where m_0 is the initial weight of the crushed glass and m_t is the residue weight at time t .

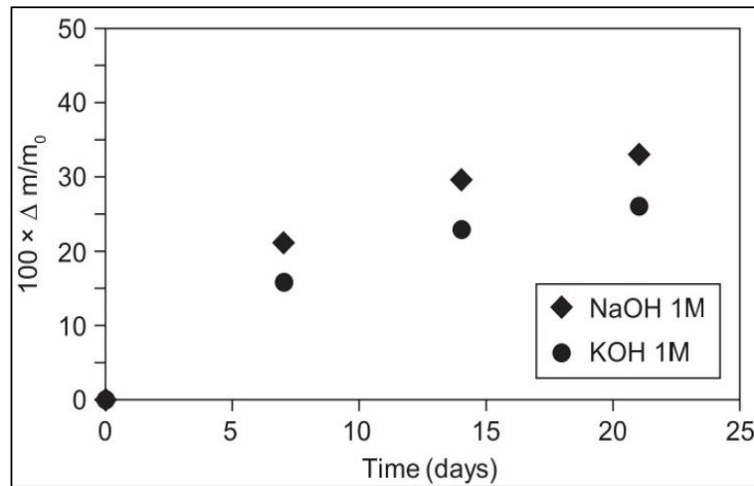


Figure 1.25 Weight loss (Δm is the difference between m_0 and m_t) of SB versus time in function of the nature of alkaline solution (NaOH and KOH) at 70°C [113].

In this investigation, the dissolution curve shown in Figure 1.26 was suggested to be divided in three steps:

1. An initial linear range as a function of time due to glass network dissolution.
2. Intermediate exposure time where the dissolution slows down. This can be due to both the back precipitation of the silica and the saturation of solution.
3. The last step was suggested to be due to the presence of carbonate species which deposited at the surface, with the consequence of inhibition of the dissolution and the ions silicate transport.

The dissolution curves could be divided into three steps (Figure 1.26). Step I consisting of a linear range as a function of time, could be explained by a glass network dissolution.

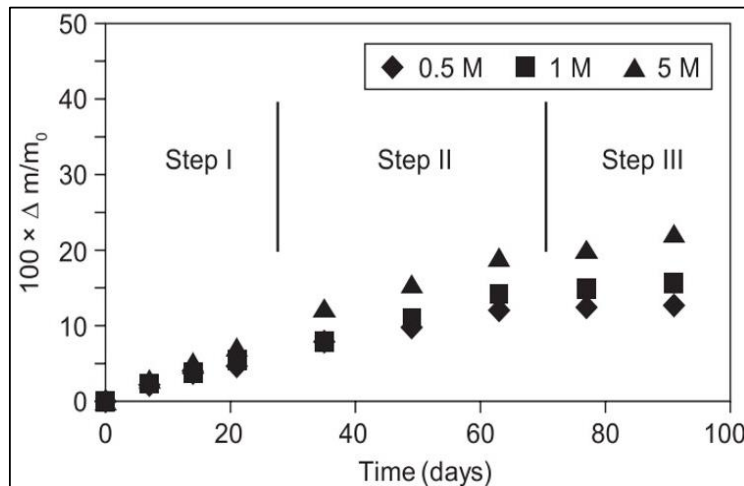


Figure 1.26 Weight loss (Δm is the difference between m_0 and m_t) of SB versus time in function of the concentration of alkaline solution (NaOH) at 70°C [113].

It was also shown that an increase in temperature increased the dissolution rate, with a relationship found of dissolution rate multiplied by 3 for a 20°C rise in temperature. Alkaline solution concentration also affects dissolution. The decreasing time dependence of dissolution curves was suggested to be due to the formation of a precipitated layer on the glass surface. This precipitated layer was suggested to be due to two possible mechanisms. The first mechanism considers that due to the glass dissolution and interdiffusion, the ion activity products in respect to mentioned silicates exceeded their solubility products. The precipitated layer is then created through the solution. A second possible mechanism assumes the direct reaction of Ca and Mg ions in a gel layer created on glass surface.

The corrosion produced by alkaline solutions such as NaOH solutions has also been studied. Molchanov and Prikhidko [114] studied the corrosion of silica glasses by NaOH solutions. They determined the degree of breakdown of the crystalline lattice of the silicate caused by alkaline treatments in quartz, quartz glass and some other laboratory glasses, using a micro-interferometer, an interference microscope for the study of glass surfaces, and a Linnik's double microscope to measure the depths of breakdown glass. They observed that the depth of corrosion of quartz glass is proportional to the concentration of the alkaline solution and to the duration of treatment. Temperature increases directly affected the depth of corrosion, in

accordance with an exponential regression. Another investigation of corrosion in acidic and basic solutions and hydrothermal, but in this case with silicon nitride materials [115], showed that there is a relationship between the amount of silica (SiO_2) and the corrosion of basic solutions. Higher content of SiO_2 in the material produces higher corrosion by the basic solutions at 90°C . Wiederhorn et al. [116] carried out an investigation about the micromechanisms of crack growth in ceramics and glasses in corrosive environments. They explained it through the *Chemical reaction rate theory*. They modified the equation of the theory in accordance to the cracks and failures to create a model. It was also mentioned that for solutions with pH higher than 9, the OH^- directly attacks the network structure.

This corrosive effect of alkali solutions in glasses was applied as a surface cleaner as well. It was used to clean the surface of glass, due to the removal of organic compounds from the surface and the etching effect on glass surface [117].

Wei et al. [118,119] studied the environmental resistance and mechanical performance of basalt and GFs (E-glass) and their tensile behaviour after chemical treatments. They studied the effect of NaOH and HCl on the performance of both types of fibres. The fibres were treated with 2 M solutions in both cases and 97 and 98°C respectively for periods of times between 30 minutes and 3 hours. The effect of NaOH on both fibre types mass loss ratio and strength maintenance ratio (being strength maintenance ratio, the strength after a period of treating time divided by the strength before any treatment in %) loss with respect to time can be seen in Figure 1.27 [118] and Figure 1.28 [118]. Mass loss ratio is the mass of the fibre after t treatment time divided by the mass of the fibre before any treatment in % and strength maintenance ratio is the strength of the fibre after t treatment time divided by the strength of the fibre before any treatment in %.

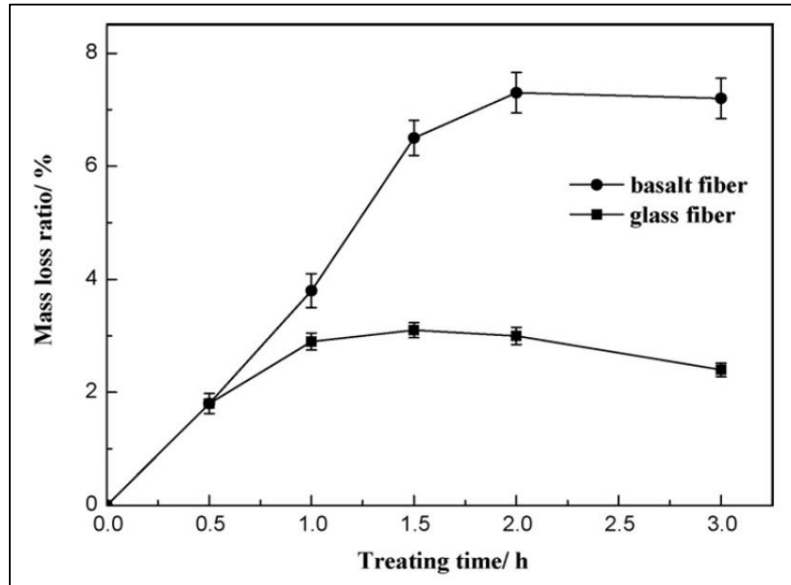


Figure 1.27 Mass loss ratio-treating time behaviour (alkali treatment). The error bars represent the standard deviation [118].

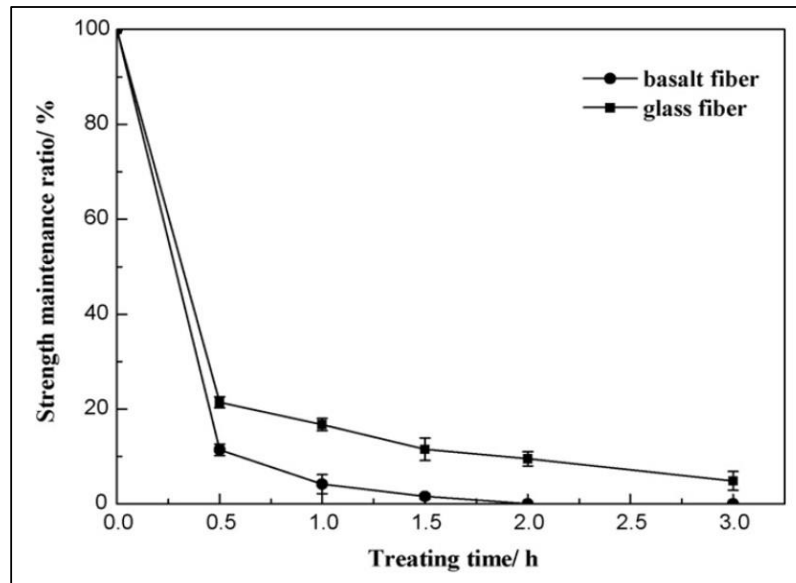


Figure 1.28 Strength maintenance ratio-treating time behaviour at 98^oC (alkali treatment). The error bars represent the standard deviation [118].

They showed that the treatment time significantly affects the mass loss and the strength retention of the GFs. This corrosion suffered by both types of fibres in alkaline media is mainly controlled by the dissolving of the SiO₂ network. The hydroxyl ions

of the solution disrupt the siloxane bonds in the glass and the silicates generating a migration into the solution. They also showed SEM pictures, as can be seen in Figure 1.29 [118], of the surface of GFs after NaOH treatment, clearly deteriorated. They also showed that the mechanical performance of GFs after NaOH treatments decreased, suggesting that tensile strength decreases with increasing the treatment time.

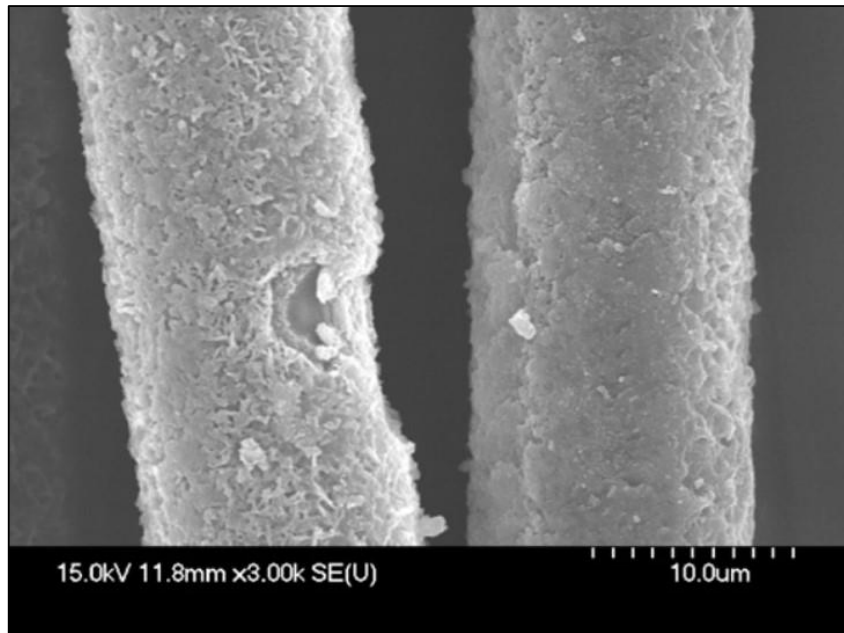


Figure 1.29 SEM images of the GF (E-glass) surfaces after treatment in NaOH solution [118].

Sodium Hydroxide reactions with GF oxide components

The possible reactions of NaOH with GF can be modelled by considering the oxide components used to make the glass and are listed below.

1. $\text{SiO}_2 + 2 \text{NaOH} \rightarrow \text{Na}_2\text{SiO}_3 + \text{H}_2\text{O}$
2. $\text{Al}_2\text{O}_3 + 6 \text{NaOH} + 3 \text{H}_2\text{O} \rightarrow 2 \text{Na}_2\text{Al}(\text{OH})_4$
3. $\text{CaO} + 2 \text{NaOH} \rightarrow \text{Ca}(\text{OH})_2 + \text{Na}_2\text{O}$
4. $\text{MgO} + 2 \text{NaOH} \rightarrow \text{Mg}(\text{OH})_2 + \text{Na}_2\text{O}$

Several sub-products might appear due to the reaction of NaOH with the GFs. They might deposit on GF surface as the NaOH reaction proceeds.

In summary, it has been reported by numerous investigations that NaOH can have significant negative effects on a variety of different types of glass. It is corrosive to the glass structure and has been shown to negatively impact the tensile strength of glass fibres.

In this investigation, NaOH is going to be used to recover mechanical properties of thermal treated GFs (mechanically damaged). It is going to focus on the concentration and treatment time effect of NaOH on E-glass fibres. It is based on the reactions between the NaOH and the E-glass compound. It might etch the damaged GF surface providing a similar effect as HF provides recovering the mechanical properties of GFs.

The OH group on GF surface after NaOH treatment is going to be characterised as a regenerative effect of NaOH treatment. Fourier Transform Infrared Spectroscopy (FTIR) was used for this purpose, as other authors used it before to investigate silica based structures, analysing OH bonds with silica groups and many other [120–123].

From this review, it can be seen that the research on the strength of glass fibre has been carried out mainly in three aspects: fundamental interest in the strength of glass fibres, understanding the behaviour of the strength of given and thermally conditioned glass fibres and improving the strength of glass fibres through chemical treatments. On the other hand, the research on silane coupling agents has been carried out in the conditioning of silane coupling agents and their adsorption and deposition on glass fibre surfaces. The former is now facing questions such as how to recover GF strength of damaged GFs, especially after thermal processes at high temperatures, like HF is able to perform it, but with less hazardous chemicals. The latter needs to change preparation conditions of silanes, particularly the commonly used APS, in order to improve the beneficial effect of them on GF strength. Additionally, structure changes should be determined to try to correlate with any substantial difference on GF strength due to the different preparation conditions.

Chapter 2 Experimental

2.1 Materials

2.1.1 Glass fibres

Boron-free-E-glass fibres under the trade name of Advantex® supplied by Owens Corning-Vetrotex were investigated in this work. The fibre rovings were produced on a pilot scale bushing and were received as 20 kg continuous single end square edge packages. The roving had a nominal tex of 1200 g/m and a nominal fibre diameter of 17 µm. No sizing had been applied to the fibres which had only been water sprayed using the normal cooling sprays under the bushing [69], these samples are referred to commercially uncoated or as received GFs. The sized fibres were coated with a normal rotating cylinder sizing applicator containing a 1% APS hydrolysed solution in distilled water. All fibre packages were subsequently dried at 105°C for 24 hours [71,81]. These samples are referred to as commercially coated GFs.

2.1.2 Chemicals

The chemicals that have been used were purchased from Sigma Aldrich. The silanes were as follows:

- γ -Aminopropyltriethoxy Silane (APS) ($\geq 98\%$)
- γ -Methacryloxypropyltrimethoxy Silane (MPS) (98%)
- γ -Glycidoxypyltrimethoxy Silane (GPS) ($\geq 98\%$)

The rest of the chemicals used are listed below:

- Acetic acid (CH_3COOH) ($\geq 99.7\%$)
- Deionised water (H_2O)
- Deuterated water (D_2O)
- Chloroform (CHCl_3) ($\geq 99\%$)
- 1,4-Dioxane ($\text{C}_4\text{H}_8\text{O}_2$) ($\geq 99.8\%$)
- Sodium hydroxide (NaOH)
- Hydrochloric acid (HCl) (37%)

2.2 Silanes solution treatments

Silanes used in this investigation were prepared with combining different pH values, temperatures and concentrations. The initial treatments followed recommendations from other researchers' investigations in which they showed benefits of different conditions [124]. Further investigation of the conditions was subsequently carried out after analysing the first treatments. All the silane preparations were studied by applying them to unsized GF bundles.

Silane preparation was carried out in deionised water by adjusting the pH of the deionised water, if needed, using a solution of dilute acetic acid (5%). The pH of the deionised water was measured using a pH meter, previously calibrated using 4, 7 and 10 buffer solutions provided with the pH meter [124]. The solutions were prepared using a plastic container with the lid closed at 1% in volume (v/v).

For APS hydrolysis, the reaction by-product is ethanol (C_2H_6O). The boiling points of ethanol and water are 78.4 and 100⁰C respectively, but when it is mixed with water, they formed an aqueous solution with an azeotrope. The liquid composition of this azeotrope is 95.5% in ethanol and 4.5% in water (percentage by weight), whose boiling point is 78.2⁰C.

Elevated temperature (83⁰C) was applied to the APS solution for a time of 5 hours in order to evaporate most of the ethanol by-product. Water is also evaporated in small proportions due to the azeotrope and steam is generated due to the surface tension created on the solution surface, enhance by the elevated temperature (i.e. 83⁰C).

Once the molecules of water-ethanol start to evaporate the closed lid caused water molecules to condense. However, the ethanol molecules remain mostly in vapour phase, as the temperature is above the boiling temperature of ethanol.

For MPS and GPS the hydrolysis reaction by-product is methanol (CH_4O , the boiling point being 65⁰C). Consequently, two different temperatures (73⁰C and 83⁰C) above the boiling point of methanol were investigated for the preparation of MPS and GPS solutions. MPS and GPS were prepared in 1% (v/v), varying the parameters as shown in Table 2.1. It should be noted that these silane preparation methods were based on previous work carried out for bundle tension tests (Appendix 7.3).

The purpose of opening or closing the lid is in regard to the main by-products of the silanes and to the steam generated when heating the solution. Leaving the lid open allows the release of ethanol/methanol vapour along with steam. If the lid is closed the steam condenses and is returned to the silane solution. The lid was either left closed the whole preparation time or opened two times during the process. Hence “open” refers to the lid being initially closed and then completely opened two times, once after 1.5 hours and another time after 3 hours, both for a duration of 15 minutes. The aim of this procedure was to avoid too much water evaporation.

Table 2.1 Silanes 1% (v/v) preparation.

	1	2	3	4	5	6	7	8	9
Silane	APS	APS	MPS	MPS	MPS	MPS	MPS	GPS	GPS
pH	7.5	7.5	7.5	5.0	7.5	5.0	5.0	7.5	5.0
Preparation time (h)	24	5	24	24	5	5	5	24	24
T (°C)	25	83	25	25	73	73	83	25	25

Once the silane solutions were ready for use, glass fibre bundles were completely immersed in the silane solution for 15 minutes, as suggested in the paper by Yue and Quek [125], who showed that the immersion time is not a critical factor in the silane deposition on the GF surface. The samples were then removed from the solution and dried by placing the bundles in an oven at 110°C for 15 minutes using a specially designed rig (Figure 2.1 and Figure 2.2), using a nut, bolt and washer to prevent fibre breakage. The bundles were completely suspended preventing any contact with, and hence damage to, the fibres [81]. Finally, they were left at RT overnight before being prepared and tested.

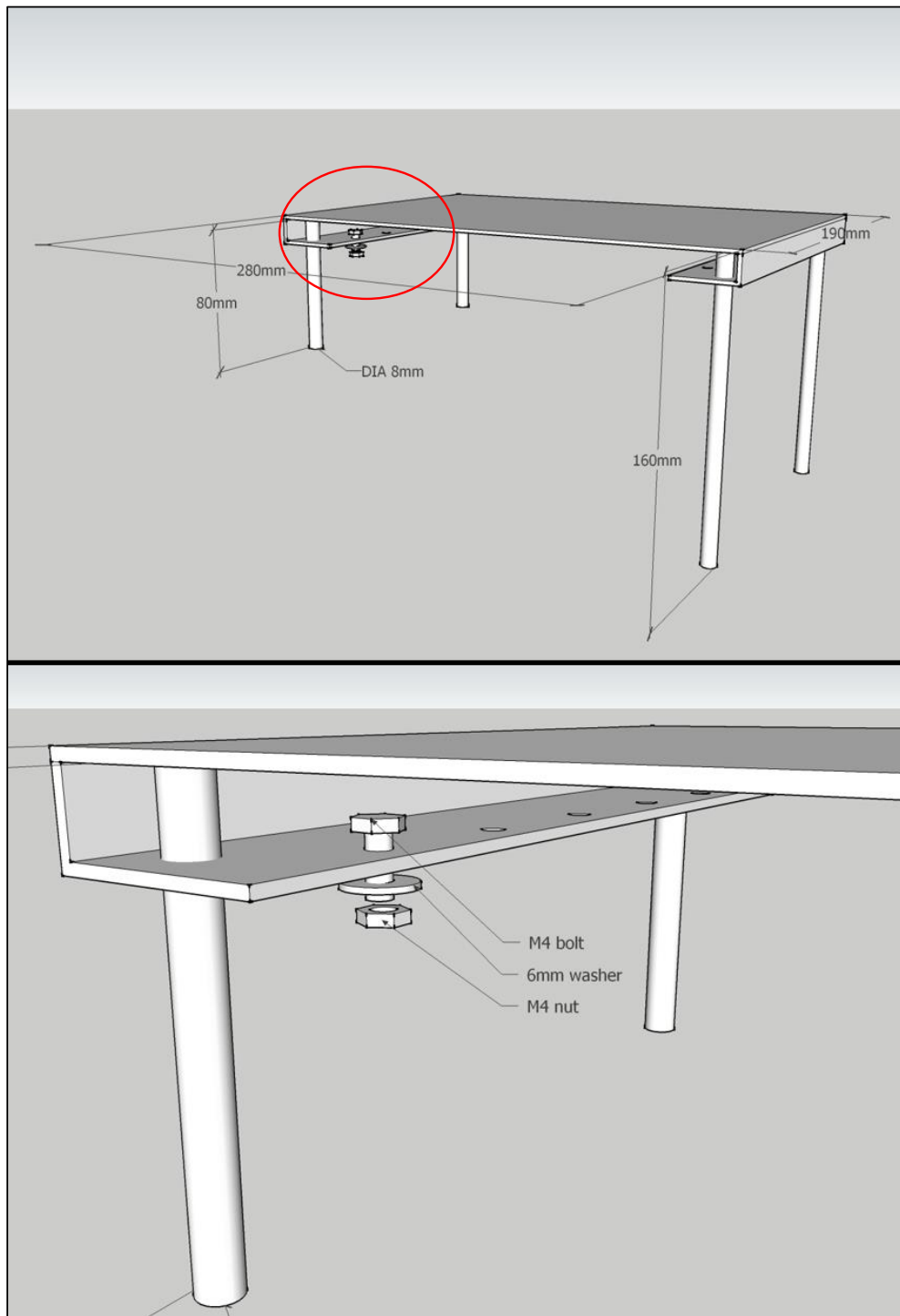


Figure 2.1 Bundles Steel Rig.



Figure 2.2 Bundles Steel Rig. A) GF Bundle. B) Nut, bolt and washer.

2.3 Thermal degradation (TD)

A specially designed steel rig using a nut (Figure 2.2 and Figure 2.1), bolt and washer to prevent fibre breakage, was used to heat treat the bundles. Care was taken to ensure that no damage was suffered by the bundle, damage due to tensile stresses and contact between them, which may cause friction and consequently damage. Once the furnace had been preheated at the required temperature (from 350⁰C up to 600⁰C) for 1 hour, the rig was inserted into the furnace for 25 minutes. Thereupon it was removed from the furnace leaving it cooling to RT for at least 30 minutes [50,126].

To ensure an accuracy of $\pm 15^{\circ}\text{C}$, a thermocouple was also used to check the furnaces temperature.

The thermal degradation temperatures were as follows (Table 2.2):

Table 2.2 Range of thermal degradation temperatures.

Temperature (⁰ C)	25	350	375	400	425	450	475	500	550	600
----------------------------------	----	-----	-----	-----	-----	-----	-----	-----	-----	-----

A wide range of thermal degradation temperatures have been studied, with special focus on temperatures between 350 and 500°C, at intervals of 25°C. Two higher temperatures were also used, 550 and 600°C, to approach the glass T_g .

2.4 Acid and base treatments

2.4.1 HCl treatment

The HCl was used in a 10% v/v in deionised water solution. The solution was prepared by diluting HCl 37% with deionized water in a plastic container, producing 250cm³ of solution. Once the concentration of the HCl was 10% v/v, the thermally degraded GF bundles (250 mm gauge length) were completely immersed in it, leaving them for 1 hour at room temperature. Thereupon the GFs bundles were rinsed in deionized water for at least 1 minute [111]. If this was the only treatment applied to the GFs bundles, a drying process followed, which consisted of placing the bundles in an oven at 110°C for 15 minutes. The oven was preheated for 1 hour [50].

2.4.2 NaOH treatments

The NaOH was prepared in deionised water solution at different concentrations. The concentrations used were 1.5, 3, 5 and 10 M (mol/l). The solutions were prepared using a 0.5 l flask. The NaOH pellets were measured using a balance (Mettler Toledo XS205 DualRange) and were poured inside the flask. Once the amount of NaOH needed for the desired concentration was inside the flask, deionised water was added gradually while continuously shaking the flask. This was done to avoid the possibility of splashes due to the highly exothermic reaction. Once the pellets were properly dissolved, the 0.5 l solution from the flask was poured into a plastic container and then introduced into an oven, which was preheated for 15 minutes at 95°C for 2 hours to ensure that the temperature of the solution was reached. When the solution was ready to use, thermally degraded commercially coated GF bundles (250 mm gauge length) were completely immersed in it for different period of times: 5, 10, 15, 20 and 30 minutes. Depending on the further treatments applied to this GFs, right after this treatment, they were either rinsed for 1 minute in HCl 37% at RT and then deionised water or they were rinsed in hot water (95°C) for one minute as well. The aim of these

post treatments is to remove as much residue from the GF surface as possible. The post treatment used in any case will be explained.

2.5 Single fibre tension test

Card frames were cut from 250 g/m² grade card with tabs with a central cut-out that matched the gauge length chosen for the test, i.e. 20 mm gauge length, as the template shown in Figure 2.3.

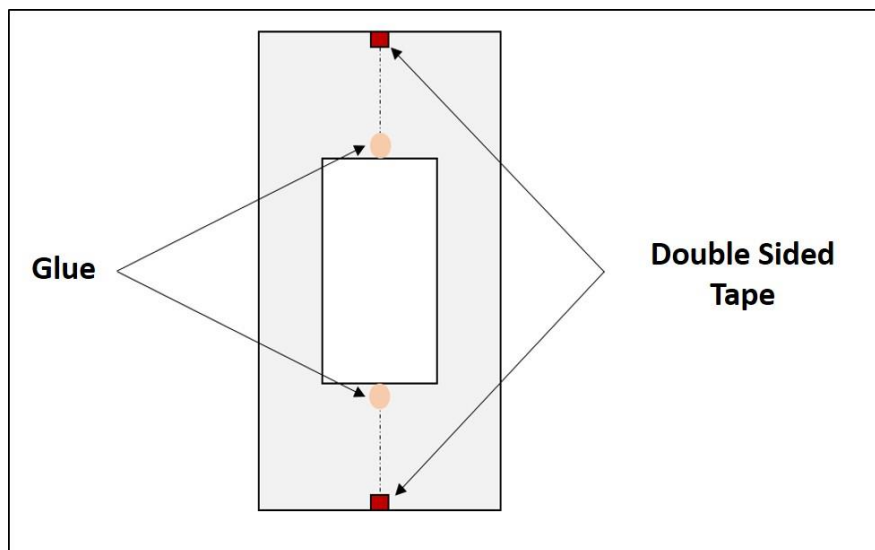


Figure 2.3 Single fibre test template.

Single fibres were meticulously separated from the GF bundle. One end of a bundle is taped to a lamp frame in front of a dark background for better visibility as can be seen in Figure 2.4. Instead of separating a fibre from the free end, the upper part of the bundle was partially cut to let the outermost fibres stick out. A fibre was then gently pulled outward-downward from the upper free end and eventually separated from the bundle. This would avoid fibre rubbing during the separation as much as possible [127].



Figure 2.4 Single fibre separation from GF bundle.

Individual fibres were glued onto a card tabs with a central window cut out to match the desired gauge length for the test as shown in Figure 2.3. It should be noted that the gauge length is actually defined by the distance between the fibre exit points from the glue. The glue should, thus, be placed at the contact point between the fibre and the slot.

Single fibres were fixed to the card at both sides of the window using Loctite™ Gel Superglue, helping with double side tape to prefix the GF before applying the Superglue.

The cross-sectional area of every sample was estimated from a diameter measurement and assuming circular cross-section uniformity of the GFs along the gauge length. An Olympus GX51 optical microscope at 500x magnification was used to obtain a digital photo of each fibre, as can be seen in Figure 2.5. During handling of the fibre in the microscope, care was taken to avoid fibre damage through contact with the microscope objective.

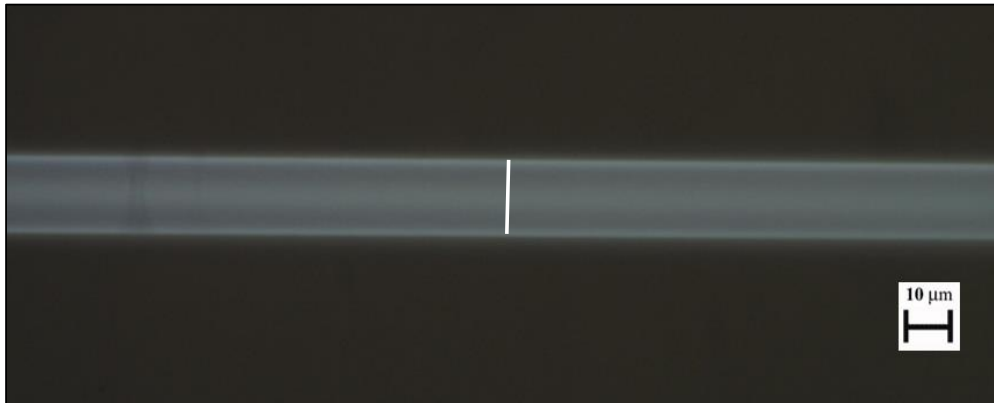


Figure 2.5 Measurement of GF diameter using an optical microscope.

Single fibre tensile properties were determined following the method described in ASTM C1557-03 [128] using an Instron 3342 universal testing machine equipped with a 10 N load cell and operated through the software Instron Bluehill® 2. According to ASTM C1557-03, the axis of the fibre should be coaxial with the line of action of the testing machine within $\delta \leq l_0 / 50$ to prevent bending strain and/or stress concentrations at the point of fibre exit from the tab. δ is the tolerance and l_0 is the fibre gauge length.

The tab ends of the specimen were gripped in the universal testing machine. Once it had been mounted in the test machine, a section of the tab was carefully cut away, leaving the specimen free to be loaded during the test.

Strain estimation was taken from the machine displacement. Only tests where the sample broke within the gauge length were taken into consideration for further data processing, while discarding samples that broke at a distance of 3 mm or less from the clamps. In Figure 2.6 a typical load-extension curve is shown. Due to GFs being brittle, they exhibited a sharp drop in stress after ultimate failure stress.

Fibre strength was then calculated from the load at break at the cross-sectional area, $A = \pi D^2 / 4$, calculated using individual diameter D .

The value of the apparent Young's modulus of the fibre can be determined by the slope of the fitting line in Figure 2.6. Bluehill® 2 software has an Automatic Young's Modulus function which calculates it automatically.

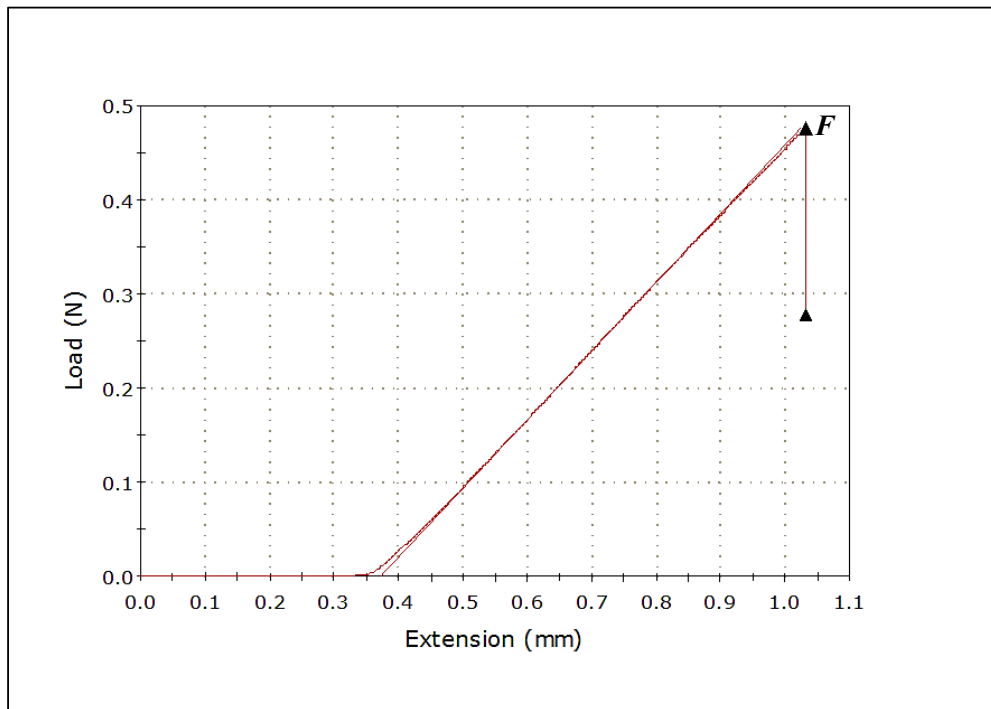


Figure 2.6 Typical load-extension curve for a single fibre test.

The modulus was calculated as follows:

- Searches the data between the first data point with a value greater or equal to the 2% of the maximum load and the maximum load value.
- Carries out a zero-slope yield calculation in order to determine if there is a yield point in the data.
- Uses the first data point as the start value and the yield point or the maximum load point as the end value. It does not matter which one occurs first.
- Divides the data on the extension axis between the start and end values into 6 equal regions with 0% overlap.
- Applies a least square fit algorithm to all of the points in each region in order to determine each slope.
- The pair of consecutive regions that has the highest slope sum is determined.
- From this pair, the region with the highest slope is determined and the modulus is assigned to that region.

In this investigation, Young's modulus was not calculated as the research was mainly focused on the recovery of thermally degraded GFs. Indeed, only one gauge length (20 mm) was chosen to carry out this investigation, and different gauge lengths should be tested if a correct calculation of the Young's modulus would be needed to be determined. This can be explained from the effect of both the gauge length and the compliance. Firstly, there is an inverse relationship between the length of the fibre and the Young's modulus. Then another factor that may affect the resulting modulus is the system compliance, that could be produced by the card frame and/or the glue used to prepare the samples.

The loading rate was adjusted according to the fibre gauge length. The strain rate of 1.5 %/min was used. The tests were carried out at RT and 50% relative humidity.

2.6 Nuclear Magnetic Resonance (NMR)

Samples for the NMR analysis were prepared following the same procedure as shown in section 2.2 for RT and APS prepared at elevated temperatures (ET) but using deuterated water (D₂O) instead of deionised water. Due to instrument sensitivity, 20 cm³ of solution were prepared with 25 % in v/v of APS (i.e. 5 cm³). After the solutions were prepared, the same volume of reference compound was added to them. The reference compound used was 1,4-Dioxane. A reference compound is needed in order to have a fixed value which allow measurement of the changes of other unknown compounds (e.g. from reactions, evaporation, etc.). Using a micropipette, 0.4 cm³ (8 % of the volume of APS in initial solution) of 1,4-Dioxane was added to all the solutions prepared. Once the solutions were ready to analyse they were placed into the NMR using liners, where a liner is a thin tube (with diameters usually of 5 mm) needed to analyse liquid samples, in this case, different APS solutions.

In this particular case, special liners were purchased due to the impossibility of using traditional glass liners with APS as it would react with them. 5 mm Teflon® Tube Liners (8" or 9" length) were purchased from Fluorchem Ltd. ¹H analysis was carried out using an AV3 00 9.4 T Bruker Ultrashield NMR.

¹H analysis provides the chemical shifts measurements based on the resonance position of the bare proton nucleus as the primary standard. A reference compound,

1, 4-Dioxane, is added in each sample and always in the same proportion. It acts as an inert internal standard in the medium (i.e. it does not react/change with the other components). Based on its value the rest of the integrals are calculated and compared in order to have a quantitative relationship between them.

2.7 Fourier Transform Infrared (FTIR)

In order to better understand the positive effect of hot hydrolysed APS on GF strength, APS was prepared at RT and ET (i.e. 83⁰C) and analysed in solutions of water (H₂O) and deuterated water (D₂O). Fourier Transform Infrared Spectroscopy (FTIR) (Appendix A) equipment was used to test for any differences in the polymer in solution as well as the by-products of the reactions, i.e. ethanol (C₂H₆O). Interferometer FTIR equipment was chosen since nowadays almost all commercially available mid-IR instruments are FTIR spectrometers. The advantages are shown below:

- I. Spectral quality.
- II. Data collection speed.
- III. Reproducibility of data.
- IV. Ease of maintenance and use.

Analysis was carried out using three different FTIR instruments which were:

- I. Agilent Technologies 5500 Series Portable FTIR Spherical Diamond Attenuated Total Reflectance (ATR). It uses a type IIa diamond crystal as the interface between the sample and the IR energy. Each spectrum consisted of 128 scans with 4 wavenumbers resolution for liquids with 2 μm depth penetration at 2000 wavenumbers.
- II. Agilent Technologies 5500 Series Portable FTIR Dialpath (transmission). It uses a proprietary liquid transmission sampling accessory called *TumbIIR*, patented by Agilent Technologies. Each spectrum consisted of 128 scans with 4 wavenumbers resolution for liquids with 3 different paths calibrated at 29, 106 and 890 μm.
- III. Agilent Technologies 4100 Exoscan FTIR with the Diffuse Reflectance Infrared Fourier Transform (DRIFT). It uses a single bounce diamond as the

sample interface. Each spectrum consisted of 128 scans with 4 wavenumbers resolution for solids with depth penetration from 200 to 400 μm .

The liquid samples analysed using the ATR and the Dialpath were prepared at RT and ET using different solvents: deionised water and deuterated water. The concentration used was 10% in v/v of APS. The total volume used was 10 cm^3 for each sample. The analysis was carried out at RT and the path used to analyse the solutions for higher resolution was the 29 μm , due to the other two resolutions being higher than needed. The usual wavenumber resolution for liquids and solids are 4 μm and 8 μm respectively.

Films analysed using the DRIFT were also prepared in deionised and deuterated water at 10% concentration using lids to dry and analysed them as the one show in Figure 2.7. Once the solution was ready, a few drops were poured into the middle cavity of the lid until it was filled. The lid with the solution was then dried using an oven at 83 $^{\circ}\text{C}$ for 3 hours and 48 hours.

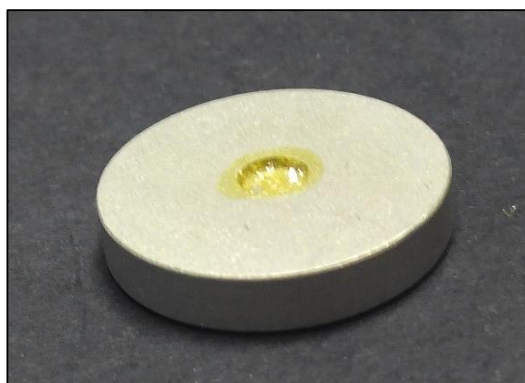


Figure 2.7 Lid used to prepare APS films for DRIFT analysis.

For the GF surface study of the treatments effects on hydroxyl groups the samples were prepared from treated GF bundles. They were carefully converted into a thicker GF bundle of 50 mm length, to ensure a higher homogeneity of the results obtained. The original GF bundle of 250 mm length was cut in 5 bundles of 50 mm length. They were carefully overlapped, avoiding touching any part of them except the extremes. Then, they were fixed together using masking tape at both ends of the bundles, creating a new thicker and shorter GF bundle.

2.8 Scanning Electron Microscope (SEM)

The Scanning Electron Microscope used was a HITACHI SU-6600, a high resolution analytical variable pressure, field emission scanning electron microscope.

Single fibres were meticulously separated from the GF bundle. Then, using a special designed SEM pan, coated with a carbon sticker, the fibres are fixed onto it. The samples were coated in gold using an Edwards S150 sputter coater, to obtain a clearer picture of the fibre surface.

The SEM was used to carry out examination of the commercially coated GF surfaces, thermally degraded, before and after chemical and silane treatments and combinations of both that were applied.

Chapter 3 Results and Discussion

3.1 Regeneration of glass fibre strength

3.1.1 Strength of as received and commercially coated glass fibres

Table 3.1 Average single fibre strength of as received and commercially silane coated GFs.

	Average Tensile Strength (GPa)	95% Confidence Limit (GPa)
As received	1.28	± 0.06
Commercially silane coated	2.26	± 0.12

At least 60 individual fibre samples have been tested for as received and commercially coated. The results can be seen in Table 3.1. The average fibre tensile strength of commercially coated fibres was found to be almost double that of the as received unsized GFs. The error was found to be lower for the as received than the commercially coated ones. As explained above, these results were expected due to the coating effect of GF surface. They confirm the protective effect of APS coating on fibre properties that might be affected by surface defects.

As explain in 1.3.3, the surface defects distribution results in a length dependence of glass fibre tensile strength. The longer the test sample, the most statistically probable it is for that sample to have severe flaws, which affect the measured strength of the fibre. Consequently, there is a direct relationship between the length of the fibre and its measured strength. The results obtained for the 20 mm gauge length used here match with results obtained by other authors [71,82,129].

3.1.2 Strength of as received self-coated glass fibres

Based on previous work results (Appendix 7.3), the effect of three silanes was investigated. These silanes were APS, MPS and GPS. Single fibre tests have shown the effect on strength of GFs, considerably reducing the non-desirable interfibre

friction effect, which clearly occurs during bundle tests, but it does not happen in single fibre tests. The preparation of silanes was carried out varying the pH and temperature of the solution, following the same procedure as for bundle test preparation.

Between 30 and 150 individual fibre samples have been tested for different silanes and preparation conditions, as shown below in Table 3.2.

Table 3.2 Average single fibre strength for as received GFs self-coated with silanes prepared in different conditions.

Silane	T (°C)	Time (h)	Solution pH	Average Tensile Strength (GPa)	Confidence limit (95%)
APS	RT	24	7.5	1.40	± 0.19
APS	83	5	7.5	1.83	± 0.06
MPS	RT	24	7.5	1.13	± 0.19
MPS	RT	24	5.0	1.74	± 0.13
MPS	73	5	7.5	1.41	± 0.21
MPS	73	5	5.0	1.61	± 0.22
MPS	83	5	5.0	1.32	± 0.27
GPS	RT	24	7.5	1.78	± 0.13
GPS	RT	24	5.0	1.75	± 0.17

The average fibre strength for these three different silanes prepared in different conditions, used for coating as received GFs show that the preparation of APS under ET, i.e. 83°C, further improve the mechanical properties of GFs in comparison with RT APS. Apparently, APS conditioning under ET produces a change in the silane when it is still in solution which results in a remarkable increase in GF strength. The GF strength is increased to values almost 40% higher than the baseline, uncoated GFs. In comparison with the RT APS coated GFs, which has only an increase of barely 7%. This is a large increase. With the simple application of temperature to release ethanol

vapour by opening the lid, the APS conditioning makes a positive effect which is reflected in fibre strength when it is applied to the as received GFs.

The extensive investigation carried out with MPS preparation conditions shows that this silane has a better effect on GF strength when the pH has been adjusted to 5. Preparation under elevated temperature conditions, both 73⁰C and 83⁰C, did not produce any significant effect in comparison to MPS preparation at RT. The highest fibre strength has been achieved at RT preparation adjusting the pH to 5. It has to be pointed out that when MPS was prepared at its natural pH and/or ET, the solution become cloudy and several droplets could be seen in suspension, suggesting that self-polymerisation had occurred.

The investigation carried out with GPS showed that the silane solution pH did not appear to have any significant effect on the treated GF strength. When GPS was prepared under ET (73⁰C), the solution appearance was similar to the one seen for MPS in similar conditions, which was the reason no further fibre strength tests were carried out.

In summary, the best ways to prepare these three commonly used silanes in order to raise single fibre strength appear to be:

- I. APS: natural pH and elevated temperatures (83⁰C).
- II. MPS: adjusting the pH to 5.0 and RT.
- III. GPS: adjusting the pH to 5.0 or natural pH and RT.

Comparing the best results obtained for the three silanes, from a fibre strength point of view, they have the same positive effect. On the other hand, when the GF bundles were coated with these three different silanes, before preparation of the single fibre samples, the behaviour was different. The bundles coated with GPS and MPS show a particular malleable behaviour, without apparently any rigidity, whilst the GF bundle coated with the APS show a rigid behaviour and more attachment between the fibres when they were separated to prepare the single fibre samples. This may be related to the reactivity of the APS and may suggest that APS single fibre strength is higher, but due to this stronger attachment between the fibres, the fibre friction produced is higher

and is reflected in a lower fibre strength, while with the other two silanes, apparently, this effect is lower and probably is translated in a lower fibre friction effect.

3.1.3 Strength statistical analysis of as received, commercially silane coated and as received self-coated with RT and ET APS GFs

Data from single fibre strength measurements are often subjected to further detailed statistical analysis such as Weibull analysis [31,33], which has been explained above (1.3.4).

Single fibre tension tests for as received GFs, as received GFs coated with RT and ET APS and commercially coated GFs are presented using the Weibull method in Figure 3.1:

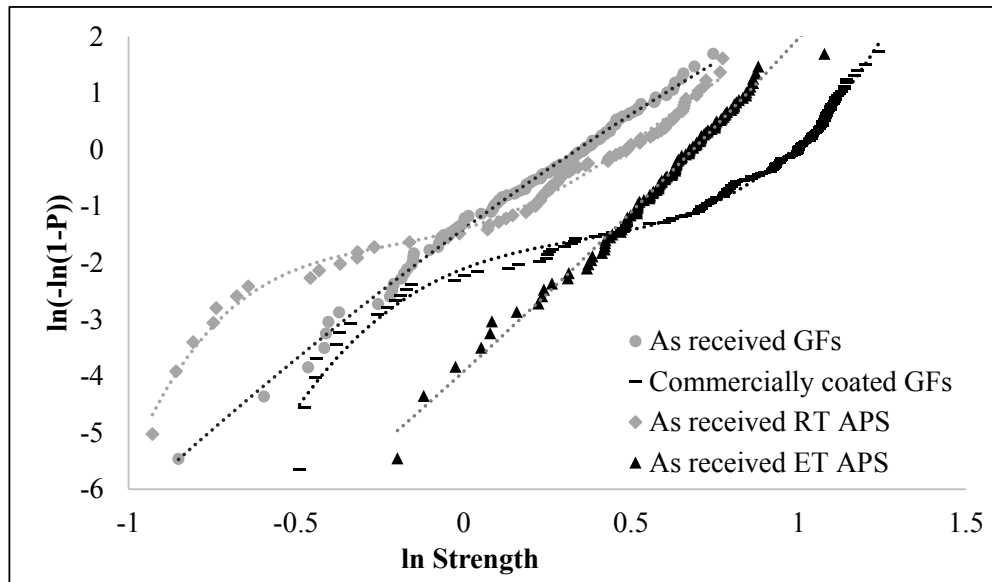


Figure 3.1 Weibull plot of as received GFs, self-coated with RT and ET APS and commercially coated GFs.

The comparison of Weibull plots in Figure 3.1 between as received GFs, as received GFs self-coated with RT and ET APS and commercially coated GFs, probably cover the full range of behaviours observed in Weibull analysis of the data from all fibres and conditions [33,81].

At higher strength values, data obtained for the as received and ET APS Self-coated GFs follow a linear relationship, i.e. unimodal flaw distribution but at lower strengths

the data exhibit a downward deviation in curvature. This has been shown to be caused by the experimental inability to access very low strength values, and as a consequence, the data is poorly fitted by a straight line [33].

The data for the RT APS and commercially coated GFs exhibited a more complex fibre strength distribution, with apparently 3 different regions, suggesting that the failure of fibres is controlled by at least two different types of flaw. Due to this, a multimodal Weibull distribution could be used to describe them.

Although Weibull analysis could be used to further discuss the strength results obtained, a more robust method is rather more reliable to use in order to have less possible uncertainties. Due to this, probability of failure (P_F) has been used to analyse the single fibre tension test results because of its robustness and a less complex theoretical background.

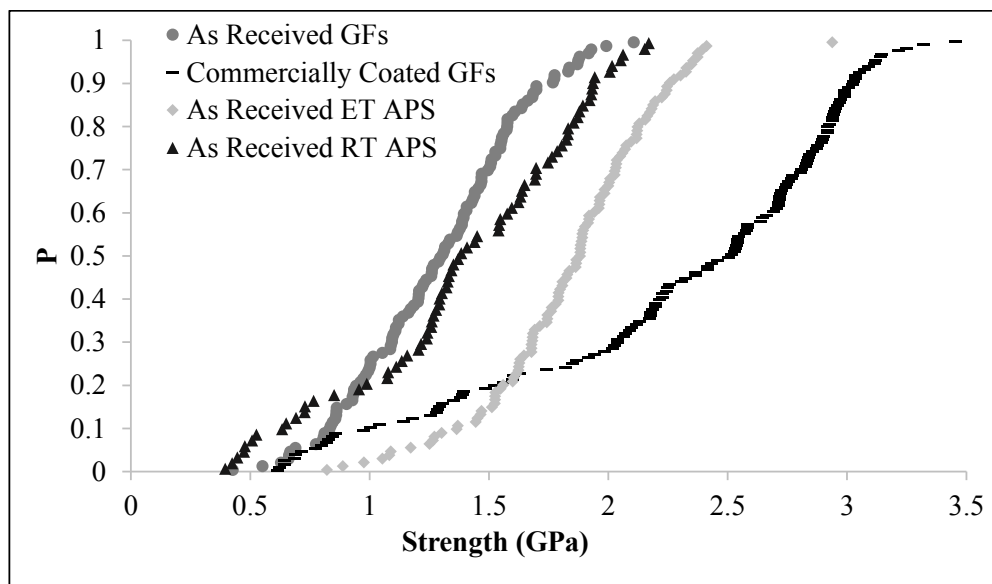


Figure 3.2 Cumulative failure probability for as received GFs, self-coated with RT and ET APS and commercially coated GFs.

Figure 3.2 shows the cumulative failure probability data for as received GFs, self-coated with RT and ET APS and commercially coated GFs. It can be observed that there is a clear separation from commercially coated GFs and as received and self-coated RT APS GFs; this region is likewise spanned by self-coated ET APS.

The first noticeable difference between the 4 different distributions is the appearance of bimodality for commercially coated, RT APS and ET APS GFs whilst for as received GFs it appears to be unimodal. Based on that, it can be clearly suggested that APS is the main reason for this distribution difference. Commercially silane coated GFs show a broad strength distribution that appears to be split in low and high strength regions at 40-50%. It is narrower for ET APS GFs and even narrower for RT APS GFs.

As received GFs are completely different than the commercially silane coated GFs, as shown by the strength values for the last one on the right of the as received GFs. This clearly shows that the commercially coating, i.e. APS, has a significant effect on the retention of fibre strength for high strength values.

When self-coated RT APS GFs are compared with as received GFs, another effect is suggested to happen. Although for high strength values RT APS seems to have a slightly positive effect, for low values it's the opposite, something that does not happen when ET APS is used as self-coating. All the strength values for this treatment are on the right of as received GFs, which clearly shows that on applying this treatment the strength of as received GFs is improved, not reaching values as high as commercially coated but high enough to appreciate the positive effect.

When RT and ET APS GF strength distributions are compared, a couple of important differences can be seen (Figure 3.3). The first one is that whilst for RT APS the distribution splits at around 25%, for ET APS it seems to split at 10%. This suggests that the coating protection provided by ET APS is more evenly distributed than the one by RT APS. The other obvious difference is that the whole ET APS distribution is on the right of RT APS. This clearly means that the positive effect of ET APS on GFs is comparatively higher for all the strength range. For these two treatments the main difference has been the temperature at which they have been prepared. It may be suggested that some fundamental structural changes in occur to the APS when it is prepared in this way and that this change causes an increase in the mechanical performance of GFs.

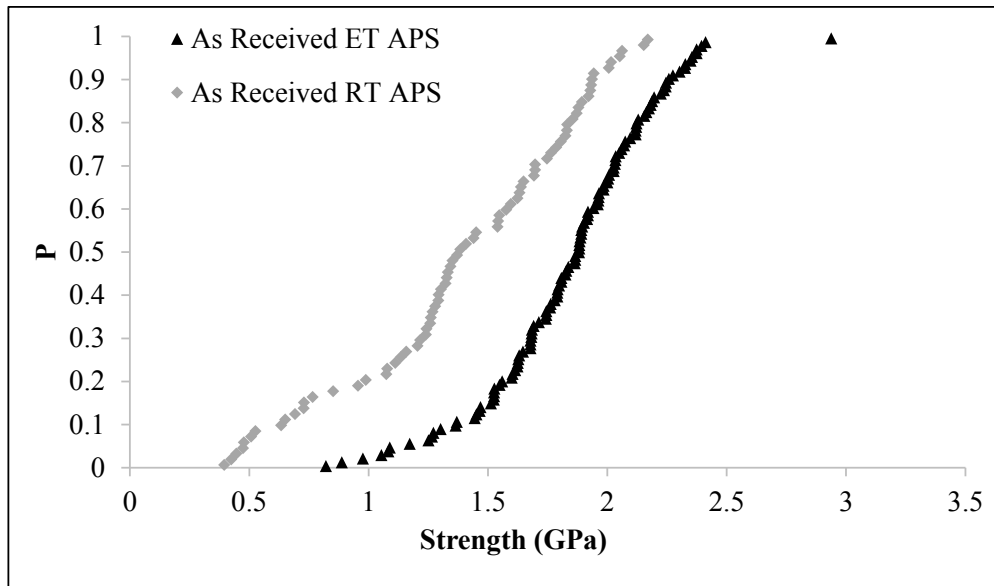


Figure 3.3 Cumulative failure probability for self-coated RT and ET APS GFs.

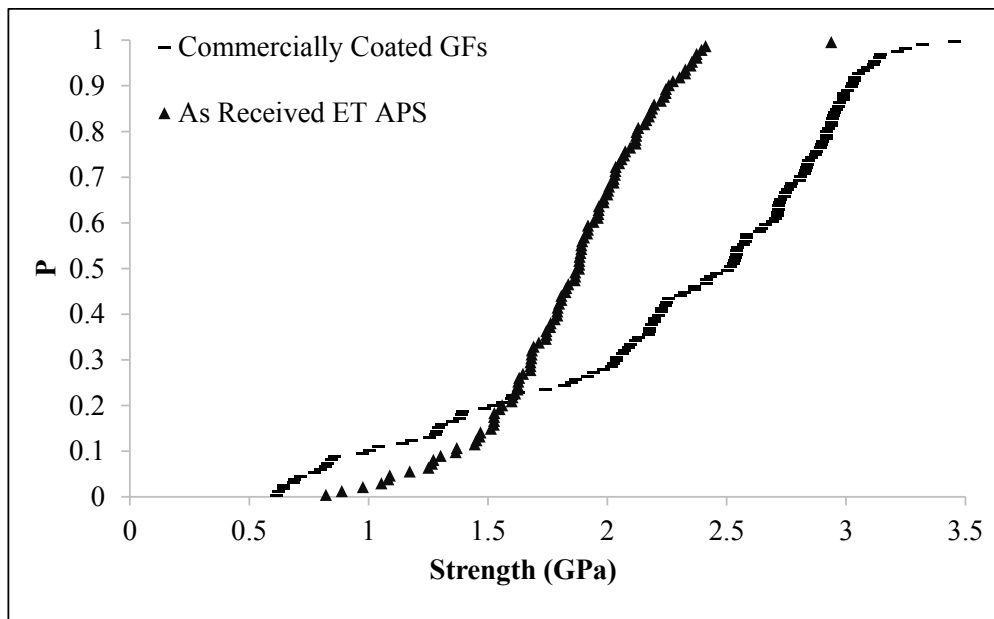


Figure 3.4 Cumulative failure probability for self-coated ET APS and commercially silane coated GFs.

It can be also seen that when commercially coated and ET APS distributions are compared (Figure 3.4), the first one is evidently on the right, except for low strength values, where ET APS is on the right. These trend differences suggest that both

treatments have something intrinsically different, maybe due to structural differences as suggested above for RT and ET APS.

Another comparison has been made between RT APS and commercially coated GF strength distributions (Figure 3.5). Although the strength distribution for commercially coated is clearly on the right, as mentioned above using Weibull analysis, a trend similarity can be seen between them, with the big difference that the strength distribution for commercially coated is quite broad and for RT APS in substantially narrower.

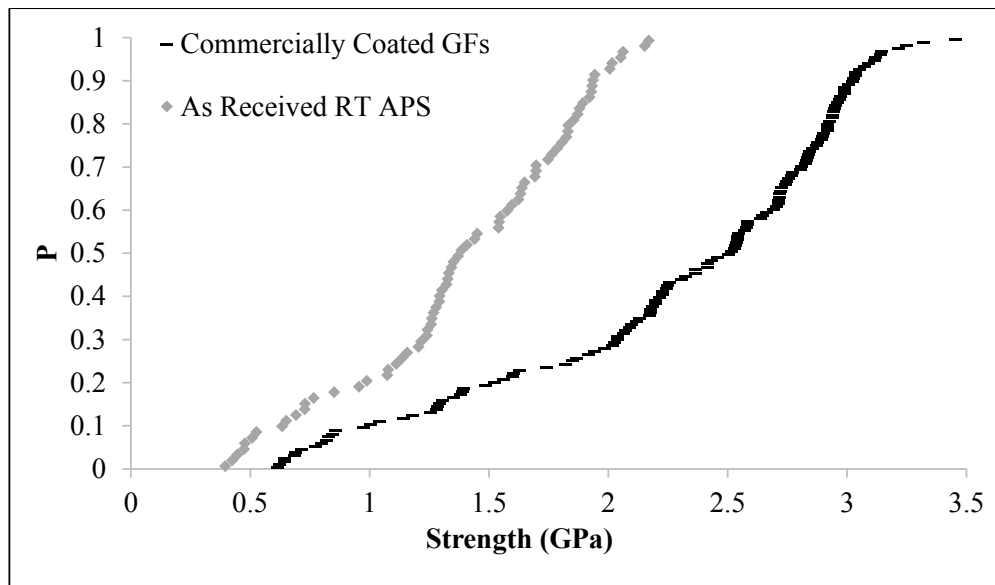


Figure 3.5 Cumulative failure probability for self-coated RT APS and commercially silane coated GFs.

3.1.4 Thermally degraded GFs

Table 3.3 shows results from single fibre tensile testing of the different commercially coated GFs TD at different temperatures (Table 2.2).

In agreement with other authors, there is a clear relationship between the loss in strength with temperature. The higher the temperature is, the higher the decrease will be on GF strength. In Figure 3.6 the results in GF strength versus temperature are plotted to better illustrate the effect of temperature on GF strength.

Table 3.3 Average single fibre strength for commercially silane coated GFs at different TD temperatures.

Temp. (°C)	25	350	375	400	425	450	475	500	550	600
Average (GPa)	2.23	1.76	1.69	1.22	0.86	0.67	0.60	0.56	0.74	0.65
Conf. Limit 95%	0.17	0.20	0.16	0.18	0.09	0.04	0.06	0.05	0.06	0.05

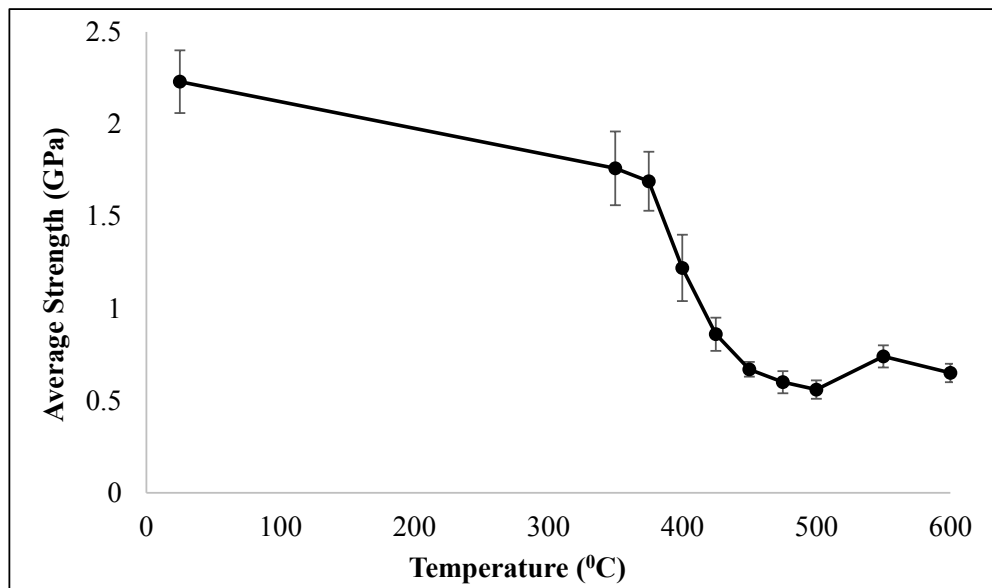


Figure 3.6 Plot of the average single fibre strength for commercially coated GFs at different TD temperatures.

It is clear that there is a significant effect of temperature on GF strength from RT up to 600°C. The strength is decreased to values of around 0.5-0.7 GPa, which is basically a loss of 78-69% of the initial value. Other researchers have investigated this reduction in strength and proposed that it is probably caused by two factors. The first and obvious one is, once again, temperature effect, assuming a shrinkage and structural relaxation occurs as a consequence of the temperatures with structural changes. This was not further studied with length contraction as other researcher have already reported on this phenomenon [16]. It has to also be pointed out that the structural relaxation due to water diffusion, can occur even at temperatures as low as 350°C [130].

The second effect is fibre-fibre friction, which can cause serious damage on GF surfaces and probably create new flaws and cracks. It is well known that silanes protect GFs from frictional damage [81] and may offer some protection against a limited range of temperatures. In this case, high temperatures is likely to cause degradation of the organic part of the APS and the consequent loss of protection of this organic part of the polysiloxane layer on the fibre surface probably contributes significantly to the loss of average fibre strength [81,129].

On the other hand, an effect related to thermal conditioned GFs has been noticed. When the bundles of commercially coated GFs were removed after TD at high temperatures (450°C and higher), the bundle behaviour was observed to be very rigid and inflexible. This behaviour has been discussed and a self-crosslinking of the APS has been proposed. However, it should be noted that when composites are thermally recycled, the matrix is burnt out from the around fibres along with the organic part of the silane which may have bonded to the matrix. In the current project, the organic part of the silane is not crosslinked to any matrix, and is probably free at room temperature. High temperature may induce the Si-OH groups of the silane to self-crosslink providing the bundles their rigid behaviour.

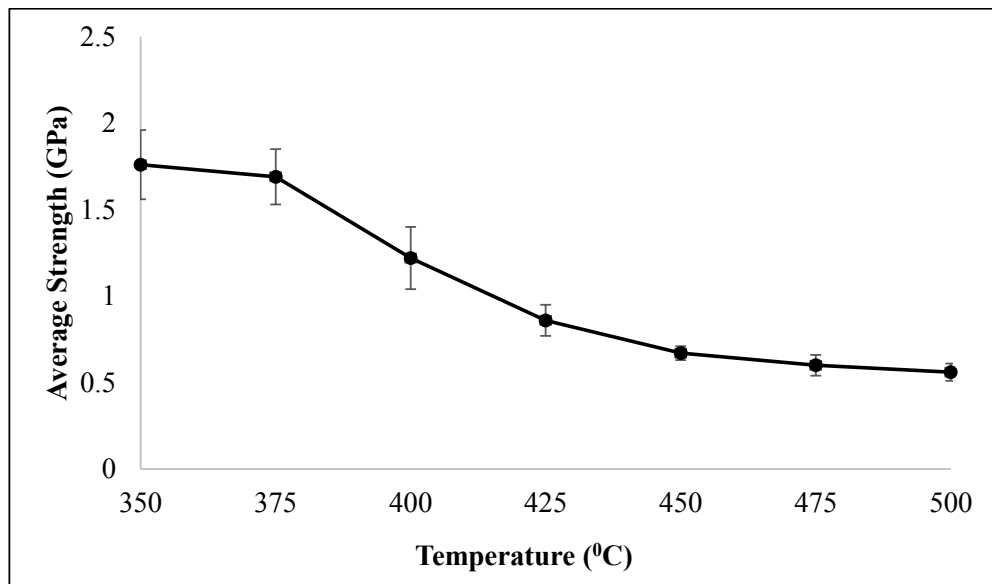


Figure 3.7 Plot of the average single fibre strength for commercially coated GFs at different TD temperatures between 350 and 500°C.

Particularly attention was taken with TD temperatures between 350 and 500⁰C. Between these two temperatures the highest drop on GF strength occurs as can be seen in Figure 3.7. The largest drop occurs between 375 and 450⁰C. These results also suggest that the degradation of the silane is most severe for temperatures of 400⁰C and higher.

Clearly, after the silane is degraded and partially removed from the GF surface, the fibre strength starts to drastically decrease up to 450⁰C, above which the incremental strength loss is not as considerable and the average strength is approximately unchanged within the experimental error.

The relative strength stability for temperature treatments between 450 and 600⁰C (0.5-0.7 GPa), can be misleading. While the average fibre strength results are similar, it is quite probable that more severe structural changes happen with increasing temperature. This was proposed by Thomason [33]. He explained that for a number of successful single fibre results, there are always a large number of fibres which break during sample preparation and mounting. The level of this breakage depending on a complex combination of factors (e.g. force required to remove the fibre from the bundle and experience and abilities of the operator). Consequently, the possibility of not being able to test the weakest fibres of the specimens after higher treatment temperatures probably increases with increasing temperature.

A Young's modulus study was not carried out on these samples since only one gauge length was investigated. As explained in previous chapters, the compliance effect prohibits a proper analysis of the results obtained on fibre modulus when only one gauge length has been used.

3.1.5 Effect of chemical treatments on the strength of thermally conditioned commercially coated GFs

3.1.5.1 HCl treatment

HCl was used in an attempt to increase the concentration of OH⁻ on the surface of heat treated GF. As was discussed in the literature review [111] this may improve the re-attachment of the silane coupling agent to the heat cleaned fibre surface. In this case, the commercially coated GFs were thermally degraded only at 450⁰C [50]. The

range of different treatments and the average single fibre strength after these treatments were applied is shown in Table 3.4.

Table 3.4 Average single fibre strength for 450°C commercially coated thermally degraded GFs with different combinations using HCl 10% v/v.

TD (°C)	HCl 10% v/v (h)	APS 1% (min)	MPS 1% (min)	Av. Strength (GPa)	Conf. Limit 95%
450	-	-	-	0.67	0.04
450	1	-	-	0.57	0.04
450	-	15	-	0.66	0.07
450	-	-	15	0.73	0.06
450	1	15	-	0.80	0.05
450	1	-	15	0.85	0.09

The results obtained show that the HCl treatment has no apparent direct benefit on fibre strength; in fact, the fibres suffer a slight decrease in fibre strength after treatment in HCl. The combination of HCl 10% v/v for 1 hour followed by MPS 1% v/v for 15 minutes showed the highest average strength increase. None of the combinations shown has a clear beneficial effect on fibre strength with increases of only up to 0.18 GPa. The values shown in Table 3.4 are probably not suitable for the reusability of the GFs in composite materials with specific mechanical requirements.

Based on the work carried out by J. Baselga et al. [111], which showed the increase of the hydroxyl group (OH) in the GF surface after being immersed for a period of time in HCl, the effect of RT APS and MPS on strength recovery show a positive effect on GF average strength in comparison with the simple silane treatment. In addition, no reduction in fibre diameter of GF immersed in 10% HCl at RT was reported and hence there was no etching effect similar to that observed with HF treatment.

Results showed that the commonly used RT APS silane, does make a small positive effect on GF strength with HCl treatment; although this positive effect is probably not enough to meet the requirements for reusability. It is suggested that the positive effect

is not higher due to the damage caused during the thermal degradation of the GFs which is severe enough to not be recovered with only silane treatment.

With regard to the MPS, a higher average strength is achieved for the combination of HCl and MPS. Apparently, MPS has a better effect on GF average strength when it is applied directly to the thermally degraded GFs or after HCl treatment. MPS may be a silane to take into real consideration when acid treatments will be applied in order to recover GF strength (i.e. HF treatment) instead of APS, as it seems to be, based on the results obtained, that the performance of APS after HCl treatment is poorer than MPS after HCl [50].

3.1.5.2 NaOH treatment

The effect of NaOH on the mechanical performance of thermally degraded commercially coated GFs was also studied. Two process parameters were systematically varied to investigate the resultant effects of this chemical on GF average single fibre strength. These parameters were:

1. the NaOH concentration.
2. the treatment time.

NaOH concentration effect

As discussed in the literature review, NaOH solution can react with silica-based glass. Furthermore, the solution was presented to be more reactive with glass when maintained at a higher temperature and when present in caustic concentrations, i.e. with molarities of 1.5mol/L (M) or higher. Therefore, to both achieve sufficiently high temperature yet also remain below the solution's boiling point, 95⁰C was chosen as the temperature at which NaOH was applied. All the NaOH treatment solutions used were heated for at least 2 hours in the oven to ensure that the solution reached the desired temperature. The thermally degraded GFs were then completely immersed in the preheated solution for 10 minutes, leaving the container with the solution and the bundle in the oven. The concentrations of NaOH solution in deionised water used for the treatments were: 1.5, 3, 5 and 10M (as explained in 2.4.2). These four NaOH concentrations were applied to GFs that had been thermally degraded at three different

temperatures, 400, 450 and 500⁰C for 25 minutes. The average single fibre strength after these treatments are shown in Table 3.5 and Figure 3.8.

The results obtained show that the most interesting concentration of NaOH is 3M, due to the fact that it is the one that achieves higher average fibre strength. However, it is noted that, for temperatures of 500⁰C or above, the average strength cannot be restored to the target value for any of the molarities used under these conditions. It is therefore suggested that NaOH is suitable to repair the damage caused by thermal degradation temperatures of 450⁰C or below only. Whilst a limitation to the capabilities of the use of NaOH to recover tensile strength of more severely thermally degraded GFs, it is notable that these results clearly show increases to the average strength to more than reasonable values suitable enough for the treated GF to be reused in composites.

Table 3.5 NaOH concentration effect on average single fibre strength of thermally degraded commercially coated GFs.

Temperature (⁰ C)	NaOH solution molarity	0	1.5	3	5	10
	(mol/l)					
400	Av.Strength (GPa)	1.22	1.22	2.1	1.46	1.71
	Conf. limit 95%	0.18	0.16	0.19	0.17	0.21
450	Av.Strength (GPa)	0.67	0.81	1.78	1.58	1.28
	Conf. limit 95%	0.04	0.08	0.18	0.15	0.21
500	Av.Strength (GPa)	0.56	0.51	0.61	0.53	0.59
	Conf. limit 95%	0.05	0.12	0.17	0.04	0.06

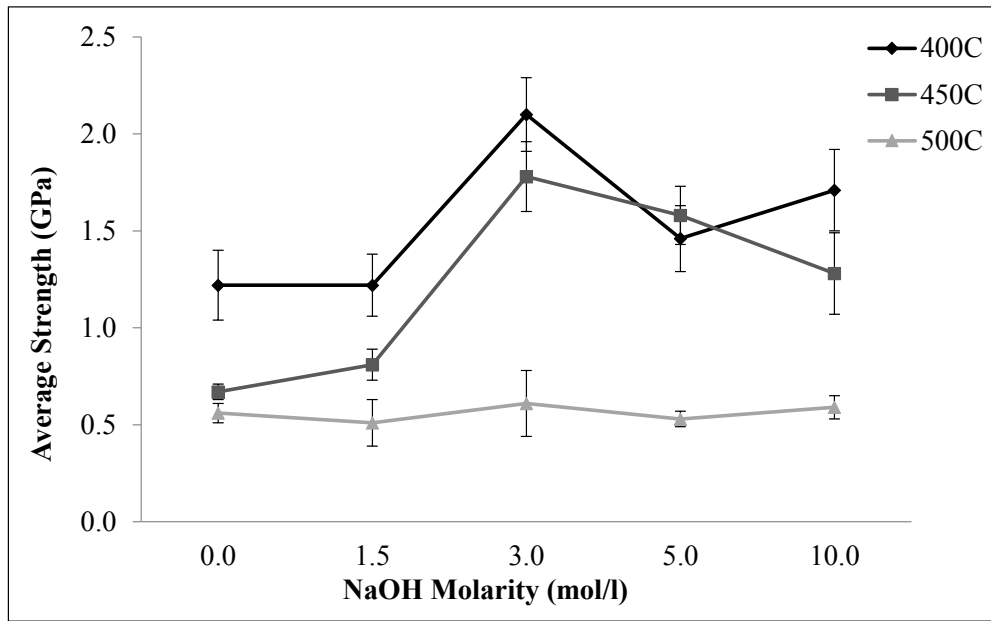


Figure 3.8 NaOH solution concentration effect on average single fibre strength of TD commercially coated GFs.

NaOH treatment time effect

Once the most suitable concentration of NaOH solution was found, i.e. 3M, a treatment time effect investigation was also carried out with commercially coated GFs heat treated at 400°C for 25 minutes. Table 3.6 presents the data obtained for single fibre tensile strength vs. NaOH solution immersion time.

Table 3.6 3M NaOH solution treatment time effect on average single fibre strength of TD commercially coated GFs.

Treatment time (min)	0	5	10	30	120
Av. Strength (GPa)	1.22	1.74	1.88	1.63	1.39
Conf. limit 95%	0.18	0.17	0.18	0.14	0.16

The results in Table 3.6 showed that the most effective treatment times are 5 and 10 minutes, with 10 minutes treatment apparently providing slightly higher strength recovery, although both results are within experimental error. Considering this

information, NaOH immersion time of 10 minutes was employed for all future NaOH treatment experiments undertaken

The above results also suggested that for longer NaOH treatment times, the initially positive effect of NaOH on GF average strength may be lost at longer treatment times. This can be seen in that for NaOH treatments of longer 10 minutes the average fibre strength starts to decrease again. As mentioned before, this may be due to a harmful effect of prolonged exposure to NaOH on the GF surface, or excess of deposition of NaOH and other subproducts as will be explained with SEM pictures (3.6)

3.1.6 Effect of ET APS on the strength of thermally degraded commercially coated GFs

The positive effect on single fibre strength shown by ET APS for the as received GFs (3.1.2) was also investigated on TD commercially coated GFs. Three thermal degradation temperatures have been applied: 400, 450 and 500°C. ET APS was then applied for 15 minutes, with the same procedure as explained in chapter 2.2. The results obtained for GF average strength are shown in Table 3.7.

Table 3.7 Average single fibre strength of TD commercially coated GFs self-coated with ET APS.

		400°C	450°C	500°C
TD	Av.Strength (GPa)	0.81	0.67	0.56
	Conf.limit 95%	0.06	0.04	0.05
TD + ET APS	Av.Strength (GPa)	1.68	0.69	0.56
	Conf.limit 95%	0.16	0.04	0.06

As can be observed in Table 3.7, ET APS maintains a significant beneficial effect on 400°C TD commercially coated GFs, exhibiting a substantial single fibre tensile strength increase following re-coating. However, for 450°C and higher, no significantly positive benefit of re-coating with ET APS was observed. These results suggest that ET APS still has a positive effect due to protection provided by them and probably a healing effect, when the GFs are still not severely damaged due to the temperature effect. For higher temperatures, the GF become seriously affected by the temperature effect, ET APS cannot increase the fibre strength because the damage

suffered by the GFs is more severe and a APS coating alone is not enough to significantly recover the fibre strength loss.

3.1.7 Effect of pre-washing of APS from commercially coated GFs

On removal from the oven after thermal degradation at temperatures of 450⁰C or higher, it was noticed that the mechanical rigidity of the commercially coated GFs had significantly increased, behaving as a stick-like, non-flexible bundle.

It was proposed that this untypical rigid behaviour of the GF bundles was caused by a crosslinking reaction of the APS that coated the GFs facilitated by the high TD temperatures, at which APS is supposed to degrade. It is theorized that this crosslinking effect may not be observed in fibres retrieved from recycling of composite materials, as partial silane reaction with the composite matrix would have occurred. This suggested crosslinking reaction may be the cause of this extremely rigid behaviour.

To minimise the occurrence of this silane crosslinking effect, a simple pre-treatment was carried out on the fibre bundles. Prior to thermal conditioning, the bundles were completely immersed in deionised water at 70⁰C for 4 hours, with the intention of removing part of the silane coating in order to minimise as much crosslinking as possible. Immediately after the bundles were dried in a furnace at 110⁰C overnight to ensure they were completely dried before any subsequent TD was performed.

As shown in Figure 3.9, the effect of the prewashing clearly positively affected the strength of the fibres for 450 and 500⁰C thermally degraded GFs, but not for 600⁰C. For these first two temperatures, it may be said that prewashing completely or partially removes the silane, avoiding the damage due to the crosslinking created during the thermal degradation. For GFs TD at 600⁰C it is thought that the damage caused by the heat treatment on the fibre is more severe than the friction effect that may occur due to the silane crosslinking and hence dominates the resultant tensile strength.

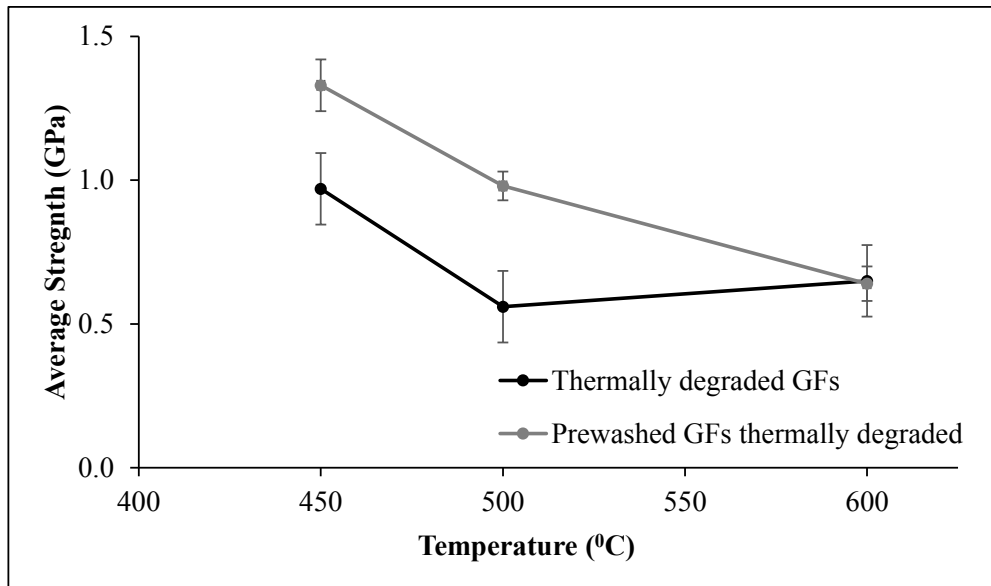


Figure 3.9 Prewashing effect on average single fibre strength of TD commercially coated GFs.

3.1.8 Combined effect of Prewashing, HCl, NaOH and ET APS

Considering the results of these individual chemical treatments on single fibre tensile strength of TD GFs, several combinations have been investigated to identify any synergistic effects on TD GF tensile strength recovery.

The combined treatments investigated were as follows:

- Prewash (PW) followed by TD and then ET APS.
- PW followed by TD and then NaOH 3M for 10 minutes and finally washed with HCl 37%.
- PW followed by TD and then NaOH 3M for 10 minutes, then washed with deionised water and finally ET APS.

In the last of these combinations, after NaOH treatment, the GFs were washed with deionised water instead of HCl due to a previously observed negative effect on APS when it is applied following an acid treatment [50]. The results for the treatments listed above, for 3 different thermal degradation temperatures are shown in Table 3.8. These results can also be seen in Figure 3.10.

Table 3.8 Summary of average single fibre strength of the commercially coated GFs TD at different temperatures using new treatment combinations.

	1	2	3	4	5	
Treatment	TD	PW+TD	PW+TD+ APS	PW+TD+ NaOH	PW+TD+ NaOH+APS	
450°C	Av.Strength (GPa)	0.67	1.33	1.33	1.51	1.85
	Conf.limit 95%	0.04	0.09	0.09	0.11	0.10
500°C	Av.Strength (GPa)	0.56	0.98	1.22	1.44	1.66
	Conf.limit 95%	0.05	0.05	0.09	0.08	0.10
600°C	Av.Strength (GPa)	0.65	0.64	0.89	1.42	1.54
	Conf.limit 95%	0.05	0.06	0.05	0.08	0.08

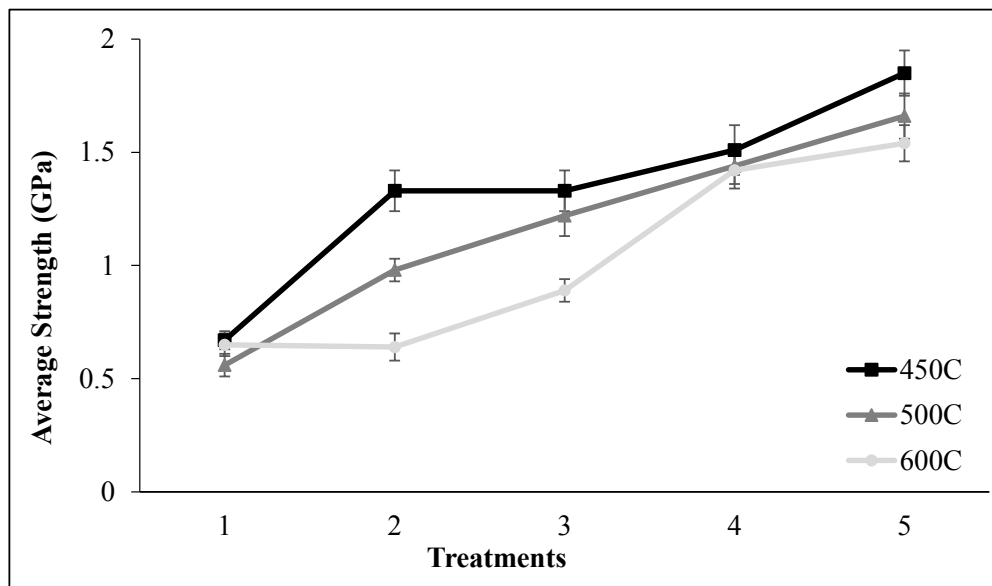


Figure 3.10 Average single fibre strength for the different treatment combinations.1: TD; 2: PW and TD; 3: PW, TD and ET APS; 4: PW, TD, NaOH; 5: PW, TD, NaOH and ET APS.

The results obtained for 1 and 2 have been discussed previously in sections 3.1.4 and 3.1.7. Regarding treatment 3, the combination in which both PW and ET APS is applied, it is noted that there is no significant strength increase over treatment 2 when the TD temperature is 450⁰C. However, a significant strength increase was obtained for TD at the two higher temperatures. For the first temperature (i.e. 450⁰C), the reason why ET APS gave no apparent additional positive effect might be due to the fact that additional protection from a further APS coating is not needed at all due to the fact that the GF surface damage caused by the thermal conditioning is not as severe at this lower temperature. Consequently, the flaws are probably not healed at all. For the two higher temperatures there is a clear increase in fibre strength, confirming that ET APS has a beneficial effect on the fibre surface, protecting the fibre and also possibly healing some of the surface flaws.

Treatment 4 was the application of the hot alkali solution, i.e. NaOH 3M at 95⁰C to prewashed TD commercially coated GFs. A significant increase in fibre strength from this treatment is clearly observed for all three TD temperatures. In particular for the TD 600⁰C sample, the NaOH treatment increases the fibre strength up to 1.42 GPa, which is more than twice the base line value of 0.65 GPa. For the two lower TD temperatures the increase is also significant, reaching values around 1.50 GPa. These results clearly show the beneficial effect of NaOH on TD GF tensile strength. As outlined previously, the positive effect of NaOH is perceived to be due to the chemical reaction of the NaOH solution with the GF surface and the consequent etching which removes the defects present on the GF surface which were caused by the TD treatments.

Treatment 5 is a combination of all of the previous treatments: PW, NaOH and ET APS. The results on fibre strength regeneration are the greatest of all of the different combinations applied, with values of average fibre strength values greater than 1.50 GPa for all TD temperatures and TD at 450⁰C achieving an average strength of 1.85 GPa. This combination has two principal beneficial implications. The first is that of the high recovery in fibre strength exhibited by the GFs, which is sufficient to make them potentially suitable for reuse in composite applications. Secondly, by applying the ET APS, the GFs are both protected against external factors (e.g. friction between fibres, moisture, etc. during further processing) and ready to be used in a composite,

where the silane enhances the fibre-matrix interface needed to produce a suitable composite.

These results clearly show that this combination of treatments offers high potential with respect to tensile strength regeneration in TD GFs. There is no doubt that significant strength recovery has been demonstrated beyond the values required to facilitate reuse in composite applications, using a relatively low cost chemical such as NaOH. However, the problem that remains to be solved is the excess of residual deposits on GF surface that sometimes appears (as shown in 3.6). This residue may negatively affect the performance of recycled regenerated fibres in composites through hindering the creation of a suitable interface.

3.2 NMR investigation of ethanol removal from APS solution

NMR was used to investigate the effect of temperature upon ethanol removed from APS solution. As explained in 2.2, the by-product from the hydrolysis of APS is ethanol and the boiling point of the azeotrope of ethanol-water solution is 78.2°C, hence a temperature of 83°C was maintained for 5 hours to ensure vapourisation.

First, an APS proton (¹H) NMR spectra in an anhydrous medium has been obtained using RT chloroform, to give a reference point of the non-reacted APS. This baseline reference is shown in Figure 3.11:

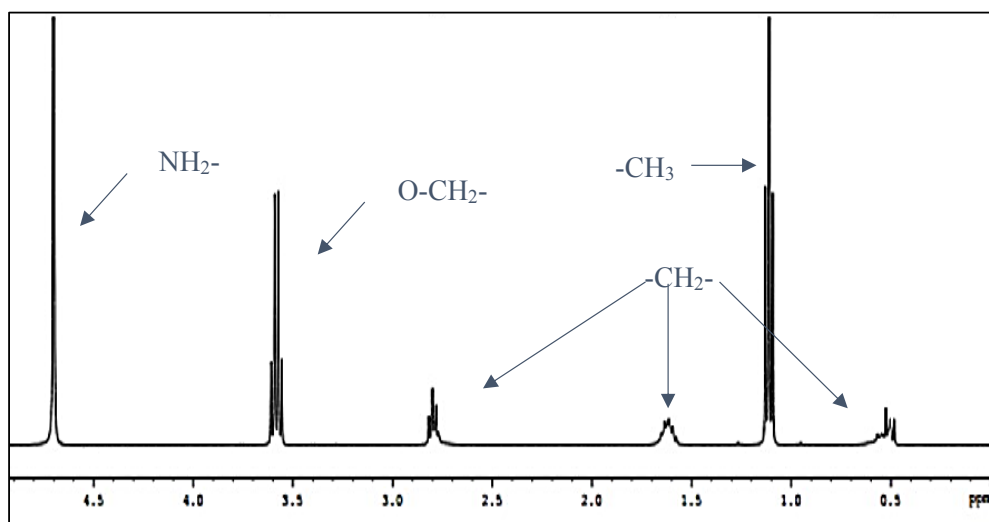


Figure 3.11 ¹H NMR spectrum of APS in Chloroform at 20°C (RT).

The proton chemical shifts obtained correspond to different hydrogens bonded to the carbons that form the APS molecule. These signals obtained from the APS in chloroform can be seen in Figure 3.11. The predicted chemical shifts for protons in APS (from KnowItAll® Software database) are shown in Figure 3.12:

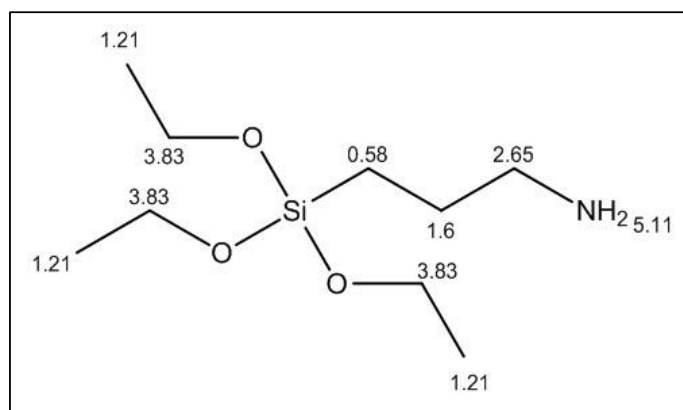


Figure 3.12 Predicted ^1H chemical shifts (ppm) for γ -APS.

The predicted proton chemical shifts obtained are at almost the same chemical shift as those obtained in chloroform. These signals obtained from the APS in chloroform and the predicted proton shift for 1, 4-Dioxane in D_2O are summarised in Table 3.9. It is notable that *ppm*, which appear in the X axis of the protons shifts spectra, are referred to Tetramethylsilane (TMS), which is generally used as the standard to determine chemical shift of compounds, so δ_{TMS} is equal to 0 ppm.

Table 3.9 ^1H chemical shifts of carbons which form the APS and 1, 4-Dioxane at RT.

^1H	ppm
CH_2 (Propyl group)	2.25/1.59/0.66
CH_2 (Ethyl group)	3.85
CH_3 (Ethyl group)	1.26
NH_2 (Amine group)	4.80
1, 4-Dioxane [131]	3.75

Since the volume of reference compound added was the same in each sample, the integral of 1, 4-Dioxane proton chemical shift was given the value of 1. Based on this reference value the remaining integrals are calculated and compared in order to have a quantitative relationship between them.

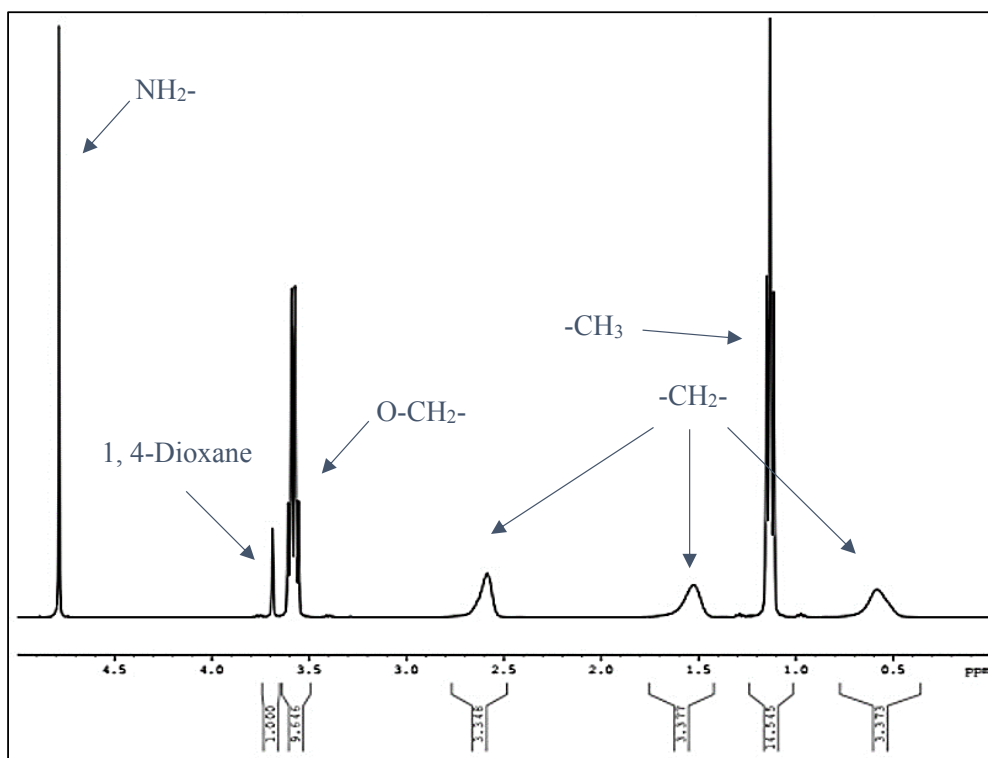


Figure 3.13 ^1H chemical shifts of 25% v/v RT APS in D_2O .

The difference between RT APS and ET APS can be seen in Figure 3.13 and Figure 3.14. The integral values corresponding to the CH_3 and O-CH_2 groups, which correspond to the ethanol, are significantly lower for ET APS in comparison with RT APS.

Comparing both preparation conditions, the ethanol removed from the solution shows clearly that whilst the RT APS still contains 100% of the ethanol released from the APS hydrolysis, the ET APS has lost almost 80% of the ethanol produced.

It also can be seen from the NMR data that the ^1H shifts corresponding to the CH_2 from the propyl group (at 2.6/1.5/0.5 ppm) have changed, i.e. there are wider ^1H chemical shifts when both ET APS and RT APS are compared with APS in chloroform

(Figure 3.11). Furthermore, APS in chloroform ^1H chemical shifts are composed of three small sharp peaks, whilst for the hydrolysed RT and ET APS, it is only one peak. This may be related to the polymerisation of the APS.

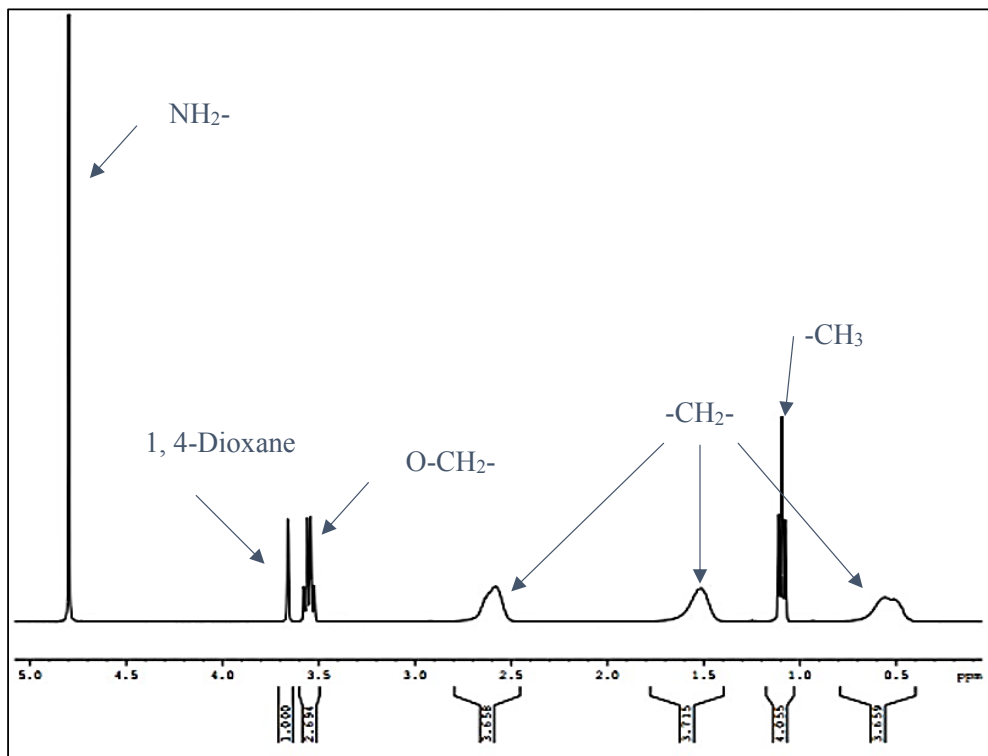


Figure 3.14 ^1H chemical shifts of 25% v/v ET APS in D_2O .

These results show that changing the temperature at which the APS solution is prepared significantly affects the ^1H chemical shifts related to the ethanol/ethyl group. A clear difference between RT APS and ET APS can be seen for those chemical shifts. This could suggest that the decreases in these chemical shifts are due to the removal of ethanol from the solution, and the small chemical shifts corresponding the O-CH_2 and CH_3 , which still can be seen in Figure 3.14, may be due to non-reacted ethyl groups. Comparing the integral results, as shown in Figure 3.15, it can be seen that up to 80% of the ethanol/ethyl produced by the APS hydrolysis can be removed from the solution.

Further analysis was carried out to better understand the relationship between the temperature and the effectiveness of ethanol removal from the solution during the APS

preparation process (^1H chemical shifts can be shown in 7.2.1). The results are shown in Figure 3.15:

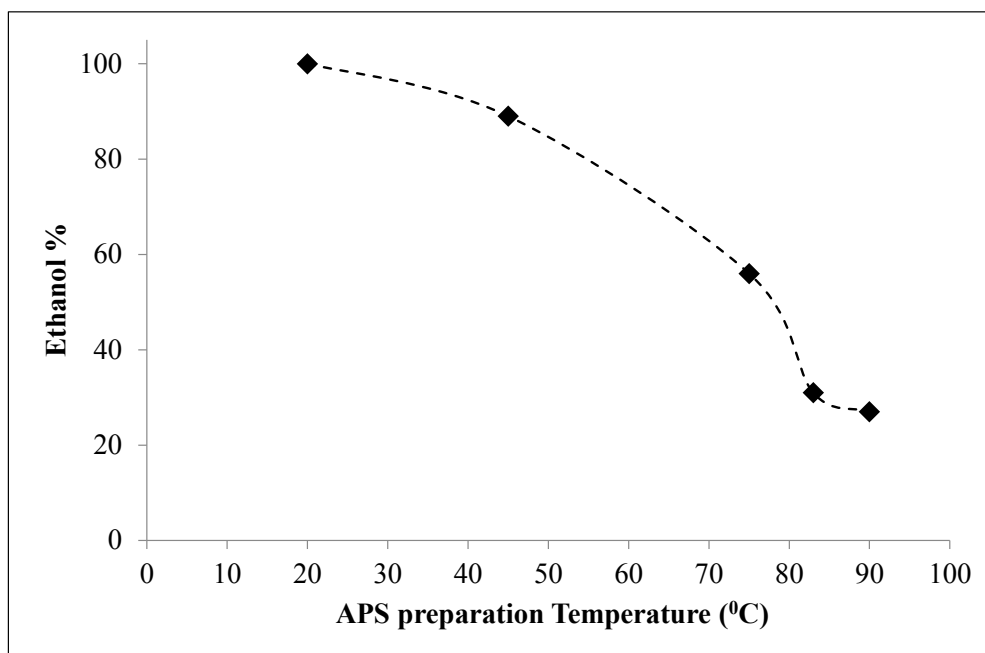


Figure 3.15 Ethanol presence during 25% v/v APS in D_2O preparation at different temperatures.

These results show the presence of a relationship between the hydrolysis temperature and the fraction of ethanol lost from the solution, suggesting that at a temperature of 80°C or above, a significant percentage of ethanol can be removed from the solution. For temperatures higher than 80°C , the data presented in Figure 3.15 indicates that the extent of the ethanol removal becomes relatively constant. This can be explained from the reaction rate of APS.

It is suggested that for RT APS that the ethanol/ethyl remaining in solution is almost 100% of the initial concentration, and that this is predominantly due to ethanol [47]. It is possible that a small fraction of the ethanol is released but this is probably insignificant in comparison to the ethanol remaining in solution.

In summary, these results show that increasing the temperature of the APS solution increased the effectiveness of ethanol removal from the solution. It is suggested that temperature may also affect the self-condensation of APS and therefore the

polymerisation of APS, but this cannot be further investigated using NMR due to their limitations. These results suggest that a polymerisation occurred for both RT and ET APS preparations, but not to a sufficient extent such that the differences between them could be conclusively observed.

3.3 FTIR characterisation of ET APS

Based on the improvement shown in GF strength results obtained in 3.1.2, APS was identified as an interesting candidate for further study. Consequently, RT and ET APS were further investigated using FTIR spectroscopy with various interfaces in order to determine any structural differences between them.

3.3.1 FTIR characterisation of ET APS in solution

3.3.1.1 Attenuated Total Reflection (ATR) spectra

The ATR results presented in Figure 3.16 show spectra of 10% v/v APS solution in deionised water, prepared at RT and ET, with the spectra of an ethanol–water mixture with the equivalent amount of ethanol released when 100% of the APS hydrolysis would have been reached (i.e. 7.5% v/v ethanol solution in deionised water) also shown for reference purposes.

There are several regions of the spectra of particular importance for the structural differences between the APS prepared at RT and ET. In particular, one region is between 3100 and 2700 cm^{-1} and the other is between 1350 and 850 cm^{-1} . These regions of the spectra are magnified in Figure 3.17 and Figure 3.18 for clarity.

The spectral region between 3100 and 2700 cm^{-1} (Figure 3.17) shows four bands, two whose intensities are attributed mainly to ethanol and the other two whose intensities are attributed mainly to the polymerised APS: 2985 cm^{-1} is assigned to be the band of asymmetric stretching $(\text{C-H})_{\text{CH}_3}$, 2940 cm^{-1} is $(\text{C-H})_{\text{CH}_2}$ asymmetric stretching with a major contribution from the propyl group of the APS, 2905 cm^{-1} is $(\text{C-H})_{\text{CH}_3}$ symmetric stretching, and 2875 cm^{-1} is $(\text{C-H})_{\text{CH}_2}$ symmetric stretching with major contribution from the propyl group of the APS and also from ethanol [49,51,77,121].

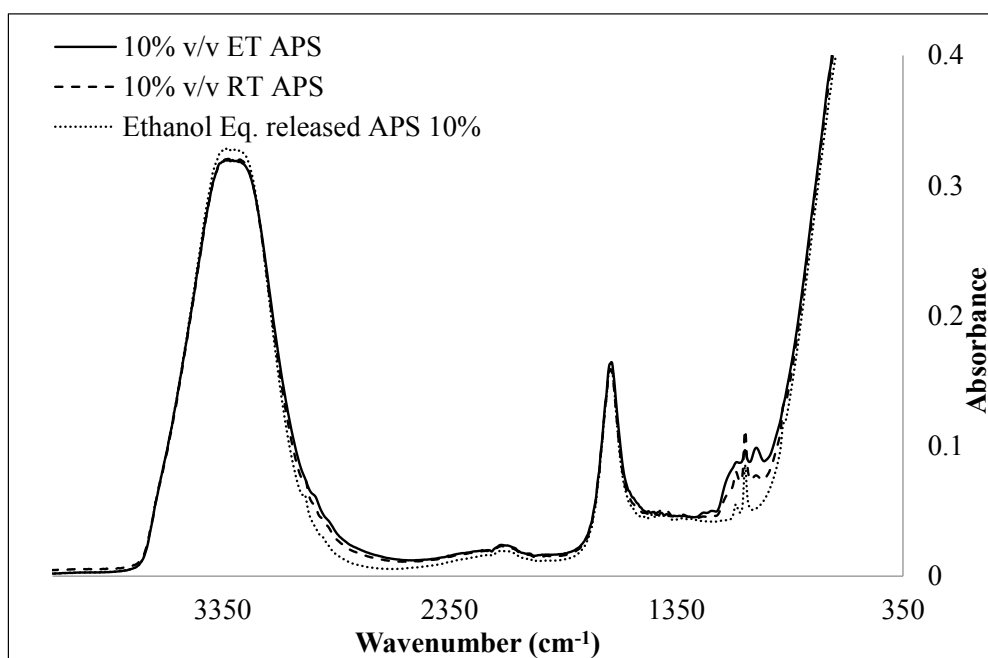


Figure 3.16 ATR spectra of 10% v/v APS in deionised water solution prepared at RT and ET, and an equivalent % of ethanol released by APS in deionised water solution (7.5% v/v).

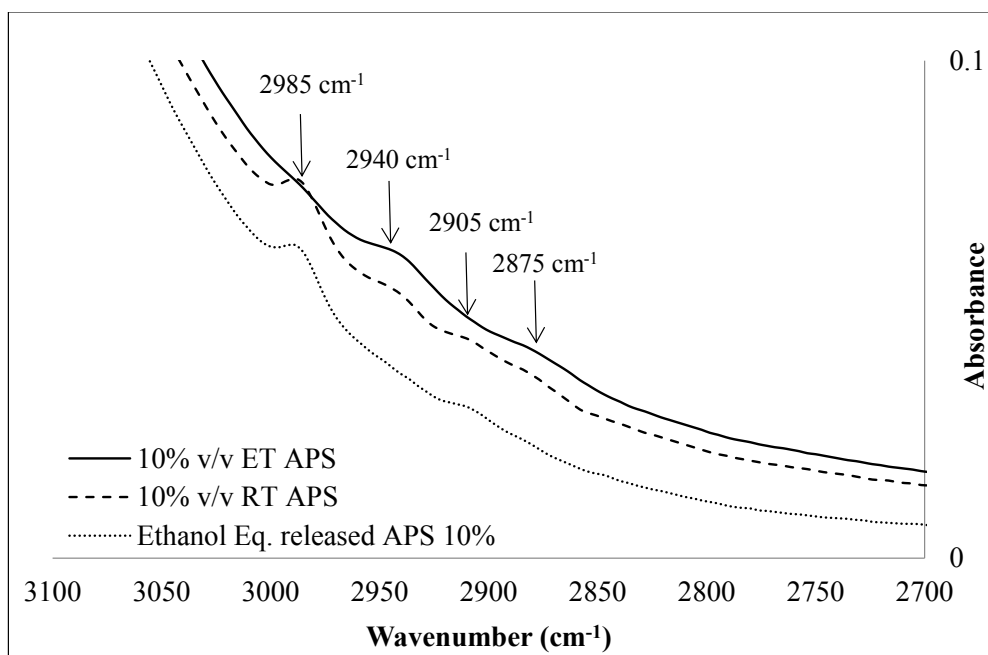


Figure 3.17 Magnification of ATR spectra of 10% v/v APS in deionised water solution prepared at RT and ET, and an equivalent % of ethanol released by APS in deionised water solution (7.5% v/v) between 3100 and 2700 cm^{-1} .

In Figure 3.18, in the spectral region between 1350 and 850 cm^{-1} , five different bands can be seen: $(\text{C-O})_{\text{COH}}$ symmetric stretching from the ethanol and also contribution of $(\text{C-O})_{\text{SiOC}}$ symmetric stretching from the unhydrolysed APS, and $(\text{C-O})_{\text{COH}}$ asymmetric stretching of the ethanol at 1085 cm^{-1} and 1045 cm^{-1} . (Si-O-Si) symmetric stretching from the polymerised APS and a minor contribution of (Si-OH) deformation at 995 cm^{-1} due to hydrolysed APS, ethanol skeleton at 875 cm^{-1} and a broad band between 1150 and 1020 cm^{-1} which corresponds to (Si-O-Si) asymmetric stretching of the polymerised APS [51,77,78,121,132,133].

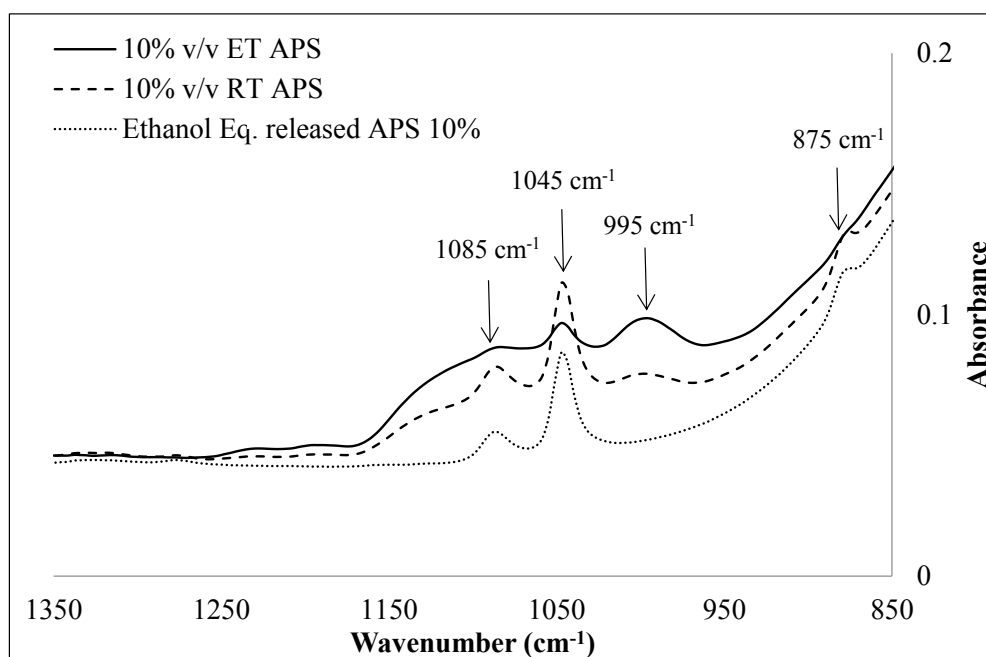


Figure 3.18 Magnification of ATR spectra of 10% v/v APS in deionised water solution prepared at RT and ET, and an equivalent % of ethanol released by APS in deionised water solution (7.5% v/v) between 1350 and 850 cm^{-1} .

The ATR spectra of 10% v/v APS solution in deuterated water (D_2O) prepared at RT and ET, with the spectra of an ethanol- D_2O mixture with the equivalent amount of ethanol released when 100% of the APS hydrolysis would have been reached (i.e. 7.5% v/v ethanol solution in D_2O), are shown in Figure 3.19.

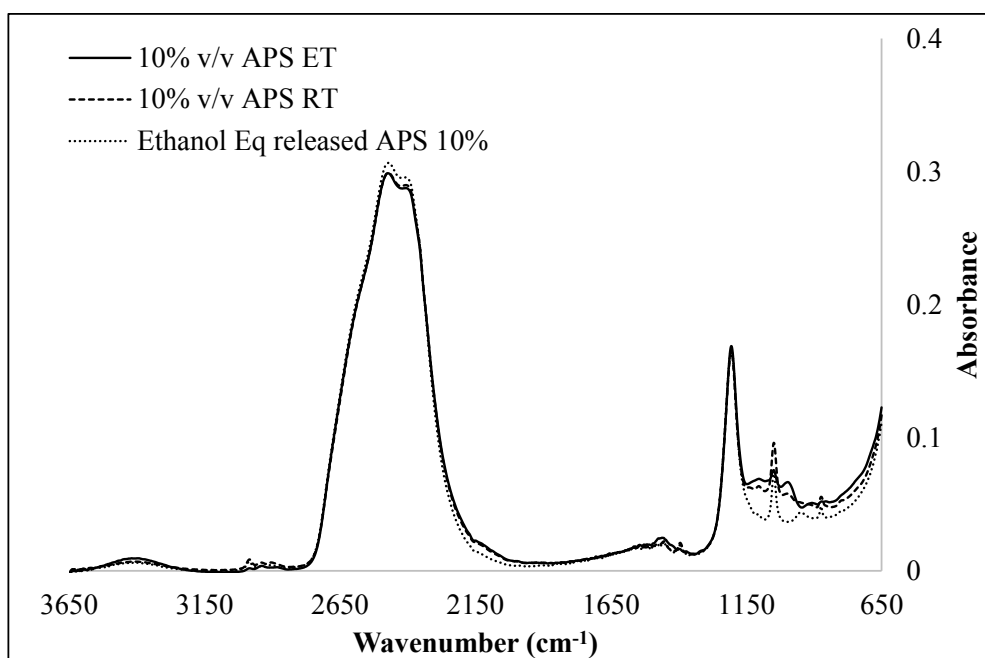


Figure 3.19 ATR spectra of 10% v/v APS in D₂O solution prepared at RT and ET, and an equivalent % of ethanol released by APS in D₂O (7.5% v/v).

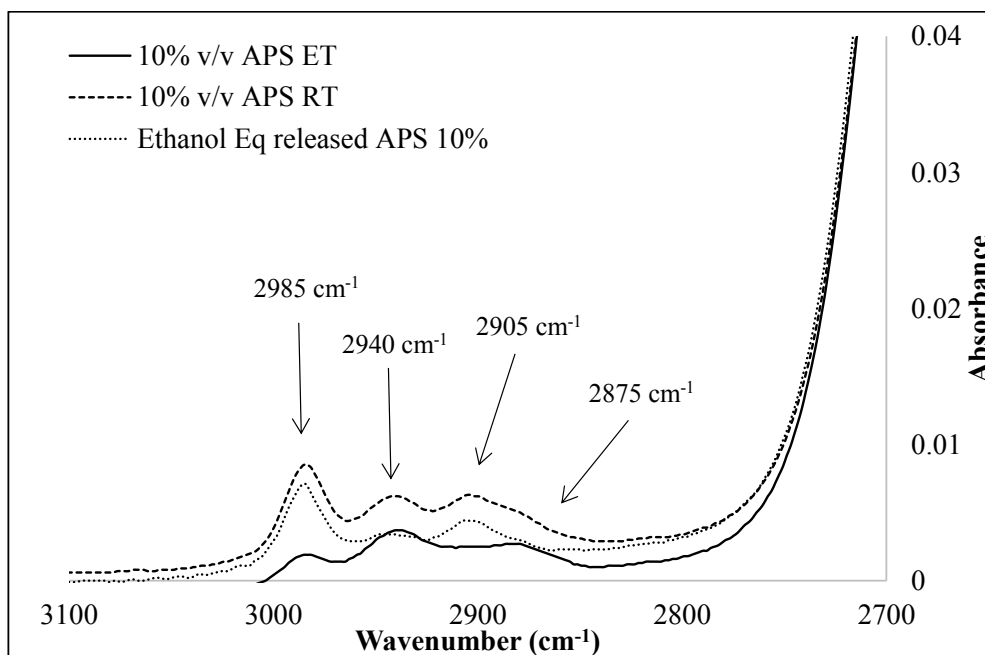


Figure 3.20 Magnification of ATR spectra of 10% v/v APS in D₂O solution prepared at RT and ET, and an equivalent % of ethanol released by APS in D₂O (7.5% v/v) between 3100 and 2700 cm⁻¹.

There are also three regions of particular interest in the spectra, of which two are in the same range as for APS in deionised water solution, with another one between 1600 and 1250 cm^{-1} . These three regions are shown magnified in Figure 3.20, Figure 3.21 and Figure 3.22. Since the solution is in D_2O , the broad bands due to the (OH) of the deionised water, shift to the broad bands caused by the (OD) of the deuterated water (on the order of 800 cm^{-1} less than OH), which facilitates greatly the distinguishing and determination of bands that were previously hidden.

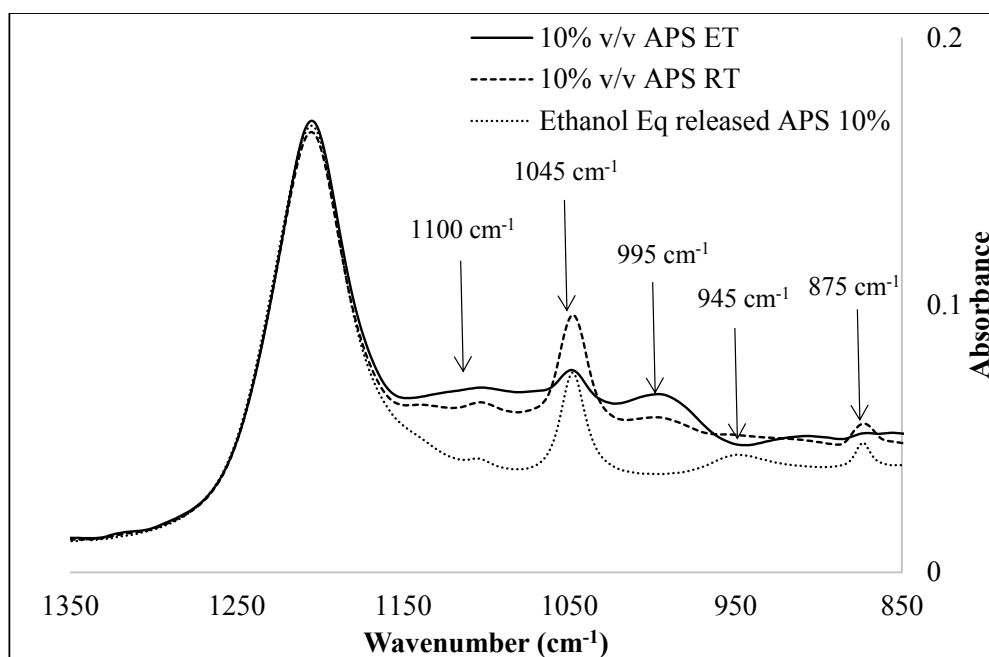


Figure 3.21 Magnification of ATR spectra of 10% v/v APS in D_2O solution prepared at RT and ET, and an equivalent % of ethanol released by APS in D_2O (7.5% v/v) between 1350 and 850 cm^{-1} .

Figure 3.21 shows the spectral region between 1350 and 850 cm^{-1} where seven different bands can be seen: $(\text{C-O})_{\text{COH}}$ symmetric stretching from ethanol and a contribution of $(\text{C-O})_{\text{SiOC}}$ symmetric stretching from unhydrolysed APS at 1100 cm^{-1} as well, $(\text{C-O})_{\text{COH}}$ asymmetric stretching at 1045 cm^{-1} of ethanol, (Si-O-Si) symmetric stretching of polymerised APS at 995 cm^{-1} , $(\text{C-O})_{\text{COD}}$ symmetric stretching at 945 cm^{-1} from ethanol, ethanol skeleton at 875 cm^{-1} and a broad band between 1150 and 1020 cm^{-1} that corresponds to the (Si-O-Si) asymmetric stretching from the polymerised APS [45,51,77,78,133,135–137].

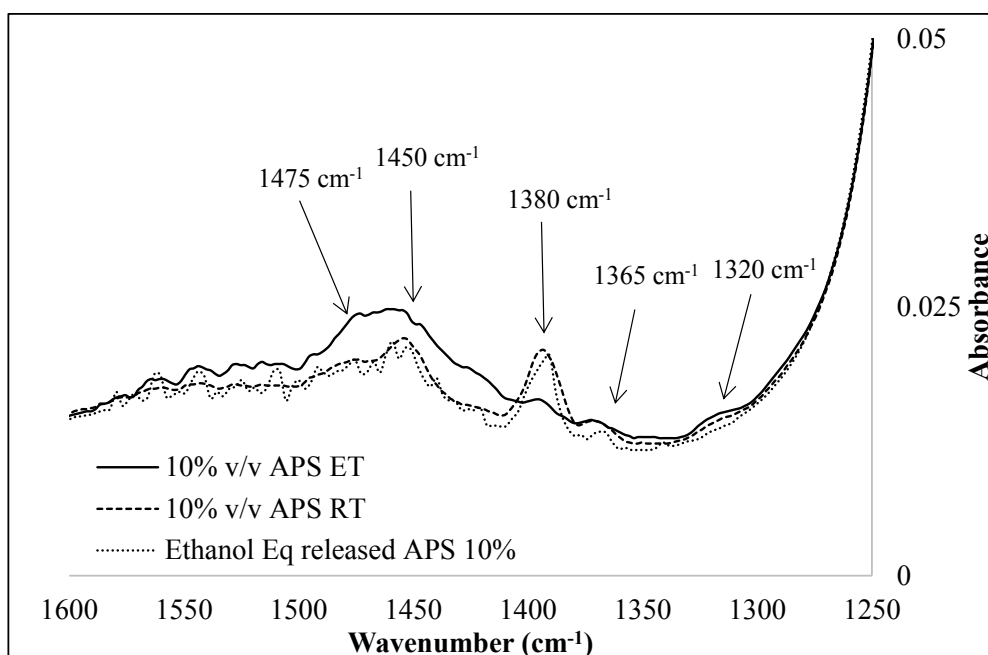


Figure 3.22 Magnification of ATR spectra of 10% v/v APS in D₂O solution prepared at RT and ET, and an equivalent % of ethanol released by APS in deionised water solution (7.5% v/v) between 1600 and 1250 cm⁻¹.

A new spectral region is observed between 1600 and 1250 cm⁻¹ (Figure 3.22). Five different bands can be determined: NH₂ deformation at 1475 cm⁻¹ from the APS [136], asymmetric deformation of CH₃ at 1450 cm⁻¹, symmetric deformation of CH₃ at 1380 cm⁻¹, twisting CH₂ mode at 1365cm⁻¹ and wagging CH₂ at 1320 cm⁻¹ with major contribution from the propyl group of the APS [49,132].

Since the quality of the spectra between 1600 and 1250 cm⁻¹ is poor, identical solutions have also been analysed using a Dialpath multitransmission instrument. This equipment has a higher sensitivity than the previously employed ATR, which resulted in better quality spectra for this region.

3.3.1.2 Dialpath Transmission spectra

The spectra of the same samples analysed with ATR, i.e. 10% v/v APS in deionised water and D₂O solution prepared at RT and ET, are shown in Figure 3.23 and Figure 3.24. It can clearly be seen that this is the same spectra as obtained with the ATR but with a significant reduction in the noise that appears in the region of the OH stretching

(3700-3100 cm^{-1}). This is due to the signal being much stronger in comparison with the sensitivity of the equipment previously used. Bands that could be seen in the ATR appear here as expected, but in different regions. These bands are now easier to differentiate due to the higher sensitivity of the technique.

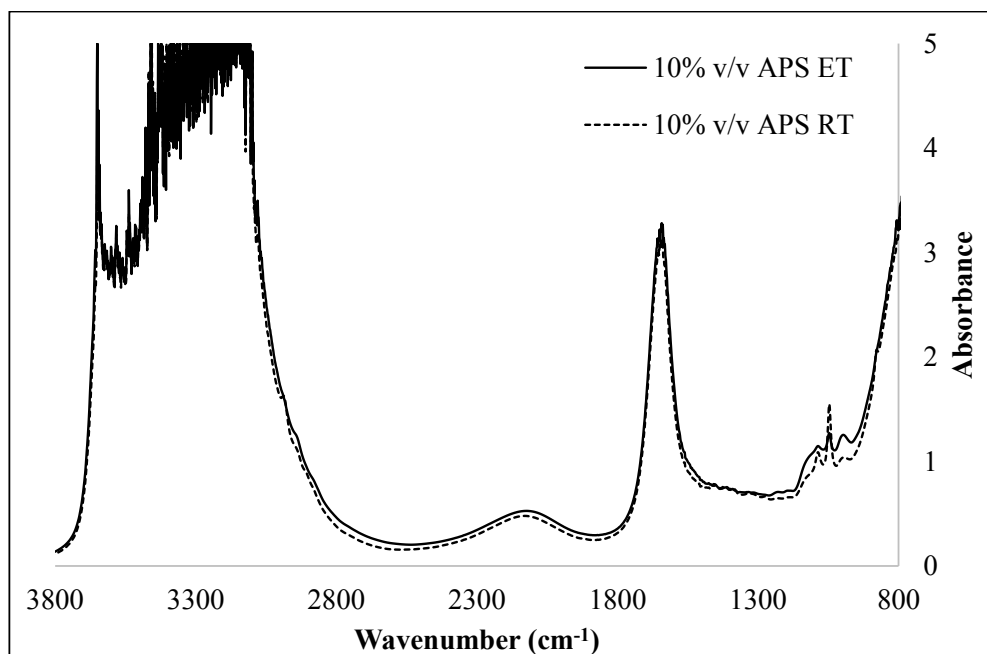


Figure 3.23 Dialpath transmission spectra of 10% v/v APS in deionised water solution prepared at RT and ET.

The Dialpath spectra (Figure 3.24) do not show any new bands for the deionised water solution in comparison with the ATR spectra shown in Figure 3.16. However, 10% v/v APS in D_2O solution was further analysed with the Dialpath to clarify the bands that appear in the region between 1600 and 1250 cm^{-1} .

The region mentioned above is magnified in Figure 3.25 where the same bands can be seen as in Figure 3.22, but now with a higher sensitivity due to the use of the Dialpath multitransmission interface. NH_2 deformation at 1475 cm^{-1} with apparently partial reaction with atmospheric CO_2 to form amine-bicarbonate salt [136,138], asymmetric deformation of CH_3 at 1450 cm^{-1} , symmetric deformation of CH_3 at 1380 cm^{-1} , twisting CH_2 mode at 1365 cm^{-1} and wagging CH_2 at 1320 cm^{-1} with major contribution from the propyl group of the APS [49,132].

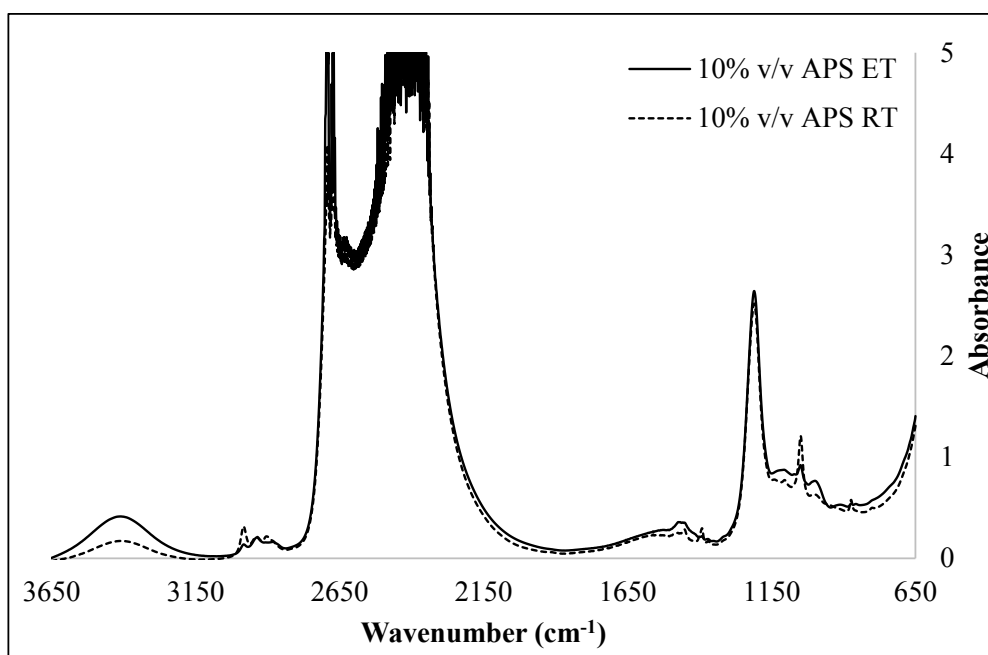


Figure 3.24 Dialpath transmission spectra of 10% v/v APS in D₂O solution prepared at RT and ET.

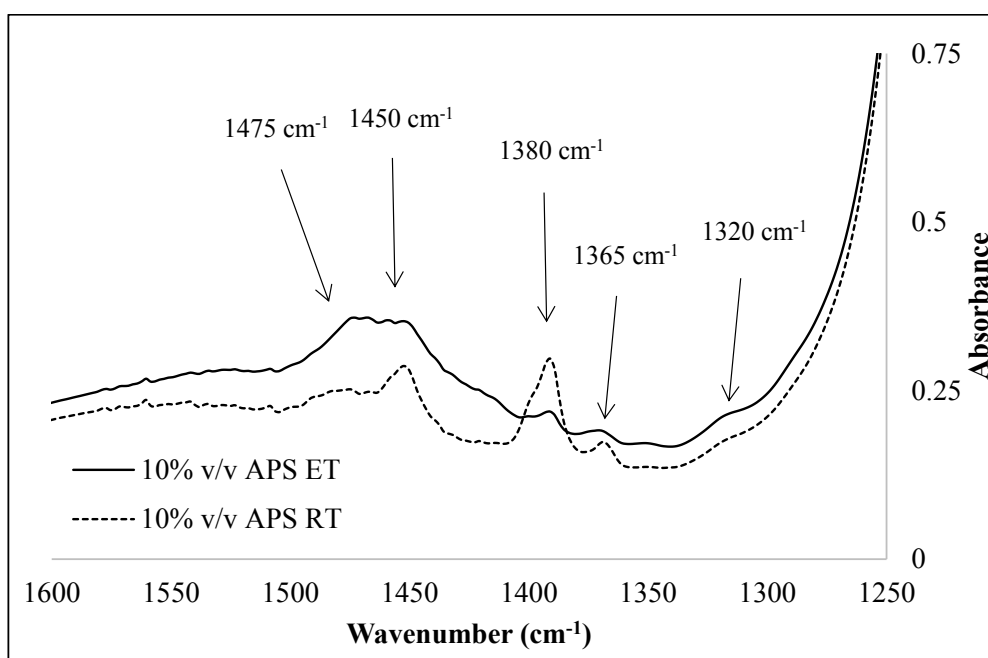


Figure 3.25 Magnification of dialpath transmission spectra of 10% v/v APS 10 in D₂O solution prepared at RT and ET between 1600 and 1250 cm⁻¹.

3.3.1.3 Discussion

The results presented in sections 3.3.1.1 and 3.3.1.2 of the ATR and Dialpath transmission spectra may be related to the single fibre tensile strength results (Table 3.2) obtained and shown in 3.1.2 for ET APS. Due to the preparation of ET APS, various changes were observed to occur in the network of the polymerised silane, which shall be explained below. These changes are thought to be of significance to the higher increases in GF strength observed.

As can be seen in Figure 3.17 (ATR spectra), the first significant difference relates to the ethyl group associated with the ethoxy group on the unhydrolysed silane and the ethanol solution. In the same figure, the bands at 2985 and 2905 cm^{-1} due to the presence of (CH_3) are higher intensity for RT APS and ethanol, whilst conversely for ET APS their intensity is very low. The bands at 2940 cm^{-1} and 2875 cm^{-1} for the (CH_2), which relate mainly to the propyl chain of the APS, are higher intensity for ET APS than for RT APS and ethanol solution. As can be seen in Figure 3.17 (ATR spectra) they are barely present for the ethanol solution. This suggests that the presence of ethanol ($\text{CH}_3\text{CH}_2\text{-OH}$) released or remaining ethyl groups ($\text{CH}_3\text{-CH}_2\text{-O-}$) is minimised for the ET APS, whilst conversely the propyl group gives rise to a stronger band for the ET APS than for the RT APS. This is suggested to be due to a molecular weight effect. This is suggested to be due to a molecular weight effect related to the size of the polymer molecules. As the molecules become more polymerised, the ratio of the number of intermediate groups (e.g. Si-O-Si) to end groups (e.g. Si-OH) increases, i.e. the relative intensities of end groups to intermediate groups decrease with increasing polymer molecular weight. As can be seen for the propyl group in Figure 3.17, the effect is reflected with a stronger intensity baseline. Although the amount of APS in solution is the same for ET APS and RT APS (10% v/v), and the band is expected to be of similar intensity, the propyl group band is stronger for the ET APS. This can be explained by the ET APS being more polymerised than the RT APS [134, 139].

In Figure 3.18 (ATR spectra) the bands at 1085 and 1045 cm^{-1} are due to the (C-O) of the ethanol and ethoxy groups of the APS, and 875 cm^{-1} due to the ethanol skeleton. It can be seen that these three bands are more intense for RT APS and the ethanol-

water solution, with the band for the ethanol skeleton showing almost zero absorbance for the ET APS. This suggests, once again, that the ethanol and most of the ethyl groups have been removed from the ET APS. The last two bands present are due to (Si-O-Si) of polymerised APS and (Si-OH) of hydrolysed APS. The wide broad band between 1150 and 1020 cm^{-1} clearly shows a higher intensity for the ET APS; furthermore, the band at 995 cm^{-1} appears to be stronger for ET APS than for RT APS, and is absent for the reference ethanol-water solution. This band at 995 cm^{-1} is due to a major contribution of (Si-O-Si) and (Si-OH). This contribution can be more clearly seen for the solution of APS in D_2O (Figure 3.21, ATR spectra). The intensity of these bands may confirm that the polymerisation of ET APS is higher than the RT APS which supports the theoretical supposition explained before that some fundamental structural changes occur in the APS when it is prepared at ET.

The aim of preparing the solutions in D_2O and analysing them with FTIR (with ATR and Dialpath interface) was to facilitate comparisons and double-check the results obtained. Due to the heavier hydrogen isotope deuterium (D or ^2H) most of the peaks were found to be the same but additional new peaks also appeared due to the H^+ and D^+ exchange and the shift of the (OH) to the (OD) band. Figure 3.20 (ATR spectra) shows the same bands with same contributions as Figure 3.17 (ATR spectra), but in this case the bands can be more easily distinguished due to the shift of the (OH) broad peak for the (OD). It can be considered that Figure 3.20 reaffirms what was explained above for analysis in deionised water solution between 3050 and 2750 cm^{-1} , in which asymmetric stretching of $(\text{C-H})_{\text{CH}_3}$, $(\text{C-H})_{\text{CH}_2}$ asymmetric stretching with a major contribution from the propyl group of the APS, $(\text{C-H})_{\text{C-H}_3}$ symmetric stretching and $(\text{C-H})_{\text{CH}_2}$ symmetric stretching with major contribution from the propyl group of the APS, were identified.

A new region of the spectra between 1600 and 1250 cm^{-1} can also be analysed when D_2O is used as a reaction solvent. Figure 3.22 (ATR spectra) and Figure 3.25 (Dialpath spectra) show a band at 1475 cm^{-1} due to the (NH_2) deformation, which corresponds to the aminopropyl chain of the APS, with apparent partial reaction with CO_2 to form an amine-bicarbonate salt. This band can be seen for ET and RT APS, but the peak for the ET APS is significantly stronger using both techniques (Figure 3.22 and Figure 3.25). This may either be related to the molecular weight effect of the polymerised ET

APS or to the NH_2 having reacted in high levels with the CO_2 , increasing the peak. Again, two bands can be seen for both (CH_3) and (CH_2) at 1450 and 1380 cm^{-1} , and at 1365 and 1320 cm^{-1} respectively. Both bands regarding the (CH_3) are weaker for the ET APS in comparison to the RT APS or the ethanol solution. The two bands corresponding to the (CH_2) are stronger for the ET APS, due to the major contribution of the propyl group of the polymerised APS. These results again show that polymerised ET APS has less ethyl from non-reacted APS molecules and less ethanol present in the solution due to a more effective removal of ethanol at elevated temperature.

Four of the bands shown in Figure 3.21 (ATR spectra) at 1045 cm^{-1} , 995 cm^{-1} , 875 cm^{-1} and a broad band between 1150 and 1020 cm^{-1} are the same as in Figure 3.18 (ATR spectra). In addition, in Figure 3.21 there is one new peak at 1100 cm^{-1} with similar contributions from $(\text{C-O})_{\text{Si-O-C}}$ and $(\text{C-O})_{\text{C-OH}}$ due to the non-reacted ethyl group of the APS and due to the ethanol released and also at 945 cm^{-1} due to the presence of (C-OD) caused by the equilibrium effect between the H^+ and D^+ , mainly from ethanol. Once again, the results confirm that the presence of ethanol and non-reacted ethyl groups in ET APS solution is minimal, with a stronger and broader band than RT APS solution.

To the contrary, several authors advocate that the band at 995 cm^{-1} is due to (Si-OH) , but when the preparation process of the APS had been carried out in D_2O , no appreciable change can be observed. It would be expected that this band would shift due to the (Si-OH) changing to (Si-OD) , but in Figure 3.26 (ATR spectra) it can be seen that the peak is basically the same. As ATR may struggle to differentiate both bands, the same spectra using Dialpath transmission is shown in Figure 3.27, without any noticeable difference apart from the higher precision of the technique. This has been verified in Figure 3.28 (ATR spectra) by applying the derivative to the spectra of APS in both solutions between 1150 and 900 cm^{-1} . It can be seen that the length of the slope for APS in both solutions is practically the same, which suggests that this peak is not solely due to (Si-OH) , and that the major contribution may be attributable to another bond. This bond is essentially suggested by other authors to be (Si-O-Si) [121].

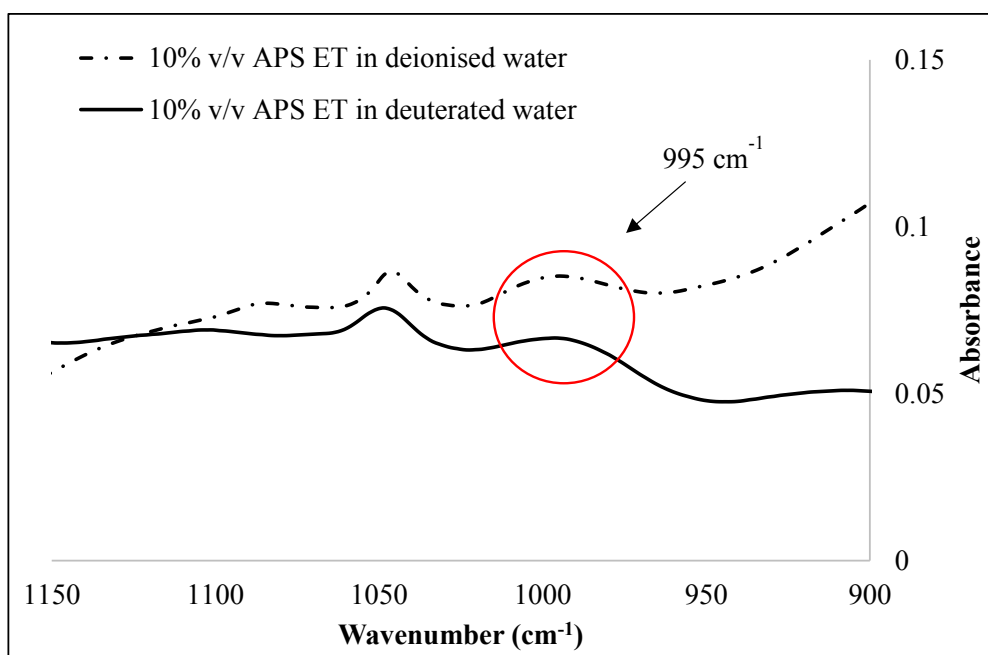


Figure 3.26 ATR spectra for 10% v/v ET APS in deionised water and D₂O between 1150 and 900 cm⁻¹.

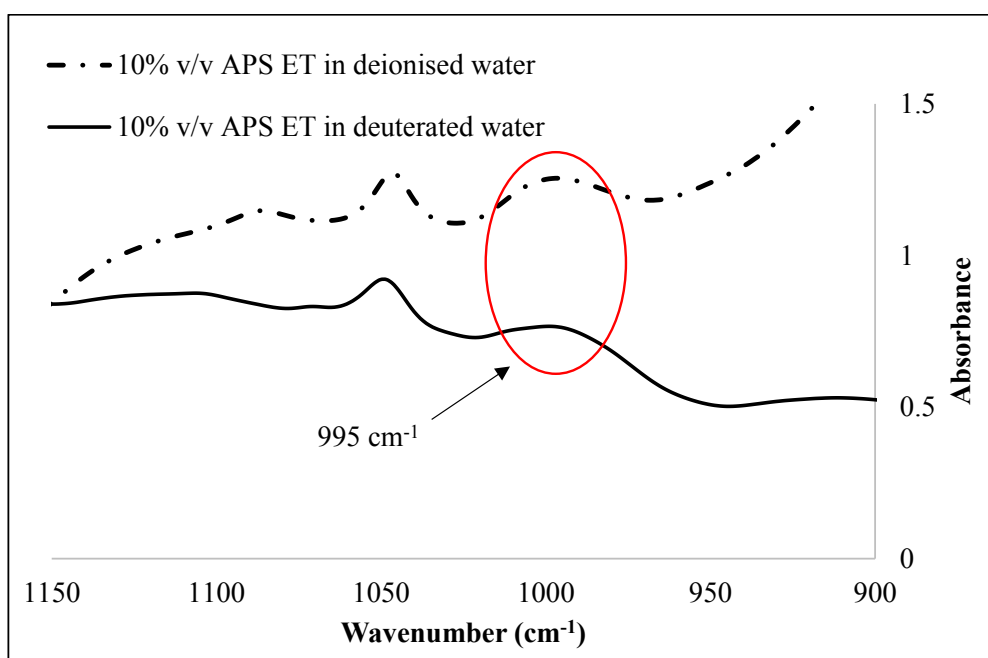


Figure 3.27 Dialpath transmission spectra for 10% v/v ET APS in deionised water and D₂O between 1150 and 900 cm⁻¹.

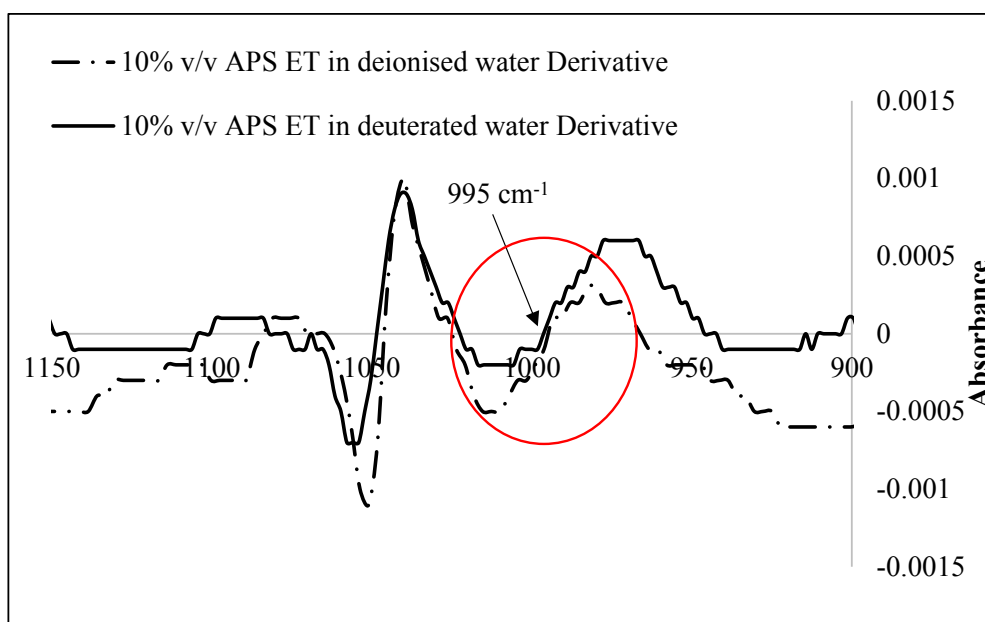


Figure 3.28 ATR derivative of the spectra for 10% v/v ET APS in deionised water and D₂O between 1150 and 900 cm⁻¹.

In summary, the spectra obtained with ATR and Dialpath showed structural differences between ET APS and RT APS solutions. These observations validate the results obtained with NMR regarding ethanol/ethyl removal from solution and suggest that the (Si-O-Si) peak which is related to the polymerisation of the APS is stronger for ET APS than for RT APS. This, once again, reaffirms what theoretically was explained in chapter 1.7, that APS self-condensation reactions are strongly accelerated by elevated temperatures. Furthermore, the peaks attributed by several authors to (Si-OH), were shown to actually be due to the presence of (Si-O-Si) and not Si-OH [121].

3.3.2 FTIR characterisation of ET APS films

3.3.2.1 Diffuse Reflectance Infrared Fourier Transform (DRIFT) spectra

Further investigation of the structure of APS films prepared from ET and RT hydrolysed 10% v/v solutions was performed using FTIR with the diffuse interface, a different technique than those previously used (ATR and Dialpath transmission). This was used to analyse the films due to its higher resolution and manageability with solids. Figure 3.29 shows the results for the films of 10% v/v APS in deionised water

solution prepared at RT and ET, then dried for 48h at 83°C. In Table 3.10 the important peaks further are defined for clarity.

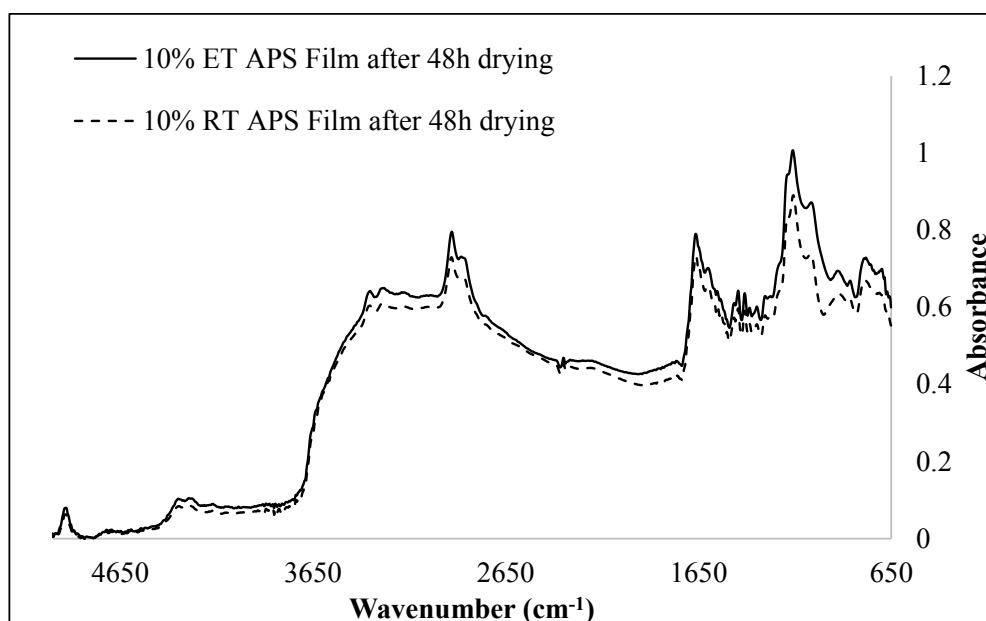


Figure 3.29 DRIFT spectra for 10% v/v APS prepared at RT and ET in deionised water, dried for 48h at 83°C.

Table 3.10 DRIFT different bands of the spectra.

Band (cm ⁻¹)	Bond
3650-3000	(OH)
3340	(N-H) _{NH2} asymmetric stretching
3270	(N-H) _{NH2} symmetric stretching
2920	(C-H) _{CH2} asymmetric stretching from (CH2-CH2-CH2)
2860	(C-H) _{CH2} symmetric stretching from (CH2-CH2-CH2)
1660	(-N-H-) _{NH} secondary amine
1605	(N-H) _{NH2} deformation
1160-1050	(Si-O-Si)

The same films were prepared in deuterated water. Both spectra are shown in Figure 3.30. The spectra are very similar to those obtained from the solutions in deionised water, and so it was concluded that D₂O appears to interact with APS in the same manner.

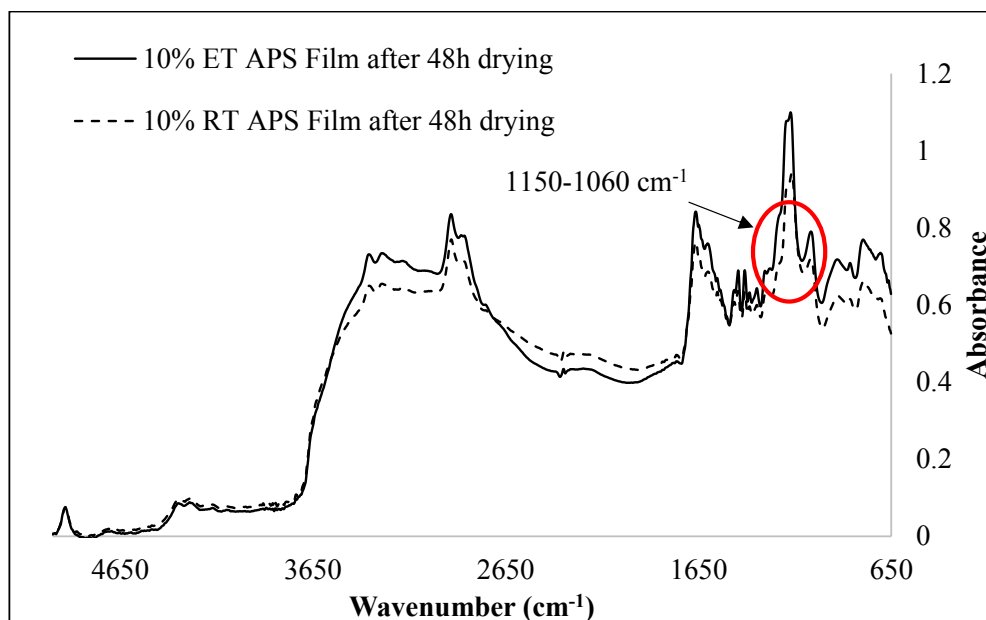


Figure 3.30 DRIFT spectra for 10% v/v APS prepared at RT and ET in D₂O, dried for 48h at 83°C.

In general terms, the ET hydrolysed APS film has higher intensity bands, which is suggested to be related to a molecular weight effect. On the other hand, most of the bands are apparently of a relatively similar size, except for the band that corresponds to the (Si-O-Si), which seems to be of higher intensity for the ET APS film than for RT APS film. This also suggests enhanced polymerisation of APS when it is prepared at ET, increasing the (Si-O-Si) bonding (1160-1050 cm⁻¹) and producing a higher polymer. This again supports what was observed for APS solutions regarding their polymerisation. It is suggested that ET preparation of APS causes an increase in polymerisation rate and hence, increases the molecular weight of the polymer chain of APS. This in turn seems to positively affect the mechanical properties of GFs, probably caused by a higher grade of flaw healing.

3.4 ET APS polymerisation Hypothesis

As shown above, there are significant differences in the strength of GFs which have been coated with APS prepared at RT or ET (i.e. 83°C for 5 hours). Since the physical application of different APS solutions was identical, this observation must be related to the method of APS preparation prior to application to the GF surface.

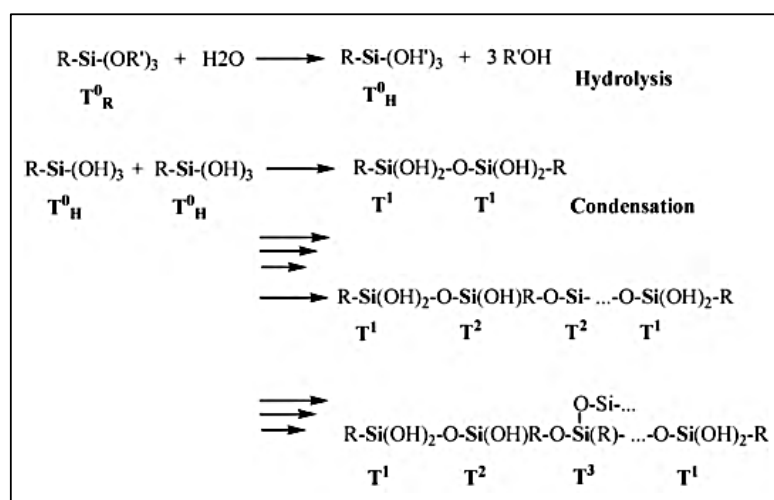


Figure 3.31 The different species formed during the hydrolysis reaction determined with solid state NMR relaxation time measurements. Molecule structures are T^0_{R} : pristine silane; T^0_{H} : silanol group from hydrolysis; T^1 : dimer or chain end; T^2 : linear link; T^3 : three dimensional [140].

Figure 3.31 presents the different species formed during the silane hydrolysis reaction. A summary of the preparation reaction sequence with the different species formed is also shown. It can be seen that the by-products of the hydrolysis reaction are alcohol molecules. Alcohols, in general, have a low boiling point (usually under 80°C), and in the particular case of APS, where the by-product alcohol is ethanol, the boiling point is 78.4°C. As explained in chapter 2.2, due to being in an aqueous medium (i.e. deionised water or D₂O), this forms an azeotrope at 78.2°C whose liquid composition is 95.5% ethanol and 4.5% water (percentage by weight). Elevated temperature (83°C) is applied to the APS solution for a period of 5 hours in order to evaporate most of the ethanol by-product produced.

Due to the lid being closed, water molecules were able to condense whilst ethanol molecules remained mostly in the vapour phase, as the temperature of the solution was

maintained above the boiling point of ethanol, i.e. above 78.4°C though below the boiling point of water.

The molecular structures involved in the hydrolysis and condensation reactions, which are the ones that determine the differences between the resultant structures of the same silane prepared in different ways, are as follows:

- T¹ structure: dimer or chain end.
- T² structure: linear link.
- T³ structure: three dimensional.

Regarding the APS preparation at natural pH and either at RT or ET, the table below is a comparison between them [47,51,140,141]:

Table 3.11 Comparison between RT and ET APS.

<u>RT APS</u>	<u>ET APS</u>
<i>Hydrolysis</i>	
Without pH modification, <u>hydrolysis is an automatic process</u>	
After short periods of time for APS in water, there is few or no non-hydrolysed APS (T ⁰ _R)	
It would be <u>T⁰_H, and ethanol</u> released as a reaction by-product	It would <u>only</u> be T ⁰ _H , as the ethanol molecules have been mostly removed due to the elevated temperature
<i>Condensation</i>	
<u>Condensation is an automatic process</u>	
Ethanol present <u>catalysed Self-condensation (T³)</u>	Self-condensation is suppressed in 100% water medium. There is <u>not ethanol present</u> , so no catalysing of self-condensation (T ³) is possible
<i>FTIR (Solutions)</i>	
<u>Low Si-O-Si peaks (DRIFT)</u>	<u>Higher Si-O-Si peaks</u>
Higher Ethanol/Ethyl peaks	Not ethanol peaks (DRIFT)
Higher peaks on Si-O-Si is a matter of molecular weight (DRIFT)	

Considering the summary presented in the table above, it can be suggested that the difference between both methods of APS preparation results in:

- A similar amount of hydrolysed molecules of APS (T_H^0) for both cases.
- The amount of dimer or end chain molecules (T^1) will be greater for APS prepared at room temperature, whilst the amount of linear link molecules (T^2) will be greater for APS prepared at elevated temperatures.
- No three dimensional molecules (T^3) are expected to form for ET APS as the medium is 100% water and most or all the ethanol has been evaporated. Conversely, for RT APS, although it is also a 100% water medium, there is ethanol present in the solution, so T^3 molecules may be expected.

It is possible that some T^3 appears for the RT APS, since the ethanol released during the hydrolysis could catalyse the formation of T^3 and so form cross-linked polymers, which often have lower density due to their higher free volume (i.e. a less compact structure). Presumably, the appearance of T^3 is also contemplated when drying the solutions to form the film in both cases, but RT APS is more likely to have higher amounts of three dimensional molecules as it may have them in solution also prior to drying.

This is in agreement with results presented by Salon et al. [47,140] and the results obtained in this work with ATR and Dialpath for APS solutions prepared at RT and ET. The results using DRIFT for dry films of APS prepared in both ways also showed a similar trend, with stronger Si-O-Si peaks for the ET APS.

Pasternack et al. [62] investigated the attachment of γ -aminopropyltriethoxysilane to silicon oxide surfaces and its dependence on solution temperature. It was suggested that the APS film prepared at 70°C in an anhydrous medium led to a stronger, denser and better-oriented APS film. Although they are completely opposite mediums (anhydrous and aqueous), the results obtained lead to a possible analogy between them; suggesting a denser APS film (molecular weight effect using the IR). Furthermore, in 3.1.2 the mechanical results showed that the APS film produced at ET is stronger than the film prepared at RT.

The foregoing suggests that, when APS is applied to the GFs and subsequently dried, the film created is attached to the GF surface creating different properties of the silane polymer layers depending on the preparation mode. The ET APS provides a better coverage protection due to the nature of the polymer produced. This ET APS

polymer has longer linear chains (T^2), but also some dimer or chain end molecules (T^1) that can heal the flaws, i.e. a combination of both effects, improving the effect of RT APS. This may be mainly due to the higher grade of T^2 to the detriment of T^1 .

3.5 DRIFT study of treatments effects on GFs

Different treatment combinations were analysed to see if, other than the effect on GFs strength, they also had an effect on the bulk hydrolysis of the fibres (OH group concentration). A bulk technique like DRIFT, with depth penetration from 200 to 400 μm , was used to analyse the treatment effects on GFs. It is interesting to analyse this parameter to better understand the possible subsequent reactions between the fibres and the silanes.

The broad band that has to be checked to see the differences is the band between 3650 and 3000 cm^{-1} . This band is the one that determines the OH groups.

The GFs were thermally degraded at 450 $^{\circ}\text{C}$ and then different treatments were applied, which were as follows:

1. Thermally degraded at 450 $^{\circ}\text{C}$ for 25 minutes (TD).
2. TD + NaOH 3M at 95 $^{\circ}\text{C}$ for 5 minutes + rinsed in water.
3. TD + NaOH 3M at 95 $^{\circ}\text{C}$ for 10 minutes + rinsed in water.
4. TD + NaOH 3M at 95 $^{\circ}\text{C}$ for 20 minutes + rinsed in water.
5. TD + NaOH 3M at 95 $^{\circ}\text{C}$ for 30 minutes + rinsed in water.
6. TD + NaOH 3M at 95 $^{\circ}\text{C}$ for 5 minutes + rinsed in HCl.
7. TD + NaOH 3M at 95 $^{\circ}\text{C}$ for 10 minutes + rinsed in HCl.
8. TD + NaOH 3M at 95 $^{\circ}\text{C}$ for 20 minutes + rinsed in HCl.
9. TD + NaOH 3M at 95 $^{\circ}\text{C}$ for 30 minutes + rinsed in HCl.

The results are shown in two separate figures. One figure compares the treatments which were rinsed in deionised water. The other figure compares the treatments which were rinsed in HCl. The aim of rinsing the fibres in either deionised water or HCl was to remove the degraded GF surface deposits caused by the NaOH treatments.

Based on the results shown in Figure 3.32, the strongest OH peaks are observed for the 20 and 30 minutes NaOH treatment, which both have similar intensities. In

comparison to 20 and 30 minute treatments, the treatments for 5 and 10 minutes present lower absorbance which are almost the same as the only thermally degraded control sample. The strong OH absorbance of GFs treated for 20 and 30 minutes in NaOH solution correspond to the decrease in intensity of the Si-O-Si band pointing downwards at 1000 cm^{-1} , which supports the idea of NaOH solution hydrolysing the bulk glass fibre network. The large peak at 1250 cm^{-1} for each spectrum is in fact a point of inflection due to the reststrahlen effect, where features at lower wavenumbers from this point (such as the Si-O-Si band) are all negative mainly because of concomitant changes in refractive index with IR absorbance.

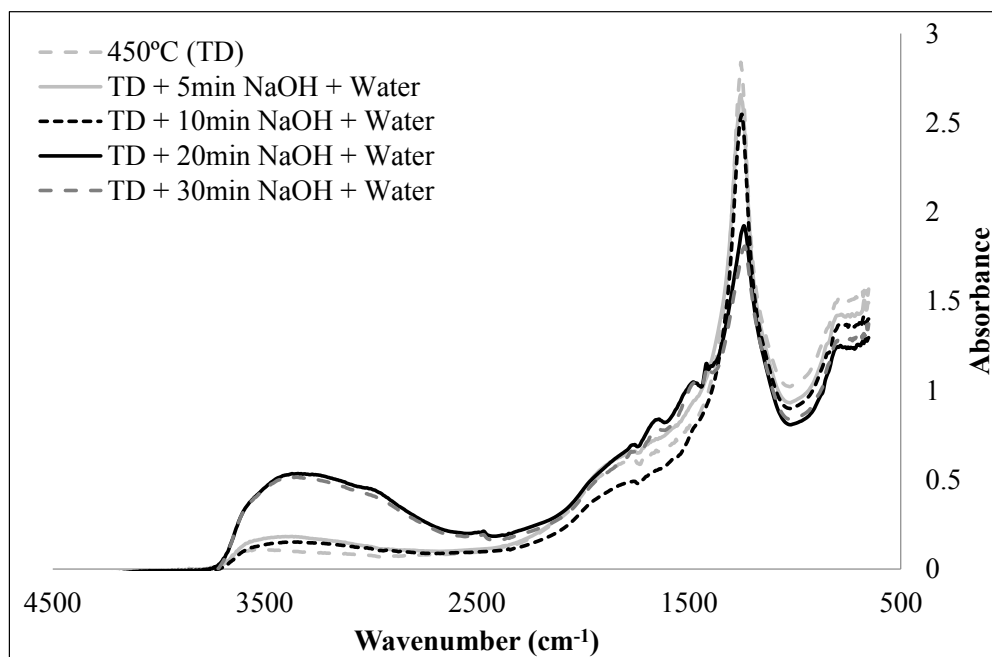


Figure 3.32 DRIFT spectra for TD commercially coated GFs treated with NaOH and then rinsed in deionised water.

In Figure 3.33, the initial treatments are the same as in Figure 3.32 but instead of washing the fibres with water they were washed with HCl. It can be seen that the strongest OH band obtained was for the 10 minutes NaOH, and the 20 and 30 minutes ones, that previously were the strongest ones, have lower absorbance.

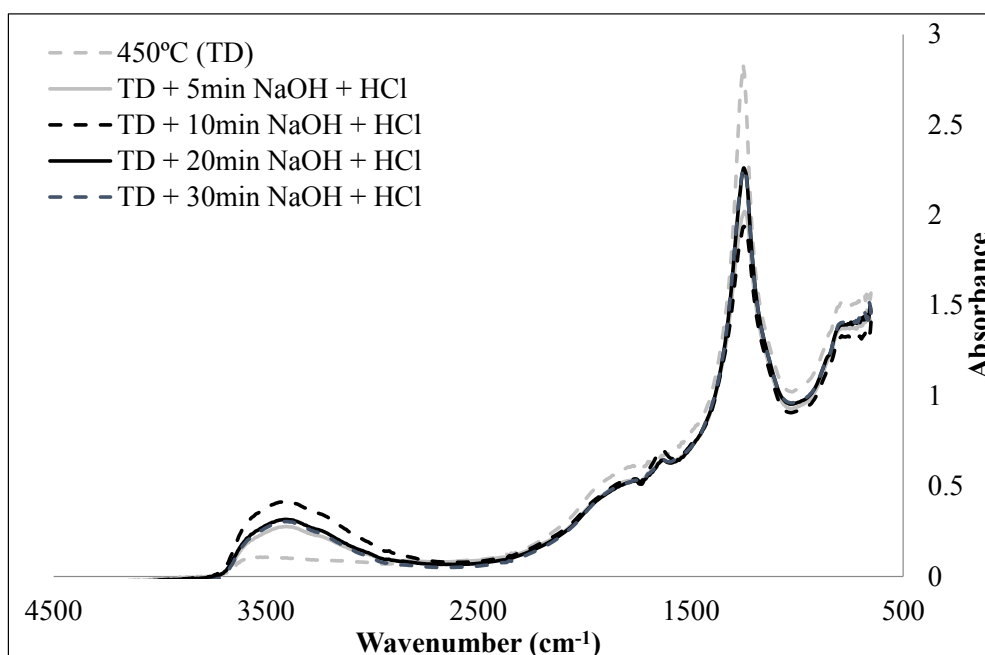


Figure 3.33 DRIFT spectra for TD commercially coated GFs treated with NaOH and then rinsed in HCl.

Comparing the band between 3650 and 3000 cm^{-1} (OH group) in Figure 3.32 and Figure 3.33 leads to the suggestion that it may be possible that the longer treatments apparently increased the OH group concentration in the GFs, but this is only an effect of the NaOH degraded GF. The level of degradation probably increases with treatment time. When the analysis was carried out with HCl washed fibres, which seems to remove most of the OH groups associated to the alkali treatment degradation, the result was different. It suggests that longer periods of time do not increase OH group concentration, but instead it decreases for treatments times longer than 10 minutes. This observation may be in agreement with the previously presented negative effect of prolonged treatments on mechanical properties.

Further analysis was carried out with DRIFT and the NaOH treatments washed with water and applying silanes, in this case RT APS and MPS (Figure 3.34). An NaOH treatment wash with water and followed by application of RT APS showed a similar trend in OH band intensity but with additional characteristic peaks of the APS. As shown in Figure 3.32, the highest OH band is for the 30 minutes NaOH treatment and the second highest is for the 20 minutes treatment.

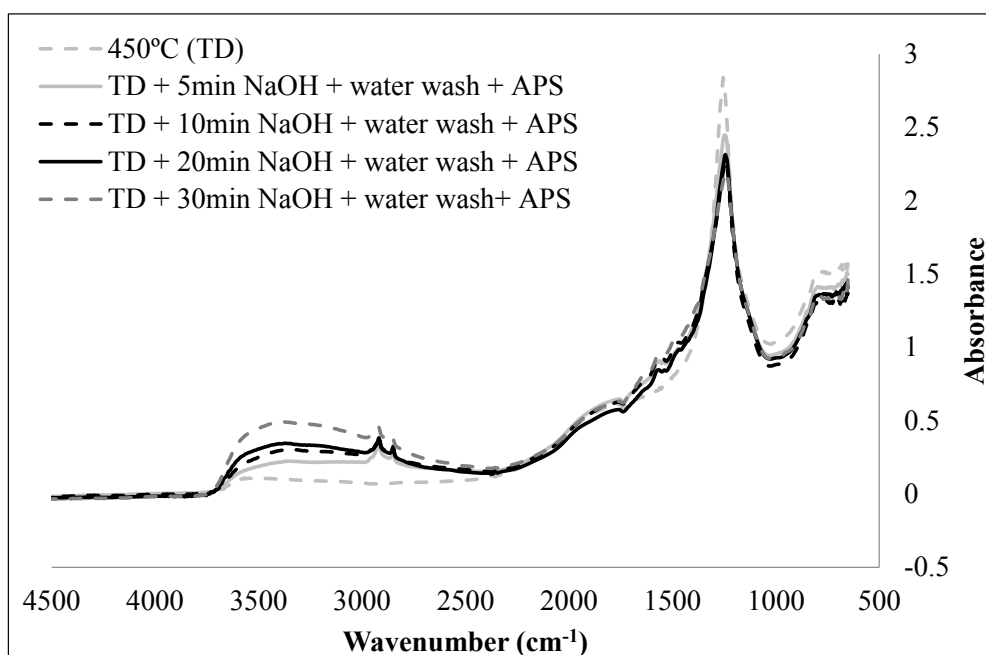


Figure 3.34 DRIFT spectra for TD commercially coated GFs treated with NaOH, wash with deionised water and then treated with APS.

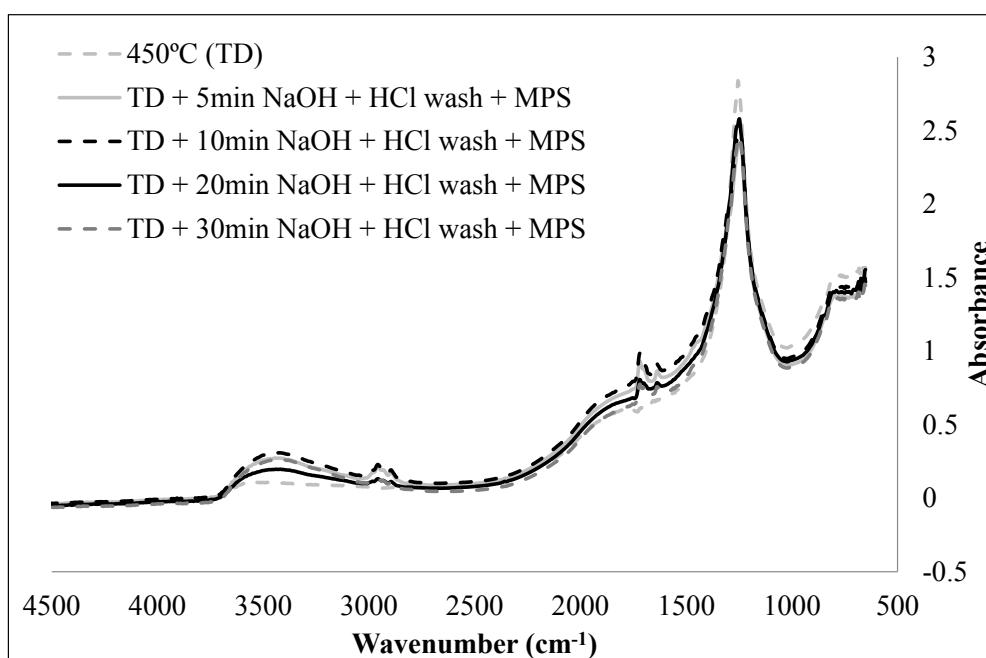


Figure 3.35 DRIFT spectra for TD commercially coated GFs treated with NaOH, wash with deionised water and then treated with MPS.

Analogously, the NaOH treatments washed with HCl were also treated with MPS (Figure 3.35). The results showed a similar trend as the ones obtained without the silane, with the addition, in this case, of the typical bands for the MPS.

These results suggest that, in terms of OH group concentration on the GF, the best option is to wash them after 10 minutes of NaOH treatment in order to have a higher concentration of OH groups and may increase the probability of reaction between the fibre and the silanes.

3.6 SEM surface characterisation

Further GF surface characterisation has been carried out using SEM. The samples examined under the SEM were the commercially coated GFs with different treatments. Initially, surface examination of GFs thermally degraded at 450°C and with subsequent application of 10% v/v HCl, MPS and RT APS was performed.

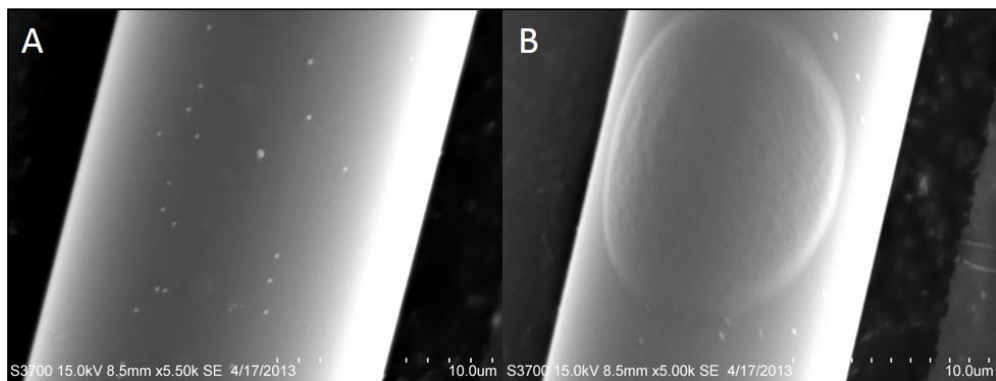


Figure 3.36 Commercially coated GFs TD at 450°C. a) Flat surface GF; b) bump in GF surface.

In Figure 3.36 a), the typical appearance of TD GF can be seen, with an apparent smooth surface and some little particles which may be due to residues of the sizing after the thermal degradation. In picture b) a bump in GF surface is shown. It may be due to the TD of the coating.

The SEM picture of the TD GF with the chemical treatment of 1 hour immersed in 10% v/v HCl shown in Figure 3.37 has the same appearance as the thermal degraded GF, without significant visual differences.

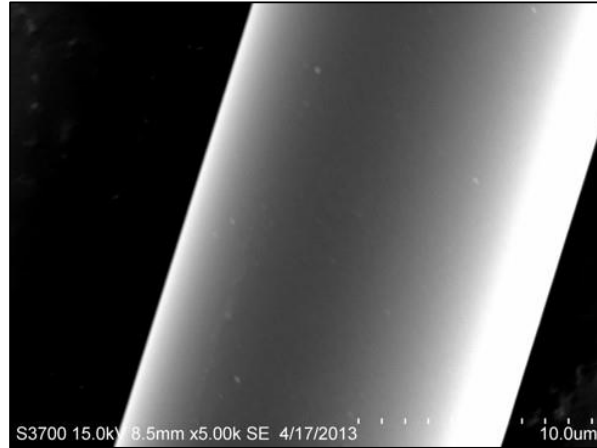


Figure 3.37 Commercially coated GF TD at 450⁰C with HCl 10% v/v for 1 hour treatment surface.

The SEM pictures were also used to compare the GFs shown above, self-coated with two different silanes, RT APS and MPS. In Figure 3.38 silane deposits are clearly visible. The difference between these two samples is that the deposition of the MPS appears more homogeneous in comparison with the deposition of RT APS.

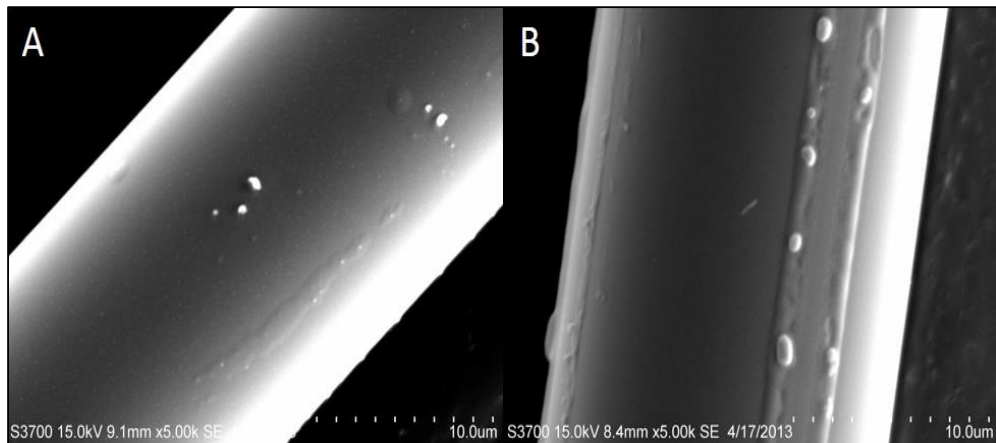


Figure 3.38 Commercially coated GFs TD at 450⁰C coated with a) MPS b) RT APS.

For combinations of HCl rinsing and subsequent silane application, Figure 3.39 shows that the amount of MPS on HCl treated GF surface appears to be higher than that with RT APS. Comparing Figure 3.39 with Figure 3.38 it can be seen that HCl treatment prior to silanisation seems to increase the MPS deposition on TD GFs but appears to have a negative effect on RT APS deposition. On the other hand, the combination of HCl and MPS treatment seems to leave a less homogenous surface coverage.

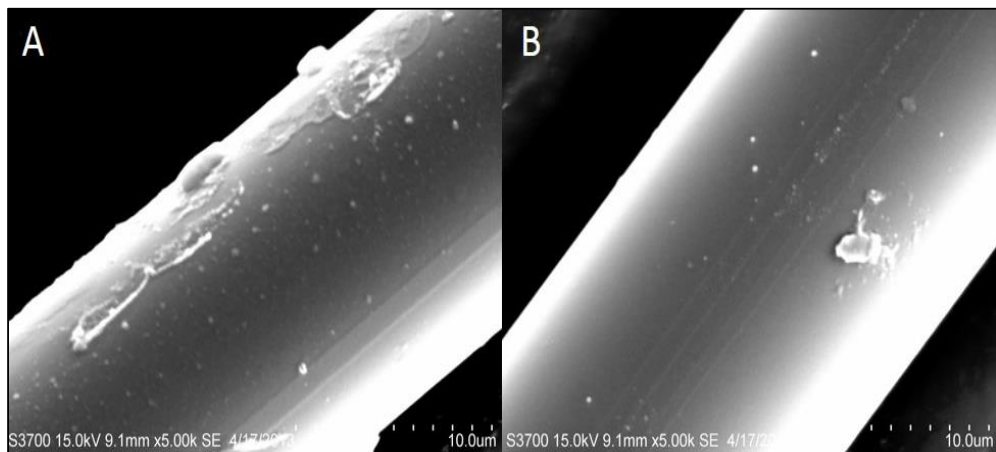


Figure 3.39 Commercially coated GFs TD at 450⁰C treated with a)10% v/v HCl and MPS b)10% v/v HCl and RT APS.

Further SEM surface examination has performed to investigate the dust seen when NaOH treated GFs were carefully separated from the bundle in order to prepare the single fibre test samples. The surface examination was carried out with as received GFs treated with different NaOH concentrations, different treatment times and washing them with deionised water and 37% v/v HCl. At the beginning of this investigation the GFs were soaked in the hot alkali solution for 5 hours and then they were analysed under the SEM, to check the effect on GF surface.

Heavy deposits can clearly be seen on the GF surface in Figure 3.40. In both pictures (A and B), a tridimensional structure, similar to a coral, is deposited onto the GF surface. It is most likely to be a typical NaOH degraded GF surface, but minor contributions of NaOH and other subproducts cannot be discarded.

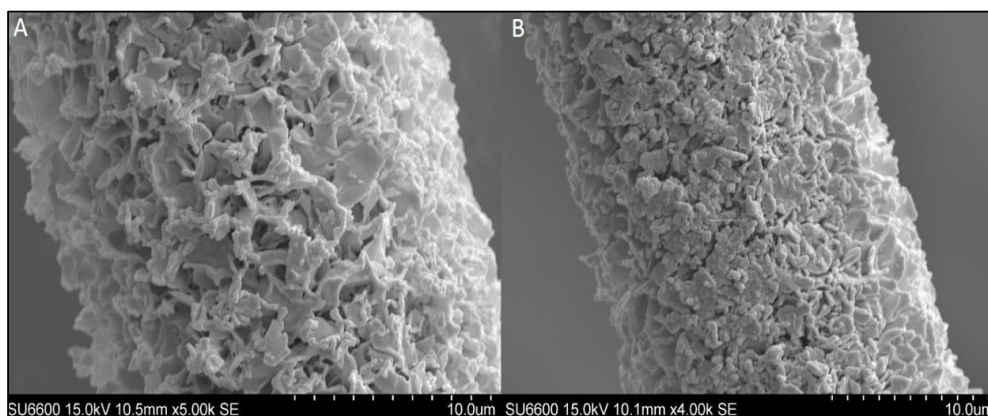


Figure 3.40. As received GFs treated 5 hours with NaOH 3M.

When these fibres are rinsed in HCl to remove the deposits, two different observations were made which are illustrated in Figure 3.41. In picture A most of the tridimensional structure has disappeared, but a kind of subproduct layer remains on the surface, leaving the fibre inside. On the other hand, in picture B, most of the subproduct has been removed from the surface, but there is still subproducts remaining. These pictures can be compared with those in Figure 3.42 which shows GFs treated with 3M NaOH for 10 minutes without any subsequent washing process. A lot of residue can also be seen on this GF surface, but as might be expected at a much lower level compared to the 5 hours treatment.

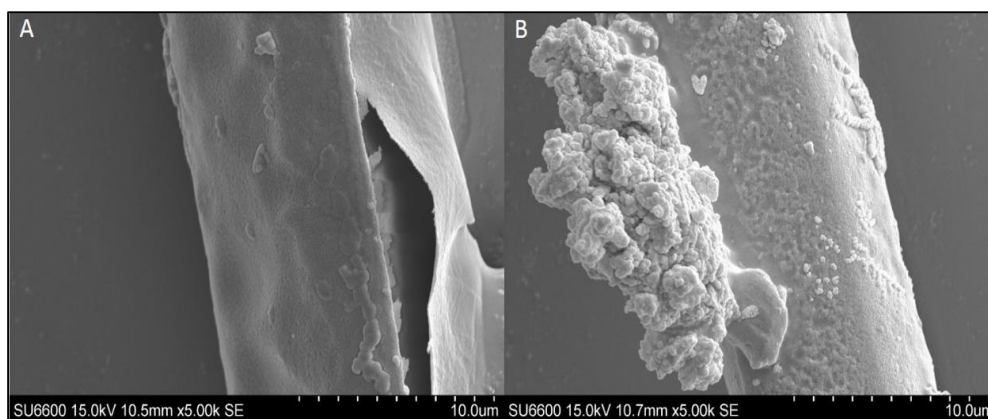


Figure 3.41. As received GFs treated 5 hours with NaOH 3M and washed with 37% v/v HCl.

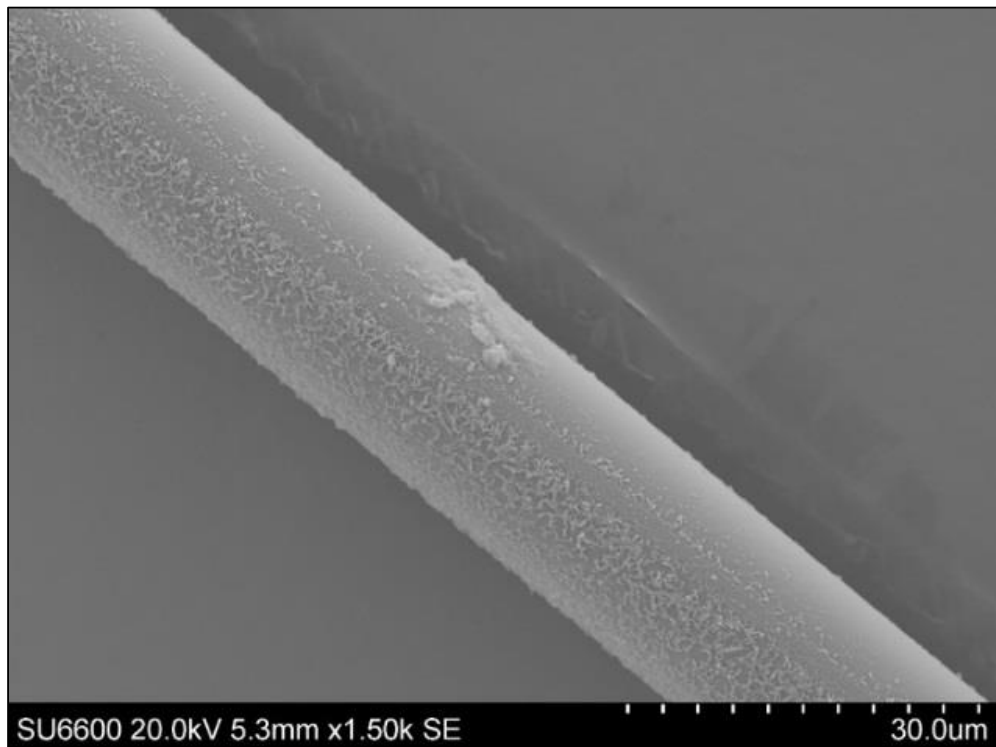


Figure 3.42. As received GFs treated 10 minutes with NaOH 3M.

Figure 3.43 presents images of GFs treated with NaOH 3M for 10, 20 and 30 minutes and subsequently washed with HCl. This images would appear to show that, the longer the NaOH treatment, the more residue that remains on the surface after washing with HCl. This confirms that the longer that the NaOH is applied, the more surface residue is obtained.

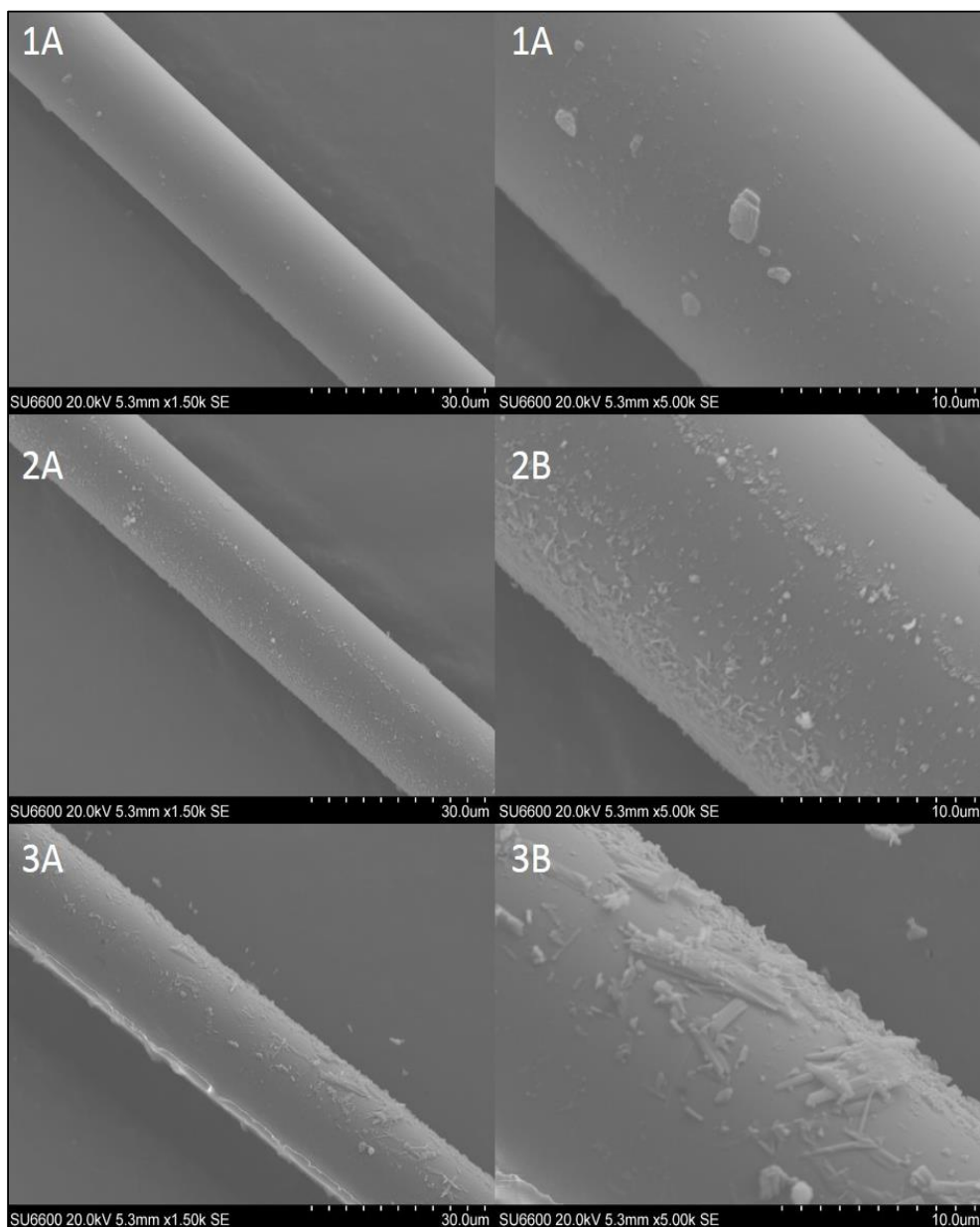


Figure 3.43 As received GFs treated 1A, 1B) 10 minutes NaOH 3M washed with HCl, 2A, 2B) 20 minutes NaOH 3M washed with HCl and 3A, 3B) 30 minutes NaOH 3M washed with HCl.

Chapter 4 Conclusions

The single fibre tensile test was used to characterise the mechanical properties of as received GFs, commercially coated GF, as received GFs self-coated with three different silanes prepared in different ways, TD commercially coated GFs and TD commercially coated GFs treated with different combinations of PW, silanes, HCl and NaOH. The strength of commercially coated GFs was almost twice the strength of as received GF. Since the manufacturing conditions and glass formulation of these fibre samples were identical, the differences in fibre strength were attributable directly to the APS on surface of the coated fibres. The results suggested that the APS effect was mainly from the protection and repairing of the GFs surface.

The as received GFs were also self-coated with different silanes (APS, MPS and GPS) prepared under different conditions. The results on fibre strength suggested that the best conditions to prepare MPS and GPS solutions were at room temperature and at a solution pH of 5.0-5.5. MPS and GPS solutions prepared at elevated temperature (73⁰C) for 5 hours become cloudy and several droplets in suspension could be seen, probably due to the self-polymerisation of the silane. The results for MPS at elevated temperature did not have any positive effect on single fibre strength. APS preparation at ET, i.e. 83⁰C, for 5 hours opening the lid twice (every 1.5 hours), at solution medium natural pH, was found to be the best condition to improve the mechanical properties of coated as received GFs. The strength of the as received GFs coated with ET prepared APS was found to be up to 30% higher in comparison with the as received GFs coated with APS prepared at RT.

NMR was used to determine the amount of the ethanol by-product remaining in solution when APS was prepared at RT and higher temperatures. The ethanol remaining in solution for RT APS was found to be 100% of the initial amount, knowing that it is not possible to differentiate between ethanol and ethyl group related peaks.

On the other hand, a study of ethanol released when APS is prepared at 83⁰C or above showed that the remaining ethanol level is almost constant at around 20 to 25% of the initial amount.

FTIR equipment was used to determine the structural differences in dried APS films which had been prepared at RT and ET in solution. ATR and Dialpath transmission IR spectra were used to analyse the solutions. It was found that there were several differences between them. The bands related to the ethanol/ethyl compound showed more intense peaks for RT APS, which matches with the results of the NMR analysis. The amount of ethanol/ethyl for ET APS sample appeared to be much lower than for the RT APS sample. On the other hand, the bands related to the polymerisation of APS (Si-O-Si) showed higher peaks for the ET APS, suggesting that the ET APS polymerised at a higher rate than the RT APS. Although not as clear as the analysis carried out for solutions, DRIFT analysis also showed that the degree of polymerisation of molecular weight of ET APS was larger than RT APS. It further showed that the bands related to the polymerisation of APS seemed to be higher for ET APS film. This also supports what was found from the APS solution analyses.

Regarding the band analysis, it was found that at 995 cm^{-1} , which has been suggested as related to (Si-OH), the results suggested that this band has a major contribution from (Si-O-Si) rather than (Si-OH). This was suggested to be due to the results obtained with D_2O , which clearly contradict what was previously stipulated by other authors.

It has to be pointed out that, although the solution concentrations used for NMR and IR investigations were higher than the concentration used for GF coating, they were chosen in order to meet the sensitivity limits of the equipment used. The signals obtained for lower concentrations, did not allow clear detection of weak signals such as $(\text{C-H})_{\text{CH}_3}$ and $(\text{C-H})_{\text{CH}_2}$, as they could be seen as small peaks for higher concentrations. It should also be noted that silane concentration has an effect on their hydrolysis and condensation. However, the differences shown, suggest that something different happened when APS is prepared at RT and ET, either at higher or lower concentrations.

The strength of commercially coated GFs which had been heat treated at different temperatures was analysed in further detail. A severe drop in GF strength was observed with the increase in TD temperature. A large decrease in fibre strength was observed for conditioning temperatures between 350 and 450°C while at temperatures below

350⁰C it was less severe. For TD temperatures of 450⁰C up to 600⁰C, the strength became apparently stable, at a very low average value of around 0.5-0.7 GPa. The results obtained were consistent with the observations of other investigations of the temperature effect on GF mechanical properties. The results suggested that at temperatures around 350⁰C the APS coating on the GFs started to degrade and disappear, consequently reducing the protection provided by the APS layer with the addition of fibre structural relaxation due to water diffusion. On the other hand, the effect of high temperatures creating cracks and flaws may also contribute to the strength loss observed in these results. The relative average strength stability seen for conditioning temperatures between 450 and 600⁰C, can be misleading. While the average strength results were similar in this conditioning temperature range, it is quite probable that more severe structural changes were occurring with the temperature increase.

The HCl treatment did not have the effect expected on TD commercially coated GFs. Treatment with HCl, which allegedly increases the concentration of OH groups on GF surface, was expected to have an effect on mechanical properties of the TD GFs due to a better attachment of the silane to the GFs. The results did not show any substantial increase in GF strength. The best effect was obtained for the HCl and MPS treatment, with an increase of 27% on fibre strength, but this value was still not considered sufficient recovery for effective reusability as a reinforcement. On the other hand, it was observed that HCl treatment had a negative effect in combination with APS applied to TD GFs. This was probably due to the fact that APS does not have a good performance in acidic environments.

NaOH treatment was found to significantly increase fibre strength. TD commercially coated GFs treated with NaOH reached quite high values. This was found to be a promising treatment to take into consideration for the recovery of the recycled GFs. The best conditions for NaOH treatment were found to be for 3 M concentration, at 95⁰C for a period of 10 minutes. Due to the alkali degradation products found on the surface after NaOH treatment it is highly recommended to immerse GFs in HCl to remove these alkali degradation products. Another thing to take into consideration is that if GFs that are going to be treated and have any kind of

layer (i.e. silane), it is necessary to remove all or most part of the silane before applying any treatment, as was also shown.

The study using the FTIR (DRIFT) to characterise the GF after the NaOH treatments led to the conclusion that the 10 minutes NaOH treatment produced a higher increase of the OH in the GF sub-surface. The treatment combinations of NaOH with APS and MPS did not show anything else relevant, apart from the addition of the typical bands due to the silanes to the NaOH FTIR spectra.

Chapter 5 Summary and future work

It is well known that the mechanical properties of glass fibres (GFs) recycled from glass reinforced plastics (GRP) at high temperatures suffer a large loss in room temperature (RT) fibre strength. This is controlled by several factors, within which are mechanical damage (mainly due to fibre-fibre interaction), the effect of high temperature on GF structure (e.g. thermal compaction, flaw initiation and growth and relaxation) and the effect of temperature on surface coatings (e.g. coating degradation and the corresponding increased sensitivity to fibre surface damage).

The aim of this project was to supply experimental data leading to:

- A better understanding of the relative influence of these factors on GF RT strength.
- A better understanding of the effects on GF mechanical properties when coated with different silanes.
- To find a solution for this issue enabling the reuse of regenerated recycled GF as a reinforcement in composites.

Towards accomplishing this aim, three major work programmes have been conducted:

1. Estimation of the beneficial effect of a wide range of silanes on mechanical properties of as received uncoated GFs. This investigation was carried out to identify the effect of silane on repairing the mechanical damage mainly caused by fibre-fibre friction and mechanical handling damage. The measurement of fibre strength at RT was carried out after coating the fibres with the different silanes, and in some cases, in different ways of silane preparation. A new procedure developed for APS coating solution preparation led to a substantial improvement in the effect of APS on GF strength. This process resulted in two patent applications (WO2015/011490 and WO2016/116764).
2. The characterisation of the APS prepared at high temperature was carried out using nuclear magnetic resonance (NMR) and Fourier Transform Infrared spectroscopy (FTIR). Differences were identified between the results for

traditional RT silane preparation and this new ET method for preparing the APS.

3. Estimation of the thermal degradation of GF strength and its recovery was carried out to better understand the effect of temperature on GF strength. The results were consistent with the observations of other investigations, which showed that the exposure of GFs to thermal degradation at composite recycling temperatures, drastically reduced GF strength. Then a process using NaOH treatment was developed, finding the best conditions to treat the thermally degraded GFs with NaOH, regenerating the fibre strength to levels suitable for reuse as composite reinforcement materials. Then a combination of NaOH treatment with APS prepared at ET was also carried out, adding a further washing step between the NaOH treatment and the silane coating step, which produced further promising results. A summary of the main results presented in each chapter is given below:

As received untreated GFs were used to characterise the effect of three different silanes on single fibre strength at RT. The silanes used were γ -Aminopropyltriethoxy Silane (APS), γ -Methacryloxypropyltrimethoxy Silane (MPS) and γ -Glycidoxypropyltrimethoxy Silane (GPS). They were prepared in two different ways, varying the preparation time, pH and temperature. The highest average strength was found to be 1.83 GPa for as received GFs coated with APS prepared for 5 hours at 83°C and solution medium natural pH. Average strength for as received GFs coated with MPS and GPS, both prepared for 24 hours at RT and acidic pH for MPS and acidic or basic pH for GPS, were found to be 1.74 and 1.78 GPa respectively.

These results emphasised the importance of silane hydrolysis conditions. New conditions were developed for APS preparation with an important impact on the GF mechanical performance.

After obtaining these results, the characterisation of APS was identified as an interesting field for further research. An investigation of different conditions of pH and temperature applied when APS is prepared was carried out using ^1H NMR and FTIR equipment. The amount of the by-product (i.e. ethanol) in solution when APS is prepared at RT and other temperatures was investigated with NMR. It was found that

the ethanol and/or ethyl groups remaining in solution when APS is prepared at RT is 100% of the initial one. On the other hand, when APS was prepared at elevated temperature of 83⁰C (ET) the remaining concentration of ethanol and/or ethyl groups was found to be around only 20-25% of the initial one.

FTIR was used to determine the structural differences of APS prepared in both ways, RT and ET. ATR and Dialpath transmission were used to analyse solutions and several differences were found between them. The bands related to ethanol and ethyl groups showed higher peaks for RT APS whilst for ET APS seems to be much lower. This matches with the results of the NMR analysis. The bands related to the polymerisation of APS (Si-O-Si) showed a higher rate for ET APS than the RT APS. Moreover, DRIFT analysis, being not as clear as the analysis carried out for solutions, showed that the degree of polymerisation of ET APS was larger than RT APS, further supporting what was found in the APS solutions analyses.

Using cumulative failure probability analysis some interesting differences were found between both treatments. ET APS improved the strength and probably the flaw uniformity of as received GFs. Differences between ET and RT APS strength results. ET APS results showed a more even distribution, with a deviation of only 10% whereas with RT APS it was 25-30%. This suggested that ET APS preparation protects GFs in a more homogeneous way, with a more even distribution. Furthermore, it was found that RT APS GFs exhibited a similar behaviour to the commercially silane coated GFs. It was also suggested that ET APS preparation may provide a better silane performance than the classic APS preparation (i.e. RT APS).

Glass fibre strength characterisation of commercially silane coated GFs conditioned at different temperatures was carried out at RT. A severe drop in GF strength was observed with the increase of TD temperature. In particular, a large drop in fibre strength was observed for conditioning temperatures between 350 and 450⁰C, with a less severe decrease between RT and 350⁰C. For temperatures from 450⁰C up to 600⁰C, the strength apparently became stable, with a very low average fibre strength of around 0.50-0.70 GPa. The results obtained were consistent with the observations of other investigations effect of temperature on GF mechanical properties. These results suggested that the APS coating on the GF surface started to degrade at

temperatures around 350⁰C, with a consequent reduction of the protection provided by APS layer and probably the occurrence of structural relaxation in the GF due to water diffusion.

On the other hand, the effect of high temperature in creating cracks and flaws may also contribute to the strength loss seen in these results which are also consistent with the creation of defects for high temperatures. The relative average strength stability found for conditioning temperatures between 450 and 600⁰C, can be misleading. While the average strength results were similar in this conditioning temperature range, it is quite probable that more severe structural changes were occurring with increasing temperature.

Different chemical treatments were investigated in order to recover the strength of TD commercially coated GFs. An investigation of two different chemicals was carried out on GF strength of GFs conditioned at temperatures up to 600⁰C. This investigation was carried out using average fibre strength analysis, SEM, and DRIFT.

Hydrochloric acid (HCl) was used to chemically treated TD commercially coated GFs at 450⁰C for 25 minutes. The treatment did not have the expected effect. The combination of HCl and then coating the fibres with APS or MPS at room temperature did result in a limited increase in average fibre strength, but with values still below 1.0 GPa. The highest increase in average fibre strength was found to be for the combination of HCl and MPS, which resulted in a 27% increase in average fibre strength.

The use of sodium hydroxide (NaOH) treatment was also investigated. This was found to have a significant effect on average fibre strength when applied for 10 minutes at a temperature of 95⁰C and a concentration of 3M. Average fibre strength reached values up to 1.8 GPa for GFs thermally degraded at 450⁰C, but without any noticeable increase for higher temperatures.

A washing pretreatment (PW) was also applied before the TD process in order to remove part of the APS layer on GF surface to avoid possible undesirable reactions of the APS layer during the TD process. It was found that this PW treatment substantially influenced the performance of both ET APS and particularly NaOH treatments. The

combination of the PW treatments and NaOH had a very significant effect, even on TD GFs at 600⁰C, with average fibre strengths up to 1.5 GPa obtained. The GFs TD and treated with the PW and NaOH treatment, were also coated with APS.

It was also found that after the NaOH treatment significant residue was apparent on the GF surface, which presumably could interfere with the adhesion of APS to the GF surface. Two different options were applied to remove these deposits. HCl was applied after NaOH treatment, which removed most of the residues on the GF surface, with the inconvenience that the acidity left on GF surface had a negative effect on the deposition of APS. The second option was to rinse the fibres in elevated temperature water after the NaOH treatment with the same purpose. The results showed that for the deposition of APS this was a better choice but the remaining residue on the GF surface was still significant.

The results obtained from DRIFT analysis of TD GFs chemically treated with NaOH further support what was explained above and provided further information about the most effective NaOH treatment time. The first results obtained for TD then NaOH treated GFs showed an intense peak at around 3400 cm⁻¹ with longer NaOH treatment time. It could be misleading as the DRIFT measured the OH groups from the compounds on the GF surface, mainly due to residual NaOH. When these analyses were repeated on the same GFs washed with HCl, the higher OH⁻ band was found to be for a treatment time of 10 minutes, this time being the turning point from which the OH⁻ band started to decrease again. These results clearly showed that there is a promising potential treatment to significantly regenerate the performance of recycled GFs from GRP.

The strength performance of the GFs treated with different silanes, TD and chemically treated has been the main focus throughout this work and this makes the mechanical characterisation of the GF strength become an essential routine. The results obtained in this work open an interesting possibility in terms of cost-effective treatments to recover the GF strength of recycled GFs from GRP with the purpose of using them as suitable materials for reinforcing composite materials again.

From the foregoing summary the following directions for **future work** on this subject can be identified as:

1. Further investigation of the chemical treatment times is needed in order to find the lower limit of preparation time.
2. Further verification of the structural differences between RT and ET APS is needed. Matrix-Assisted Laser Desorption/Ionization (MALDI-TOF) or other similar equipment is suggested to further investigate the polymer size differences. To look for characteristic differences, Light Scattering (e.g. Dynamic Light Scattering) and Gel Permeation Chromatography (GPC) are techniques to consider for this purpose, as they are well known techniques used in polymer analysis. A well prepared ^1H NMR analysis of the RT and ET APS solutions may also be of interest in order to further understand the reactions occurring during the preparation time.
3. The NaOH treatment should be further investigated in order to find a better way to remove the residues from the GF surface which will then improve the adhesion of the silanes to the regenerated GFs.
4. Further investigation of the HCl as an alternative treatment to recover the GF strength of recycled GFs is needed. It has the potential of not leaving any residues. It has to be applied in a similar way as NaOH, i.e. at high temperatures (e.g. 90°C for 25% v/v HCl).

Chapter 6 References

- [1] Loewenstein KL. The Manufacturing Technology of Continuous Glass Fibres. Amsterdam: Elsevier, 1993.
- [2] Sugarman B. Strength of Glass (A Review). *Journal of Material Science* 2 1967;2:275–83.
- [3] Meyers M, Chawla K. Mechanical behavior of materials. 2nd ed. Cambridge University Press, 2009.
- [4] Thomason JL, Jenkins P, Yang L. Glass fibre strength – A review with relation to composite recycling. *Fibers* 2016; 4, 18.
- [5] Wallenberger FT, Watson JC, Li H. Glass Fibers. ASM Handbook Volume 21: Composites. In: Miracle DB, Donaldson SL, Eds.. Composites 21st ed. ASM International: Novelt, OH, USA, 2001, pp. 1-8.
- [6] Gupta PK. Glass fibers for composite materials. Fibre reinforcements for composite materials, Chapter 2. In: Brunzell AR, Ed., Amsterdam: Elsevier, 1988. pp. 19-71.
- [7] Hull D, Clyne TW. An introduction to Composite Materials. 2nd ed. Cambridge solid state science series, 1996.
- [8] Loewenstein KL. The manufacture of continuous glass fibres. *Platinum Metals Rev.* 1975;19:82–7.
- [9] Gupta PK. Strength of glass fibers. *Fiber Fract.* Elices M, Lorca J, Eds. 1st ed. Elsevier Science 2002, 129–151.
- [10] Thomason JL. Glass Fibre Sizings: a review of scientific literature. Blurb Incorporated, 2012. ISBN 978-0-9573814-3-8. Available online: <http://www.blurb.com/b/6244677-glass-fibre-sizings> (accessed September 5th, 2017).
- [11] Jones FR. Handbook of Polymer-Fibre Composites. Essex and New York: Polymer Science and Technology, 1994.
- [12] Jones FR, Wang D. ToF-SIMS and XPS Studies of the interaction of silanes and matrix resins with glass surfaces. *Surface Interface Analysis* 1993; 20:457–67.
- [13] Bartenev GM. The structure and strength of glass fibers of different chemical composition. *Materials Science and Engineering* 1968;4:22–8.
- [14] Goldstein M. Glass Fibers with Oriented Chain Molecules. *Journal of the American Ceramic Society* 1955; 38:1953–6.
- [15] Brannan RT. Further Evidence Against the Orientation of Structure in Glass Fibers. *Journal of the American Socciety* 1953;36:230–231.
- [16] Otto WH. Compaction effects in glass fibers. *Journal of the American Ceramic*

Society 1958; 44:68–72.

- [17] Kaw AK. *Mechanics of Composite Materials*. 2nd ed. Boca Raton, London, New York, Taylor&Francis Group, 2006.
- [18] Kolesov YI, Kudryavtsev MY, Mikhailenko NY. Types and compositions of glass for production of continuous glass fibre (review). *Glass and Ceramics* 2001;58:197–202.
- [19] Wallenberger FT. *Fiberglass and Glass Technology*. Boston, MA: Springer US, 2010.
- [20] Lawn BR. *Fracture of brittle solids*. 2nd ed. Cambridge solid state science series, 1993.
- [21] Schmitz GK, Metcalfe AG. Stress Corrosion of E-Glass Fibres. *I&EC Product Research and Development* 1965; 5:1–8.
- [22] Griffith AA. The Phenomena of Rupture and Flow in Solids. *Philosophical Transactions of the Royal Society of London* 1921;221:163–98. .
- [23] Schmitz GK, Metcalfe AG. Stress Corrosion of E-Glass Fibers. *Product Research Development*, 1966; 5:1–8.
- [24] Jones FR, Rock JW. On the mechanism of stress corrosion of E-glass fibres. *Journal of Material Science Letters* 2, 1983; 415–418.
- [25] Charles RJ. Static Fatigue of Glass. I. *Journal of Applied Physics*, 1958; 29:1549-1552.
- [26] Charles RJ. Static Fatigue of Glass. II. *Journal of Applied Physics* 1958; 29:1554-1560.
- [27] Rodriguez EL. Corrosion of glass fibres. *Journal of Material Science Letter* 6 1987; 6:718–720.
- [28] Kurkjian CR, Gupta PK, Brow RK, Lower N. The intrinsic strength and fatigue of oxide glasses. *Journal of Non-Crystalline Solids* 2003;316:114–124.
- [29] Bartenev GM, Sidorov AB. The Effect of Length of Glass fibers on their Strength. *Glass and Ceramics* 1965; 22:597–599.
- [30] Otto WH. Relationship of Tensile Strength of Glass Fibers to Diameter. *Journal of the American Ceramic Society* 1955 38:122–124.
- [31] Weibull W. *A Statistical Theory of the Strength of Materials*. Royal Technical University, Stockholm, 1939.
- [32] Weibull W. A Statistical Distribution Function of Wide Applicability. *Journal of Applied Mechanics* 1951; 293–297.
- [33] Thomason JL. On the application of Weibull analysis to experimentally determined single fibre strength distributions. *Composites Science and Technology* 2013; 77:74–80.
- [34] Beetz JCP. The analysis of carbon fibre strength distributios exhibiing multiple

- modes of failure. *Fibre Science and Technology* 1982; 16:45–59.
- [35] Zinck P, Mader E, Gerard JF. Role of silane coupling agent and polymeric film former for tailoring glass fiber sizings from tensile strength measurements. *Journal of Material Science* 2001; 36:5245–5252.
- [36] Masson JJ, Bourgain E. Some guidelines for a consistent use of the Weibull statistics with ceramic fibres. *International Journal of Fracture* 1992; 55:303–319.
- [37] Asloun EM, Donnet JB, Guilpain G, Nardin M, Schultz J. On the estimation of the tensile strength of carbon fibres at short lengths. *Journal of Material Science* 1989; 24:3504–3510.
- [38] Mader E, Jacobasch H-J, Grundke K, Gietzelt T. Influence of an optimized interphase on the properties of polypropylene/glass fibre composites. *Composites Part A: Applied Science and Manufacturing* 1996; 27:907–912.
- [39] Plueddemann EP. *Silane coupling agents*. 2nd ed. New York: Plenum Press, 1991.
- [40] Plueddemann EP. Silane primers for epoxy adhesives. *Adhesion Science Technology* 1988; 2:3–5.
- [41] Shokoohi S, Arefazar A, Khosrokhavar R. Silane Coupling Agents in Polymer-based Reinforced Composites: A Review. *Reinforced Plastics and Composites* 2008; 27:473–485.
- [42] Mittal KL, Ed.. *Silanes and Other Coupling Agents*. Volume 4. Boca Raton: VSP, 2007.
- [43] Pape PG, Plueddemann E. Methods for improving the performance of silane coupling agents. *Adhesion Science Technology* 1991; 5:831–842.
- [44] Thomason JL. Interfaces and interfacial effects in glass reinforced thermoplastics. 28th Risø Int. Symposium Material Science, Risø National Laboratory, Roskilde, Denmark 2007.
- [45] Briard R, Barthel E, Laurent G, Heitz C. Glass strengthening by organosilane water-based coatings. In: *Silanes and Other Coupling Agents*. Mittal KL, Ed., 2007; vol. 4 pp 99-112.
- [46] Thomason JL, Adzima LJ. Sizing up the interphase : an insider's guide to the science of sizing. *Composites Part A: Applied Science and Manufacturing* 2001; 32:313–321.
- [47] Salon M-CB, Bayle P-A, Abdelmouleh M. Kinetics of hydrolysis and self condensation reactions of silanes by NMR spectroscopy. *Colloids Surfaces A: Physicochemical and Engineering Aspects* 2008; 312:83–91.
- [48] Osterholtz FD, Pohl ER. Kinetics of the hydrolysis and condensation of organofunctional alkosysilanes: a review. *Journal of Adhesion Science Technology* 1992; 6:127–149.

- [49] Naviroj S, Culler SR, Koenig JL, Ishida H. Structure and adsorption characteristics of silane coupling agents on silica and E-glass fiber; dependence on pH. *Journal of Colloid and Interface Science* 1984; 97:308–317.
- [50] Sáez E, Yang L, Thomason JL. Investigation of Strength Recovery of Recycled Heat Treated Glass Fibres through Chemical Treatments. 19th International Conference on Composites Matererials, Montreal 2013.
- [51] Peña-Alonso R, Rubio F, Rubio J, Oteo JL. Study of the hydrolysis and condensation of γ -Aminopropyltriethoxysilane by FT-IR spectroscopy. *Journal of Material Science* 2007; 42:595–603.
- [52] Ogasawara T, Yoshino A, Okabayashi H, O'Connor CJ. Polymerization process of the silane coupling agent 3-aminopropyltriethoxy silane – ¹H NMR spectra and kinetics of ethanol release. *Colloids Surfaces A: Physicochemical and Engineering Aspects* 2001; 180:317–322.
- [53] Witucki GL. Silane primer: chemistry and applications of alkoxy silanes. *Journal of Coatings Technoloy* 1993; 65:57–60.
- [54] Johansson OK, Stark FO, Vogel GE, Fleischmann RM. Evidence for Chemical Bond Formation at Silane Coupling Agent Interfaces. *Journal of Composite Materials* 1967; 1:278–292.
- [55] Kaas RL, Kardos JL. The Interaction of Alkoxy Silane Coupling Agents with Silica Surfaces. *Polymer Engineering Science* 1971; 11:11-18.
- [56] Droste DH, Dibenedetto a. T. The glass transition temperature of filled polymers and its effect on their physical properties. *Journal of Applied Polymer Science* 1969; 13:2149–2168.
- [57] Kwei TK, Kumins CA. Polymer-Filler Interaction: Vapor Sorption Studies. *Journal of Applied Polymer Science* 1964; 8:1483–1490.
- [58] Shenoy A V. Rheology of filled polymer systems. 1st ed. Springer-Science and Busines Media, Pune, India 1999.
- [59] Ishida H, Koenig JL. The Reinforcement Mechanism of Fiber-Glass Reinforced Plastics Under Wet Conditions: A Review. *Polymer Engineering and Science* 1978; 18:128–145.
- [60] Throckmorton PE, Browne MF. The Effect of Surface Tension and Strength of Glass Fiber Reinforced Plastics. 20th Annual Technology Conference of the Reinforced Plastics Division, Chicago: 1965, Section 15-A.
- [61] Bascom WD. Some Surface Chemical Aspects of Glass-Resin Composites Part 1- Wetting Behavior of Epoxy Resins on Glass Filaments.pdf. 20th Annual Techology Conference of the Reinforced Plastics Division, Chicago: 1965, Section 15-B, 1-14.
- [62] Pasternack RM, Rivillon Amy S, Chabal YJ. Attachment of 3-(Aminopropyl)triethoxysilane on silicon oxide surfaces: dependence on solution temperature. *Langmuir* 2008; 24:12963–12971.

- [63] H.Ishida, S.Naviroj, Koenig JL. The Influence of a Substrate on the Surface Characteristics of Silane Layers. In: *Physicochemical Aspects of Polymer Surfaces*. Mittal KL, Ed., New York, 1983; vol. 1, Part 1, pp. 91–104.
- [64] Ishida H. Controlled Interphases in Glass Fiber and Particulate Reinforced Polymers: Structure of Silane Coupling Agents in Solutions and on Substrates. *The Interfacial Interactions in Polymeric Composites* 1993; 169–199.
- [65] Wang D, Jones FR, Denison P. TOF SIMS and XPS study of the interaction of hydrolysed γ -aminopropyltriethoxysilane with E-glass surfaces. *Journal of Adhesion Science and Technology* 1992; 6:79–98.
- [66] Liu XM, Thomason JL, Jones FR. XPS and AFM study of interaction of organosilane and sizing with e-glass fibre surface. *Journal of Adhesion* 2008; 84:322–338.
- [67] Culler SR, Ishida H, Koenig JL. Structure of silane coupling agents adsorbed on silicon powder. *Journal of Colloid and Interface Science* 1985; 106:334–346.
- [68] Izmailova LK, Bartenev GM. Investigating the production cycles for glass fibers without surface defects. *Steklo I Keramika* 1964; 21:12–16.
- [69] Thomason JL, Kalinka G. A technique for the measurement of reinforcement fibre tensile strength at sub-millimetre gauge lengths. *Composite Part A: Applied Science and Manufacturing* 2001; 32:85–90.
- [70] Zinck P, Pays MF, Rezakhanlou R, Gerard JF. Mechanical characterisation of glass fibres as an indirect analysis of the effect of surface treatment. *Journal of Material Science* 1999; 34:2121–2133.
- [71] Yang L, Thomason JL. Effect of silane coupling agent on mechanical performance of glass fibre. *Journal of Material Science* 2012; 48:1947–1954.
- [72] White L, Tripp C. Reaction of (3-Aminopropyl)dimethylethoxysilane with Amine Catalysts on Silica Surfaces. *Journal of Colloid and Interface Science* 2000; 232:400–407.
- [73] Vrancken KC, De Coster L, Van Der Voort P, Grobet PJ, Vansant EF. The Role of Silanols in the Modification of Silica Gel with Aminosilanes. *Journal of Colloid and Interface Science* 1995; 170:71–77.
- [74] Arora PS, Matison JG, Provas A, Smart RSC. Aminohydroxysiloxanes on E-Glass Fibers. *Langmuir* 1995; 11:2009–2017.
- [75] Howarter JA, Youngblood JP. Optimization of silica silanization by 3-aminopropyltriethoxysilane. *Langmuir* 2006; 22:11142–11147.
- [76] Vandenberg ET, Bertilsson L, Liedberg B, Uvdal K, Erlandsson R, Elwing H, et al. Structure of 3-aminopropyl triethoxy silane on silicon oxide. *Journal of Colloid and Interface Science* 1991; 147:103–118.
- [77] Culler SR, Ishida H, Koenig JL. The Silane Interphase of Composites: Effects of Process Conditions on Gamma-Aminopropyltriethoxysilane. *Polymer Composites* 1986; 7:231–238.

- [78] Ishida H, Naviroj S, Tripathy SK, Fitzgerald JJ, Koenig JL. The structure of an Aminosilane Coupling Agent in Aqueous solution Partially Cured Solids. *Journal of Polymer Science* 1982; 20:701–718.
- [79] Yang L, Thomason JL. The thermal behaviour of glass fibre investigated by thermomechanical analysis. *Journal of Material Science* 2013; 48:5768–5775.
- [80] Feih S, Boiocchi E, Mathys G, Mathys Z, Gibson AG, Mouritz AP. Mechanical properties of thermally-treated and recycled glass fibres. *Composites Part B* 2011; 42:350–358.
- [81] Thomason JL, Yang L, Meier R. The properties of glass fibres after conditioning at composite recycling temperatures. *Composites Part A* 2014; 61:201–208.
- [82] Jenkins PG, Thomason JL, Meier R. Separation of mechanical and thermal degradation of thermally conditioned sized glass fibre. 15th European Conference on Composite Materials, Venice 2012.
- [83] Aslanova MS. The Strength and chemical composition of glass. *Steklo I Keramika* 1967; 24:1–4.
- [84] Aslanova MS, Ivanov NV, Balashov YS. Effect of chemical composition on the relaxation properties of thin glass fibers. *Steko I Keramika* 1970; 21–4.
- [85] Narayanaswamy OS. A Model of Structural Relaxation in Glass. *Journal of the American Ceramic Society* 1971; 54:491–498.
- [86] Garofalini SH, Webb III EB. Relaxation of silica glass surfaces before and after stress modification in a wet and dry atmosphere: molecular dynamics simulations 1998: 47–57.
- [87] Proctor BA, Whitney I, Johnson JW. The Strength of Fused Silica. *Proceedings of the Royal Society of London, Ser A, Mathematical Physical Science* 1967; 297:534–557.
- [88] Duan RG, Roebben G, Biest O Van der. Glass microstructure evaluations using high temperature mechanical spectroscopy measurements. *Journal of Non-Crystalline Solids* 2003; 316:138–145.
- [89] Bartenev GM, Motorina LI. Effect of tensile stresses on the strength of heat-treated glass fibres. *Mekhanika Polimerov* 1965;1:89–92.
- [90] Sakka S. Effect of Reheating on Strength of Glass Fibers. *Bulletin of the Institute for Chemical Research* 1957; 34:316–320.
- [91] Thomas WF. An investigation of the factors likely to affect the strength and properties of glass fibres. *Physics and Chemistry of Glasses* 1960; 1:4–18.
- [92] Cameron NM. Effect of prior heat treatment on the strength of glass fibers measured at room temperature. *Journal of the American Ceramic Society* 1965; 385.
- [93] Piggott MR, Yokom JC. The Weakening of silica fibres by heat treatment. *Glass*

Technology 1968.

- [94] Aslanova MS. The Effect of Different Factors on the Mechanical Properties of Glass Fibers. *Steklo I Keramika* 1960; 17:10–15.
- [95] Dorzhiev DB, Khazanov VE, Gorbachev VV. Some features of the structure and strength of a magnesium aluminosilicate fiber. *The Soviet Journal of Glass Physics and Chemistry* 1990; 15:99–102.
- [96] Tomozawa M, Kim D-L, Agarwal A, Davis KM. Water diffusion and surface structural relaxation of silica glasses. *Journal of Non-Crystalline Solids* 2001; 288:73–80.
- [97] Tomozawa M, Hepburn RW. Surface structural relaxation of silica glass: A possible mechanism of mechanical fatigue. *Journal of Non-Crystalline Solids* 2004; 345–346:449–460.
- [98] Tomozawa M, Lezzi PJ, Hepburn RW, Blanchet T a., Cherniak DJ. Surface stress relaxation and resulting residual stress in glass fibers: A new mechanical strengthening mechanism of glasses. *Journal of Non-Crystalline Solids* 2012; 358:2650–2662.
- [99] Spiernings GACM. Review: Wet chemical etching of silicate glasses in hydrofluoric acid based solutions. *Journal of Material Science* 1993; 28:6261–6273.
- [100] Ray NH, Stacey MH. Increasing the Strength of Glass by Etching and Ion-Exchange. *Journal of Material Science* 1969; 4:73–79.
- [101] Bartenev GM. Constitution and strength of glass fibers. *International Journal Fracture Mechanics* 1969; 5:179–186.
- [102] Levengood WC. Study of Moisture-Condensation Patterns on Glass and Crystalline Surfaces. *Journal of the American Ceramic Society* 1955; 38:179–183.
- [103] Inniss D, Zhong Q, Kurkjian CR. Chemically Corroded Pristine Silica Fibres: Blunt or Sharp Flaws?. *Journal of the American Ceramic Society* 1993; 76:3173–3177.
- [104] Takahagi T, Nagai I, Ishitani A, Kuroda H, Nagasawa Y. The formation of hydrogen passivated silicon single-crystal surfaces using ultraviolet cleaning and HF etching. *Journal of Applied Physics* 1988; 64:3516–3521.
- [105] Takahagi T, Ishitani A, Kuroda H, Nagasawa Y. Fluorine-containing species on the hydrofluoric acid etched silicon single-crystal surface. *Journal of Applied Physics* 1991; 69:803–807.
- [106] Tso ST, Pask JA. Reaction of Glasses with Hydrofluoric Acid Solution. *Journal of the American Ceramic Society* 1982; 65:360–362.
- [107] Yang L, Sáez E, Thomason J. Regeneration of Thermally Recycled Glass Fibre for Cost-Effective Composite Recycling : Increasing the strength of thermally conditioned glass fibres by HF treatment. 16th European Conference on

Composite Materials, Sevilla 2014.

- [108] Yang L, Sáez E, Nagel U, Thomason JL. Can thermally degraded glass fibre be regenerated for closed-loop recycling of thermosetting composites? *Composites Part A* 2015; 72:167-174.
- [109] Iliescu C, Jing J, Tay FEH, Miao J, Sun T. Characterization of masking layers for deep wet etching of glass in an improved HF/HCl solution. *Surface and Coatings Technology* 2005; 198:314–318.
- [110] Machavaram VR, Badcock RA., Fernando GF. Fabrication of intrinsic fibre Fabry-Perot sensors in silica fibres using hydrofluoric acid etching. *Sensors and Actuators A* 2007; 138:248–260.
- [111] Baselga J, Aznar AJ, Gonzalez J. Microstructural and wettability study of surface pretreated glass fibres. *Journal of Material Process and Technolgy* 1999; 92–93:129–134.
- [112] Smith RD, Corbin PE. Attack of Glasses By Alkaline Solutions. *Journal of the Ameraican Ceramic Society* 1949; 32:195–198.
- [113] Kouassi SS, Andji J, Bonnet J, Rossignol S. Dissolution of waste glasses in high alkaline solutions. *Ceram Silikáty* 2010; 54:235–240.
- [114] Molchanov VS, Prikhidko NE. Corrosion of silicate glasses by alkaline solutions. *Bulletin of the Academy of Science of the USSR, Division of Chemical Science* 1995; 6:1179–1184.
- [115] Herrmann M, Schilm J, Michael G, Meinhardt J, Flegler R. Corrosion of silicon nitride materials in acidic and basic solutions and under hydrothermal conditions. *Journal of the European Ceramic Society* 2003; 23:585–594.
- [116] Wiederhorn SM, Fuller ER, Thomson R. Micromechanisms of crack growth in ceramics and glasses in corrosive environments. *Metal Science* 1980; 14:450–458.
- [117] Cras J., Rowe-Taitt C., Nivens D., Ligler F. Comparison of chemical cleaning methods of glass in preparation for silanization. *Biosensors and Bioelectronics* 1999; 14:683–688.
- [118] Wei B, Cao H, Song S. Environmental resistance and mechanical performance of basalt and glass fibers. *Material Science Engineering A* 2010; 527:4708–4715.
- [119] Wei B, Cao H, Song S. Tensile behavior contrast of basalt and glass fibers after chemical treatment. *Materials and Design* 2010; 31:4244–4250.
- [120] Almeida RM, Pantano CG. Structural investigation of silica gel films by infrared spectroscopy. *Journal of Applied Physics* 1990; 68:4225.
- [121] Innocenzi P. Infrared spectroscopy of sol–gel derived silica-based films: a spectra-microstructure overview. *Journal of Non-Crystalline Solids* 2003; 316:309–319.

- [122] Alessi A, Agnello S, Buscarino G, Gelardi FM. Raman and IR investigation of silica nanoparticles structure. *Journal of Non-Crystalline Solids* 2013; 362:20–24.
- [123] Pandurangi RS, Seehra MS, Razzaboni BL, Bolsaitis P. Surface and bulk infrared modes of crystalline and amorphous silica particles: a study of the relation of surface structure to cytotoxicity of respirable silica. *Environmental Health Perspectives* 1990; 86:327–336.
- [124] Reilly SP, Thomason JL. Effects of silane coating on the properties of glass fibre and glass fibre reinforced epoxy resin. 14th European Conference on Composite Materials, Budapest 2010.
- [125] Quek MY, Yue CY. The interfacial properties of fibrous composites. *Journal of Material Science* 1994; 29:2487–2490.
- [126] Sáez E, Yang L, Thomason JL. Regeneration of Thermally Recycled Glass Fibre for Cost-effective Composite Recycling: Increasing the Strength of Thermally Conditioned Glass Fibres using Cost effective ReCoVeR Treatments. European Conference on Composite Materials, Sevilla 2014.
- [127] Yang L (2011). A Physical Approach To Interfacial Strength In Fibre Reinforced Thermoplastic Composites. PhD thesis, University of Strathclyde, Glasgow, United Kingdom.
- [128] ASTM. Standard Test Method for Tensile Strength and Young's Modulus of Fibers. 2008.
- [129] Jenkins PG, Yang L, Liggat JJ, Thomason JL. Investigation of the strength loss of glass fibre after thermal conditioning. *Journal of Material Science* 2014; 50:1050–1057.
- [130] Davis KM, Tomozawa M. Water diffusion into silica glass : structural changes in silica glass and their effect on water solubility and diffusivity. *Journal of Non-Crystalline Solids* 1995; 185:203–220.
- [131] Gottlieb HE, Kotlyar V, Nudelman A. NMR Chemical Shifts of Common Laboratory Solvents as Trace Impurities. *Organic Chemistry* 1997; 62:7512–7515.
- [132] Culler S., Ishida H, Koenig J. FT—IR characterization of the reaction at the silane/matrix resin interphase of composite materials. *Journal of Colloid Interface Science* 1986; 109:1–10.
- [133] Heitz C, Laurent G, Briard R, Barthel E. Cross-condensation and particle growth in aqueous silane mixtures at low concentration. *Journal of Colloid Interface Science* 2006; 298:192–201.
- [134] Chalmers JM. Handbook of vibrational spectroscopy. Volume 2: Anomalies, artifacts and common errors in using vibrational spectroscopy techniques. In: Chalmer JM, Griffiths PR, Eds. *Sampling Techniques for Vibrational Spectroscopy*. John Wiley and Sons; 2006, p. 2327-2347.
- [135] Ishida H, Koenig JL. Fourier transform infrared spectroscopic study of the

- silane coupling agent/porous silica interface. *Journal of Colloid Interface Science* 1978; 64:555–564.
- [136] McKenzie MT, Culler SR, Koenig JL. Applications of Diffuse Reflectance FT-IR to the Characterization of an E-Glass Fiber/ γ -APS Coupling Agent System. *Applied Spectroscopy* 1984; 38:786–790.
- [137] Murthy RSS, Leyden DE. Quantitative determination of (3-aminopropyl)triethoxysilane on silica gel surface using diffuse reflectance infrared Fourier transform spectrometry. *Analytical Chemistry* 1986; 58:1228–1233.
- [138] Culler SR, Naviroj S, Ishida H, Koenig JL. Analytical and spectroscopic investigation of the interaction of CO₂ with amine functional silane coupling agents on glass fibers. *Journal of Colloid Interface Science* 1983; 96:69–79.
- [139] Coates J. *Encyclopedia of analytical chemistry. Interpretation of infrared spectra, a practical approach.* Meyers RA, Ed., Chichester: John Wiley and Sons; 2000, p. 10815-10837.
- [140] Salon MB, Belgacem MN. Competition between hydrolysis and condensation reactions of trialkoxysilanes, as a function of the amount of water and the nature of the organic group. *Colloids and Surfaces A: Physicochemical and Engineering Aspects* 2010; 366:147–154.
- [141] Paquet O, Brochier Salon M-C, Zeno E, Belgacem MN. Hydrolysis-condensation kinetics of 3-(2-amino-ethylamino)propyl-trimethoxysilane. *Material Science Engineering C* 2012; 32:487–493.
- [142] Larkin PJ. *IR and Raman Spectroscopy. Principles and spectral interpretation.* Amsterdam: Elsevier, 2011.
- [143] Stuart BH. *Infrared Spectroscopy: fundamentals and applications.* Chichester: John Wiley and Sons, 2004.
- [144] Keeler J. *Understanding NMR Spectroscopy.* 2nd ed. Chichester: John Wiley and Sons, 2010.
- [145] Gerathanassis IP, Troganis A, Exarchou V, Barbarossou K. Nuclear Magnetic Resonance (NMR) Spectroscopy: Basic Principles and Phenomena, and Their Applications To Chemistry, Biology and Medicine. *Chemistry Education: Research and Practice in Europe* 2002; 3:229–252.
- [146] Atkins PW. *Physical Chemistry.* 6th ed. New York: Oxford University Press; 1998.
- [147] Banwell CN. *Fundamentals of Molecular Spectroscopy.* 3rd ed. London; McGraw Hill 1983.
- [148] Harris RK. *Nuclear Magnetic Resonance Spectroscopy (A physicochemical view).* London: Pitman Publishing; 1983.
- [149] ASTM. *Standard Test Method for Tensile Properties of Yarns by the Single-Strand Method 1.* 2012.

Chapter 7 Appendix

7.1 Fourier Transform Infrared spectroscopy (FTIR)

IR Absorption Process

The typical IR spectrometer broad band source emits all IR frequencies of interest simultaneously with the near-IR region between 14000-4000 cm^{-1} , the mid-IR region between 4000-400 cm^{-1} , and the far-IR region between 400-10 cm^{-1} respectively. Typical of absorption spectroscopy, the relationship between the intensities of the incident and transmitted IR radiation and the analyte concentration is governed by the Beer-Lambert law. The IR spectrum is obtained by plotting the intensity (absorbance or transmittance) versus the wavenumber, which is proportional to the energy difference between the ground and the excited vibrational states.

Two important components to the IR absorption process are the radiation frequency and the molecular dipole moment. The interaction of the radiation with molecules can be described in terms of a resonance condition where the specific oscillating radiation frequency matches the natural frequency of a particular normal mode of vibration. In order for energy to be transferred from the IR photon to the molecule via absorption, the molecular vibration must cause a change in the dipole moment of the molecule. This is the familiar selection rule for IR activity.

The dipole moment, μ , for a molecule is a function of the magnitude of the atomic charges (e_i) and their positions (r_i):

$$\mu = \sum e_i r_i \quad (7.1)$$

The dipole moments of uncharged molecules result from partial charges on the atoms, which can be determined from molecular orbital calculations. As a simple approximation, the partial charges can be estimated by comparison of the electro negativities of the atoms. Homonuclear diatomic molecules such as H_2 , N_2 and O_2 have no dipole moment and are IR inactive while heteronuclear diatomic molecules such as HCl , NO and CO have dipole moments and have IR active vibrations.

The IR absorption process involves absorption of the energy by the molecule if the vibration causes a change in the dipole moment, resulting in a change in the vibrational energy level. Figure 7.1 shows the oscillating electric field of the IR radiation generating forces on the molecules dipole where the oscillating electric field drives the oscillation of the molecular dipole moment and alternately increases and decreases the dipole spacing.

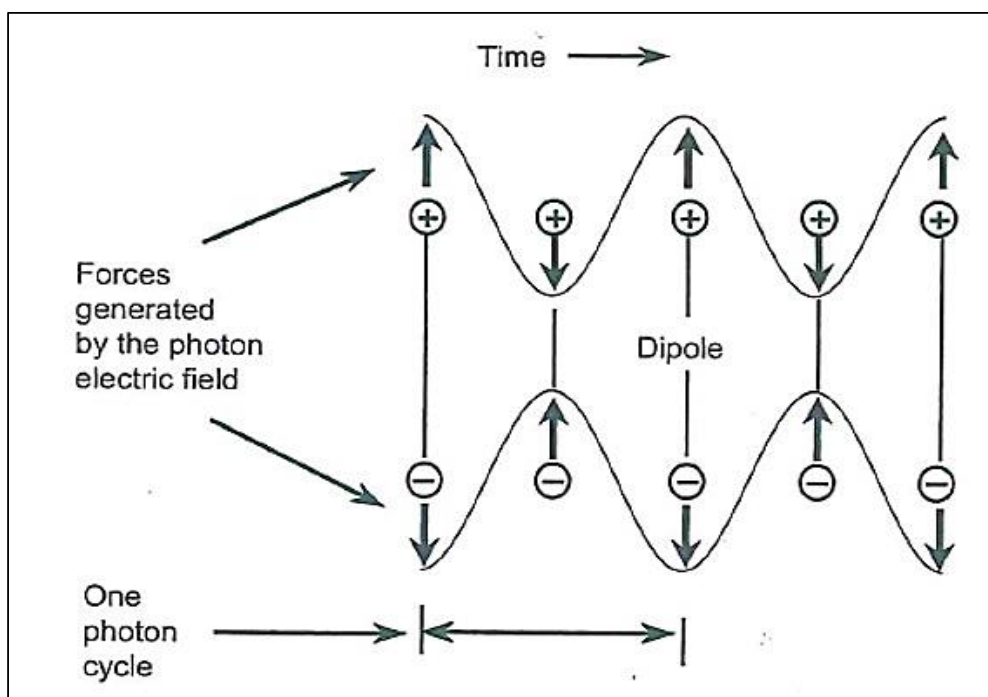


Figure 7.1 The oscillation electric field of photon generates oscillating, oppositely directed forces on the positive and negative charges of the molecular dipole. The dipole oscillates with the same frequency as the incident photon [142].

Here, the electric field is considered to be uniform over the whole molecule since the wavelength (λ) is much greater than the size of most molecules. In terms of quantum mechanics, the IR absorption is an electric dipole operator mediated transition where the change in the dipole moment, μ , with respect to a change in the vibrational amplitude, Q , is greater than zero.

$$\left(\frac{\partial \mu}{\partial Q}\right) \neq 0 \quad (7.2)$$

The measured IR band intensity is proportional to the square of the change in the dipole moment [142].

FTIR Spectrometers

In a FTIR spectrometer, sampling occurs just prior to the detector and its collimating optics. Commercial FTIR spectrometers typically operate in a single beam mode requiring sequential measurements of sample spectra whose ratio to the single beam background provide the final absorbance or % transmittance IR spectrum. The single beam background spectrum provides a wavelength-dependent throughput of the instrument and is a function of the source emission, detector response, beamsplitter properties, and residual atmospheric absorptions from carbon dioxide and water vapour [142].

Molecular vibrations

There are two types of molecular vibrations: stretching and bending. Vibrations can involve either a change in bond length (stretching) or bond angle (bending) (Figure 7.2). Some bonds can stretch in-phase (symmetric stretching) or out-of-phase (asymmetric stretching), as shown in Figure 7.3. If a molecule has different terminal atoms such as HCN, ClCN or NOCl, then the two stretching modes are no longer either symmetric or asymmetric vibrations of similar bonds, but will have varying proportions of the stretching motion of each group. In other words, the amount of coupling will vary [143].

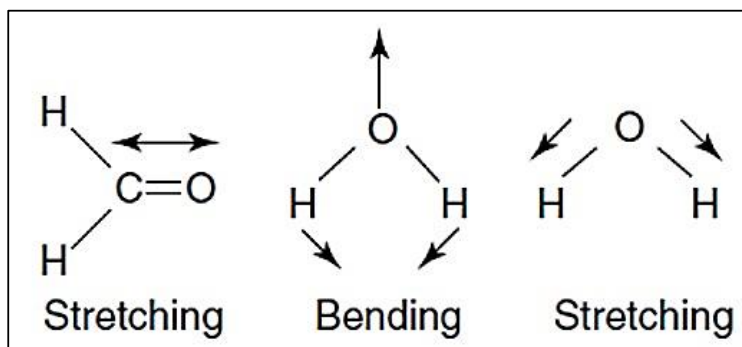


Figure 7.2 Stretching and bending vibrations [143].

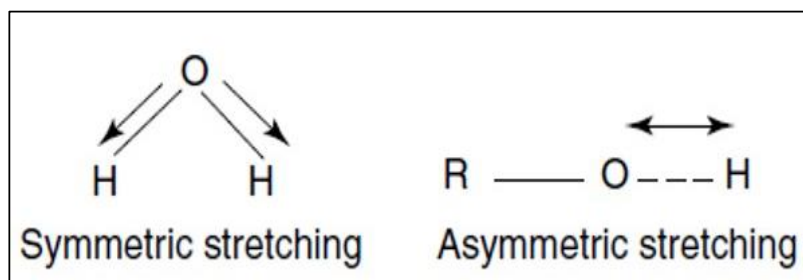


Figure 7.3 Symmetric and asymmetric vibrations [143].

Bending vibrations also contribute to infrared spectra and these are summarized in Figure 7.4. It is best to consider the molecule being cut by a plane through the hydrogen atoms and the carbon atom. The hydrogen atoms can move in the same direction or in opposite directions in this plane (which here is the plane of the page) [143].

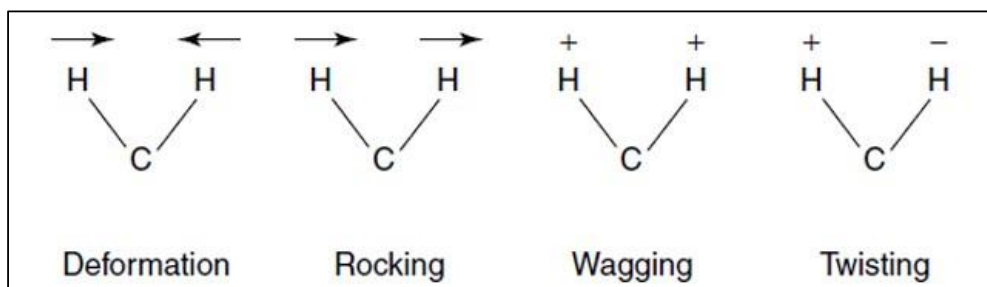


Figure 7.4 Different types of bending vibrations [143].

Symmetrical molecules will have fewer ‘infrared-active’ vibrations than asymmetrical molecules. This leads to the conclusion that symmetric vibrations will generally be weaker than asymmetric vibrations, since the former will not lead to a change in dipole moment. It follows that the bending or stretching of bonds involving atoms in widely separated groups of the periodic table will lead to intense bands. Vibrations of bonds such as C–C or N=N will give weak bands. This again is because of the small change in dipole moment associated with their vibrations. There will be many different vibrations for even fairly simple molecules. The complexity of an infrared spectrum arises from the coupling of vibrations over a large part of, or over the complete molecule. Such vibrations are called skeletal vibrations. Bands associated with skeletal vibrations are likely to conform to a pattern or fingerprint of the molecule as a whole, rather than a specific group within the molecule [143].

7.1.1 FTIR spectra

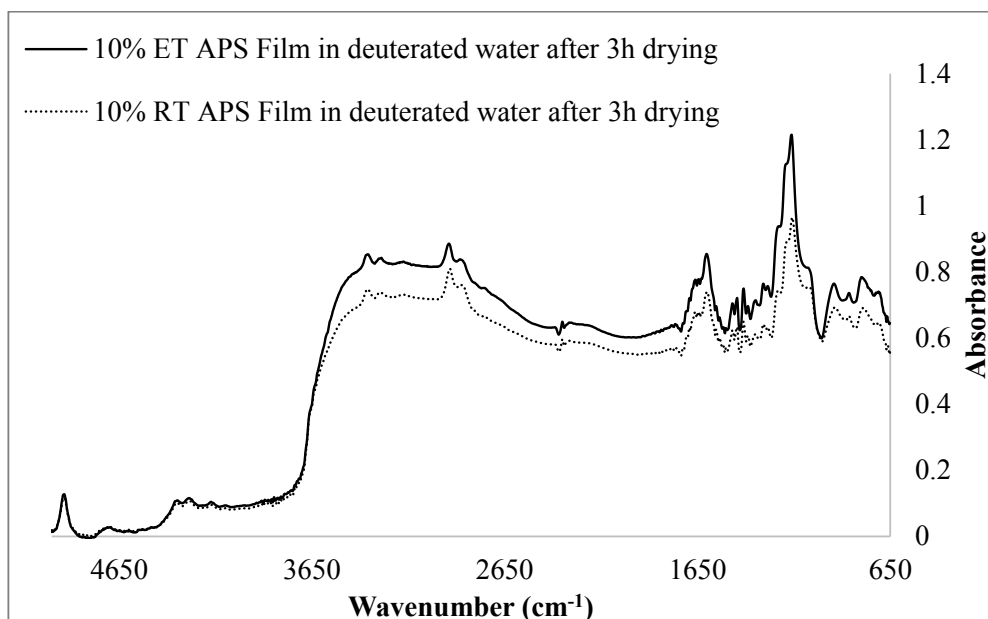


Figure 7.5 DRIFT spectra for 10% v/v APS prepared at RT and ET in D₂O, dried for 3h at 83°C.

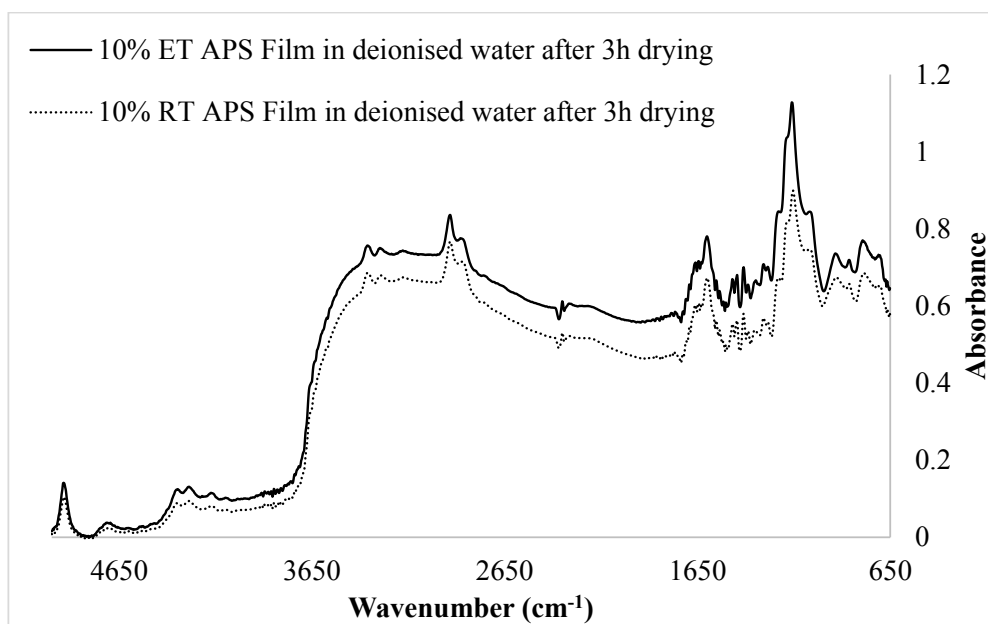


Figure 7.6 DRIFT spectra for 10% v/v APS prepared at RT and ET in deionised water, dried for 3h at 83°C.

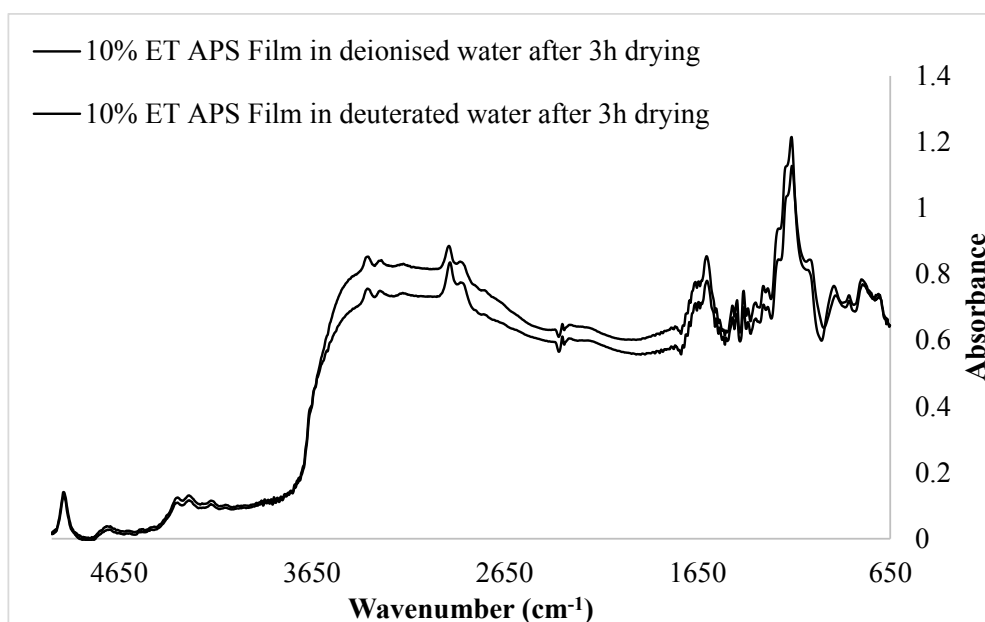


Figure 7.7 DRIFT spectra for 10% v/v ET APS prepared in deionised water and deuterated water, dried for 3h at 83°C.

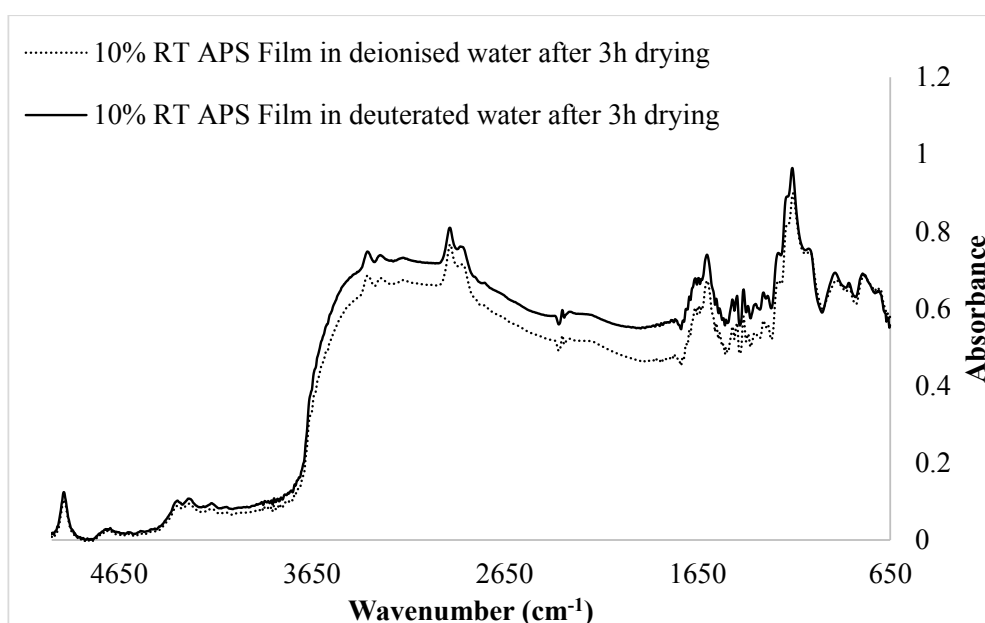


Figure 7.8 DRIFT spectra for 10% v/v RT APS prepared in deionised water and deuterated water, dried for 3h at 83°C.

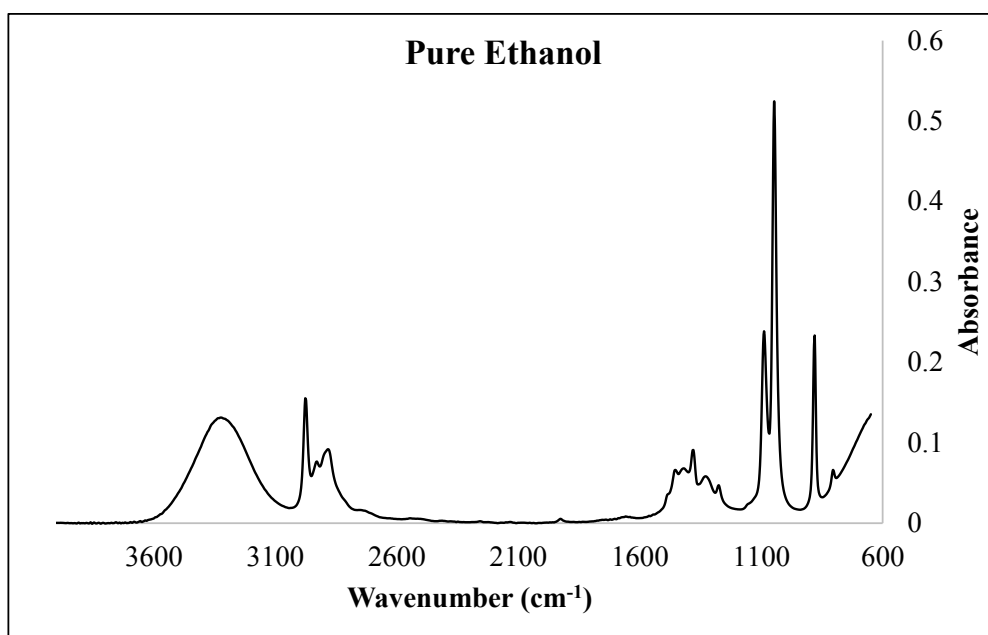


Figure 7.9 ATR spectra for pure ethanol.

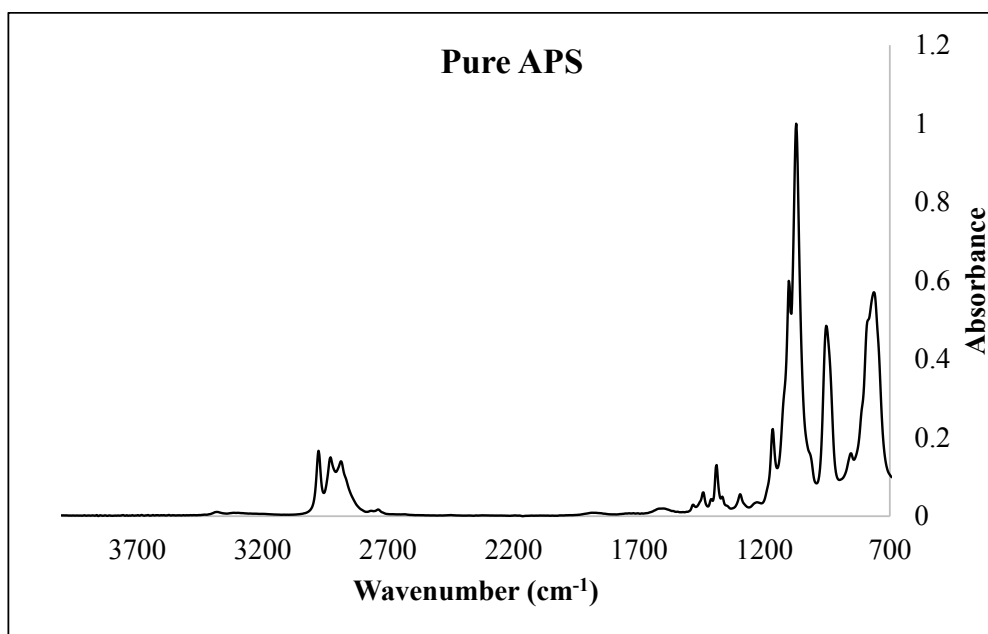


Figure 7.10 ATR spectra for pure APS.

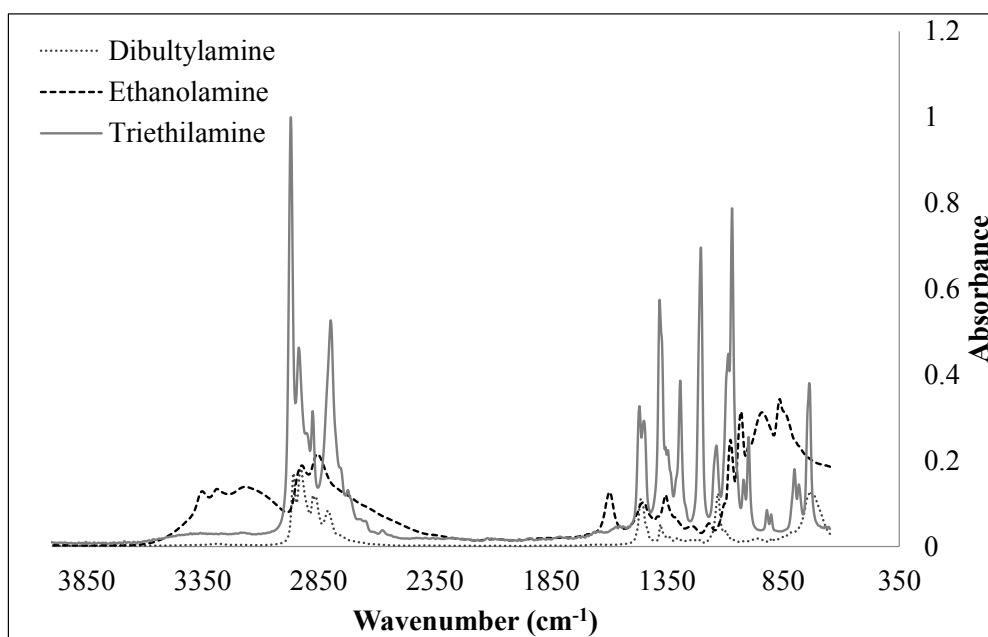


Figure 7.11 ATR spectra for dibutylamine, ethanolamine and triethylamine.

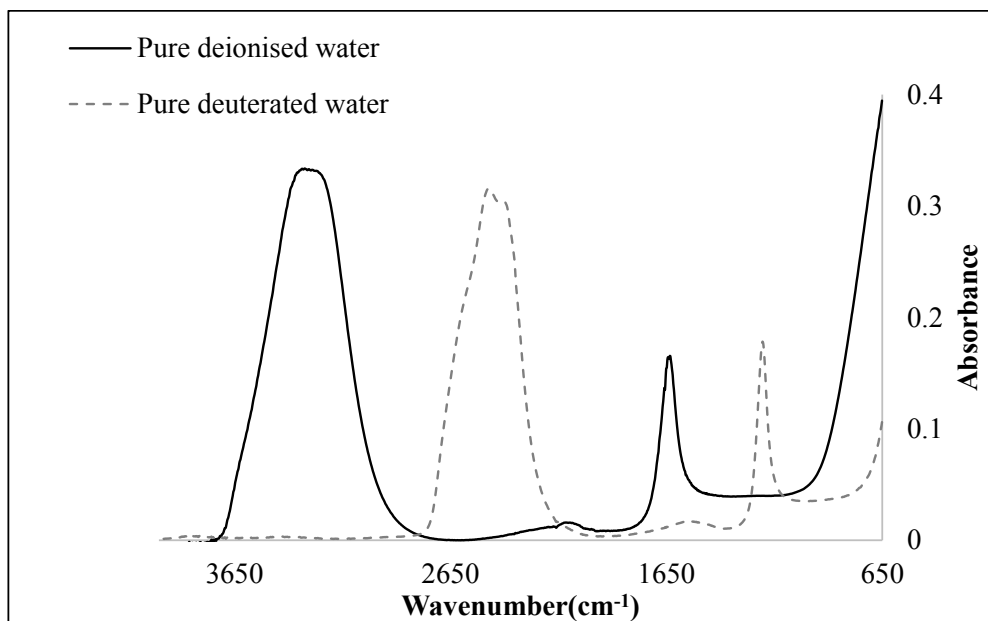


Figure 7.12 ATR spectra for pure deionised water and D₂O.

7.2 Nuclear Magnetic Resonance

NMR is another form of spectroscopy in which the spectrum is a plot of the intensity of absorption (or emission) on the vertical axis against frequency on the horizontal axis. NMR spectra appear at low frequencies, usually in the range 10 to 800 MHz, which corresponds to wavelengths from 30 m down to 40 cm.

The position of the lines are given in 'ppm' using the chemical shift scale. Shift scale is used since the frequencies of NMR lines are directly proportional to the magnetic field strength. The field dependence makes it difficult to compare absorption frequencies between spectrometers which operate at different field strengths, and to solve this problem the chemical shift scale was introduced which results in the peak positions being independent of the field strength [144].

Chemical shift scales

A simple reference compound is needed to set up the chemical shift scale. It is a line taken to define zero on the chemical shift scale. For ^1H , the one used for this study, the reference compound is tetramethyl silane (TMS), an accepted chemical standard for calibration.

The frequency separation from the reference peak, is what is going to specify the position of a peak, and this difference has to be divided by the frequency of the reference peak. Expressed mathematically the chemical shift δ is given by:

$$\delta(\text{ppm}) = 10^6 \times \frac{\nu - \nu_{\text{ref}}}{\nu_{\text{ref}}} \quad (7.3)$$

Where ν is the frequency of the NMR line and ν_{ref} is the frequency of the line from the reference compound. It is obvious that the line from the reference compound will appear at $\delta = 0$. The ratio is multiplied by 10^6 due to the fact that δ is expressed in ppm [144].

Linewidths, lineshapes and integrals

The method to resolve two peaks is based on the separation between them relative to their linewidth and their lineshape. These two properties are of great importance in

NMR. Lines in NMR are often very narrow but they might also be a few Hz in width. Nevertheless, what the linewidth should be compared with is the spread of the frequencies over which NMR lines are found for a given nucleus. Linewidths have little spread for simple molecules but can possess a large spread for complex ones.

In proton (^1H) NMR the area under a peak or multiplet is proportional to the number of protons giving rise to that feature. Hence, if two peaks of single protons are analysed, they must have the same integral; therefore, although they might have a different appearance, if one is broader it will also have a reduced peak height that will make both integrals the same [144].

^1H NMR Spectra

The vast majority of molecules of interest to chemists contain hydrogen atoms and, as this nucleus has one of the strongest resonances, it is not surprising that ^1H NMR has found the widest application [145]. Protons in different chemical groups have different shielding constants, and the resonance condition is satisfied at different ν_0 . Examining the spectrum of ethanol shown in Figure 7.13 [146], the methyl protons form one group; since all the CH bonds are identical and the shielding of each of the nuclei is the same. Such nuclei are called magnetically equivalent, and come into resonance at a position governed by their electron density. The two methylene protons are in a different part of the molecule, they therefore have a different electron density and come into resonance at a different frequency. Finally, the proton of the hydroxyl group resonates at yet another value of the applied field. Since we know that oxygen is a much better electron acceptor than carbon (oxygen has greater electronegativity), then the electron density around the hydrogen atom in C-H bonds should be considerably higher than the O-H bonds. We should thus expect $\sigma_{\text{CH}} > \sigma_{\text{OH}}$ and hence

$$\nu_{\text{CH}} = \frac{\gamma B_0}{2\pi(1 - \sigma_{\text{CH}})} < \nu_{\text{OH}} = \frac{\gamma B_0}{2\pi(1 - \sigma_{\text{OH}})} \quad (7.4)$$

Thus, for a given applied field, the CH hydrogen nucleus will precess with a smaller Larmor frequency than that of OH [146][147]. Two very important facets of NMR spectroscopy appear in Figure 7.13:

- I. Identical nuclei, i.e. ^1H nuclei, give rise to different absorption positions when in different chemical surroundings. For this reason, the separation between absorption peaks is usually referred to as chemical shift.
- II. The area of an absorption peak is proportional to the number of equivalent nuclei (i.e. nuclei with the same chemical shift). Note that in the case of ethanol, we can distinguish which group of lines corresponds to which group of protons by their relative intensities.

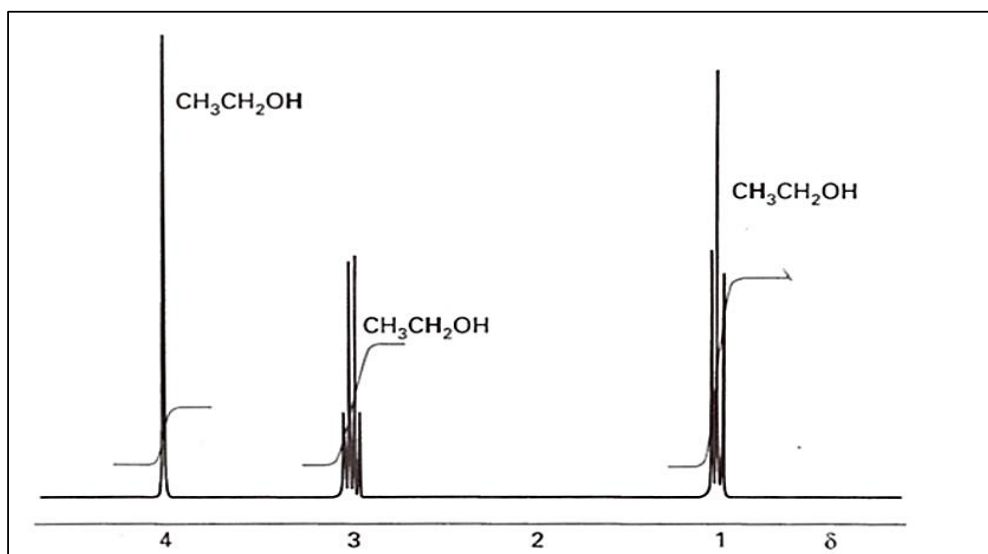


Figure 7.13 The ^1H -NMR spectrum of ethanol. The bold letters denote the protons giving rise to the resonance peak, and the step-like curve is the integrated signal (Atkins, 1998) [145].

The group intensities are in the ratio 3:2:1 because there are 3 methyl protons, 2 methylene protons and 1 hydroxyl proton. Chemical shift measurements are formally based on the resonance position of the bare proton nucleus as the primary standard. For this there is no shielding, and hence $\sigma = 0$. Since this is a quite impracticable standard, the shifts are normally quoted relative to the protons of some standard compound. Tetramethylsilane $\text{Si}(\text{CH}_3)_4$, written TMS, which has equivalent protons is a frequently chosen standard. So, we define the chemical shift in terms of the difference in resonance frequencies between the nucleus of interest (i.e. ^1H) and a reference nucleus (i.e. ^1H of TMS) by means of a dimensionless parameter δ . The δ

values are positive if the sample absorbs to high frequency of the reference absorption at constant field:

$$\delta = 10^6 \frac{(\nu_{sample} - \nu_{TMS})}{\nu_{TMS}} \quad (7.5)$$

Since shielding constants are small, the value ν_{TMS} in the denominator may be replaced by the spectrometer operating frequency ν_0 or by $|\gamma|B_0/2\pi$ with little error. Thus, δ is related to shielding constants by:

$$\delta = 10^6(\sigma_{TMS} - \sigma_{sample}) \quad (7.6)$$

The factor of 10^6 simply scales the numerical value of δ to a more convenient size: δ values are quoted in parts per million, or ppm [148]. Characteristic δ chemical shifts of a number of commonly occurring groups are shown in Figure 7.14.

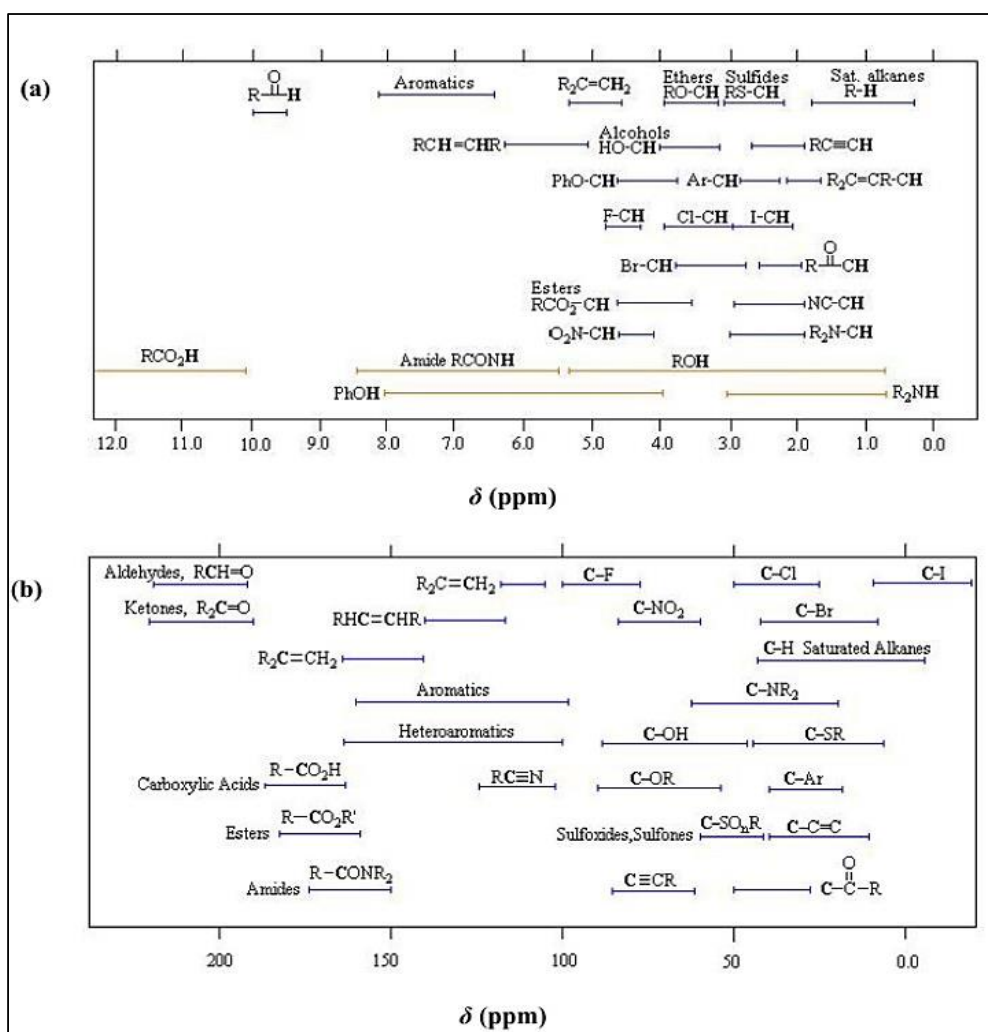
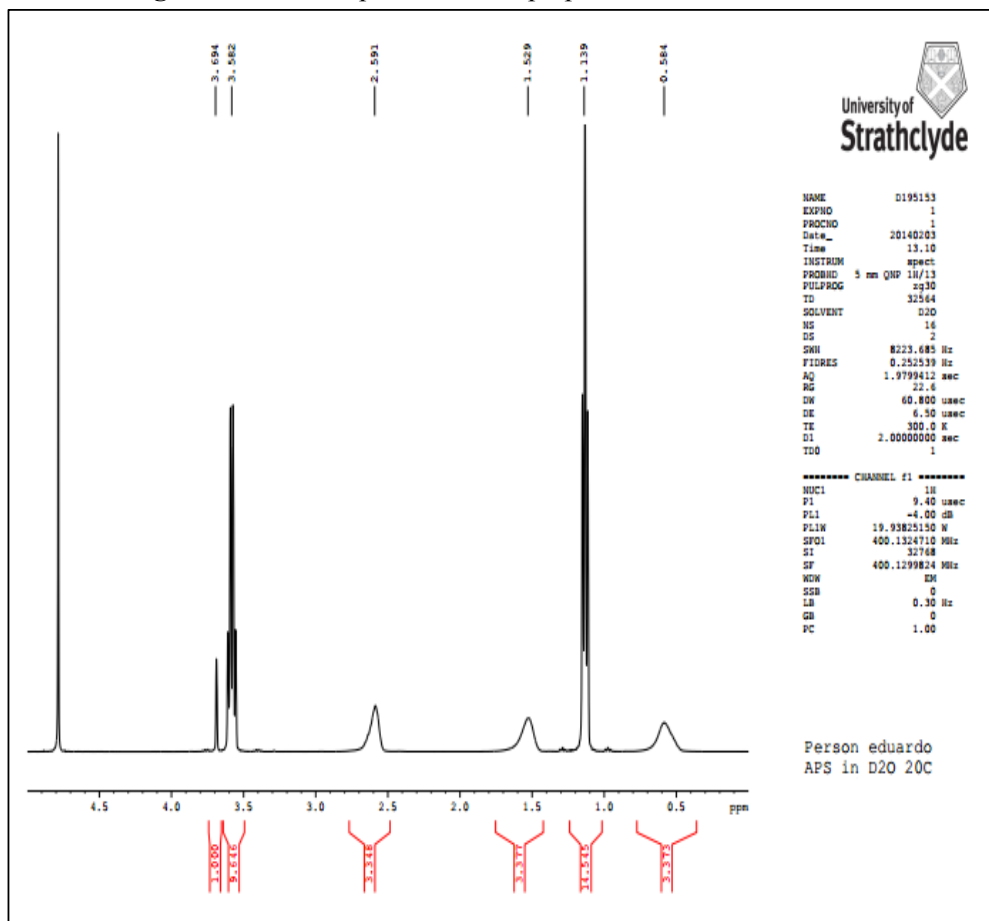


Figure 7.14 The range of typical chemical shifts for (a) ^1H resonances and (b) ^{13}C resonances.

7.2.1 NMR spectra

Figure 7.15 NMR spectra of APS prepared for 24 hours at 20°C in D₂O.



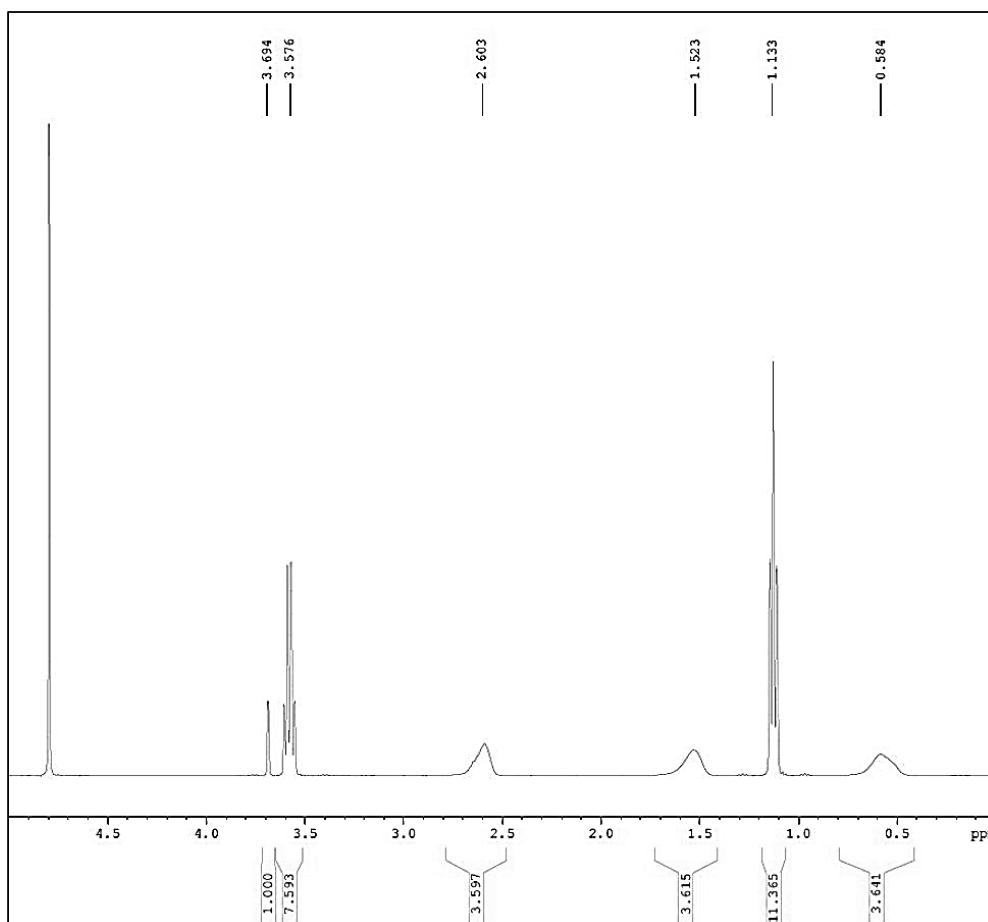


Figure 7.16 NMR spectra of APS prepared for 5 hours at 45°C in D₂O.

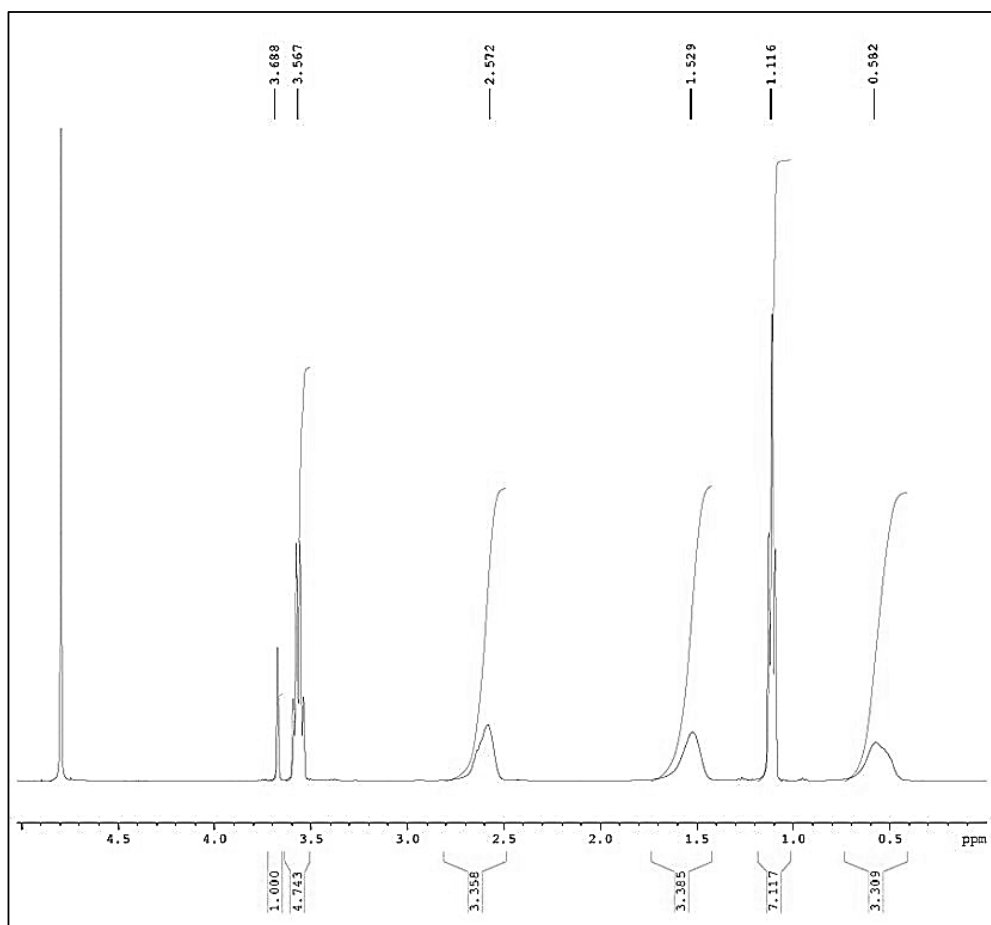


Figure 7.17 NMR spectra of APS prepared for 5 hours at 75⁰C in D₂O.

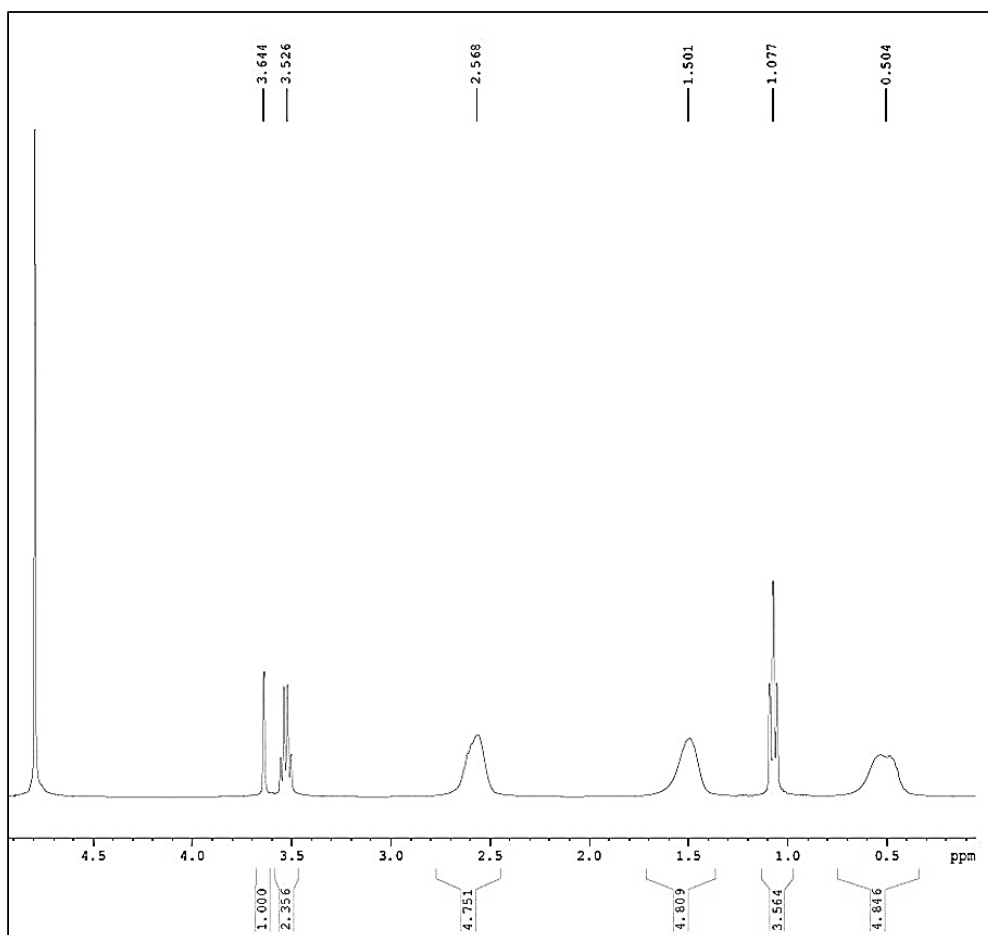


Figure 7.18 NMR spectra of APS prepared for 5 hours at 83°C in D₂O.

7.3 Bundle tension tests

7.3.1 Materials

Boron-free-E-glass fibres under the trade name of Advantex® supplied by Owens Corning-Vetrotex were investigated in this work. The fibre rovings were produced on a pilot scale bushing and were received as 20 kg continuous single end square edge packages. The roving had a nominal tex of 1200 g/m and a nominal fibre diameter of 17 µm. No sizing had been applied to the fibres which had only been water sprayed using the normal cooling sprays under the bushing [69], these samples are referred to commercially uncoated or as received GFs. The sized fibres were coated with a normal rotating cylinder sizing applicator containing a 1% γ-aminopropylsilane (APS) hydrolysed solution in distilled water. All fibre packages were subsequently dried at 105 °C for 24 hours [71,81]. These samples are referred to commercially coated GFs.

7.3.2 Chemicals

The chemicals that have been used were purchased from Sigma Aldrich. The silanes were as follows:

- γ-Aminopropyltriethoxy Silane (APS) (≥98%)
- γ-Methacryloxypropyltrimethoxy Silane (MPS) (98%)
- γ-Glycidoxypyltrimethoxy Silane (GPS) (≥98%)
- Vinyltryethoxy Silane (VS) (97%)
- γ-Mercaptopropyltrimethoxy Silane (SPS) (95%)

The rest of the chemicals used are listed below:

- Acetic acid (CH₃COOH) (≥99.7%)
- Deionised water (H₂O)

7.3.3 Silane solution preparation

Silane preparation was carried out in deionised water by adjusting the pH of the deionised water, if needed, using solution of dilute acetic acid. The pH of the deionised water was measured using a pH meter. It was calibrated using 4, 7 and 10 buffer

solutions provided with the pH meter [124]. The solutions were prepared using a plastic container with the lid closed at 1% in volume (v/v) as can be seen Table 7.1.

Table 7.1 Silanes 1% (v/v) preparation for bundle tensile tests.

Silane	MPS	SPS	VS	GPS	APS	
pH	5.0	5.0	5.0	5.0	5.0	7.5
Preparation time (h)	24	24	24	24	24	24
Conc. (%)	1	1	1	1	1	1

Some silane blends were also prepared following the same procedure. Silanes were prepared separately at 1% (v/v), as shown above. Then they were mixed in the same proportions, being the sum of both 1% (v/v), as shown in Table 7.2.

Table 7.2 Blends of silanes 1% (v/v) preparation for bundle tensile tests.

Silanes blend	MPS-GPS	MPS-SPS	MPS-APS
pH	5.0	5.0	5.0
Preparation time (h)	24	24	24
Concentration (%)	1	1	1

Since APS is the most commonly used silane in the GF industry due to its good performance, both with matrix and GFs, it was chosen to investigate the effect of temperature in the preparation of APS solutions. In Table 7.3 the different methods of APS preparation are shown.

Table 7.3 Temperature effect investigation on APS 1% (v/v) for bundle tensile tests.

Silane	APS	APS	APS
pH	7.5	7.5	7.5
Preparation time (h)	1	5	5
T (°C)	83	83	83
Lid	Closed	Closed	Open

The reasons why the lid could be left either closed or open was due to the main by-products of the silanes as well as the steam generated. Leaving the lid open allowed for the release of ethanol/methanol vapours along with steam, while if the lid was closed, it may not occur and water molecules would condense. The lid was either left closed the whole preparation time or open. Open refers to the lid being initially closed and then it was completely opened two times, once after 1.5 hours and another time after 3 hours, both times for 15 minutes respectively. The aim of this procedure is to avoid too much water evaporation.

Table 7.4 Concentration effect of MPS and APS 1 and 2% (v/v) applied to water sized GFs for bundle tensile tests.

Silane %	MPS 1%	MPS 2%	APS 1%	APS 2%
pH	5.0	7.5	7.5	7.5
Preparation time (h)	24	24	5	5
T (°C)	25	25	83	83

The silane concentration effect was also studied, preparing 2% in volume (v/v) of MPS and APS, combined with temperature effect as well. For silane preparation, every

time that temperature was involved in the preparation process, the lid was occasionally opened, as explain above.

The details of the preparation of the various silane solutions are given in above Table 7.4. Once the silanes were ready to apply, the bundles were completely immersed in the silane solution for 15 minutes. The samples were then removed from the solution and dried by placing the GF strands in an oven at 110⁰C for 15 minutes using a specially designed jig (Figure 2.1), using a nut, bolt and washer to prevent fibre breakage where the strands were completely suspended. This prevented any contact with, and hence damage to, the fibres [81]. Finally, they were left at RT overnight before being prepared and tested.

7.3.4 Experimental

GF bundles were carefully selected from the GF roving and glued onto a card tabs with a central window cut out to match the desired gauge length for the test as shown in Figure 7.19. Card frames were cut from 250 g/m² grade card and fibre bundles were fixed to the card on both sides window using Araldite Rapid Epoxy Resin.

Fibre bundle tensile properties were determined following the method described in ASTM 2256-03 [149] using a Testometric M250-2.5CT testing machine equipped with a 2.5 kN load cell. The sample gauge length was 250 mm and up to 20 bundles were tested for the as received GFs, the commercially coated GFs, and each treatment applied to the as received GFs. The tensile testing strain rate was 1.5 %/min (3.75 mm/min) and all tests were carried out at room temperature and 50% relative humidity.

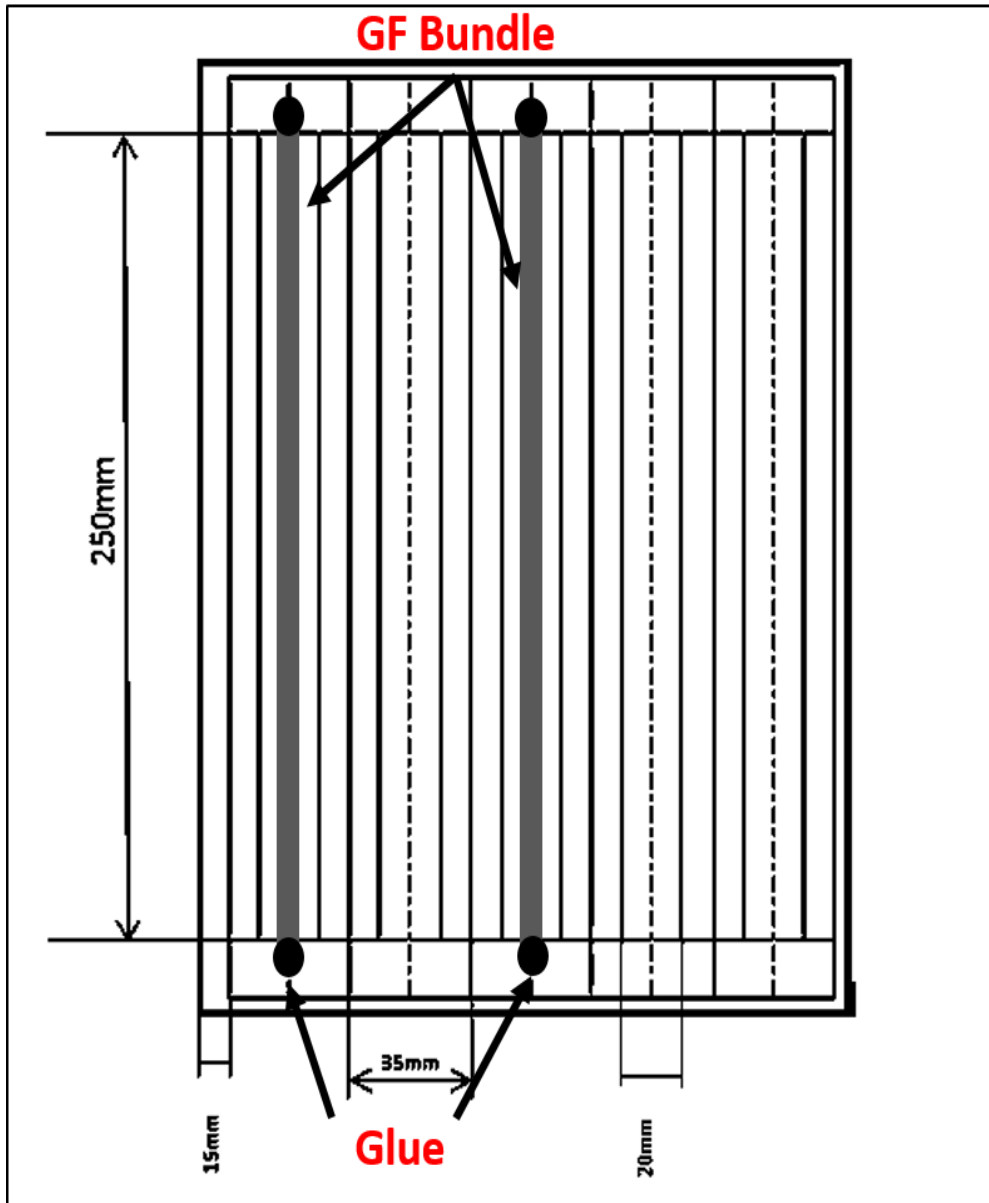


Figure 7.19 Fibre bundle template.

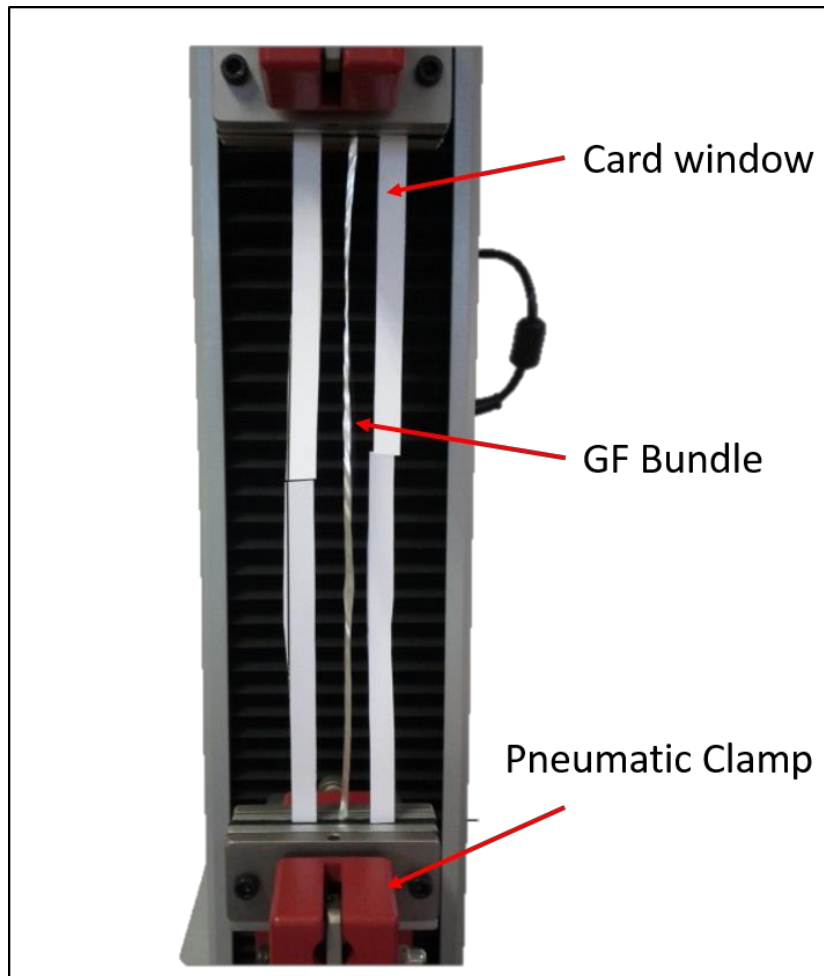


Figure 7.20 Bundle sample in Testometric M250-2.5CT

In Figure 7.21 a typical force-elongation curve for water and APS sized GF bundles is shown. Since the GF bundle has over 1000 fibres, each of which could have a different strength, not all the fibres broke at the same elongation. Instead a progressive drop in force was exhibited after the maximum force was reached while the individual fibres were breaking. Both types of GFs followed the same pattern of curve, but some differences can be seen between them. The unsized GFs showed a more irregular progression of the curve, i.e. a higher amount of small peaks can be seen due to breakage of individual filaments. On the other hand, the APS-sized GFs showed a softer progression of the curve without the presence of small peaks, which may be due to the presence of the APS sizing. It is also noticeable that once the highest load peak was reached, the downward slope was steeper for the APS-sized GFs.

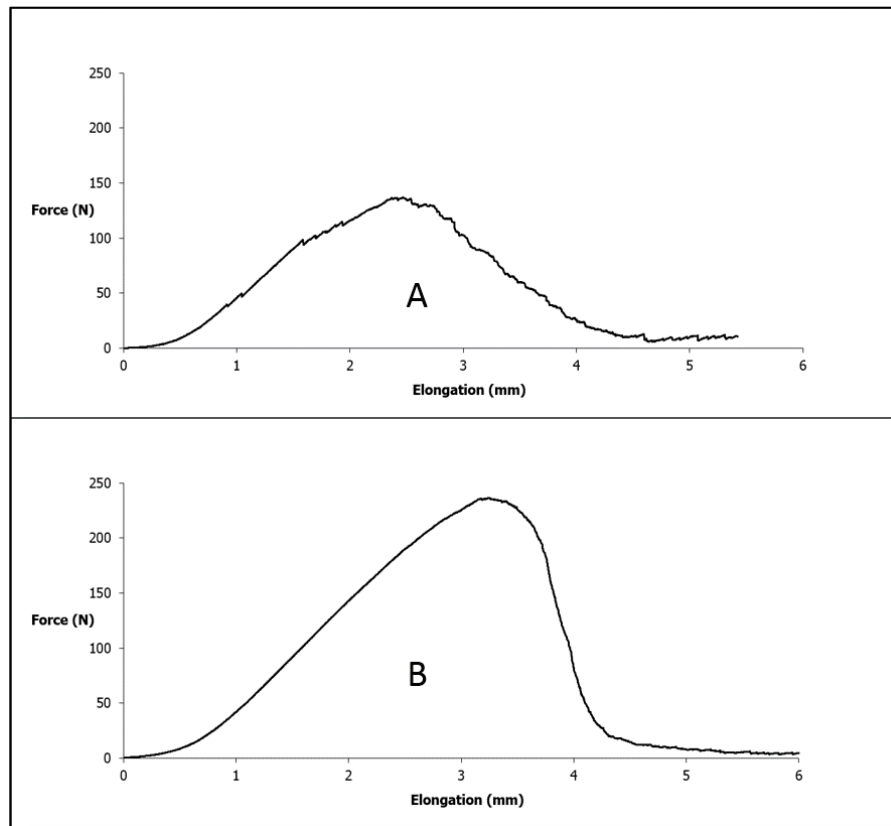


Figure 7.21 Typical force-elongation curve for a fibre bundle test. A) As received GF. B) commercially coated GF.

7.3.5 Results and discussion

In Table 7.5 results of bundle fibre average peak force for as received and commercially coated GF bundles are shown.

Table 7.5 Average peak force of as received and commercially coated GF bundles.

	Average Peak Force (N)	95% Confidence Limit (N)
Unsize	146	± 2.9
APS-Sized	224	± 7.6

The average bundle peak force of the commercially coated GFs was found to be significantly higher than for the as received GFs, the error being higher as well. These results were expected due to the coating effect on GF surface and, as a consequence,

in GF bundle peak force due to the coating preventing friction damage between fibres, i.e. surface protection effect, something that surely happens during bundle tests. On the other hand, coatings may have a repairing effect on GF surface defects, i.e. flaw healing, which may explain even more the difference in peak force between them.

Table 7.6 Average peak force for as received GFs coated with different silanes.

	Average Peak Force	Confidence Limit
	(N)	(95%)
As received GFs	146	± 2.8
MPS	198	± 15.0
SPS	156	± 13.2
VS	139	± 11.2
GPS	167	± 13.1
APS	159	± 7.6
(pH 5)		
APS	192	± 14.4
(pH 7.5)		
Commercially coated		
GFs	226	±13.8

In Table 7.6 results of fibre bundle average peak force for as received GF bundles coated with different silanes prepared as shown in Table 7.1 can be seen.

The average bundle peak force was found to increase remarkably for as received GFs coated with MPS and APS at the solution medium (i.e. deionised water) natural pH (7.5). Both reached values of almost 200 N, which is an increase of around 35% in bundle peak force, close to the value obtained for the commercially coated GFs, which was 226 N. GPS seems to have some effect as well, but in a lower range than the other two. Other silanes such as SPS and VS, apparently, have little significant effect on

bundle peak force, with values surrounding the baseline value obtained for as received GFs.

Based on the results obtained in Table 7.6, different blends have been prepared using MPS and results for three other silanes with higher levels of bundle peak force increase. (APS, GPS and SPS discarding VS for the poor results) obtained. The results obtained for the unsized GFs coated with these blends are shown in Table 7.5.

Table 7.7 Average peak force for as received GF bundles coated with different silane blends.

	n^o of Samples	Average Peak Force (N)	Confidence Limit (95%)
Unsize O.C.	25	146.2	± 2.8
MPS-GPS	7	189.5	± 18.0
MPS-SPS	7	164.2	± 15.6
MPS-APS	9	166.3	± 7.6

The only blend that showed a substantial increase in bundle peak force was the combination of MPS and GPS, whilst the effect of the other two blends were not as much as this blend. It is important to point out that none of the three combinations reached or improved on the effect of MPS itself. These results may be explained from two different points of view. For MPS-GPS and MPS-SPS the decrease in bundle peak force might be due to the GPS and SPS effect itself being lower than the MPS. The combination of both silanes with MPS decrease the effect of MPS, the decrease of MPS blend with SPS being higher than with GPS, something that can be correlated with the lower average bundle peak force found for SPS compared with GPS. On the other hand, the combination of MPS and APS, being both silanes that achieved higher values of average bundle peak force when they were applied alone, has not got as beneficial effect. It may be due to the pH used to prepare the blend. It was prepared at a solution medium pH of 5. This is the proper pH to prepare MPS but not as suitable

to prepare APS. The results suggest that this is probably the reason for the lower increase in bundle peak force.

As explained above, APS is the most commonly used silane in the GF industry and the results showed a noticeable positive effect of bundle peak force. Due to this reason, other parameters fixing the solution medium pH at 7.5 (natural) were changed to investigate if another variation in preparation parameters could improve the later effect on GFs mechanical properties.

Firstly, temperature was chosen to see its effect. Different methods of preparing APS at high temperature (83⁰C) were investigated. Time preparation and lid open or closed, as shown in Table 7.8, have been studied. The results are shown in Table 7.8:

Table 7.8 Average peak force for as received GFs coated with APS 1% (v/v) prepared at solution medium natural pH, 83⁰C and changing the preparation time and leaving the lid open or closed.

	Preparation time (h)	Lid	Average Peak Force (N)	Confidence Limit (95%)
As received GFs	-	-	146	± 2.8
1	1	Close	147	± 16.2
2	5	Close	186	± 9.4
3	5	Open	195	± 11.1
Commercially coated GFs	-	-	224	± 7.6

The results shown above suggest that 1 hour of APS preparation at 83⁰C does not have any particular effect on APS hydrolysis and condensation reactions, while 5 hours seems to have a substantial effect (5 hours being probably more time than required). It also suggests that opening the lid twice during the APS preparation does not have any remarkable effect on mechanical properties of GFs, the average peak force being the

same within experimental error. However, in order to release the by-product, i.e. ethanol, and avoid the possibility of condensation of the ethanol vapour and consequently its returning to the solution, it is recommended to use the lid opening procedure. It may help the displacement or hydrolysis reaction to the products, before self-condensation.

2% (v/v) of MPS or APS results are shown below, prepared in different ways as explained in Table 7.4.

Table 7.9 Average peak force for MPS and APS 2% (v/v) prepared in different ways.

	Average Peak Force (N)	Confidence Limit (95%)
As received GFs	146	± 2.8
MPS 1%	198	± 15.0
MPS 2%	211	± 10.1
ET APS 1%	195	± 11.1
ET APS 2%	208	± 33.7

The results suggest that an increase in the concentration of MPS and APS does not have any noticeable effect on mechanical properties of GFs, since they have the same average peak force within experimental error.

7.4 Weibull analysis plots

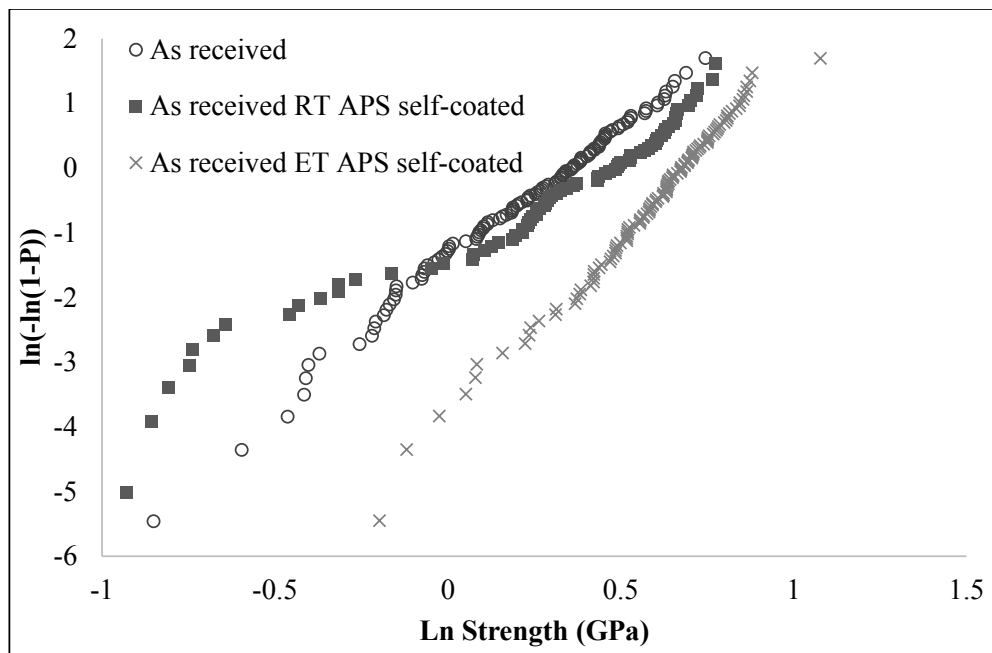


Figure 7.22 Weibull analysis. Comparison of as received GFs, RT and ET APS self-coated GFs.

Table 7.10 Summary of parameters for Weibull distribution for as received, RT APS and ET APS self-coated GFs.

	m	σ_0 (GPa)	R^2
As received GFs	4.22	1.41	0.99
ET APS self-coated	5.80	1.98	0.99

	m_1	σ_{01}	R^2_1	m_2	σ_{02}	R^2_2
ET APS self-coated	9.57	0.65	0.95	2.82	1.56	0.94

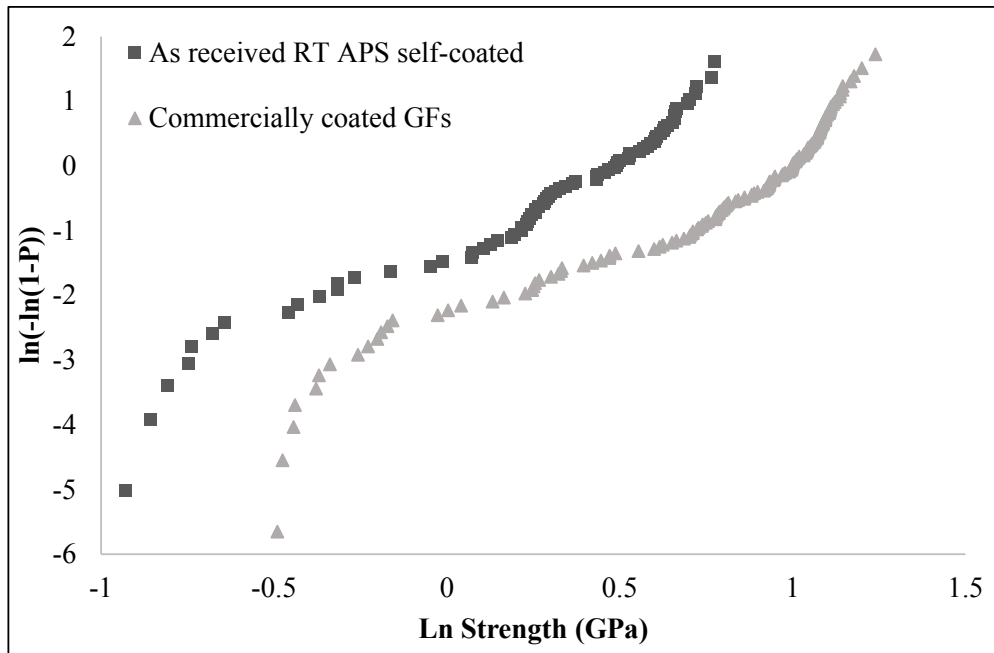


Figure 7.23 Weibull analysis. Comparison of RT APS self-coated GFs and commercially coated GFs

Table 7.11 Summary of parameters for Weibull distribution of as received RT APS self-coated and commercially coated GFs.

	m_1	σ_1	R^2_1	m_2	σ_2	R^2_2
RT APS Self-coated	9.57	0.65	0.95	2.82	1.56	0.94
Commercially coated	16.09	0.84	0.79	2.70	2.58	0.91

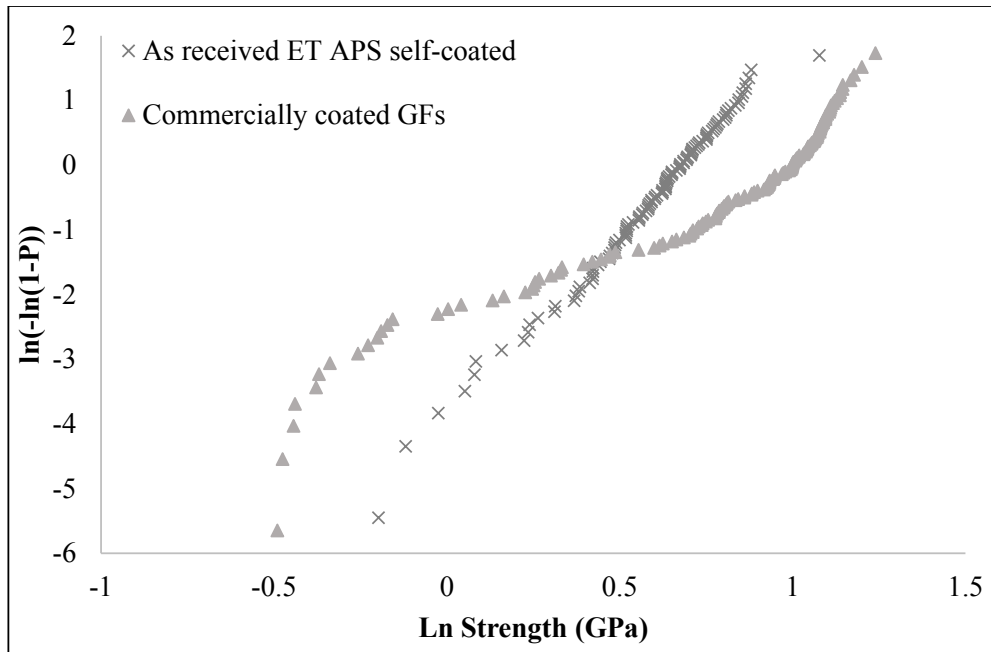


Figure 7.24 Weibull analysis. Comparison of as received ET APS self-coated and commercially coated GFs.

Table 7.12 Summary of parameters for Weibull distribution as received ET APS self-coated and commercially coated GFs.

	<i>m</i>		σ_0 (GPa)		R^2	
ET APS self-coated GFs	5.80		1.98		0.99	
	<i>m</i> ₁	σ_{01}	R^2_1	<i>m</i> ₂	σ_{02}	R^2_2
Commercially coated GFs	16.09	0.84	0.79	2.70	2.58	0.91